UNIVERSITY OF SOUTHAMPTON

FACULTY OF ENGINEERING, SCIENCE AND MATHEMATICS

Institute of Sound and Vibration Research

WAVE REFLECTION, TRANSMISSION AND PROPAGATION IN STRUCTURAL WAVEGUIDES

by

Seung-Kyu Lee

Thesis for the degree of Doctor of Philosophy

August 2006

UNIVERSITY OF SOUTHAMPTON

ABSTRACT

FACULTY OF ENGINEERING, SCIENCE AND MATHEMATICS
INSTITUTE OF SOUND AND VIBRATION RESEARCH

Doctor of Philosophy

WAVE REFLECTION, TRANSMISSION AND PROPAGATION IN STRUCTURAL WAVEGUIDES

by Seung-Kyu Lee

A generalised wave approach based on reflection, transmission and propagation of waves is presented for the analysis of one-dimensional structural waveguides. The state vector in the physical domain is transformed to the wave domain using the displacement and internal force matrices. The wave amplitudes at one point are then related to those at another point by the (diagonal) propagation matrix, which is true for deterministically varying waveguides as well as uniform waveguides. The response to external excitation, reflection and transmission at a point discontinuity, reflection at boundaries, the spectral element and the energy flow associated with waves are described in a systematic way using the matrices. Numerical results of the wave approach are always well conditioned since the positive- and negative-going wave motions are separated. The wave approach is illustrated for longitudinal and bending motions of deterministically varying straight beams, based on elementary theories such as Euler-Bernoulli theory. The energy transport velocity is derived using the relationship between power and energy. In contrast to that for uniform structures, the energy velocity for deterministically varying structures depends on position as well as frequency. The in-plane motion of uniform curved beams, in which longitudinal and bending motions are coupled, is studied as well. The energy flow associated with waves is described explicitly in terms of the wavenumbers. Numerical results for the power transmission through a U-shaped structure are presented. In conjunction with the piecewise approach, the exact results can be used in an efficient way for arbitrarily varying structures and, eventually, built-up structures. Employment of deterministically varying elements, rather than uniform elements, could lead to rapid convergence at low computational cost, especially when the non-uniformity of the structure becomes severe. The modal behaviour of a linearly tapered curved beam with clamped-free boundaries is studied and its asymptotic behaviour related to the pure bending and pure extensional motions is revealed.

TABLE OF CONTENTS

ACKNOWLEDGEMENTS

The work presented in this document was completed with the financial support of Hankook Tire Co. Ltd., Korea. I would like to appreciate their allowance to do this research. I am also deeply grateful to my supervisors Professor B.R. Mace and Professor M.J. Brennan for their help and guidance. I would like to thank to Professor D.J. Thompson and Dr. N.S. Ferguson who gave me invaluable advice during this work. I should mention Ms. Anne-Marie McDonnell for her warm help. Thanks to my parents and parents-in-law. I am sorry to my son and daughter for having little time with them during this study. My heartfelt thanks and love are to my wife Euna.

LIST OF SYMBOLS

$a,\ d$	amplitudes of waves
A	cross-sectional area
b	width
c_b	phase velocity of bending wave
c_l	phase velocity of longitudinal wave
c^E	energy transport velocity
ds	arc length
$d\theta$	arc angle
e_s	strain along the coordinate s
E	modulus of elasticity
$\mathcal{E}$	energy density, $\mathcal{E}=\mathcal{T}+\mathcal{V}$
f_{ext}	amplitude of a point external force
h	thickness
$H_\mu^{(1,2)}$	Hankel functions of the first and second kind of order μ
i	$\sqrt{-1}$
I	the second moment of area
I_μ	modified Bessel function of the first kind of order μ
k	wavenumber
k_b	bending wavenumber
$k_{b,m}$	effective flexural wavenumber of a section
k_l	longitudinal wavenumber
K_μ	modified Bessel function of the second kind of order μ
K_T	non-dimensional translational dynamic stiffness
$\bar{K}_T$	translational dynamic stiffness
K_R	non-dimensional rotational dynamic stiffness

$\bar{K}_R$	rotational dynamic stiffness
L	length
M	bending moment
M_{ext}	amplitude of a point external moment
N	normal force
P	normal force for longitudinal motion
Q	shear force
r	radial coordinate
R	radius of curvature
s	circumferential coordinate
t	time
$\mathcal{T}$	kinetic energy density
$\mathcal{V}$	potential energy density
u	longitudinal displacement of the centreline of a waveguide
U	longitudinal displacement of a point of a waveguide
w	lateral displacement of the centreline of a waveguide
W	lateral displacement of a point of a waveguide
x	coordinate along waveguide axis
z	coordinate along the normal to waveguide axis

α	ratio of tangential displacement to radial displacement
α_A	taper rate for cross-sectional area
α_I	taper rate for the second moment of area
β	wavenumber
β_s	change in curvature along the coordinate s
γ	Euler's constant, $\gamma \approx 0.577216$
ε_s	extensional strain along the coordinate s

θ	angle or phase difference between two waves
κ	curvature, $\kappa = 1/R$
λ	eigenvalue of $\mathbf{U}$, or wavelength
μ	flaring index for polynomial variation
ν	$\nu = (\mu - 1)/2$
ξ	dimensionless wavenumber, $\xi = kR$
Π	power
ρ	density
ϱ	power reflection coefficient
σ_s	extensional stress along the coordinate s
τ	power transmission coefficient
φ	rotation of the normal to the centreline, or slope due to the effect of bending
χ	radius of gyration
$\overline{\chi}$	dimensionless radius of gyration
ω	angular frequency
ω_c	cut-off frequency
$\Omega, \Omega', \Omega''$	non-dimensional angular frequency
$\mathbf{a}$, $\mathbf{b}$, $\mathbf{d}$	vector of amplitudes of waves
$\mathbf{D}$	dynamic stiffness matrix for spectral element
$\mathbf{E}$	unitary matrix, the columns of which are eigenvectors of $\mathbf{P}$
$\mathbf{f}$	vector of generalized internal forces
$\mathbf{f}_{ext}$	vector of external forces
$\mathbf{F}$	propagation matrix
$\mathcal{F}$	field transfer matrix in wave domain
$\mathcal{G}$	point transfer matrix in wave domain
$\mathbf{I}$	identity matrix

$\mathbf{I}'$	matrix consisting of 0 and 1
$\mathbf{J}$	matrix consisting of $\mathbf{0}$ and $\mathbf{I}$
$\mathbf{J}'$	diagonal matrix composed of ± 1
$\mathbf{K}_{ext}$	external dynamic stiffness matrix
$\mathbf{M}$	matrix, columns of which are eigenvectors of $\mathbf{U}$
$\mathbf{p}$	vector of amplitudes of power waves
$\mathbf{P}$	power matrix, Hermitian
$\mathbf{q}$	vector of amplitudes of waves induced by external forces
$\mathbf{R}$	reflection matrix
$\mathbf{S}$	system matrix in physical domain
$\mathbf{T}$	transmission matrix
$\mathcal{T}$	transfer matrix in wave domain
$\mathbf{u}$	physical state vector, $\mathbf{u} = \left[\mathbf{w}^T \quad \mathbf{f}^T \right]^T$
$\mathbf{U}$	transfer matrix in physical domain
$\mathbf{V}$	diagonal matrix consisting of the (real) eigenvalues of $\mathbf{P}$
$\mathbf{w}$	vector of generalized displacements
$\mathbf{y}$, $\mathbf{z}$	eigenvectors of $\mathbf{U}$
$\mathbf{0}$	zero matrix
Λ	diagonal matrix
ϕ	column vector of Φ
Φ	internal force matrix
ψ	column vector of Ψ
Ψ	displacement matrix

Superscripts

$+$	denote positive-going direction in x-axis

$-$	denote negative-going direction in x-axis
$\cap$	combined with $\mathbf{R}$ and $\mathbf{T}$, denote the case where waves are incident from the right-hand side

Subscripts

b	denote bending motion
l	denote longitudinal motion
N	denote nearfield wave

Operators

T	transpose
H	Hermitian
$*$	complex conjugate
$\mathrm{Re}(\cdot)$	real part of a quantity
$\mathrm{Im}(\cdot)$	imaginary part of a quantity
$\langle\cdot\rangle$	time-averaged

Chapter 1.

INTRODUCTION

1.1 Background

Finite element analysis is a useful tool to analyse the dynamic behaviour of structures at low frequencies. However, in the high frequency region, it requires powerful computing resources for a refined model. Statistical energy analysis, which is concerned with energy flow in a structure and is used at high frequencies, is not suitable for structures with high damping such as a tyre.

The literature, which is reviewed in the next section, suggests several alternative approaches using exact solutions such as the transfer matrix method, the dynamic stiffness method and the wave methods. These approaches are valid for all frequencies in contrast to finite element analysis, so they can be used efficiently in the high frequency region and may also be suitable for structures with high damping. Interest has been shown in the wave approach where the dynamic behaviour of a structure is described in terms of waves and their propagation, reflection and transmission in the structure. This wave approach is attractive since the associated numerical results are always well conditioned.

The present work is concerned with wave motion of various types of one-dimensional structure. In one-dimensional structures all the field quantities associated with the motion are written as functions of position along the axis of the structure. Throughout the thesis the material properties of the structures under consideration are

assumed to be linearly elastic. The geometry and/or material properties may be uniform along the length, or vary continuously.

1.2 Review of previous work

In this section the literature on wave motion of one-dimensional structures is reviewed. One-dimensional structures are first categorised according to their type and then the results of the survey are classified according to the categorisation. Special attention is paid to three cases: straight bars undergoing longitudinal motion, straight beams undergoing bending motion and curved beams, in which longitudinal and bending motions are coupled in their plane. These motions are all based on elementary theories such as Euler-Bernoulli beam theory.

1.2.1 Classification of one-dimensional structures

Figure 1-1 shows a categorisation of one-dimensional structures according to the characteristics of the material and geometric properties. The bold-faced groups in the figure are considered in this thesis. First uniform structures, where the properties are constant, and non-uniform structures are separated. Periodicity of the spatial variation divides the non-uniform structures into 3 groups: non-periodic, near periodic and periodic structures. Non-periodically varying structures can be subsequently divided into two groups: slowly varying and rapidly varying structures. When the degree of the non-uniformity is relatively small compared to a wavelength, waves can propagate along the structure with negligible reflection. These structures are classified as slowly varying structures. When the non-uniformity becomes severe, waves may not propagate freely and may be partly reflected. However, previous work has shown that there is a class of non-uniform structures where no such reflection occurs. These structures are

categorised as deterministically varying structures. Combining the categories of slow variation and deterministic variation makes another class, called near deterministically varying structures, which are similar to deterministically varying structures but not the same. Non-uniform structures, where the geometry and material properties vary in a complex manner so that the reflection of waves is significant, are classified as arbitrarily varying structures. Indeed this group includes all other structures, which have not been classified yet as one of the other groups since exact or approximate closed-form solutions for the motion are difficult to obtain.

This categorisation has been made on the assumption that the variation of the properties is prescribed by known functions. The so-called random or disordered structures, where the properties are given as random variables with a probability distribution, are beyond the scope of this thesis.

1.2.2 Uniform waveguides

A uniform structure has geometric and material properties which are invariant along its length. This group includes uniform straight bars undergoing longitudinal motion, uniform straight beams undergoing bending motion, and curved beams with constant curvature and constant properties.

Transfer matrix methods have been widely used for analysing the dynamic behaviour of elastic systems including uniform structures such as space structures. Lin and Donaldson (1969) outlined the principles of the transfer matrix method and presented a series of examples of its application including curved panel-stringer rows in aircraft. The review by Mead (1996) on wave motion in continuous periodic structures contains some references to the transfer matrix method. Easwaran *et al.* (1993) derived

the relationships between the impedance matrix and transfer matrix and investigated the properties of the matrices of symmetrical, reciprocal and conservative systems, respectively. Zhong and Williams (1995) utilized the symplectic property (see equation (2.4)) of the transfer matrices to develop a more efficient and accurate computational procedure for solving eigensolutions of the transfer matrices.

The eigenvectors of the transfer matrix describe the form of the wave motion in the structure and the eigenvalues are related to the amplitude change of the waves across the structure. Cremer, Heckl and Ungar (1973) summarized the fundamentals of the longitudinal, shear, torsional and bending waves and provided numerous examples and applications. Mace (1984) studied the vibrational behaviour of uniform, straight beams using a wave approach based on reflection, transmission and propagation of waves including the nearfield components. Milne (1987) studied the reflection of bending waves at the boundary of uniform straight beams, where conversion from a propagating wave into a nearfield wave and *vice versa* could take place. Using the fact that the dynamic stiffness matrix representing boundary conditions of a reciprocal system is symmetric, he showed that magnitudes of the reflection coefficients for the two cases are the same but the phase difference is $\pi/2$. Miller and von Flotow (1989) studied the energy flow associated with waves in structural networks of one-dimensional members such as bars and beams. In their studies, they showed that energy could be propagated through the interaction between two nearfield waves of opposite direction, which was also considered by Bobrovnitskii (1992). Ignoring the nearfield waves, Mace (1992) showed that the scattering matrix for a reciprocal system is symmetric and it is unitary (consequently the eigenvalues are of unit magnitude) for a conservative system. Mead

(1994) re-examined the phase-closure principle for the natural frequencies of finite beams. He showed that the principle, which is usually associated with propagating waves, can also be applied to nearfield waves. Beale and Accorsi (1995) presented a general matrix method, based on the work of Miller and Flotow, for the analysis of power flow in two- and three-dimensional frames consisting of uniform members such as Timoshenko beams.

For structures such as composite beams and curved beams where the various motions are coupled to each other, wave approaches are also useful in that the motions can be described in terms of independent waves. Harland *et al.* (2001) studied wave motion in straight, tunable fluid-filled beams, which is a three-mode system, using the wave approach based on the reflection, transmission and propagation of waves. Chidamparam and Leissa (1993) summarized the large amount of published literature on the in-plane, out-of-plane and coupled vibrations of curved bars, beams, rings and arches of arbitrary shape. Recognizing that fewer publications on the vibrations of loaded arches had appeared, they studied the in-plane free vibrations of loaded curved arches including centreline extensibility, and found that the centreline stretching causes a decrease of the natural frequencies and that the decrease may be important, especially for shallow arches. Wu and Lundberg (1996) investigated the transmission of energy through a circular bent section connecting two straight beams. Numerical results for various bend types with different curvatures were presented in polar radiation diagrams for bend angles between 0° and 360°. Walsh and White (2000) studied the vibrational power transmission in curved beams using four different models of beam behaviour, Love-based theory, Flügge-based theory and the corrections for rotary inertia and shear

deformation, respectively. The power along the circumferential direction was separated into extensional, bending moment and shear force components, and the time-averaged value of each component for a single wave mode obtained. Kang *et al.* (2003) applied the wave approach based on the reflection, transmission and propagation of waves for the free in-plane vibration of curved beams with constant curvature.

1.2.3 Slowly varying waveguides

When the lengthscale of the non-uniformity variation is relatively large compared to the wavelength concerned, waves can propagate along the structure with negligible reflection to a first approximation, as shown by Lighthill (1978) in his study on acoustic ducts. These structures are classified as slowly varying structures. Langley (1999) studied wave propagation along a slowly varying one-dimensional waveguide with deterministic, periodic and random variation using a perturbation method. He showed that, in these cases, the power carried by a wave component is preserved along the waveguide.

Care should be taken in using this approximation since, in some situations, the wavelength can become very long at certain frequencies, for example, a cut-off frequency which is found in the case of a beam on an elastic foundation as shown by Langley (1999). Burr *et al.* (2001) studied non-uniform Euler-Bernoulli beams under the action of non-uniform tensile force. When the lengthscale of the non-uniformity is large compared to the wavelength concerned, they showed that the coupling between the propagating waves and the nearfield waves (or the energy transfer between the two kinds of waves) becomes so small that the evolution of the two kinds can be considered separately. They derived a second order differential equation describing the asymptotic

evolution of the propagating waves, and showed that waves stop propagating and become trapped in certain conditions of non-uniformity. A similar effect was observed by Scott and Woodhouse (1992). They investigated the vibrational behaviour of an S-shaped curved plate strip and showed that certain of the normal modes would be trapped in the vicinity of the inflection point of the S-strip by a process of total internal reflection from points where the curvature reaches critical values. To understand the mode transition phenomenon in the vibration of beams having varying curvature and cross-section, Tarnopolskaya *et al.* (1996, 1999) carried out an asymptotic analysis for the transition of the high-frequency modes and a perturbation analysis for the transition of the low-frequency modes. The similarities and distinctions between the low mode and the high mode transitions were described.

1.2.4 Deterministically varying waveguides

For non-uniform waveguides with rapid variation, wave motion is in general difficult to interpret since the variation may lead to the significant reflection of waves. However, previous work has shown that there is a class of non-uniform waveguides where no such reflection occurs. Most of the work is related to acoustic waveguides (i.e. horns). For example, it is well-known that the governing equation of an acoustic horn can be solved for several specific types of horn, the so-called Salmon's family (Pierce 1981), which includes conical, exponential and catenoidal horns. Nagarkar and Finch (1971) studied a bell and suggested that a sinusoidal horn could also be included in the family. As a more general case, it was found that wave propagation in a horn, where the cross-sectional area varies as a power of the length, can be solved exactly in terms of Bessel functions (McLachlan 1955). The results for non-uniform acoustic waveguides

can be equally applied to structural waveguides with the same variation undergoing longitudinal motion or torsion, since their governing equations all have the same mathematical form (Graff 1975). Kumma and Sujith (1997) used the results to determine natural frequencies of the longitudinal vibration of some non-uniform bars.

Little attention has been paid to non-uniform beams undergoing bending motion, however, even though their motion can be interpreted in terms of waves. Cranch and Adler (1956) showed that the motion of a non-uniform beam along the x axis of density ρ, cross-sectional area A and the second moment of area I where $\rho A(x) \propto x^m$ and $EI(x) \propto x^n$ with m and n real and non-negative, can be solved in terms of Bessel functions if $n = m+2$, $n = m+4$, $n = m+6$ or $n = \frac{m+8}{3}$. The first three conditions include rectangular beams with linear, quadratic, and cubic thickness variation and with the width varying to any power. The last condition includes a rectangular beam where $A(x) \propto x^4$ and $I(x) \propto x^4$. For this condition, the equation of motion can be transformed into that of a uniform beam as shown by Abrate (1995). It has also been found that the motion of non-uniform beams with exponentially varying properties along the length can be expressed simply in terms of exponential functions (Cranch and Adler 1956, Suppiger and Taleb 1956). These analytical solutions have been used to obtain natural frequencies for beams for various boundary conditions and with intermediate constraints, e.g., see references (Conway *et al.* 1964, Mabie and Rogers 1968, Mabie and Rogers 1974, Goel 1976, Craver and Jampala 1993, Auciello and Nole 1998). Banerjee and Williams (1985) used the solutions to obtain the exact dynamic stiffness matrices for non-uniform beams with $n = m+2$. Petersson and Nijman (1998) studied

dynamic characteristics of the beams equivalent to the acoustic horn, featured by a broad-banded transition from vibrations governed by the properties at the mouth to vibrations governed by those at the throat. Using the geometrical acoustic approach, Krylov and Tilman (2004) showed that the incident flexural waves are trapped near the edge of the wedges, the thickness of which varies as a power of the length, and the waves are therefore never reflected back.

There are various previous studies using approximate or numerical methods for deterministically varying waveguides. Karabalis and Beskos (1983) presented the exact static axial and bending stiffness matrices for a linearly tapered beam element with constant width, which can be used for dynamics and stability of the structures consisting of tapered beams in an efficient way. Abrate (1995) applied the Rayleigh-Ritz approach to non-uniform bars and beams, where the cross section varies polynomially as a function of distance, under several practical boundary conditions such as fixed-free, and investigated the sensitivity of the fundamental frequencies to the non-uniformity. Auciello and Nole (1998) obtained the natural frequencies of a beam composed of two tapered beam sections with different properties with a mass at the end by using the Rayleigh-Ritz approach with the orthogonal polynomials as test functions. In particular, the approximate methods might be useful to model the vibration of higher order non-uniform structures where the analytical solutions cannot be obtained such as Timoshenko beams. For example, Gopalakrishnan and Doyle (1994) obtained axial and flexural dynamic stiffnesses of a higher order non-uniform waveguide using the displacements of the uniform deep waveguide as Ritz functions.

1.2.5 Near deterministically varying waveguides

Adding small variation to the rapid and deterministic variation will make a certain class of non-uniform structures. For example, a rectangular beam, where the thickness and width are linearly tapered but the positions of the fictitious apexes are slightly different, is one case of these structures.

The motion of these structures can be expected to be similar to that of the deterministically varying structures, which may be shown by an asymptotic approach as done for the slowly varying structures. However, there is very little existing literature concerning these structures and previous studies have mostly been concerned with more general cases, the arbitrarily varying structures, which are described in the next section 1.2.6.

1.2.6 Arbitrarily varying waveguides

Non-uniform structures, where the geometry and material properties vary in a complex manner and the magnitude of the variation is not so small, are classified as arbitrarily varying structures. Indeed this group includes all other structures which are not yet classified as one of the four groups, since exact or approximate closed-form solutions of the motion are difficult or impossible to obtain. For example, this group includes the case of non-uniform straight beams where the cross sectional area and the moment of inertia varying according to any two arbitrary powers along their length. Wang (1968) obtained the modal solutions for these non-uniform straight beams in terms of generalized hypergeometric functions. Eisenberger (1990) obtained the axial, torsional and bending stiffnesses for the non-uniform beams, where the variation is given by any polynomial functions, in terms of an infinite series.

Another approach for the motion of arbitrarily varying structures is a piecewise approximation where the structure is divided into a sequence of small segments. Each segment is modelled by an analogous element where the solution is known. The whole motion of the structure is then predicted by combining the behaviour of the elements and properties of the joints between the elements. Pease (1965) outlined this piecewise approach for a general one-dimensional Sturm-Liouville problem. Gallagher and Lee (1970) studied the numerical errors occurring in the piecewise representation of the arbitrarily varying beams using two types of segment modelling. One is the stepped representation, where the segment is modelled as a uniform beam element, and the other is the tapered representation, where the segment is modelled as a tapered beam element. The numerical results showed that the tapered representation could reduce the numerical errors effectively. They also showed that the conventional stepped representation would not assure the upper bound of the natural frequencies. Hodges *et al.* (1994) studied the vibration of the tapered beam using the transfer matrix method.

1.2.7 Summary of review

The purpose of this survey has been to review the published literature on wave motion of one-dimensional structures. The one-dimensional structures, the properties of which are linearly elastic and are prescribed by known functions, have been classified according to their type into the five groups as in Figure 1-1: the uniform, slowly varying, deterministically varying, near deterministically varying, and arbitrarily varying structures.

The motion of uniform structures has been investigated extensively using various methods. One of them is the approach based on the transfer matrix method, which is

widely used due to its conciseness. However, numerical difficulties may occur at high frequencies. These difficulties are related to the existence of nearfield waves, decaying or increasing along the length. In the wave approach based on the reflection, transmission and propagation of waves, the positive- and negative-going wave motions are separated and all computations are conducted in the direction of wave propagation so that the associated numerical results are always well conditioned (Yong and Lin 1989).

Besides uniform structures, existing literature has shown that there is a class of non-uniform structures, called deterministically varying structures, where exact closed-form solutions exist. Compared to the studies of modal behaviour of the structures using these solutions, little work has been attempted to interpret the motion in terms of waves, especially for the cases concerning beams undergoing bending motion.

The motion of the slowly varying or near deterministically varying structure could be estimated from that of the analogous structure for which an exact solution exists, i.e., the uniform structure and deterministically varying structure, respectively. However, care should be taken in this approximation since, in some situations, the wavelength can become very long at certain frequencies, for example, a cut-off frequency. The motion of the arbitrarily varying structure could be investigated by a piecewise approach where the structure is modelled by a series of small elements.

1.3 Objectives

The review results suggest that the wave approach based on reflection, transmission and propagation of waves is suitable for uniform structures since it does not require powerful computing resources and is well conditioned. However, most built-

up structures are too complicated to apply the wave approach easily. This research was planned to solve the problem. First it was proposed that a systematic formulation of the wave approach should be presented so that wave behaviour even in complex cases can be investigated in a concise way using the formulation. Application of the wave approach is illustrated in this thesis for several elementary structures. Especially curved beams drew interest since they are an important element in many built-up structures. The review results also showed that little work has been attempted to interpret the motion of deterministically varying structures in terms of waves. Thus application of the wave approach to deterministically varying structures was proposed. This work is important since employment of a single deterministically varying element, rather than a series of uniform elements, in the piecewise approach to arbitrarily varying structures could reduce computational cost.

In brief, the objectives of this research were:

- Development of a systematic formulation of the wave approach based on reflection, transmission and propagation of waves for the analysis of one-dimensional structures
- Study of wave behaviour in uniform structures such as curved beams with constant curvature
- Study of wave behaviour in deterministically varying structures
- Application of the wave approach including nearfield waves to various problems such as energy flow in a series of uniform and non-uniform structures

1.4 Outline of the thesis

This thesis provides a general overview and gives specific examples of a wave approach based on reflection, transmission and propagation of waves to one-dimensional structures. The complexity of the examples increases throughout the thesis. It is arranged as follows:

In chapter 2, a generalised wave approach based on reflection, transmission and propagation of waves is presented in a systematic way for the wave analysis of the motion of one-dimensional structures. The state vector in the physical domain is transformed to the wave domain using the displacement and internal force matrices. The wave amplitudes at one point are then related to those at another point by the diagonal propagation matrix. The response to external excitation, reflection and transmission of waves at a point discontinuity, reflection of waves at boundaries, and the energy flow associated with waves are described using the matrices. The relationship between this wave method and two other methods - the dynamic stiffness method and the transfer matrix method is established.

In chapter 3, the wave approach is applied to cases concerning straight uniform bars undergoing longitudinal motion. The bars are a single-mode system, where only two opposite-going propagating waves occur. The response of the bars to external excitation, reflection and transmission of waves at a point discontinuity, and reflection of waves at boundaries are described in a systematic way. These examples give a simple, clear demonstration of the application of the wave approach. The energy flow associated with waves is investigated and the power reflection and transmission coefficients are introduced.

In chapter 4, the wave approach is applied to cases concerning straight uniform beams undergoing bending motion. The motion is based on Euler-Bernoulli theory neglecting effects of the shear deformation and rotary inertia. Thus the beams are a two-mode system, where two propagating waves and two nearfield waves occur. Two issues related to nearfield waves are discussed in this chapter: the energy flow and numerical conditioning problem. It is shown explicitly that the energy can be transported by interaction of two opposite-going nearfield waves. It is also shown that the present wave approach always provides well-conditioned numerical results while the transfer matrix method may lead to numerical difficulties related to nearfield waves at high frequencies.

In chapter 5, the wave approach is applied to cases concerning a deterministically varying structure - straight bars where the area varies as a power of the length. The response of the non-uniform bars to external forces is investigated and the reactive behaviour due to non-uniformity is revealed. The energy transport velocity, the velocity at which energy is carried by waves, is derived using the relationship between power and energy. In contrast to that of uniform bars, it is not equal to the phase velocity and depends on position as well as frequency.

In chapter 6, the wave approach is applied to cases concerning a two-mode deterministically varying structure – straight beams where the area and second moment of area vary as a power of the length, respectively. The response of the non-uniform beams to external forces is investigated numerically, and it is shown that the stiffness and mass-dominant behaviour due to non-uniformity are separately represented by the propagating and nearfield waves. The energy transport velocity is obtained as well. In contrast to that of uniform beams, it is not equal to twice the phase velocity and depends on position as well as frequency.

In chapter 7, the wave approach is applied to cases concerning thin, uniform, curved beams based on Flügge theory. The beams provide coupling of the radial and tangential displacements, which does not occur in the examples of the previous four chapters. The dispersion relation is rather complicated and an ambiguity may arise in defining the dispersion curve for each wave. A criterion is suggested here: the imaginary value of the wavenumber of a positive-going wave should be negative and the energy transport velocity associated with a positive-going wave should be positive. The energy flow associated with waves is also revealed explicitly in terms of wavenumbers. Numerical results for the energy transmission through a U-shaped structure are presented as well.

In chapter 8, further applicability of the wave approach is described. Besides the previous examples, several different kinds of uniform structures and deterministically varying structures are listed. In conjunction with the piecewise modelling, the wave approach can be applied to arbitrarily varying structures. In the approach, the arbitrarily varying structure is divided into a series of small segments, and then each segment is modelled by a known structural element. It is shown that modelling using deterministically varying elements can be efficient compared to modelling using uniform elements. A general procedure of the wave approach for obtaining the natural frequencies and mode shapes is described. Subsequently the modal behaviour of a linearly tapered curved beam with clamped-free boundaries is studied.

In chapter 9, the thesis is summarised and recommendations are made for future studies.

1.5 Contributions from this thesis

Several original contributions are made in this work, which are:

- A systematic formulation for the wave approach based on reflection, transmission and propagation of waves is presented. The wave generation by external excitation, the spectral elements and the energy flow associated with waves, which were not dealt in previous work of, e.g. Harland *et al.* (2001), are described in a systematic way using the formulation. The properties of the reflection, transmission and propagation matrices are also obtained for a reciprocal system from the property of the transfer matrix, which is symplectic in the physical domain.
- The wave behaviour in deterministically varying structures, which are not uniform but in which no wave mode conversion occurs, is studied. It is shown that the wave approach based on reflection, transmission and propagation of waves can be applied in the same way as that for uniform structures. Examples include straight bars undergoing longitudinal motion, where the area varies as a power of the length, and straight beams undergoing bending motion, where the area and second moment of area vary as a power of the length, respectively. The energy transport velocity, which depends on position as well as frequency, for the bars and beams is obtained exactly. The results can be used for an efficient piecewise approach to arbitrarily varying structures in that employment of a single deterministically varying element, rather than a series of uniform elements, can provide rapid convergence to the exact results at low computational cost, especially when non-uniformity of the structure is severe.

- The wave approach is applied to the in-plane motion of uniform, curved beams with constant curvature based on Flügge theory. Even though the radial and tangential displacements of the beam are coupled together, waves propagate independently so that the problem could be simplified in the wave domain. A criterion is suggested for the dispersion relation for each wave in the beam: the imaginary value of the wavenumber of a positive-going wave should be negative and the energy transport velocity associated with a positive-going wave should be positive. Energy flow associated with waves in the beam is described explicitly in terms of the wavenumbers.
- A series of examples of the application of the wave approach are presented. It is shown that the wave approach can be used as an efficient and well-conditioned computational method even in cases where nearfield waves cannot be neglected. Examples include power transmission through a U-shaped structure and the modal behaviour of a linearly tapered, curved beam.

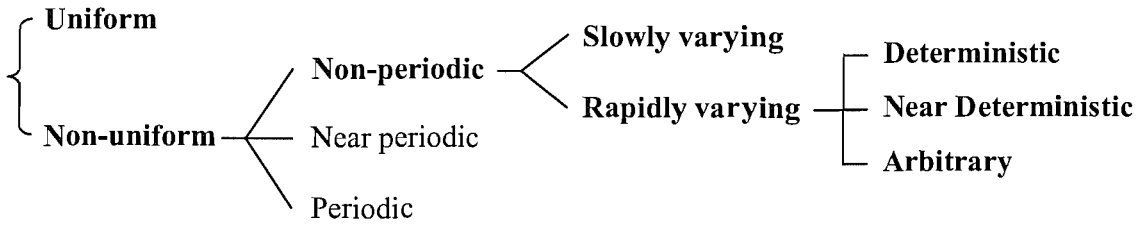

Figure 1-1. A categorisation of one-dimensional structures: the bold-faced groups are considered in this thesis.

Chapter 2.

A GENERALISED WAVE APPROACH

2.1 Introduction

The aim of this chapter is to review the wave approach based on reflection, transmission and propagation of waves and to present a generalised and systematic formulation of the approach for the motion of one-dimensional structures. All examples in this thesis are reciprocal and conservative systems: the transmission of vibration from one position to another position has a simple relation to the transmission in the opposite (or reciprocal) direction, and energy is not dissipated. General forms for the properties of the transfer matrix, which is symplectic for a reciprocal system in the physical domain, are obtained in the wave domain and then the properties of the reflection, transmission and propagation matrices are studied. Systematic formulations are presented for wave generation by external sources, for the spectral elements, and for reflection and transmission of waves by a discontinuity or boundary where external dynamic stiffnesses are attached. The reader may wish to refer to chapter 3 alongside this chapter as it gives a simple concrete example.

This wave approach gives exact and efficient computation, irrespective of frequency, for cases concerning uniform structures and deterministically varying structures. Examples concerning uniform structures are presented in chapters 3, 4 and 7 and examples concerning deterministically varying structures are presented in chapters 5 and 6. In conjunction with the piecewise approach, the wave approach can be used as

an efficient and well-conditioned method for cases concerning arbitrarily varying structures, examples for which are presented in chapter 8.

In section 2.2, the physical quantities for the motion of one-dimensional structures are grouped into a vector and the governing equations are expressed as first order differential equations. The solution of the governing equations defines the transfer matrix in the physical domain. The properties of the transfer matrix are reviewed for a reciprocal system and/or conservative system: the transfer matrix in the physical domain is symplectic for a reciprocal system and K-unitary for a conservative system.

In section 2.3, the transformation from the physical domain into the wave domain is made using the eigenvectors of the transfer matrix in the physical domain. General forms for the properties of the transfer matrix are presented in the wave domain.

At any point on the structure the waves can be divided into two groups, positive-going and negative-going waves. In section 2.4, the positive- and negative-going wave motions are separated. In uniform structures and deterministically varying structures, the waves propagate freely without coupling to each other if there is no discontinuity in their path. The diagonal propagation matrix is introduced for free wave propagation.

From section 2.5 to section 2.8, various wave phenomena in one-dimensional structures are described: generation of waves by external excitation, reflection and transmission at discontinuities, and reflection at boundaries. In section 2.9, the energy flow associated with waves is studied.

The transfer matrix methods and the spectral element (dynamic stiffness) methods have been widely used for the analysis of dynamic systems. In section 2.10, the relationships between these two approaches and the present wave approach are established.

2.2 State of a cross-section in the physical domain

Consider a one-dimensional structure where the principal axis is the x-axis as shown in Figure 2-1. The geometric and/or material properties of the structure may vary continuously along the x-axis. A cross-section of the one-dimensional structure supports n degrees of freedom. For example, a bar undergoing longitudinal motion is a single-mode system, with n=1, where the longitudinal displacement u and the internal force P are of interest. Throughout this thesis, the time dependence of the motion is assumed to be of the form of $e^{i\omega t}$ with angular frequency ω but the explicit time dependence is suppressed for clarity.

A n-dimensional vector $\mathbf{w}(x)$ is composed of the generalized displacements of the cross-section at a position x. When the corresponding internal forces are also grouped into a vector $\mathbf{f}(x)$, the state of the cross-section at x is expressed as

$$\mathbf{u}(x) = \begin{Bmatrix} \mathbf{w} \\ \mathbf{f} \end{Bmatrix} \tag{2.1}$$

where the $2n$-dimensional vector $\mathbf{u}$ is termed the physical state vector. For a bar undergoing longitudinal motion, $\mathbf{w} = \{u\}$, $\mathbf{f} = \{P\}$, and $\mathbf{u} = \begin{bmatrix} u & P \end{bmatrix}^T$ where the superscript T denotes the transpose. The governing equations of motion are then written in first-order form as

$$\frac{d\mathbf{u}}{dx} = \mathbf{S}\mathbf{u} \tag{2.2}$$

where $\mathbf{S}$ is termed the system matrix in the physical domain. The system matrix $\mathbf{S}$ reflects the nature of the structure. For a reciprocal system, any eigenvalue of $\mathbf{S}$ is always accompanied by another with the same magnitude but opposite sign (Langley

1999). Physically the eigenvalues of **S** are the local wavenumbers associated with waves at the cross-section so that, for a reciprocal system, the number of positive-going waves is equal to that of negative-going waves.

The integral form of equation (2.2), even though it is not easy to obtain in general, gives the transfer matrix **U** between two different points x_1 and x_2 in the physical domain as

$$\mathbf{u}(x_2) = \mathbf{U}(x_2, x_1)\mathbf{u}(x_1) \tag{2.3}$$

For a reciprocal system, the transfer matrix **U** is symplectic (Langley 1999), i.e.,

$$\mathbf{U}^T\mathbf{J}\mathbf{U} = \mathbf{J} \tag{2.4}$$

where the matrix **J**, consisting of the $n \times n$ identity matrix **I** and the $n \times n$ null matrix **0**, is given by

$$\mathbf{J} = \begin{bmatrix} \mathbf{0} & \mathbf{I} \\ -\mathbf{I} & \mathbf{0} \end{bmatrix} \tag{2.5}$$

Equation (2.4) indicates that, if λ is an eigenvalue of **U** and **y** is the corresponding right eigenvector, then $1/\lambda$ is also an eigenvalue and **Jy** is the corresponding left eigenvector. Throughout this thesis, it is assumed that the eigenvalues are single roots and for each eigenvalue there is a single eigenvector (i.e., the transfer matrix **U** is semisimple), which is true for a substantial number of problems.

For a conservative system, the transfer matrix **U** is K-unitary (Langley 1999), i.e.,

$$\mathbf{U}^H\mathbf{J}\mathbf{U} = \mathbf{J} \tag{2.6}$$

where the superscript H is the Hermitian operator. Equation (2.6) indicates that, if λ is an eigenvalue of **U** and **y** is the corresponding right eigenvector, then $1/\lambda^*$ is also an

eigenvalue and $\mathbf{Jy}^*$ is the corresponding left eigenvector, where the superscript * denotes the complex conjugate. If the magnitude of λ is unity (i.e., for propagating waves), then $\lambda = 1/\lambda^*$ so that the pair reduces to just a single wave component. Thus a counterpart to the component is not guaranteed in the case: the number of positive-going waves may not be equal to the number of negative-going waves in a conservative but non-reciprocal system (e.g., a waveguide where the lossless medium moves with a velocity).

For a reciprocal and conservative system, the transfer matrix **U** is real and the eigenvalue groups of the type $\left(\lambda \quad \lambda^* \quad 1/\lambda \quad 1/\lambda^*\right)$ arise. If the magnitude of λ is unity or λ is purely real (i.e., for propagating or nearfield waves), it reduces to $\left(\lambda \quad 1/\lambda\right)$.

2.3 State of a cross-section in the wave domain

In this section, the state of a cross-section is described in the wave domain. The number of wave modes is equal to the number of degrees of freedom supported by the cross-section. The waves either transport energy in the direction they are travelling or, if no energy flow is associated with the wave its amplitude will decay in that direction (e.g., for nearfield waves).

Consider a $2n$-dimensional vector **a** consisting of the (complex) amplitudes of waves. A transformation from the physical domain to the wave domain is described as

$$\mathbf{u}(x) = \mathbf{M}(x)\mathbf{a}(x) \tag{2.7}$$

where the columns of the $2n \times 2n$ matrix **M** are given by the (right) eigenvectors of **U**. Under the transformation given by equation (2.7), equation (2.3) is written in the wave domain as

$$\mathbf{a}(x_2) = \mathcal{T}(x_2, x_1)\mathbf{a}(x_1) \tag{2.8}$$

where $\mathcal{T}$ is the transfer matrix in the wave domain and is given by

$$\mathcal{T}(x_2, x_1) = \mathbf{M}^{-1}(x_2)\mathbf{U}(x_2, x_1)\mathbf{M}(x_1) \tag{2.9}$$

For a reciprocal system, equation (2.9) can be substituted into equation (2.4) to yield

$$\mathcal{T}^T\mathbf{M}^T(x_2)\mathbf{J}\mathbf{M}(x_2)\mathcal{T} = \mathbf{M}^T(x_1)\mathbf{J}\mathbf{M}(x_1) \tag{2.10}$$

Equation (2.10) is the most general form defining the property of $\mathcal{T}$ for a reciprocal system. The orthogonality relation between the eigenvectors of $\mathbf{U}$ indicates that the matrix $\mathbf{M}^T(x)\mathbf{J}\mathbf{M}(x)$ in equation (2.10) is given by

$$\mathbf{M}^T(x)\mathbf{J}\mathbf{M}(x) = \begin{bmatrix} 0 & \mathbf{\Lambda}(x) \\ -\mathbf{\Lambda}(x) & 0 \end{bmatrix} \tag{2.11}$$

where $\mathbf{\Lambda}$ is a diagonal matrix. When $\mathbf{M}$ is normalised to be such that $\mathbf{M}^T\mathbf{J}\mathbf{M} = \mathbf{J}$ (Zhong and Williams 1992), equation (2.10) simplifies to

$$\mathcal{T}^T\mathbf{J}\mathcal{T} = \mathbf{J} \tag{2.12}$$

Note that equation (2.12) is of the same form as equation (2.4).

For a conservative system, equation (2.9) can be substituted into equation (2.6) to yield

$$\mathcal{T}^H\mathbf{M}^H(x_2)\mathbf{J}\mathbf{M}(x_2)\mathcal{T} = \mathbf{M}^H(x_1)\mathbf{J}\mathbf{M}(x_1) \tag{2.13}$$

Since the matrix $\mathbf{M}^H\mathbf{J}\mathbf{M}$ in equation (2.13) is skew-Hermitian (i.e., $\mathrm{i}\mathbf{M}^H\mathbf{J}\mathbf{M}$ is Hermitian), a suitable choice of the basis results in

$$\mathrm{i}\mathbf{M}^H\mathbf{J}\mathbf{M} = \mathbf{J}' \tag{2.14}$$

where $\mathbf{J}'$ is diagonal matrix composed of ± 1, the positive elements are related to the energy flow transported toward the positive direction, and the negative elements are

related to the energy flow transported toward the negative direction. The number of the positive elements in $\mathbf{J}'$ may differ from the number of the negative elements for a conservative and non-reciprocal system. The basis, where equation (2.14) holds, is called the power wave basis. In this basis, equation (2.13) reduces to

$$\mathcal{T}^H \mathbf{J}' \mathcal{T} = \mathbf{J}' \tag{2.15}$$

The transformation to the power wave basis is discussed again in section 2.8 where the energy flow associated with waves is studied.

Wave motion in a reciprocal and conservative system satisfies equations (2.10) and (2.13). Thus it follows that

$$\left[\mathbf{M}^*(x_2)\right]^{-1} \mathbf{M}(x_2)\mathcal{T} = \mathcal{T}^* \left[\mathbf{M}^*(x_1)\right]^{-1} \mathbf{M}(x_1) \tag{2.16}$$

All examples in this thesis are for a reciprocal and conservative system, so wave motion in the examples satisfies equation (2.16).

2.4 Positive- and negative-going wave motions

Henceforth, the wave motions are separated into positive- and negative-going groups according to the direction in which waves travel: the wave vector $\mathbf{a}$ is divided into two vectors $\mathbf{a}^+(x)$ and $\mathbf{a}^-(x)$, where the superscripts '+' and '−' denote the corresponding direction of propagation. For a reciprocal system, the dimensions of the two vectors $\mathbf{a}^+(x)$ and $\mathbf{a}^-(x)$ are the same. In this case equation (2.7) is re-expressed as (Harland *et al.* 2001)

$$\begin{Bmatrix} \mathbf{w} \\ \mathbf{f} \end{Bmatrix} = \begin{bmatrix} \Psi^+ & \Psi^- \\ \Phi^+ & \Phi^- \end{bmatrix} \begin{Bmatrix} \mathbf{a}^+ \\ \mathbf{a}^- \end{Bmatrix} \tag{2.17}$$

where $\Psi^{\pm}$ and $\Phi^{\pm}$ are the displacement and internal force matrices. Note that the matrix $\mathbf{M}$ is divided into 4 sub-matrices here. They satisfy

$$\begin{aligned} \left(\Psi^{+}\right)^{T}\Phi^{+} &= \left(\Phi^{+}\right)^{T}\Psi^{+}, \\ \left(\Psi^{-}\right)^{T}\Phi^{-} &= \left(\Phi^{-}\right)^{T}\Psi^{-}, \\ \left(\Psi^{+}\right)^{T}\Phi^{-} - \left(\Phi^{+}\right)^{T}\Psi^{-} &= \mathbf{\Lambda} \end{aligned} \qquad (2.18a,b,c)$$

Equation (2.18c) reduces to $\left(\Psi^{+}\right)^{T}\Phi^{-} - \left(\Phi^{+}\right)^{T}\Psi^{-} = \mathbf{I}$ under suitable normalisation. Then it follows that $\mathbf{M}^{T}\mathbf{J}\mathbf{M} = \mathbf{J}$.

Consider now two points x_1 and x_2 on the structure as shown in Figure 2-2, where the amplitudes of waves at the points are given in a vector form as $\mathbf{a}^{+}(x)$ and $\mathbf{a}^{-}(x)$. In uniform structures and (by definition) in deterministically varying structures, waves propagate independently without coupling to each other if there is no discontinuity in their path, i.e., $\mathcal{T}$ is diagonal. In these cases, equation (2.8) is expressed as

$$\begin{Bmatrix} \mathbf{a}^{+}(x_2) \\ \mathbf{a}^{-}(x_1) \end{Bmatrix} = \begin{bmatrix} \mathbf{F}^{+} & \mathbf{0} \\ \mathbf{0} & \mathbf{F}^{-} \end{bmatrix} \begin{Bmatrix} \mathbf{a}^{+}(x_1) \\ \mathbf{a}^{-}(x_2) \end{Bmatrix} \qquad (2.19)$$

where $\mathbf{F}^{+}$ and $\mathbf{F}^{-}$ are diagonal, and are termed the positive and negative propagation matrices, respectively, between the two points. For a reciprocal system, there is a simple relation between them. Note that the transfer matrix $\mathcal{T}$ is given by

$$\mathcal{T} = \begin{bmatrix} \mathbf{F}^{+} & 0 \\ 0 & \left(\mathbf{F}^{-}\right)^{-1} \end{bmatrix} \qquad (2.20)$$

Substituting equation (2.20) into equation (2.10) gives

$$\mathbf{\Lambda}(x_2)\mathbf{F}^{+} = \mathbf{F}^{-}\mathbf{\Lambda}(x_1) \qquad (2.21)$$

Equation (2.21) further reduces to $\mathbf{F}^+ = \mathbf{F}^-$ for a suitable basis where $\mathbf{M}^T\mathbf{J}\mathbf{M} = \mathbf{J}$ holds.

In this section the state vector in the physical domain has been transformed to the wave domain using the displacement and internal force matrices, in which the positive-going and negative-going wave motions are separated. The wave amplitudes at one point are then related to those at another point by the (diagonal) propagation matrix. These matrices provide a foundation for a systematic application of the wave approach. In the following sections, wave motions in various cases, such as generation of waves by external excitation, reflection and transmission at discontinuities, and reflection at boundaries, are described in a systematic way using these matrices.

2.5 Wave generation by external excitation

Consider a point on a one-dimensional waveguide excited by local harmonic forces $\mathbf{f}_{ext}e^{i\omega t}$ as shown in Figure 2-3(a). Waves $\mathbf{q}^+$ and $\mathbf{q}^-$ are then induced in the positive and negative directions respectively. Combined with equation (2.17), the continuity and equilibrium conditions at the excitation point are expressed as

$$\begin{aligned} \Psi^+\mathbf{q}^+ &= \Psi^-\mathbf{q}^-, \\ -\Phi^+\mathbf{q}^+ + \Phi^-\mathbf{q}^- &= \mathbf{f}_{ext} \end{aligned} \qquad \text{(2.22a,b)}$$

Consequently $\mathbf{q}^+$ and $\mathbf{q}^-$ are given by

$$\begin{aligned} \mathbf{q}^+ &= \left[-\Phi^+ + \Phi^-\left(\Psi^-\right)^{-1}\Psi^+\right]^{-1}\mathbf{f}_{ext}, \\ \mathbf{q}^- &= \left[\Phi^- - \Phi^+\left(\Psi^+\right)^{-1}\Psi^-\right]^{-1}\mathbf{f}_{ext} \end{aligned} \qquad \text{(2.23a,b)}$$

Combined with the relationships between the displacement and internal force matrices given by equation (2.18), equation (2.23) reduces to

$$\mathbf{q}^{+} = \mathbf{\Lambda}^{-1}\left(\mathbf{\Psi}^{-}\right)^{T}\mathbf{f}_{ext},$$
$$\mathbf{q}^{-} = \mathbf{\Lambda}^{-1}\left(\mathbf{\Psi}^{+}\right)^{T}\mathbf{f}_{ext} \qquad (2.24a,b)$$

Now suppose that the forces are applied at the left-hand end of the waveguide as shown in Figure 2-3(b). Since the equilibrium condition at the end is

$$-\mathbf{\Phi}^{+}\mathbf{q}^{+} = \mathbf{f}_{ext} \qquad (2.25)$$

the induced waves $\mathbf{q}^{+}$ are given by

$$\mathbf{q}^{+} = -\left(\mathbf{\Phi}^{+}\right)^{-1}\mathbf{f}_{ext} \qquad (2.26)$$

Similarly, if the right-hand end of a waveguide is excited as shown in Figure 2-3(c), the induced waves $\mathbf{q}^{-}$ are given by

$$\mathbf{q}^{-} = \left(\mathbf{\Phi}^{-}\right)^{-1}\mathbf{f}_{ext} \qquad (2.27)$$

2.6 Reflection and transmission at a local discontinuity

If there is a point discontinuity such as mass attachment in the propagation path, some of the energy carried by the waves may be back-scattered. Let the amplitudes of waves at the left-hand side of the discontinuity be given in vectors $\mathbf{a}^{+}$ and $\mathbf{a}^{-}$, and the amplitudes at the right-hand side in $\mathbf{b}^{+}$ and $\mathbf{b}^{-}$. Then they are related by

$$\begin{Bmatrix}\mathbf{a}^{-}\\ \mathbf{b}^{+}\end{Bmatrix} = \begin{bmatrix}\mathbf{R} & \hat{\mathbf{T}}\\ \mathbf{T} & \hat{\mathbf{R}}\end{bmatrix}\begin{Bmatrix}\mathbf{a}^{+}\\ \mathbf{b}^{-}\end{Bmatrix} \qquad (2.28)$$

where $\mathbf{R}$ and $\mathbf{T}$ are the reflection and transmission matrices for waves incident on the discontinuity from the left-hand side, and $\hat{\mathbf{R}}$ and $\hat{\mathbf{T}}$ are those for waves incident on the discontinuity from the right-hand side.

For a reciprocal system, simple relations hold for the reflection and transmission matrices. Note that the transfer matrix for the discontinuity is given by

$$\mathcal{T} = \begin{bmatrix} \mathbf{T} - \hat{\mathbf{R}}\hat{\mathbf{T}}^{-1}\mathbf{R} & \hat{\mathbf{R}}\hat{\mathbf{T}}^{-1} \\ -\hat{\mathbf{T}}^{-1}\mathbf{R} & \hat{\mathbf{T}}^{-1} \end{bmatrix} \tag{2.29}$$

Substituting equation (2.29) into equation (2.10) gives

$$\begin{aligned} \mathbf{\Lambda}(x_1)\mathbf{R} &= \mathbf{R}^T\mathbf{\Lambda}(x_1), \\ \mathbf{\Lambda}(x_2)\mathbf{T} &= \hat{\mathbf{T}}^T\mathbf{\Lambda}(x_1), \\ \mathbf{\Lambda}(x_2)\hat{\mathbf{R}} &= \hat{\mathbf{R}}^T\mathbf{\Lambda}(x_2) \end{aligned} \tag{2.30a,b,c}$$

For a suitable basis where $\mathbf{M}^T\mathbf{J}\mathbf{M} = \mathbf{J}$ holds, equation (2.30) further reduces to be such that $\mathbf{R} = \mathbf{R}^T$, $\hat{\mathbf{R}} = \hat{\mathbf{R}}^T$, and $\mathbf{T} = \hat{\mathbf{T}}^T$.

The reflection and transmission matrices can be obtained from the continuity and equilibrium conditions at the discontinuity. For example, consider a point discontinuity as shown in Figure 2-4 where two coaxial waveguides with different properties are joined together and external dynamic components, represented by the dynamic stiffness matrix $\mathbf{K}_{ext}$, are attached. The continuity and equilibrium conditions at the discontinuity are given by

$$\begin{aligned} \mathbf{w}_a &= \mathbf{w}_b, \\ -\mathbf{f}_a + \mathbf{f}_b &= \mathbf{K}_{ext}\mathbf{w}_a \end{aligned} \tag{2.31a,b}$$

where the subscripts a and b denote the left- and right-hand waveguides respectively. Note that equation (2.31) is not a general form covering all possible situations - for example, a beam with a simple support is not covered.

Now suppose that the positive-going waves of amplitudes $\mathbf{a}^+$ are incident from the left-hand side and there is no negative-going wave from the right-hand side, i.e., $\mathbf{b}^- = 0$. Then equation (2.31) is re-written as

$$\begin{aligned} \Psi_a^{+}\mathbf{a}^{+} + \Psi_a^{-}\mathbf{a}^{-} &= \Psi_b^{+}\mathbf{b}^{+}, \\ -\Phi_a^{+}\mathbf{a}^{+} - \Phi_a^{-}\mathbf{a}^{-} + \Phi_b^{+}\mathbf{b}^{+} &= \mathbf{K}_{\text{ext}}\Psi_b^{+}\mathbf{b}^{+} \end{aligned} \qquad (2.32a,b)$$

Thus the reflection and transmission matrices for waves incident on the discontinuity from the left-hand side are given by

$$\begin{aligned} \mathbf{R} &= -\left[\mathbf{K}_{\text{ext}}\Psi_a^{-} - \Phi_b^{+}\left(\Psi_b^{+}\right)^{-1}\Psi_a^{-} + \Phi_a^{-}\right]^{-1}\left[\mathbf{K}_{\text{ext}}\Psi_a^{+} - \Phi_b^{+}\left(\Psi_b^{+}\right)^{-1}\Psi_a^{+} + \Phi_a^{+}\right], \\ \mathbf{T} &= \left[\mathbf{K}_{\text{ext}}\Psi_b^{+} + \Phi_a^{-}\left(\Psi_a^{-}\right)^{-1}\Psi_b^{+} - \Phi_b^{+}\right]^{-1}\left[\Phi_a^{-}\left(\Psi_a^{-}\right)^{-1}\Psi_a^{+} - \Phi_a^{+}\right] \end{aligned} \qquad (2.33a,b)$$

The matrices $\widehat{\mathbf{R}}$ and $\widehat{\mathbf{T}}$ for waves incident on the discontinuity from the right-hand side can also be obtained in a similar way: assume $\mathbf{a}^{+} = 0$ now and solve the continuity and equilibrium conditions.

2.7 Reflection and transmission by multiple discontinuities

In the previous section, the reflection and transmission of waves at a discontinuity have been described in a systematic way. Expanding the results, in this section, reflection and transmission of waves by multiple discontinuities are described.

First consider two discontinuities at points x_1 and x_2 as shown in Figure 2-5 where external dynamic components are attached and coaxial waveguides are joined. Waves $\mathbf{a}^{+}$ are incident upon discontinuity 1 from the left-hand side. When the relevant waves at the discontinuites are denoted by $\mathbf{a}^{-}$, $\mathbf{b}^{\pm}$, $\mathbf{c}^{\pm}$ and $\mathbf{d}^{+}$, the relationships between the waves are

$$
\begin{aligned}
\mathbf{b}^{+} &= \mathbf{T}_1\mathbf{a}^{+} + \hat{\mathbf{R}}_1\mathbf{b}^{-}, \\
\mathbf{c}^{+} &= \mathbf{F}^{+}\mathbf{b}^{+}, \\
\mathbf{c}^{-} &= \mathbf{R}_2\mathbf{c}^{+}, \\
\mathbf{b}^{-} &= \mathbf{F}^{-}\mathbf{c}^{-} \\
\mathbf{a}^{-} &= \mathbf{R}_1\mathbf{a}^{+} + \hat{\mathbf{T}}_1\mathbf{b}^{-}, \\
\mathbf{d}^{+} &= \mathbf{T}_2\mathbf{c}^{+}
\end{aligned}
\qquad (2.34a,b,c,d,e,f)
$$

where $\mathbf{R}_1$, $\mathbf{T}_1$ etc., are the reflection and transmission matrices at the discontinuities, and $\mathbf{F}^{+}$ and $\mathbf{F}^{-}$ are the propagation matrices between the discontinuities. Rearranging equations (2.34) in terms of the incident waves $\mathbf{a}^{+}$, the reflected waves $\mathbf{a}^{-}$ and the transmitted waves $\mathbf{d}^{+}$ are given by

$$
\begin{aligned}
\mathbf{a}^{-} &= \left[\mathbf{R}_1 + \hat{\mathbf{T}}_1\mathbf{F}^{-}\mathbf{R}_2\mathbf{F}^{+}[\mathbf{I} - \hat{\mathbf{R}}_1\mathbf{F}^{-}\mathbf{R}_2\mathbf{F}^{+}]^{-1}\mathbf{T}_1\right]\mathbf{a}^{+}, \\
\mathbf{d}^{+} &= \left[\mathbf{T}_2\mathbf{F}^{+}[\mathbf{I} - \hat{\mathbf{R}}_1\mathbf{F}^{-}\mathbf{R}_2\mathbf{F}^{+}]^{-1}\mathbf{T}_1\right]\mathbf{a}^{+}
\end{aligned}
\qquad (2.35a,b)
$$

The matrix $[\mathbf{I} - \hat{\mathbf{R}}_1\mathbf{F}^{-}\mathbf{R}_2\mathbf{F}^{+}]^{-1}$ in equations (2.35) can be expanded as

$$
[\mathbf{I} - \hat{\mathbf{R}}_1\mathbf{F}^{-}\mathbf{R}_2\mathbf{F}^{+}]^{-1} = \mathbf{I} + \left(\hat{\mathbf{R}}_1\mathbf{F}^{-}\mathbf{R}_2\mathbf{F}^{+}\right) + \left(\hat{\mathbf{R}}_1\mathbf{F}^{-}\mathbf{R}_2\mathbf{F}^{+}\right)^2 + \ldots \qquad (2.36)
$$

The second term in equation (2.36) represents one round trip of waves between the two discontinuities, and the third term represents two round trips, etc. Thus the reflected waves $\mathbf{a}^{-}$ have components from the direct reflection of the incident waves by discontinuity 1 (i.e., $\mathbf{R}_1\mathbf{a}^{+}$), while the remaining components arise from waves which are initially transmitted through discontinuity 1 and are then subsequently reflected back-and-forth at the two discontinuities. The net reflected waves are thus the superposition of the direct and subsequent reflected components. Similarly the transmitted waves $\mathbf{d}^{+}$ consist of the direct components transmitted through the two

junctions (i.e., $\mathbf{T}_2\mathbf{F}^+\mathbf{T}_1\mathbf{a}^+$), and the components from the subsequent reflections between the two discontinuities.

Even though equation (2.35) is obtained for the case where two discontinuities are imposed, it is indeed a general expression and can be applied to a case where three and more discontinuities are imposed in an iterative manner. In this situation, discontinuities 1 and 2 do not represent a single discontinuity, respectively, but can be thought to represent groups of discontinuities, respectively. Subsequently the matrices $\mathbf{R}_1$, $\mathbf{T}_1$, $\widehat{\mathbf{T}}_1$, $\widehat{\mathbf{R}}_1$, $\mathbf{R}_2$, and $\mathbf{T}_2$ are now *global* reflection and transmission matrices for the groups of discontinuities.

2.8 Reflection at boundaries

Consider waves of amplitudes $\mathbf{a}^+$ incident upon the right-hand end of a waveguide. Then the amplitudes of the reflected waves, $\mathbf{a}^-$, are

$$\mathbf{a}^- = \mathbf{R}\mathbf{a}^+ \tag{2.37}$$

where $\mathbf{R}$ is the reflection matrix of the boundary.

The reflection matrix can be obtained from the boundary conditions at the end. For example, consider a boundary as shown in Figure 2-6 where external dynamic components, represented by the dynamic stiffness matrix $\mathbf{K}_{ext}$, are attached. The boundary condition is given by

$$\mathbf{f} = -\mathbf{K}_{ext}\mathbf{w} \tag{2.38}$$

Combining equation (2.38) with equation (2.17) gives

$$\mathbf{\Phi}^+\mathbf{a}^+ + \mathbf{\Phi}^-\mathbf{a}^- = -\mathbf{K}_{ext}\left(\mathbf{\Psi}^+\mathbf{a}^+ + \mathbf{\Psi}^-\mathbf{a}^-\right) \tag{2.39}$$

Finally substituting equation (2.37) into equation (2.39) gives

$$\mathbf{R} = -\left(\mathbf{K}_{ext}\Psi^{-} + \Phi^{-}\right)^{-1}\left(\mathbf{K}_{ext}\Psi^{+} + \Phi^{+}\right) \tag{2.40}$$

The reflection matrices for two common boundary conditions – free and clamped boundaries, can be obtained by letting $\mathbf{K}_{ext} = 0$ (for a free boundary) and $\mathbf{K}_{ext} = \infty$ (for a clamped boundary), respectively, in equation (2.40).

Similarly the reflection matrix of the left-hand boundary where negative-going waves are converted into positive-going waves can be obtained. In this case the equilibrium condition is given by

$$\mathbf{f} = \mathbf{K}_{ext}\mathbf{w} \tag{2.41}$$

Consequently the reflection matrix $\widehat{\mathbf{R}}$ of the left-hand boundary is given by

$$\widehat{\mathbf{R}} = -\left(\mathbf{K}_{ext}\Psi^{+} - \Phi^{+}\right)^{-1}\left(\mathbf{K}_{ext}\Psi^{-} - \Phi^{-}\right) \tag{2.42}$$

2.9 Energy flow

Even though waves propagate independently, the net energy flow associated with the waves is not necessarily given by the simple sum of the individual energy flow associated with each wave, i.e. there exists the energy flow associated with the interaction between two waves. Following the work done by Miller and von Flotow (1989), the energy flow associated with waves is described in a systematic way in this section.

For time harmonic motion, the time-averaged power Π at a point is given in terms of the displacement and internal force vectors by

$$\Pi = -\left\langle \left[\mathrm{Re}\left(\frac{\partial}{\partial t}\left(\mathbf{w}e^{i\omega t}\right)\right)\right]^{T} \cdot \mathrm{Re}\left(\mathbf{f}e^{i\omega t}\right)\right\rangle \tag{2.43}$$

where $\mathrm{Re}(\cdot)$ denotes the real part of the quantity, $\langle\cdot\rangle$ indicates a time averaged quantity and the superscript T is the transpose operator. Equation (2.43) can be re-written as

$$\begin{aligned}\Pi &= -\left\langle \left[\mathrm{Re}\left(\mathrm{i}\omega \mathbf{w} e^{\mathrm{i}\omega t}\right)\right]^T \cdot \mathrm{Re}\left(\mathbf{f} e^{\mathrm{i}\omega t}\right)\right\rangle \\ &= \frac{\mathrm{i}\omega}{4}\left\{\mathbf{w}^H\mathbf{f} - \mathbf{f}^H\mathbf{w}\right\}\end{aligned} \tag{2.44}$$

where the superscript H is the Hermitian operator. Equation (2.44) gives the energy flow in terms of the physical quantities. When the transformation from the physical domain to the wave domain is made, the time averaged power is expressed in terms of wave amplitudes by

$$\Pi = \frac{1}{2}\mathbf{a}^H\mathbf{P}\,\mathbf{a} \tag{2.45}$$

where $\mathbf{a} = \left[\left\{\mathbf{a}^+\right\}^T \quad \left\{\mathbf{a}^-\right\}^T\right]^T$ and the matrix $\mathbf{P}$ is given by

$$\mathbf{P} = \frac{\mathrm{i}\omega}{2}\left[\begin{bmatrix}\left(\Psi^+\right)^H\Phi^+ & \left(\Psi^+\right)^H\Phi^- \\ \left(\Psi^-\right)^H\Phi^+ & \left(\Psi^-\right)^H\Phi^-\end{bmatrix} - \begin{bmatrix}\left(\Phi^+\right)^H\Psi^+ & \left(\Phi^+\right)^H\Psi^- \\ \left(\Phi^-\right)^H\Psi^+ & \left(\Phi^-\right)^H\Psi^-\end{bmatrix}\right] \tag{2.46}$$

Note that $\mathbf{P} = \frac{\mathrm{i}\omega}{2}\mathbf{M}^H\mathbf{J}\mathbf{M}$ according to the notation in section 2.2 before dividing positive- and negative-going wave motions. Since the matrix $\mathbf{P}$ is Hermitian, the power Π is always real for any combination of wave components.

If the matrix $\mathbf{P}$ is diagonal, it means that the energy will be transported independently by a single wave component. For example, assume that only a pair of opposite-going propagating waves is associated with a reciprocal and conservative system. For the pair, the eigenvalues are $\left(\lambda \quad \lambda^*\right)$ and the corresponding eigenvectors are $\mathbf{M} = \left[\mathbf{y} \quad \mathbf{y}^*\right]$, where $\mathbf{y}$ is a column vector satisfying $\mathbf{U}\mathbf{y} = \lambda\mathbf{y}$ and the superscript *

denotes the complex conjugate. If the eigenvectors are normalised such that $\mathbf{M}^T\mathbf{J}\mathbf{M} = \mathrm{i}\mathbf{J}$ (the factor i is introduced in order to be consistent with examples in this thesis, e.g., the longitudinal motion), then it follows that

$$\mathrm{i}\mathbf{M}^H\mathbf{J}\mathbf{M} = \mathbf{J}' \tag{2.47}$$

where $\mathbf{J}'$ is a diagonal matrix composed of ± 1. Note that $\mathrm{i}\mathbf{M}^H\mathbf{J}\mathbf{M}$ is diagonal (thus $\mathbf{P}$ is diagonal) in this case, which indicates that propagating waves transport the energy independently.

However, for waveguides such as beams undergoing bending motion as considered by Bobrovnitskii (1992), there is energy flow associated with the interaction between two components and the matrix $\mathbf{P}$ is not diagonal. Assume now that there is only a pair of opposite-going nearfield waves in the reciprocal and conservative system. The eigenvalues and corresponding eigenvectors are all real in this case, i.e., $\mathbf{M} = \mathbf{M}^*$. Thus, on the basis $\mathbf{M}^T\mathbf{J}\mathbf{M} = -\mathbf{J}$ (the factor -1 is introduced in order to be consistent with examples in this thesis, e.g., nearfield waves of the bending motion), it follows that

$$\mathrm{i}\mathbf{M}^H\mathbf{J}\mathbf{M} = -\mathrm{i}\mathbf{J} \tag{2.48}$$

Equation (2.48) indicates that nearfield waves cannot transport the energy but the interaction between two opposite-going nearfield waves can do so.

If waves are oscillating but decaying (i.e., the wavenumbers are complex), an eigenvalue group of the type $\left(\lambda \quad \lambda^* \quad 1/\lambda \quad 1/\lambda^*\right)$ arise and the corresponding eigenvectors are $\mathbf{M} = \left[\mathbf{y} \quad \mathbf{y}^* \quad \mathbf{z} \quad \mathbf{z}^*\right]$ where $\mathbf{z}$ is a column vector satisfying $\mathbf{U}\mathbf{z} = \lambda^{-1}\mathbf{z}$. This group of waves is seen in the motion of curved beams in chapter 7. Thus, on the basis of $\mathbf{M}^T\mathbf{J}\mathbf{M} = -\mathbf{J}$, it follows that

$$\mathrm{i}\mathbf{M}^{H}\mathbf{J}\mathbf{M} = -\mathrm{i}\begin{bmatrix} \mathbf{0} & \mathbf{I}' \\ -\mathbf{I}' & \mathbf{0} \end{bmatrix} \tag{2.49}$$

where

$$\mathbf{I}' = \begin{bmatrix} 0 & 1 \\ 1 & 0 \end{bmatrix} \tag{2.50}$$

In this case the energy flow is associated with the interaction between a pair of waves with eigenvalues $\left(\lambda \quad 1/\lambda^{*}\right)$, as indicated by Langley (1996). In general, all three wave types (propagating, nearfield and complex waves) may be associated with the motion. Even in this case such an analysis according to the type of waves is possible: the scaling factors for the normalisation may differ but the structure of $\mathrm{i}\mathbf{M}^{H}\mathbf{J}\mathbf{M}$ does not change.

When $\mathbf{P}$ is not diagonal, a further transformation can be considered. Since $\mathbf{P}$ is Hermitian, the power matrix can be written as

$$\mathbf{P} = \mathbf{E}\mathbf{V}\mathbf{E}^{-1} \tag{2.51}$$

where $\mathbf{E}$ is a unitary matrix (i.e. $\mathbf{E}^{H}\mathbf{E} = \mathbf{I}$) consisting of the eigenvectors of $\mathbf{P}$, and $\mathbf{V}$ is a diagonal matrix consisting of the (real) eigenvalues of $\mathbf{P}$. Substituting equation (2.51) into equation (2.45) gives

$$\Pi = \frac{1}{2}\mathbf{p}^{H}\mathbf{V}\mathbf{p} \tag{2.52}$$

where $\mathbf{p} = \mathbf{E}^{-1}\mathbf{a}$. Since $\mathbf{V}$ is diagonal, equation (2.52) indicates the energy is transported independently by the individual components of $\mathbf{p}$. Note that suitable normalisation of the eigenvectors will lead to the elements of $\mathbf{V}$ being ± 1. This basis is called the power wave basis.

2.10 Relationship with other methods

A wave approach based on the reflection, transmission and propagation of waves has been developed in a systematic manner. In this section, relationships with two other approaches - one is the wave approach based on the transfer matrix method and the other is the dynamic stiffness method - are established.

2.10.1 Wave analysis based on transfer matrix method

The transfer matrix $\mathcal{T}$ in the wave domain has been introduced earlier in section 2.3. Figure 2-7 shows a drawing analogous to the Holzer-Myklestad model (Meirovitch 1997), in which each station represents a point discontinuity such as external dynamic components and junctions between different waveguides. If positive- and negative-going waves are grouped together, the left-hand side wave vector $\mathbf{a}_j^l$ of a station j is defined as

$$\mathbf{a}_j^l = \begin{Bmatrix} \mathbf{a}^+ \\ \mathbf{a}^- \end{Bmatrix}_j^l \tag{2.53}$$

where the superscript l and subscript j refer to the left-hand side of the station j. The right-hand side wave vector $\mathbf{a}_j^r$ of the station j is expressed in terms of $\mathbf{a}_j^l$ as

$$\mathbf{a}_j^r = \mathcal{G}_j \mathbf{a}_j^l \tag{2.54}$$

where the matrix $\mathcal{G}_j$ is termed a point transfer matrix. Considering the reflection and transmission of waves at the station (discontinuity), $\mathcal{G}_j$ is expressed as

$$\mathcal{G}_j = \begin{bmatrix} \mathbf{T}_j - \hat{\mathbf{R}}_j \hat{\mathbf{T}}_j^{-1} \mathbf{R}_j & \hat{\mathbf{R}}_j \hat{\mathbf{T}}_j^{-1} \\ -\hat{\mathbf{T}}_j^{-1} \mathbf{R}_j & \hat{\mathbf{T}}_j^{-1} \end{bmatrix} \tag{2.55}$$

where $\mathbf{R}_j$ and $\mathbf{T}_j$ are the reflection and transmission matrices for waves incident on the station j from the left-hand side, and $\hat{\mathbf{R}}_j$ and $\hat{\mathbf{T}}_j$ are the reflection and transmission matrices for waves incident on the station j from the right-hand side.

The wave vector $\mathbf{a}_{j+1}^l$ at the left-hand side of the station $j+1$ is related to $\mathbf{a}_j^r$ such that

$$\mathbf{a}_{j+1}^l = \mathcal{F}_j \mathbf{a}_j^r \tag{2.56}$$

where the matrix $\mathcal{F}_j$ is called a field transfer matrix from station j to station $j+1$. Since there is no discontinuity between two points, the matrix $\mathcal{F}_j$ is given by

$$\mathcal{F}_j = \begin{bmatrix} \mathbf{F}_j^+ & 0 \\ 0 & \left(\mathbf{F}_j^-\right)^{-1} \end{bmatrix} \tag{2.57}$$

where $\mathbf{F}_j^{\pm}$ are the propagation matrices for the positive- and negative-going waves, respectively, between the two stations. Note that the inverse of $\mathbf{F}_j^-$ is used for the propagation of negative-going waves, which is one of distinct differences between the wave approach based on the transfer matrix method and the wave approach based on reflection, transmission and propagation of waves.

Successively applying equations (2.56) and (2.54) for each station yields

$$\begin{aligned} \mathbf{a}_1^l &= \mathcal{F}_0 \mathbf{a}_0^r \\ \mathbf{a}_1^r &= \mathcal{G}_1 \mathcal{F}_0 \mathbf{a}_0^r \\ \mathbf{a}_2^l &= \mathcal{F}_1 \mathcal{G}_1 \mathcal{F}_0 \mathbf{a}_0^r \\ &\vdots \end{aligned} \tag{2.58a,b,c,...}$$

Thus the waves at the right-hand side of station 0 are related to the waves at the left-hand side of station n as

$$\mathbf{a}_n^l = {}_n^l\mathcal{T}_0^r \mathbf{a}_0^r \tag{2.59}$$

where the matrix ${}_n^l\mathcal{T}_0^r$ is a transfer matrix in the wave domain and is given by

$${}_j^l\mathcal{T}_0^r = \mathcal{F}_{n-1}\mathcal{G}_{n-1}\mathcal{F}_{n-2}\cdots\mathcal{F}_1\mathcal{G}_1\mathcal{F}_0 \tag{2.60}$$

Note that, when reciprocal systems are cascaded, the resulting system should still be reciprocal (Easwaran *et al.* 1993). Thus the matrix ${}_n^l\mathcal{T}_0^r$ also satisfies equation (2.12).

If the system is finite, i.e. boundary conditions are imposed at the ends, their effects are considered after the transfer matrix for the whole system is constructed. For example, if stations 0 and n are the left and right ends of the system, the wave vectors $\mathbf{a}_0^r$ and $\mathbf{a}_n^l$ can be written as

$$\mathbf{a}_0^r = \begin{Bmatrix} \hat{\mathbf{R}}_0\mathbf{a}^- \\ \mathbf{a}^- \end{Bmatrix}_0^r, \qquad \mathbf{a}_n^l = \begin{Bmatrix} \mathbf{a}^+ \\ \mathbf{R}_n\mathbf{a}^+ \end{Bmatrix}_n^l \tag{2.61a,b}$$

where $\hat{\mathbf{R}}_0$ and $\mathbf{R}_n$ are the reflection matrices for the boundaries. Substituting equations (2.61a,b) into (2.59) describes the wave motion in the finite system.

Equations (2.59), (2.60) and (2.61) comprise the formulation of the wave analysis based on the transfer matrix method, where waves at a point are related to the others by cascading the field transfer matrix between two stations and the point transfer matrix at each station. Compared to the wave approach based on reflection, transmission and propagation of waves, it may be attractive in that it provides in a concise form the relationship between waves at different points. However, there are two kinds of numerical difficulties that may occur when using the wave approach based on the transfer matrix method (Pestel and Leckie 1963). The first occurs when the transmission matrix is singular and its inverse matrix in equation (2.55) does not exist. In fact, the

transmission matrix will always be singular if either one of the displacements or the internal forces is zero at the discontinuity. For example, if the stiffness of an intermediate elastic support is very large compared to the bending stiffness of the beam, numerical difficulties may arise. The second difficulty is related to the field transfer matrix, which includes the inverse of the propagation matrix, $\left(\mathbf{F}^{-}\right)^{-1}$, as shown in equation (2.57). For example, if there exists a wave decaying along the path such as a nearfield wave, the field transfer matrix will be ill-conditioned. It means that the round-off error in the computational process for obtaining the inverse of the propagation matrix could be significant. This numerical error due to ill-conditioning of the field transfer matrix is demonstrated in section 4.9.

2.10.2 Derivation of spectral elements

A spectral element is a finite (or infinite) section of a structure described by a dynamic stiffness matrix, which relates the displacements and internal forces at the ends of the element (Doyle 1997). In this subsection, spectral elements are derived in terms of the displacement, internal force and propagation matrices.

Consider again the two points x_1 and x_2 on the waveguide in Figure 2-2. The displacements at these points are

$$\mathbf{w}_1 = \Psi_1^{+}\mathbf{a}_1^{+} + \Psi_1^{-}\mathbf{a}_1^{-}, \qquad \mathbf{w}_2 = \Psi_2^{+}\mathbf{a}_2^{+} + \Psi_2^{-}\mathbf{a}_2^{-} \tag{2.62a,b}$$

Since the amplitudes of the waves are related by the propagation matrices as in equation (2.19), equation (2.62) can be written as

$$\begin{Bmatrix}\mathbf{w}_1\\ \mathbf{w}_2\end{Bmatrix} = \begin{bmatrix}\Psi_1^{+} & \Psi_1^{-}\mathbf{F}^{-}\\ \Psi_2^{+}\mathbf{F}^{+} & \Psi_2^{-}\end{bmatrix}\begin{Bmatrix}\mathbf{a}_1^{+}\\ \mathbf{a}_2^{-}\end{Bmatrix} \tag{2.63}$$

Similarly, the internal forces at the two points are given by

$$\begin{Bmatrix} \mathbf{f}_1 \\ \mathbf{f}_2 \end{Bmatrix} = \begin{bmatrix} \Phi_1^+ & \Phi_1^- \mathbf{F}^- \\ \Phi_2^+ \mathbf{F}^+ & \Phi_2^- \end{bmatrix} \begin{Bmatrix} \mathbf{a}_1^+ \\ \mathbf{a}_2^- \end{Bmatrix} \tag{2.64}$$

Combining equations (2.63) and (2.64) gives

$$\begin{Bmatrix} -\mathbf{f}_1 \\ \mathbf{f}_2 \end{Bmatrix} = \mathbf{D} \begin{Bmatrix} \mathbf{w}_1 \\ \mathbf{w}_2 \end{Bmatrix} \tag{2.65}$$

where the dynamic stiffness matrix $\mathbf{D}$ for the section of the waveguide is

$$\mathbf{D} = \begin{bmatrix} -\Phi_1^+ & -\Phi_1^- \mathbf{F}^- \\ \Phi_2^+ \mathbf{F}^+ & \Phi_2^- \end{bmatrix} \begin{bmatrix} \Psi_1^+ & \Psi_1^- \mathbf{F}^- \\ \Psi_2^+ \mathbf{F}^+ & \Psi_2^- \end{bmatrix}^{-1} \tag{2.66}$$

The matrix $\mathbf{D}$ is symmetric ($\mathbf{D} = \mathbf{D}^T$) for a reciprocal system, and it is real for a reciprocal and conservative system.

For a semi-infinite element (referred to as a "throw-off" element by Doyle (1997)), the dynamic stiffness matrix (spectral element) is

$$\mathbf{D}^{\pm\infty} = \mp \Phi^{\pm} \left(\Psi^{\pm} \right)^{-1} \tag{2.67a,b}$$

where $\Psi^{\pm}$ and $\Phi^{\pm}$ are now the displacement and internal force matrices at the boundaries of the semi-infinite waveguide, respectively.

2.11 Summary

A generalised wave approach based on reflection, transmission and propagation of waves has been presented in a systematic way for the motion of one-dimensional structures. The state vector in the physical domain was transformed to the wave domain using the displacement and internal force matrices, in which the positive- and negative-going wave motions were separated. The wave amplitudes at one point were then related to those at another point by the (diagonal) propagation matrix. These matrices provide a foundation for a systematic application of the wave approach. Wave motion in

various cases such as generation of waves by external excitation, reflection and transmission at discontinuities, and reflection at boundaries were then described in a systematic manner using the matrices. The property of the reflection, transmission and propagation matrices for a reciprocal system were also described: see equations (2.21) and (2.30).

The transfer matrix in physical domain is symplectic for a reciprocal system and K-unitary for a conservative system. General forms for the properties of the transfer matrix were obtained in the wave domain: see equations (2.10), (2.13) and (2.16). The relationship between the present wave approach and the transfer matrix method was also established. In contrast to the present wave approach, two kinds of numerical difficulties may occur using the transfer matrix method. The first occurs in the case where the transmission matrix is singular. For example, if the stiffness of an intermediate elastic support is very large compared to the bending stiffness of the beam, numerical difficulties may arise. The second difficulty is related to the field transfer matrix including the inverse of the propagation matrix. For example, if there exists a nearfield wave, the field transfer matrix will be ill-conditioned so that the round-off error in the computational process for obtaining the inverse of the propagation matrix could be significant. This numerical error due to ill-conditioning of the field transfer matrix is demonstrated in section 4.9. However, the wave approach does not suffer such numerical difficulties since the positive and negative propagation relationships are separated. The spectral elements were also derived in terms of the displacement, internal force and propagation matrices.

The energy flow associated with waves was also described in matrix form. Even though waves transport disturbances independently (i.e., the propagation matrix is

diagonal), it does not mean that the waves can also transport the energy independently: the energy flow could be associated with the interaction between waves, e.g., for a conservative system, a pair of waves for which the eigenvalues of the transfer matrix are the inverse of the complex conjugate of each other. Further transformation to the power wave basis, where the energy is transported independently by individual (power) waves, could be considered in such a case.

In the following chapters, the wave approach is applied to various types of one-dimensional structure. The complexity of the cases increases throughout the thesis. In chapters 3 and 4, longitudinal and bending wave motions in uniform structures are studied and, in chapters 5 and 6, those motions in deterministically varying structures are studied. In chapter 7, the motion of uniform curved beams where longitudinal and bending motions are coupled is studied. In chapter 8, further application of the wave approach to, e.g., arbitrarily varying structures, is described.

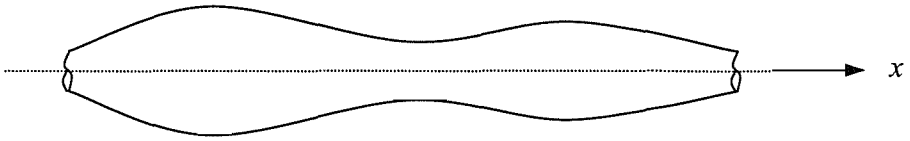

Figure 2-1. A one-dimensional waveguide where geometric and/or material properties may vary continuously along the x-axis.

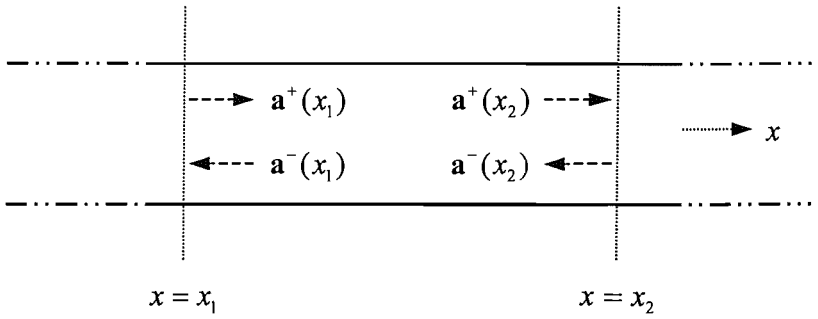

Figure 2-2. Propagation of waves between two points.

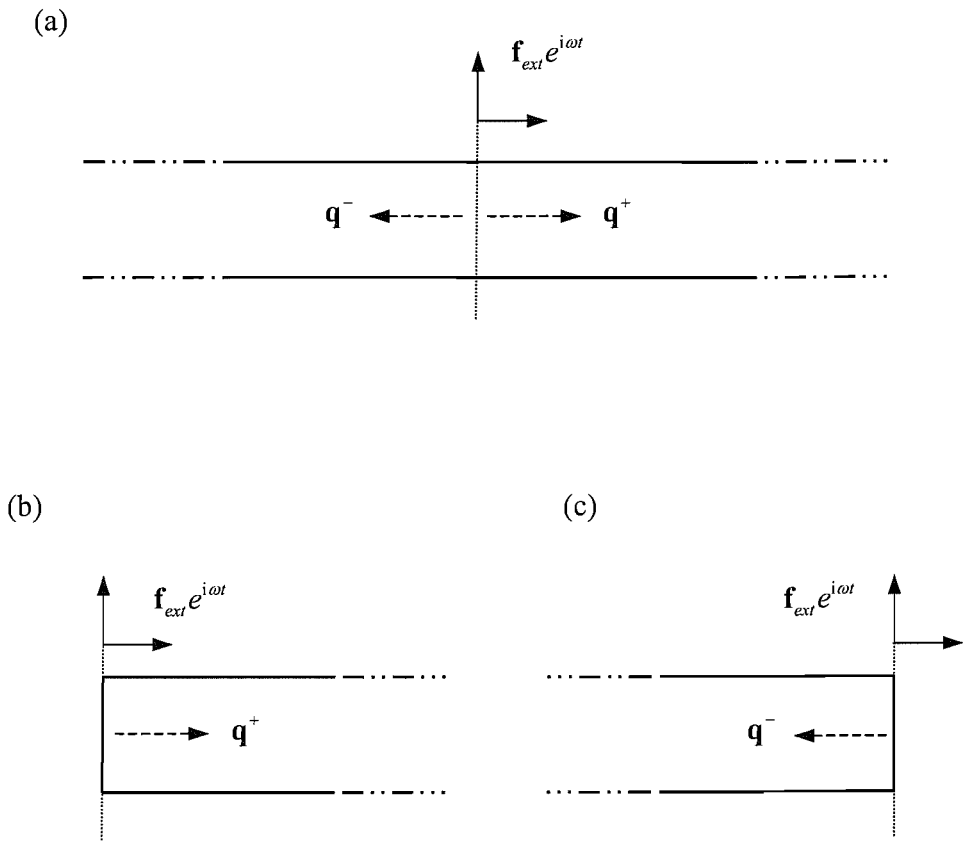

Figure 2-3. Induction of waves by local harmonic forces and moments: (a) applied at a point, (b) applied at left-hand end, (c) applied at right-hand end.

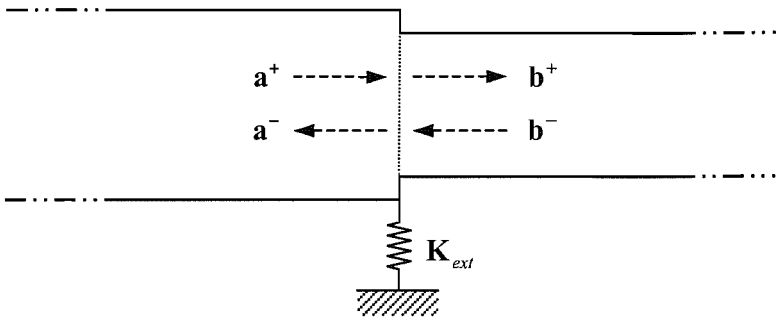

Figure 2-4. Reflection and transmission of waves at a local discontinuity.

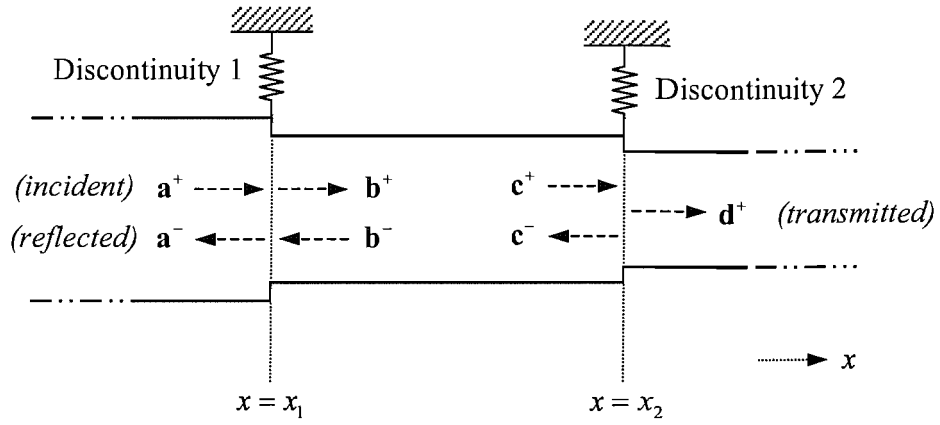

Figure 2-5. Reflection and transmission of waves through two discontinuities.

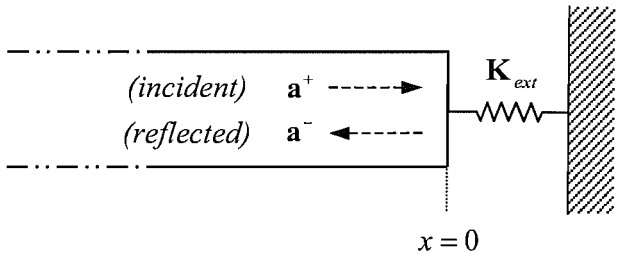

Figure 2-6. Reflection of waves at an end supported by generalised dynamic stiffnesses, which are expressed as a matrix $\mathbf{K}_{ext}$.

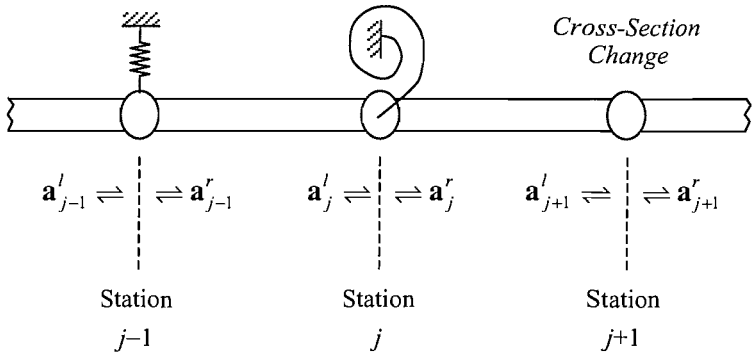

Figure 2-7. Wave analysis by the transfer matrix method.

Chapter 3.

WAVE MOTION IN UNIFORM, STRAIGHT BARS

3.1 Introduction

The general wave approach based on reflection, transmission and propagation of waves, developed in chapter 2, is applied in this chapter to cases concerning uniform, straight bars undergoing longitudinal motion. While the systematic formulation of chapter 2 is not strictly necessary for these simple cases since the bars are a single-mode system, the work will give a clear demonstration of the application of the method.

In section 3.2, the governing equation for uniform, straight bars undergoing longitudinal motion is reviewed. The motion is based on the elementary theory neglecting the higher effects such as the inertia associated with Poisson contraction, which is considered in chapter 8. For clarity no damping is present as well, thus the axial displacement of the bars consists of two propagating waves. In section 3.3, the displacement, internal force, and propagation matrices for the bars are defined. Note that these matrices have only a single element because there is just one wave mode.

Using the matrix formulation, wave generation by a force, reflection and transmission of waves at discontinuities, reflection of waves at boundaries, and spectral elements are described in sections 3.4 to 3.7. In section 3.8, the energy flow associated with waves is discussed and the power reflection and transmission coefficients are introduced.

In section 3.9, a numerical example for wave behaviour in straight bars, where the cross-sectional area changes twice discontinuously, is presented. Results obtained by two wave approaches, one based on reflection, transmission and propagation of waves and the other based on the transfer matrix method, are compared.

3.2 Equation of motion

The axial displacement $u(x,t)$ for the free vibration of a bar at position x and time t is governed by the differential equation (Graff 1975)

$$\frac{\partial}{\partial x}\left[EA\frac{\partial u}{\partial x}\right]=\rho A\frac{\partial^2 u}{\partial t^2} \tag{3.1}$$

where ρ is the density of bar, E is the modulus of elasticity and A is the cross-sectional area. The corresponding tensile axial force P as shown in Figure 3-1 is

$$P=EA\frac{\partial u}{\partial x} \tag{3.2}$$

The motion is based on the elementary theory where the inertia associated with Poisson contraction in the normal directions to the cross-section is assumed to be negligible and the axial displacement across the cross-section is assumed to be uniform. The longitudinal motion including the inertia effect is described in chapter 8.

Equation (3.1) can be easily solved when the material and geometric properties are constant with position x. If the time dependence of the motion is assumed to be of the form $e^{i\omega t}$ with angular frequency ω but suppressed here for clarity, the solution for the motion of a uniform bar is given by

$$u(x)=C_1 e^{-ik_l x}+C_2 e^{ik_l x} \tag{3.3}$$

where C_1 and C_2 are arbitrarily constants, and the wavenumber k_l is given by

$$k_l = \sqrt{\rho\omega^2 / E} \tag{3.4}$$

Since there is no damping in the bar, k_l is real and positive. Substituting equation (3.3) into equation (3.2) yields

$$P(x) = -\mathrm{i}EAk_l C_1 \mathrm{e}^{-\mathrm{i}k_l x} + \mathrm{i}EAk_l C_2 \mathrm{e}^{\mathrm{i}k_l x} \tag{3.5}$$

The first and second terms of the right-hand side of equation (3.3) or equation (3.5) represent a positive-going wave and a negative-going wave, respectively: as time increases, the disturbance (u and P) is transported toward the positive (right) direction by the first term while the disturbance is transported toward the negative (left) direction by the second term. The magnitude of the disturbance does not decay since the wavenumber k_l is real, i.e., they are propagating waves.

3.3 The wave description

The transformation from the physical domain to the wave domain using vectors and matrices was expressed as equation (2.7). Following the formulation, the physical state vectors for this longitudinal motion are defined as

$$\mathbf{w} = \{u\}, \qquad \mathbf{f} = \{P\} \tag{3.6a,b}$$

The wave vectors are defined as

$$\mathbf{a}^+ = \{a^+\}, \qquad \mathbf{a}^- = \{a^-\} \tag{3.7a,b}$$

where a^+ and a^- are the amplitudes of a positive-going wave and a negative-going wave, respectively, and are given by

$$a^+ = C_1 \mathrm{e}^{-\mathrm{i}k_l x}, \quad a^- = C_2 \mathrm{e}^{\mathrm{i}k_l x} \tag{3.8a,b}$$

Then the displacement and internal force matrices describing the relationships between the physical state vectors and the wave vectors are given by

$$\begin{aligned} \Psi^+ &= [1], & \Psi^- &= [1], \\ \Phi^+ &= [-\mathrm{i}EAk_l], & \Phi^- &= [\mathrm{i}EAk_l] \end{aligned} \tag{3.9a,b,c,d}$$

These matrices are independent of position in this case, which is not true in cases concerning non-uniform bars. These matrices also satisfy equation (2.18), i.e.,

$$\begin{aligned} \left(\Psi^+\right)^T \Phi^+ &= \left(\Phi^+\right)^T \Psi^+, \\ \left(\Psi^-\right)^T \Phi^- &= \left(\Phi^-\right)^T \Psi^-, \\ \left(\Psi^+\right)^T \Phi^- - \left(\Phi^+\right)^T \Psi^- &= \mathbf{\Lambda} \end{aligned} \tag{3.10a,b,c}$$

where the diagonal matrix $\mathbf{\Lambda}$ for this case is

$$\mathbf{\Lambda} = [\mathrm{i}2EAk_l] \tag{3.11}$$

The propagation matrix $\mathbf{F}$ for propagation of waves between two points, a distance L apart, in a uniform straight bar is given by

$$\mathbf{F} = \left[\mathrm{e}^{-\mathrm{i}k_l L}\right] \tag{3.12}$$

In this case the positive and negative propagation matrices are the same, which would be expected from symmetry between two points. Generally, the relation between them is given by equation (2.21), i.e., $\mathbf{\Lambda}(x_2)\mathbf{F}^+ = \mathbf{F}^-\mathbf{\Lambda}(x_1)$. Thus it follows that $\mathbf{F}^+ = \mathbf{F}^-$.

3.4 Wave generation by local excitation

The displacement, internal force and propagation matrices were defined for the motion of uniform straight bars. The matrices provide a foundation for analysis of wave behaviour in various cases concerning the bars. First the response of a uniform straight bar to an external point force is investigated in this section.

Consider a uniform straight bar, the left-hand end of which is excited by a harmonic point force $f_{ext}e^{i\omega t}$ as shown in Figure 3-2(a). A general formulation for waves induced by external sources applied to the left-hand end was given in equation (2.26), i.e.,

$$\mathbf{q}^{+} = -\left(\Phi^{+}\right)^{-1}\mathbf{f}_{ext} \tag{3.13}$$

Since Φ^{+} is given by equation (3.9c) and $\mathbf{f}_{ext} = \{f_{ext}\}$, the amplitudes $\mathbf{q}^{+}$ of the induced wave in this case is given by

$$\mathbf{q}^{+} = \left\{\frac{1}{iEAk_l}\right\} f_{ext} \tag{3.14}$$

When the right-hand end is excited by the force $f_{ext}e^{i\omega t}$ as shown in Figure 3-2(b), the induced wave $\mathbf{q}^{-}$ can be obtained by substituting equation (3.9d) and $\mathbf{f}_{ext} = \{f_{ext}\}$ into equation (2.27). Therefore it follows that

$$\mathbf{q}^{-} = \left\{\frac{1}{iEAk_l}\right\} f_{ext} \tag{3.15}$$

Equations (3.14) and (3.15) show that the displacement of the bar lags in phase behind the external force by $\pi/2$, therefore, the velocity is in phase with the external force.

Now a point of the bar is excited by the force as shown in Figure 3-2(c). The continuity condition at the point makes the amplitudes of the positive- and negative-going waves induced by the force identical at the excitation point in this case, i.e.,

$$\mathbf{q}^{+} = \mathbf{q}^{-} \tag{3.16}$$

The equilibrium condition at the point is given by

$$-\Phi^{+}\mathbf{q}^{+} + \Phi^{-}\mathbf{q}^{-} = f_{ext} \tag{3.17}$$

Substituting equations (3.9c) and (3.9d) into equation (3.17) gives

$$\mathbf{q}^{+} = \left\{ \frac{1}{\mathrm{i}2EAk_l} \right\} f_{ext} \tag{3.18}$$

3.5 Reflection and transmission at discontinuities

Consider two identical semi-infinite bars connected by a translational dynamic stiffness $\bar{K}_T$ as shown in Figure 3-3(a). The continuity and equilibrium conditions in this case are

$$\begin{aligned} P_1 &= P_2, \\ P_1 &= \bar{K}_T \left(u_2 - u_1 \right) \end{aligned} \tag{3.19a,b}$$

where the subscripts 1 and 2 refer to the left-hand and right-hand sides of the stiffness, respectively. Since the left-hand bar and the right-hand bar are identical in this case, equation (3.19) is written as

$$\begin{aligned} \mathbf{a}^{+} - \mathbf{a}^{-} &= \mathbf{b}^{+}, \\ \mathbf{a}^{+} - \mathbf{a}^{-} &= \mathrm{i}K_T \left(\mathbf{b}^{+} - \mathbf{a}^{+} - \mathbf{a}^{-} \right) \end{aligned} \tag{3.20a,b}$$

where the dimensionless stiffness $K_T = \bar{K}_T / EAk_l$ is introduced. Thus the reflection and transmission matrices for the connection are given by

$$\mathbf{R} = \left[\frac{1}{1 - \mathrm{i}2K_T} \right], \qquad \mathbf{T} = \left[-\frac{\mathrm{i}2K_T}{1 - \mathrm{i}2K_T} \right] \tag{3.21a,b}$$

Note that there is no reflection if $K_T \to \infty$ (rigid connection) and there is no transmission if $K_T = 0$ (no connection).

Consider now two semi-infinite bars with different geometric shapes and/or material properties, which are directly connected as shown in Figure 3-3(b). The continuity and equilibrium conditions at the junction are

$$u_1 = u_2, \qquad P_1 = P_2 \tag{3.22a,b}$$

where the subscripts 1 and 2 refer to the left-hand and right-hand sides of the junction, respectively. Equation (3.22) is written in terms of the amplitudes of waves as

$$\mathbf{a}^+ + \mathbf{a}^- = \mathbf{b}^+, \qquad \mathbf{a}^+ - \mathbf{a}^- = \gamma \mathbf{b}^+ \tag{3.23a,b}$$

where $\gamma = (EAk_l)_2 / (EAk_l)_1$. Thus the reflection and transmission matrices for the junction are given by

$$\mathbf{R} = \left[\frac{1-\gamma}{1+\gamma}\right], \qquad \mathbf{T} = \left[\frac{2}{1+\gamma}\right] \tag{3.24a,b}$$

If the Young's moduli of the two bars are the same but the cross-sectional areas are different, then the reflection and transmission matrices reduce to

$$\mathbf{R} = \left[\frac{A_1 - A_2}{A_1 + A_2}\right], \qquad \mathbf{T} = \left[\frac{2A_1}{A_1 + A_2}\right] \tag{3.25a,b}$$

As would be expected, the reflection and transmission matrices $\hat{\mathbf{R}}$ and $\hat{\mathbf{T}}$ for the case where the wave is incident from the right-hand side of the junction, can simply be obtained by exchanging the subscripts 1 and 2 in equation (3.25).

3.6 Reflection at boundaries

Consider a semi-infinite bar with a boundary supported by a translational dynamic stiffness $\bar{K}_T$ as shown in Figure 3-4. The equilibrium condition at the boundary is

$$P = -\bar{K}_T u \tag{3.26}$$

Then equation (3.26) is rewritten as

$$\mathbf{a}^+ - \mathbf{a}^- = -\mathrm{i}K_T \left(\mathbf{a}^+ + \mathbf{a}^-\right) \tag{3.27}$$

where $K_T = \bar{K}_T / EAk_l$. Thus the reflection matrix $\mathbf{R}$ of the boundary is given by

$$\mathbf{R} = \left[\frac{1 + \mathrm{i}K_T}{1 - \mathrm{i}K_T} \right] \tag{3.28}$$

For two special cases - clamped ($K_T \to \infty$) and free ($K_T = 0$) boundary conditions, the reflection matrices are given by

$$\mathbf{R}_c = [-1], \qquad \mathbf{R}_f = [1] \tag{3.29a,b}$$

where the subscripts c and f refer to the boundary conditions, respectively.

3.7 Spectral elements

In section 2.10.2 the dynamic stiffness matrix for an element was defined in terms of the displacement and internal force matrices. Then the dynamic stiffness matrix of the semi-infinite, or throw-off, element was given by

$$\mathbf{D}^{\pm\infty} = \mp \Phi^{\pm} \left(\Psi^{\pm} \right)^{-1} \tag{3.30a,b}$$

Substituting equations (3.9) into equation (3.30) gives the dynamic stiffness matrix for the semi-infinite bar as

$$\mathbf{D}^{\pm\infty} = \left[\mathrm{i}EAk_l \right] \tag{3.31}$$

The dynamic stiffness matrix for the finite section of length L of the bar, which is defined as equation (2.66), is

$$\mathbf{D} = \frac{EAk_l}{\sin k_l L} \begin{bmatrix} \cos k_l L & -1 \\ -1 & \cos k_l L \end{bmatrix} \tag{3.32a,b}$$

In this case, the bar is a symmetric and reciprocal system so that the dynamic system is symmetric and the diagonal elements are also equal.

3.8 Energy flow

In section 2.9, the time-averaged power associated with waves in one-dimensional structures was given as

$$\Pi = \frac{1}{2}\mathbf{a}^H \mathbf{P}\,\mathbf{a} \tag{3.33}$$

where $\mathbf{a} = \left[\left(\mathbf{a}^+\right)^T \quad \left(\mathbf{a}^-\right)^T\right]^T$ and the power matrix $\mathbf{P}$ is

$$\mathbf{P} = \frac{i\omega}{2}\left[\begin{bmatrix}\left(\Psi^+\right)^H\Phi^+ & \left(\Psi^+\right)^H\Phi^- \\ \left(\Psi^-\right)^H\Phi^+ & \left(\Psi^-\right)^H\Phi^-\end{bmatrix} - \begin{bmatrix}\left(\Phi^+\right)^H\Psi^+ & \left(\Phi^+\right)^H\Psi^- \\ \left(\Phi^-\right)^H\Psi^+ & \left(\Phi^-\right)^H\Psi^-\end{bmatrix}\right] \tag{3.34}$$

Substituting the displacement and internal force matrices for the uniform straight bar into equation (3.34) yields

$$\mathbf{P} = \omega E A k_l \begin{bmatrix}1 & 0 \\ 0 & -1\end{bmatrix} \tag{3.35}$$

In this case, the power matrix is diagonal so that energy is transported independently by each single wave component and there is no energy transported through the interaction between the positive- and negative-going components. Thus the time-averaged power associated with a positive-going wave with amplitude a^+ is

$$\begin{aligned}\Pi &= \frac{1}{2}\omega E A k_l \left|a^+\right|^2 \\ &= \frac{1}{2}\rho A \omega^2 \left|a^+\right|^2 c_l\end{aligned} \tag{3.36}$$

where $c_l = \sqrt{E/\rho}$ is the longitudinal wavespeed. It can be seen that power is proportional to the longitudinal wavespeed. The time-averaged power associated with a negative-going wave with amplitude a^- is

$$\begin{aligned}\Pi &= -\frac{1}{2}\omega EAk_l \left|a^-\right|^2 \\ &= -\frac{1}{2}\rho A\omega^2 \left|a^-\right|^2 c_l\end{aligned} \tag{3.37}$$

Compared to equation (3.36), the negative sign indicates that the energy is transported in the negative direction.

Consider the reflection and transmission of waves by a discontinuity. To indicate how much energy is reflected and transferred, the power reflection coefficient ϱ and power transmission coefficient τ can be defined by

$$\varrho = -\frac{\Pi_r}{\Pi_i}, \qquad \tau = \frac{\Pi_t}{\Pi_i} \tag{3.38a,b}$$

where Π_i, Π_r and Π_t are the incident, reflected and transmitted powers, respectively. If there is no energy dissipation, i.e., for a conservative system, the power reflection and transmission coefficients should satisfy the relationship

$$\varrho + \tau = 1 \tag{3.39}$$

For the bar undergoing longitudinal motion, where the power is defined as equation (3.36) or (3.37), when the amplitudes of the incident, reflected and transmitted waves are a^+, a^- and d^+, respectively, the power reflection and transmission coefficients at a discontinuity are given by

$$\varrho = \frac{\left|a^-\right|^2}{\left|a^+\right|^2}, \qquad \tau = \frac{(EAk_l)_2}{(EAk_l)_1}\frac{\left|d^+\right|^2}{\left|a^+\right|^2} \tag{3.40a,b}$$

where the subscripts 1 and 2 refer to left-hand and right-hand side of the discontinuity, respectively.

3.9 Numerical example

The reflection, transmission and propagation of waves in uniform straight bars have been studied in a systematic way. The results can be used for solving various problems concerning the bars. As an application of the previous work, in this section, a numerical example, where the cross-sectional area changes twice discontinuously such that $A_1 \to A_2 \to A_3$ as shown in Figure 3-5, is presented. The points at which the area changes, denoted by junction 1 and junction 2 in the figure, are separated by a distance L. Waves $\mathbf{a}^+$ are incident upon junction 1 from the left-hand side and the other relevant waves are denoted by $\mathbf{a}^-$, $\mathbf{b}^{\pm}$, $\mathbf{c}^{\pm}$ and $\mathbf{d}^+$ as shown in the figure. Note that this is a specific example of reflection and transmission of waves by two general discontinuities described in section 2.7.

3.9.1 Effect of cross-section changes

The reflection and transmission matrices at a point where the area changes are obtained by equation (3.25). Thus the matrices at junction 1 are

$$\mathbf{R}_1 = \left[\frac{A_1 - A_2}{A_1 + A_2}\right], \qquad \mathbf{T}_1 = \left[\frac{2A_1}{A_1 + A_2}\right],$$
$$\widehat{\mathbf{R}}_1 = \left[\frac{A_2 - A_1}{A_1 + A_2}\right], \qquad \widehat{\mathbf{T}}_1 = \left[\frac{2A_2}{A_1 + A_2}\right] \tag{3.41a,b,c,d}$$

and the matrices at junction 2 are

$$\mathbf{R}_2 = \left[\frac{A_2 - A_3}{A_2 + A_3}\right], \qquad \mathbf{T}_2 = \left[\frac{2A_2}{A_2 + A_3}\right]$$
$$\widehat{\mathbf{R}}_2 = \left[\frac{A_3 - A_2}{A_2 + A_3}\right], \qquad \widehat{\mathbf{T}}_2 = \left[\frac{2A_3}{A_2 + A_3}\right] \tag{3.42a,b,c,d}$$

The propagation matrix between the two junctions is

$$\mathbf{F} = \left[e^{-ik_l L} \right] \tag{3.43}$$

Then the relationships between the waves are

$$\begin{aligned}
\mathbf{b}^+ &= \mathbf{T}_1 \mathbf{a}^+ + \hat{\mathbf{R}}_1 \mathbf{b}^-, \\
\mathbf{c}^+ &= \mathbf{F}\mathbf{b}^+, \\
\mathbf{c}^- &= \mathbf{R}_2 \mathbf{c}^+, \\
\mathbf{b}^- &= \mathbf{F}\mathbf{c}^- \\
\mathbf{a}^- &= \mathbf{R}_1 \mathbf{a}^+ + \hat{\mathbf{T}}_1 \mathbf{b}^-, \\
\mathbf{d}^+ &= \mathbf{T}_2 \mathbf{c}^+
\end{aligned} \tag{3.44a,b,c,d,e,f}$$

Rearranging equation (3.44) in terms of the vector of incident waves $\mathbf{a}^+$, the vector of transmitted waves $\mathbf{d}^+$ is given by

$$\mathbf{d}^+ = \left[\mathbf{T}_2 \mathbf{F} [\mathbf{I} - \hat{\mathbf{R}}_1 \mathbf{F} \mathbf{R}_2 \mathbf{F}]^{-1} \mathbf{T}_1 \right] \mathbf{a}^+ \tag{3.45}$$

Substituting equations (3.41), (3.42) and (3.43) into equation (3.45) gives

$$\mathbf{d}^+ = \frac{4e^{-ik_l L}}{(1+\alpha_1)(1+\alpha_2) + (1-\alpha_1)(1-\alpha_2)e^{-i2k_l L}} \mathbf{a}^+ \tag{3.46}$$

where $\alpha_1 = A_2/A_1$ and $\alpha_2 = A_3/A_2$ represent the ratios of the cross-sectional areas at the junctions, respectively.

The power transmission coefficient τ was introduced as equation (3.40b). In this case, it is given by

$$\tau = \frac{A_3}{A_1} \frac{|d^+|^2}{|a^+|^2} \tag{3.47}$$

Substituting equation (3.46) into equation (3.47) gives

$$\tau = \frac{4\alpha_1 \alpha_2}{(\alpha_1 + \alpha_2)^2 + (1-\alpha_1^2)(1-\alpha_2^2)\cos^2 k_l L} \tag{3.48}$$

Equation (3.48) indicates that the maximum or minimum transmission occurs when $k_l L = \pi/2, \pi, 3\pi/2, \ldots$ and the maximum/minimum position is determined by the sign of $(1-\alpha_1)(1-\alpha_2)$. For example, if the cross-sectional areas increase monotonically such as $A_1 < A_2 < A_3$, the maximum transmission occurs when $k_l L = \pi/2, 3\pi/2, 5\pi/2, \ldots$ and the minimum transmission occurs when $k_l L = \pi, 2\pi, 3\pi, \ldots$.

Similarly, the power reflection coefficient ϱ can be calculated by obtaining the vector of reflected waves $\mathbf{a}^-$ in terms of $\mathbf{a}^+$. Indirectly, it can also be obtained using equations (3.39) and (3.48) since no damping is involved in this case.

Figure 3-6 shows numerical results of the power reflection and transmission coefficients when the area changes are $A \to 2A \to 4A$ and $A \to 2A \to A$, respectively. It can be seen that the frequencies where the maximum transmission occur in the first case become those where the minimum transmission occur in the second case. Figure 3-7 shows the power transmission coefficients when the cross-sectional area of the middle section varies. A greater area change ratio results in lower transmission efficiency.

3.9.2 Comparison to the transfer matrix method

In the previous subsection the example was studied using the wave approach based on the reflection, transmission and propagation of waves. In this subsection it is studied by using the approach based on transfer matrix method, which was presented in subsection 2.10.1.

The relationships between waves at the left-hand side of junction 1 and waves at the right-hand side of junction 2 are

$$\begin{Bmatrix} \mathbf{d}^+ \\ \mathbf{0} \end{Bmatrix} = \mathcal{T} \begin{Bmatrix} \mathbf{a}^+ \\ \mathbf{a}^- \end{Bmatrix}; \qquad \begin{Bmatrix} \mathbf{d}^+ \\ \mathbf{0} \end{Bmatrix} = \begin{bmatrix} \mathcal{T}_{11} & \mathcal{T}_{12} \\ \mathcal{T}_{21} & \mathcal{T}_{22} \end{bmatrix} \begin{Bmatrix} \mathbf{a}^+ \\ \mathbf{a}^- \end{Bmatrix} \tag{3.49}$$

where the transfer matrix $\mathcal{T}$ is given by

$$\mathcal{T} = \begin{bmatrix} \hat{\mathbf{T}}_2 - \mathbf{R}_2\mathbf{T}_2^{-1}\hat{\mathbf{R}}_2 & \mathbf{R}_2\mathbf{T}_2^{-1} \\ -\mathbf{T}_2^{-1}\hat{\mathbf{R}}_2 & \mathbf{T}_2^{-1} \end{bmatrix} \begin{bmatrix} \mathbf{F} & 0 \\ 0 & \mathbf{F}^{-1} \end{bmatrix} \begin{bmatrix} \mathbf{T}_1 - \hat{\mathbf{R}}_1\hat{\mathbf{T}}_1^{-1}\mathbf{R}_1 & \hat{\mathbf{R}}_1\hat{\mathbf{T}}_1^{-1} \\ -\hat{\mathbf{T}}_1^{-1}\mathbf{R}_1 & \hat{\mathbf{T}}_1^{-1} \end{bmatrix} \tag{3.50}$$

In equation (3.49), note the assumption that there are no negative-going waves on the right-hand side of junction 2. The transmitted waves are then obtained by

$$\mathbf{d}^+ = \left[\mathcal{T}_{11} - \mathcal{T}_{12}\mathcal{T}_{22}^{-1}\mathcal{T}_{21}\right]\mathbf{a}^+ \tag{3.51}$$

Substituting the reflection, transmission and propagation matrices given by equations (3.41), (3.42) and (3.43) into equation (3.50) gives the transfer matrix $\mathcal{T}$, and then the amplitudes of the transmitted waves are obtained by using equation (3.51).

Figure 3-8 shows the numerical results of the power reflection and transmission coefficients obtained by using the transfer matrix method when $A \to 2A \to 4A$. It is identical to Figure 3-6(a), which indicates that in this case either method can be used for the analysis of the motion of bars. This is generally true for bars, for which there is only one propagating wave mode.

3.10 Summary

The longitudinal motion of uniform straight bars has been described in terms of waves and their reflection, transmission and propagation. The displacement, internal force and propagation matrices for the bars were defined and used for the systematic analysis of wave motion for various situations such as the wave generation by a force, the reflection and transmission of waves at discontinuities, the reflection of waves at boundaries, and the derivation of the spectral elements. The energies are transported by the two propagating waves independently, and the propagation velocity is the same as the phase velocity.

The numerical results for bars where the area changes twice discontinuously were presented using the two wave approaches, one based on reflection, transmission and propagation of waves and the other based on the transfer matrix method. The numerical results showed that either method can be used for the analysis of the motion of the bars (in the next chapter where the bending motion of beams is studied, it is shown that the approach based on transfer matrix method may lead to numerical difficulties). As the changes of the area become more severe, the more the incident waves are reflected. The power also depends on the phase change of waves propagating between the two discontinuities, i.e., the product of the longitudinal wavenumber and the length between the two discontinuities.

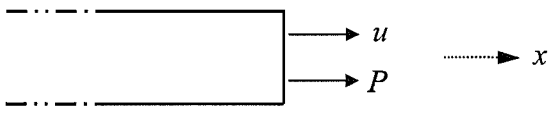

Figure 3-1. Sign convention of physical quantities for longitudinal motion.

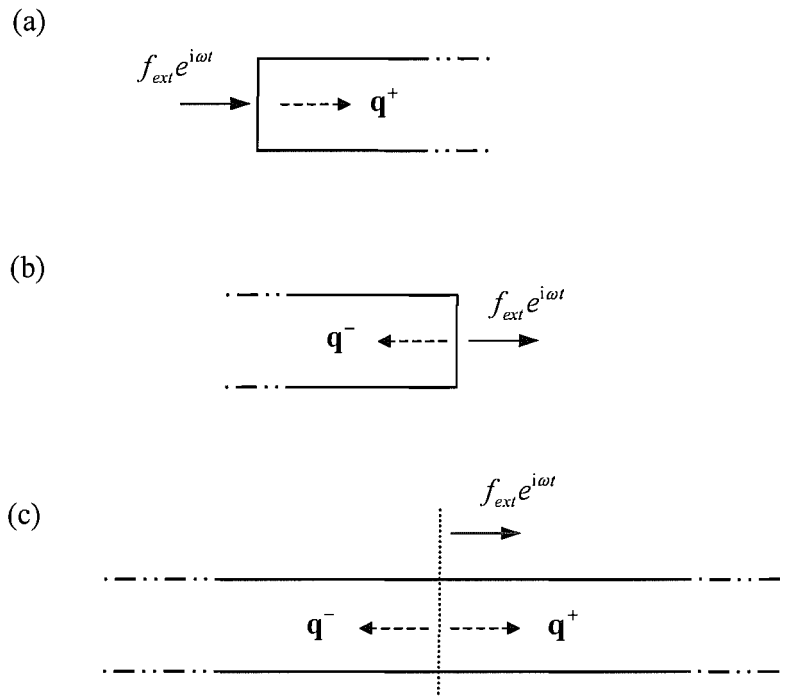

Figure 3-2. Wave generation in a uniform straight bar by a local harmonic force: (a) the left-hand end is excited, (b) the right-hand end is excited, (c) a cross-section is excited.

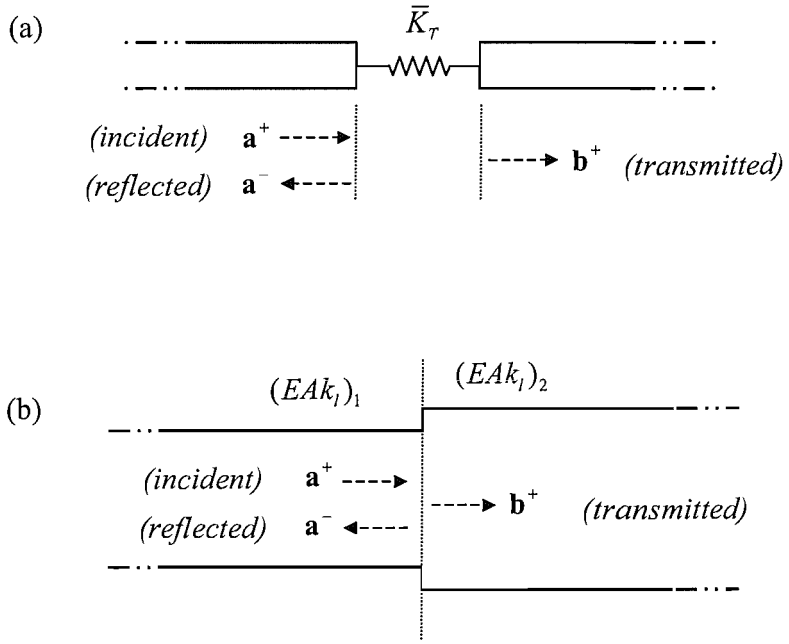

Figure 3-3. Reflection and transmission of longitudinal waves: (a) at a junction of two identical uniform straight bars connected by a translational dynamic stiffness, (b) at a junction of two different uniform straight bars connected directly.

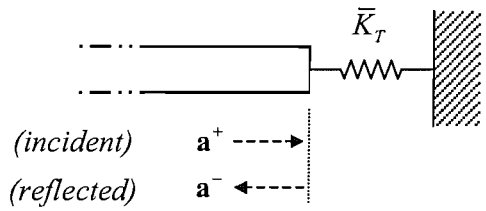

Figure 3-4. Reflection of longitudinal waves at an end of a uniform straight bar supported by a translational dynamic stiffness.

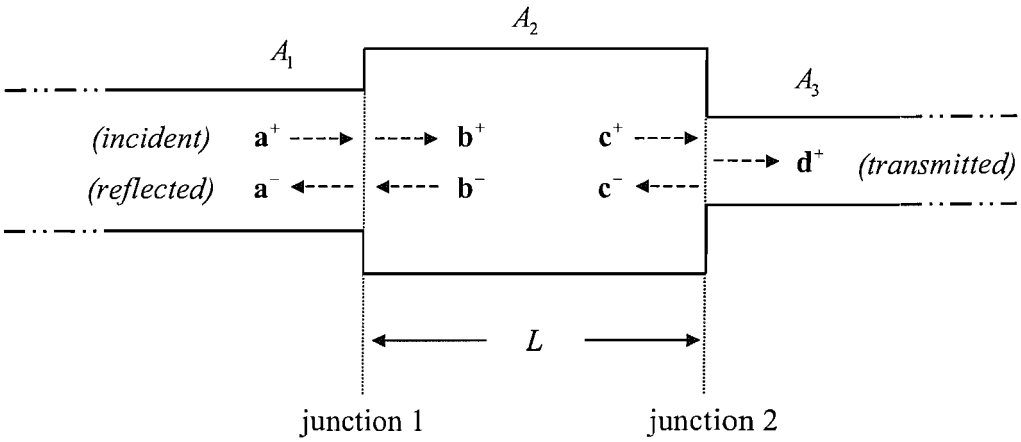

Figure 3-5. Reflection and transmission of longitudinal waves in a straight bar where cross-sectional area changes twice discontinuously, $A_1 \rightarrow A_2 \rightarrow A_3$.

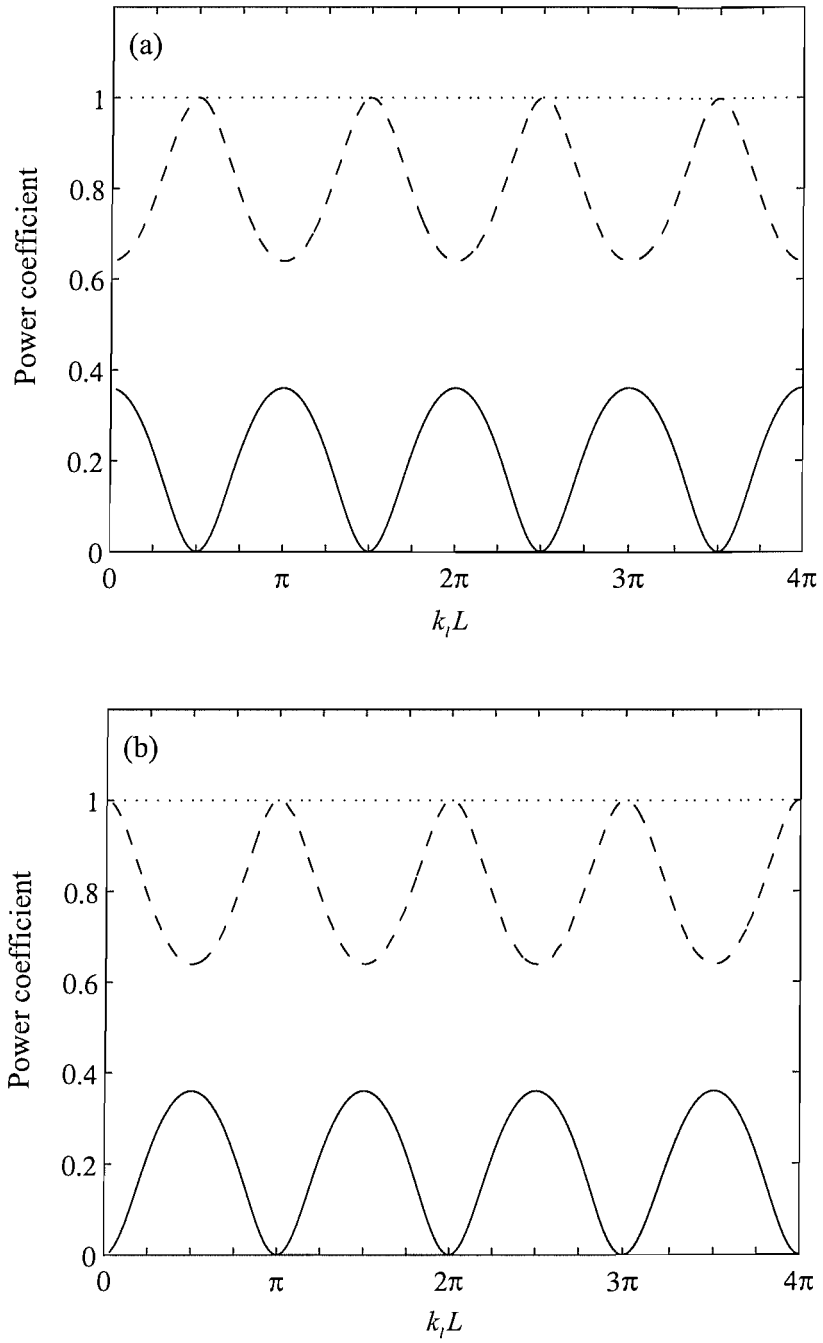

Figure 3-6. Power reflection and transmission coefficients when the area changes (a) $A \rightarrow 2A \rightarrow 4A$ and (b) $A \rightarrow 2A \rightarrow A$, respectively; ——— , reflection; ------ , transmission; ..... , total power.

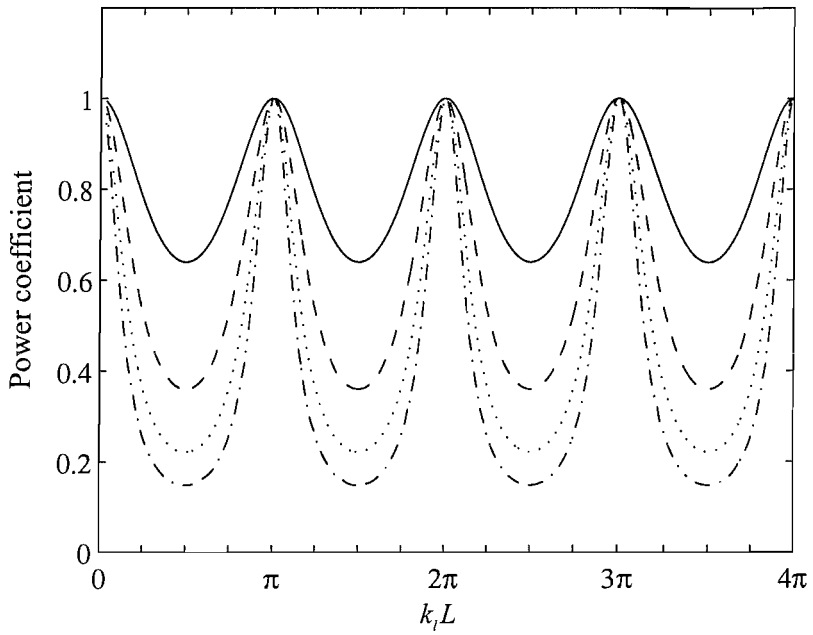

Figure 3-7. Effect of the cross-sectional area change ratio on the power transmission coefficients; ——— , $A \to 2A \to A$; ------ , $A \to 3A \to A$; ····· , $A \to 4A \to A$; -·-·-·- , $A \to 5A \to A$.

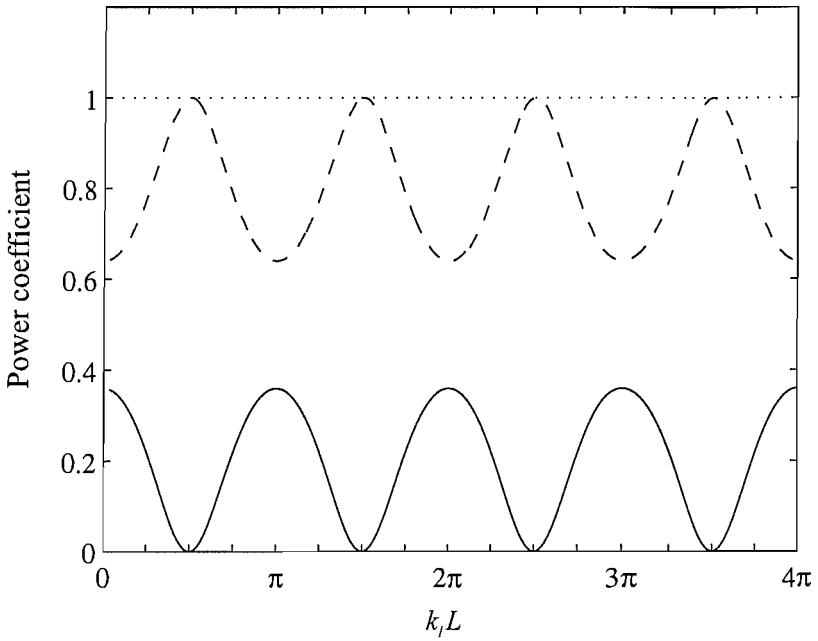

Figure 3-8. Power reflection/transmission coefficients for the two area changes, $A \rightarrow 2A \rightarrow 4A$, by using the wave method based on the transfer matrix method; ——— , reflection; ------ ,transmission; ····· , total power.

Chapter 4.

WAVE MOTION IN UNIFORM, STRAIGHT BEAMS

4.1 Introduction

In this chapter, the general wave approach based on reflection, transmission and propagation of waves is applied to cases concerning uniform, straight beams undergoing bending motion. Compared to axial vibration of the bars described in chapter 3, one distinct feature in these cases is that nearfield waves as well as propagating waves exist now. The amplitudes of nearfield waves decay very rapidly along the beam so that they are negligible when the propagation distance is longer than, typically, half the wavelength. Two issues related to nearfield waves are included in this chapter: power flow associated with nearfield waves and numerical conditioning problems associated with nearfield waves.

In section 4.2, the governing equation for uniform, straight beams undergoing bending motion is reviewed. The effects of shear deformation and rotary inertia are not considered so that the motion is based on Euler-Bernoulli theory. No damping effect is included for clarity so that the motion consists of two propagating waves and two nearfield waves. In section 4.3, the displacement, internal force, and propagation matrices for the beams are defined. Note that these matrices are now 2×2 matrices since the beam is a two-mode system.

Using the matrix formulation, wave generation by external point forces, reflection and transmission of waves at discontinuities, reflection of waves at boundaries, and

spectral elements are described in sections 4.4 to 4.7. In section 4.8, the energy flow associated with waves is discussed and the power reflection and transmission coefficients are defined.

In section 4.9, two numerical examples of application of the wave approach based on reflection, transmission, and propagation of waves are presented. The first is a beam with two simple supports. It is shown that the energy flow can be associated with the interaction of two opposite-going nearfield waves. Note that the approach based on the transfer matrix method cannot be applied to this case since the transfer matrix from the left-hand side of a simple support to the right-hand side cannot be defined. The second is a beam where the cross-sectional area changes twice discontinuously. It is illustrated that the approach based on reflection, transmission and propagation of waves always provides well-conditioned numerical results, while the approach based on the transfer matrix method may lead to numerical difficulties due to ill-conditioning at high frequencies.

4.2 Equation of motion

If the effects of shear deformation and rotary inertia are neglected, the bending displacement $w(x,t)$ for the free vibration of a beam is governed by the differential equation (Graff 1975)

$$\frac{\partial^2}{\partial x^2}\left[EI\frac{\partial^2 w}{\partial x^2}\right]+\rho A\frac{\partial^2 w}{\partial t^2}=0 \tag{4.1}$$

where I is the second moment of area. The corresponding shear force and bending moment, the convention being adopted as shown in Figure 4-1, are

$$Q = -\frac{\partial}{\partial x}\left(EI \frac{\partial^2 w}{\partial x^2} \right), \qquad M = EI \frac{\partial^2 w}{\partial x^2} \tag{4.2a,b}$$

Equation (4.1) can be easily solved when the material and geometric properties are constant with position x. If the time dependence of the motion is assumed to be of the form $e^{i\omega t}$ with angular frequency ω but suppressed here for clarity, the solution for the motion of a uniform beam is given by

$$w(x) = C_1 e^{-ik_b x} + C_2 e^{-k_b x} + C_3 e^{ik_b x} + C_4 e^{k_b x} \tag{4.3}$$

where $C_{1,2,3,4}$ are arbitrary constants, and the bending wavenumber k_b is given by

$$k_b = \sqrt[4]{\rho A \omega^2 / EI} \tag{4.4}$$

The wavenumber k_b is real and positive, unless damping is present when it will have a negative imaginary part. Note that, unlike axial vibration, k_b depends on the specific geometric shape of the beam cross-section. The corresponding shear force and bending moment can be obtained by substituting equation (4.3) into equation (4.2).

As in the axial vibration, the first and third terms of the right-hand side of equation (4.3) represent a positive-going propagating wave and a negative-going propagating wave, respectively: as time increases, the disturbance (w and the other corresponding physical quantities) is transported toward the positive (right) and the negative (left) direction by the terms, respectively, and it does not decay. The second and fourth terms represent nearfield (or evanescent) waves: the phase does not change with the distance but the magnitude decays exponentially.

4.3 The wave description

The transformation from the physical domain to the wave domain using vectors and matrices was expressed as equation (2.17). Following the formulation, the lateral displacement and the slope are grouped as a vector **w** and the corresponding shear force and bending moment are grouped as a vector **f** such that

$$\mathbf{w} = \begin{Bmatrix} w \\ \partial w/\partial x \end{Bmatrix}, \qquad \mathbf{f} = \begin{Bmatrix} Q \\ M \end{Bmatrix} \tag{4.5a,b}$$

The wave vectors are defined as

$$\mathbf{a}^{+} = \begin{Bmatrix} a^{+} \\ a_N^{+} \end{Bmatrix}, \qquad \mathbf{a}^{-} = \begin{Bmatrix} a^{-} \\ a_N^{-} \end{Bmatrix} \tag{4.6a,b}$$

where $a^{\pm}$ are the amplitudes of the propagating waves and $a_N^{\pm}$ are the amplitudes of the nearfield waves, and are given by

$$a^{+} = C_1 \mathrm{e}^{-\mathrm{i}k_b x}, \quad a_N^{+} = C_2 \mathrm{e}^{-k_b x}, \quad a^{-} = C_3 \mathrm{e}^{\mathrm{i}k_b x}, \quad a_N^{-} = C_4 \mathrm{e}^{k_b x} \tag{4.7a,b,c,d}$$

Then the displacement and internal force matrices describing the relationships between the physical state vectors and the wave vectors are given by

$$\begin{aligned} \Psi^{+} &= \begin{bmatrix} 1 & 1 \\ -\mathrm{i}k_b & -k_b \end{bmatrix}, & \Psi^{-} &= \begin{bmatrix} 1 & 1 \\ \mathrm{i}k_b & k_b \end{bmatrix}, \\ \Phi^{+} &= EI \begin{bmatrix} -\mathrm{i}k_b^{\,3} & k_b^{\,3} \\ -k_b^{\,2} & k_b^{\,2} \end{bmatrix}, & \Phi^{-} &= EI \begin{bmatrix} \mathrm{i}k_b^{\,3} & -k_b^{\,3} \\ -k_b^{\,2} & k_b^{\,2} \end{bmatrix} \end{aligned} \tag{4.8a,b,c,d}$$

Note that these matrices are independent of position in this case, which is not true in cases concerning non-uniform beams. These matrices also satisfy

$$\begin{aligned} \left(\Psi^{+}\right)^T \Phi^{+} &= \left(\Phi^{+}\right)^T \Psi^{+}, \\ \left(\Psi^{-}\right)^T \Phi^{-} &= \left(\Phi^{-}\right)^T \Psi^{-}, \\ \left(\Psi^{+}\right)^T \Phi^{-} - \left(\Phi^{+}\right)^T \Psi^{-} &= \mathbf{\Lambda} \end{aligned} \tag{4.9a,b,c}$$

where the diagonal matrix $\mathbf{\Lambda}$ is

$$\mathbf{\Lambda} = 4EIk_b^3 \begin{bmatrix} \mathrm{i} & 0 \\ 0 & -1 \end{bmatrix} \tag{4.10}$$

The propagation matrix $\mathbf{F}$ for propagation of waves between two points, a distance L apart, in a uniform straight beam is given by

$$\mathbf{F} = \begin{bmatrix} \mathrm{e}^{-\mathrm{i}k_b L} & 0 \\ 0 & \mathrm{e}^{-k_b L} \end{bmatrix} \tag{4.11}$$

In this case the positive and negative propagation matrices are the same, which would be expected from symmetry between two points. Generally, the relation between them is given by equation (2.21), i.e., $\mathbf{\Lambda}(x_2)\mathbf{F}^+ = \mathbf{F}^-\mathbf{\Lambda}(x_1)$. Thus it follows that $\mathbf{F}^+ = \mathbf{F}^-$.

4.4 Wave generation by local excitation

Consider a point of a uniform straight beam excited by a harmonic force $f_{ext}e^{\mathrm{i}\omega t}$ as shown in Figure 4-2(a). The continuity and equilibrium conditions at the point are

$$\begin{aligned} \mathbf{\Psi}^+\mathbf{q}^+ &= \mathbf{\Psi}^-\mathbf{q}^-, \\ -\mathbf{\Phi}^+\mathbf{q}^+ + \mathbf{\Phi}^-\mathbf{q}^- &= \mathbf{f}_{ext} \end{aligned} \tag{4.12a,b}$$

where the external force vector $\mathbf{f}_{ext} = \begin{bmatrix} f_{ext} & 0 \end{bmatrix}^T$. Substituting the displacement and internal force matrices given by equations (4.8) into equation (4.12) yields

$$\mathbf{q}^+ = \mathbf{q}^- = -\frac{f_{ext}}{4EIk_b^3} \begin{Bmatrix} \mathrm{i} \\ 1 \end{Bmatrix} \tag{4.13}$$

The magnitudes of the four wave components are equal. Note also that the lateral displacement, which is obtained by the sum of the amplitudes of the waves, lags in phase behind the force by $3\pi/4$.

Now suppose that the external force is applied at the left-hand end of the beam as shown in Figure 4-2(b). Since the equilibrium condition at the end is

$$-\mathbf{\Phi}^{+}\mathbf{q}^{+} = \mathbf{f}_{ext} \tag{4.14}$$

the induced waves $\mathbf{q}^{+}$ are given by

$$\mathbf{q}^{+} = -\frac{(1+\mathrm{i})f_{ext}}{2EIk_b^{\,3}}\begin{Bmatrix}1\\1\end{Bmatrix} \tag{4.15}$$

Note that the induced displacement again lags in phase behind the force by $3\pi/4$. In the final case where the external force is applied at the right-hand end as shown in Figure 4-2(c), the negative-going wave amplitude $\mathbf{q}^{-}$ is

$$\mathbf{q}^{-} = -\frac{(1+\mathrm{i})f_{ext}}{2EIk_b^{\,3}}\begin{Bmatrix}1\\1\end{Bmatrix} \tag{4.16}$$

which is the same as equation (4.15).

Now assume that the beam is excited by a time harmonic moment, instead of the force, as shown in Figure 4-3. The external force vector is now $\mathbf{f}_{ext} = \begin{bmatrix}0 & M_{ext}\end{bmatrix}^T$. For the case as shown in Figure 4-3(a), the induced waves are

$$\mathbf{q}^{+} = -\mathbf{q}^{-} = \frac{M_{ext}}{4EIk_b^{\,2}}\begin{Bmatrix}1\\-1\end{Bmatrix} \tag{4.17}$$

Note that the induced displacement at the excitation point is zero and the induced slope (or, rotation) lags in phase behind the moment by $\pi/4$. For the case as shown in Figure 4-3(b), the induced waves are

$$\mathbf{q}^{+} = \frac{(1+\mathrm{i})M_{ext}}{2EIk_b^{\,2}}\begin{Bmatrix}1\\\mathrm{i}\end{Bmatrix} \tag{4.18}$$

For the case as shown in Figure 4-3(c), the induced waves are

$$\mathbf{q}^{-} = -\frac{(1+\mathrm{i})M_{ext}}{2EIk_b^{\,2}}\begin{Bmatrix}1\\ \mathrm{i}\end{Bmatrix} \tag{4.19}$$

Compared to equation (4.18), note that the sign changes in this case.

A case where the external force and moment are applied at the same time can also be considered. Then the amplitudes of the induced waves can be obtained by simply changing the external force vector $\mathbf{f}_{ext}$ as required and following a similar procedure to that above.

4.5 Reflection and transmission at discontinuities

Consider a uniform straight beam, a point of which is supported by translational and rotational dynamic stiffnesses, $\bar{K}_T$ and $\bar{K}_R$, as shown in Figure 4-4(a). The continuity and equilibrium conditions at the point are given by

$$\begin{aligned} \mathbf{w}_a &= \mathbf{w}_b, \\ -\mathbf{f}_a + \mathbf{f}_b &= \mathbf{K}_{ext}\mathbf{w}_a \end{aligned} \tag{4.20a,b}$$

where the subscripts a and b denote the left- and right-hand sides of the discontinuity respectively, and the dynamic stiffness matrix $\mathbf{K}_{ext}$ is

$$\mathbf{K}_{ext} = \begin{bmatrix} \bar{K}_T & 0 \\ 0 & \bar{K}_R \end{bmatrix} \tag{4.21}$$

Note that, in general, $\mathbf{K}_{ext}$ could be not diagonal (but symmetric for a reciprocal system). Since the displacement and internal force matrices for the left- and right-hand sides are the same in this case, equations (4.20) can be re-expressed as

$$\begin{aligned} \Psi^{+}\mathbf{a}^{+} + \Psi^{-}\mathbf{a}^{-} &= \Psi^{+}\mathbf{b}^{+}, \\ -\Phi^{+}\mathbf{a}^{+} - \Phi^{-}\mathbf{a}^{-} + \Phi^{+}\mathbf{b}^{+} &= \mathbf{K}_{\mathrm{ext}}\Psi^{+}\mathbf{b}^{+} \end{aligned} \tag{4.22a,b}$$

Combining equations (4.8) and (4.21) with equations (4.22) gives the reflection and transmission matrices of the discontinuity (Mace 1984)

$$\mathbf{R} = \mu\mathbf{C} + \eta\mathbf{D}, \qquad \mathbf{T} = \mathbf{I} + \mu\mathbf{C} - \eta\mathbf{D}, \tag{4.23a,b}$$

where $\mathbf{I}$ is the identity matrix and

$$\mathbf{C} = \begin{bmatrix} \mathrm{i} & \mathrm{i} \\ 1 & 1 \end{bmatrix}, \quad \mathbf{D} = \begin{bmatrix} -\mathrm{i} & -1 \\ \mathrm{i} & 1 \end{bmatrix}, \quad \mu = \frac{K_T}{4-(1+\mathrm{i})K_T}, \quad \eta = \frac{K_R}{4+(1-\mathrm{i})K_R} \tag{4.24a,b,c,d}$$

where the dimensionless stiffnesses $K_T = \bar{K}_T / EIk_b^3$ and $K_R = \bar{K}_R / EIk_b$ are introduced.

For a simply supported point (namely, $K_T \to \infty$ and $K_R = 0$), the reflection and transmission matrices reduce to

$$\mathbf{R} = \frac{1}{1-\mathrm{i}} \begin{bmatrix} -1 & -1 \\ \mathrm{i} & \mathrm{i} \end{bmatrix}, \qquad \mathbf{T} = \frac{1}{1-\mathrm{i}} \begin{bmatrix} -\mathrm{i} & -1 \\ \mathrm{i} & 1 \end{bmatrix} \tag{4.25a,b}$$

Note that the coefficients of the matrices are independent of frequency and the magnitudes are $1/\sqrt{2}$. For an incident propagating wave this means that half of the energy carried by the incident wave is reflected by the simple support and the other half is transmitted. Also note that, when the amplitudes of the incident wave are of the form $\mathbf{a}^+ = \begin{bmatrix} 1 & -\mathrm{i} \end{bmatrix}^T$, i.e., such that the slope is zero, no wave will be transmitted to the right-hand side of the simple support.

Consider now a case where two beams with different geometric shapes and/or material properties are directly connected as shown in Figure 4-4(b). In this case the displacement, slope, bending moment and shear force are all continuous at the junction, namely,

$$\begin{aligned} \mathbf{w}_a &= \mathbf{w}_b \\ \mathbf{f}_a &= \mathbf{f}_b \end{aligned} \tag{4.26a,b}$$

Combined with the displacement and internal force matrices for uniform straight beams given by equations (4.8), the reflection and transmission matrices are determined to be (Mace 1984)

$$\mathbf{R} = \frac{2}{\Delta}\begin{bmatrix} -2(\beta^2-1)\gamma - \mathrm{i}\beta(1-\gamma)^2 & (1+\mathrm{i})\beta(1-\gamma^2) \\ (1-\mathrm{i})\beta(1-\gamma^2) & -2(\beta^2-1)\gamma + \mathrm{i}\beta(1-\gamma)^2 \end{bmatrix},$$
$$\mathbf{T} = \frac{4}{\Delta}\begin{bmatrix} (1+\beta)(1+\gamma) & -(1-\mathrm{i}\beta)(1-\gamma) \\ -(1+\mathrm{i}\beta)(1-\gamma) & (1+\beta)(1+\gamma) \end{bmatrix} \tag{4.27a,b}$$

where $\Delta = (1+\beta)^2(1+\gamma)^2 - (1+\beta^2)(1-\gamma)^2$, $\beta = k_{b,2}/k_{b,1}$ and $\gamma = (EIk_b^{\,2})_2/(EIk_b^{\,2})_1$. Note that the reflection and transmission matrices are independent of frequency. If, except for the thickness, the other material and geometric properties of the two beams are the same, the phase of the (1,1) element of $\mathbf{R}$ tends to $-\pi/2$ as the thickness difference increases (Mace 1984). If the two beams are identical except for their widths, b_1 and b_2, then $\beta = 1$ and the reflection and transmission matrices reduce to

$$\mathbf{R} = \frac{1}{\Delta}\begin{bmatrix} -\mathrm{i}(1-\sigma)^2 & (1+\mathrm{i})(1-\sigma^2) \\ (1-\mathrm{i})(1-\sigma^2) & \mathrm{i}(1-\sigma)^2 \end{bmatrix},$$
$$\mathbf{T} = \frac{2}{\Delta}\begin{bmatrix} 2(1+\sigma) & -(1-\mathrm{i})(1-\sigma) \\ -(1+\mathrm{i})(1-\sigma) & 2(1+\sigma) \end{bmatrix} \tag{4.28a, b}$$

where $\Delta = \sigma^2 + 6\sigma + 1$ and $\sigma = b_2/b_1$. Note that the phase of the (1,1) element of $\mathbf{R}$ is $-\pi/2$.

4.6 Reflection at boundaries

Consider a uniform straight beam where translational and rotational dynamic stiffnesses $\bar{K}_T$ and $\bar{K}_R$ are attached at the right-hand end as shown in Figure 4-5. The equilibrium condition at the end is

$$\mathbf{f} = -\mathbf{K}_{ext}\mathbf{w} \tag{4.29}$$

where the external dynamic stiffness matrix $\mathbf{K}_{ext}$ is given by equation (4.21). Thus

$$\mathbf{\Phi}^{+}\mathbf{a}^{+} + \mathbf{\Phi}^{-}\mathbf{a}^{-} = -\mathbf{K}_{ext}\left(\mathbf{\Psi}^{+}\mathbf{a}^{+} + \mathbf{\Psi}^{-}\mathbf{a}^{-}\right) \tag{4.30}$$

Substituting equations (4.8) and (4.21) into equation (4.30) gives the reflection matrix $\mathbf{R}$ of the boundary (Mace 1984)

$$\mathbf{R} = \begin{bmatrix} 1-\mathrm{i}K_T & \mathrm{i}(1-K_T) \\ -1+\mathrm{i}K_R & 1+K_R \end{bmatrix}^{-1} \begin{bmatrix} 1+\mathrm{i}K_T & \mathrm{i}(1+K_T) \\ 1+\mathrm{i}K_R & -1+K_R \end{bmatrix} \tag{4.31}$$

where $K_T = \bar{K}_T / EIk_b^{\,3}$ and $K_R = \bar{K}_R / EIk_b$.

For three common cases of interest - simply supported, clamped and free ends - the reflection matrices $\mathbf{R}$ are obtained as

$$\mathbf{R}_s = \begin{bmatrix} -1 & 0 \\ 0 & -1 \end{bmatrix}, \qquad \mathbf{R}_c = \begin{bmatrix} -\mathrm{i} & -(1+\mathrm{i}) \\ -(1-\mathrm{i}) & \mathrm{i} \end{bmatrix}, \qquad \mathbf{R}_f = \begin{bmatrix} -\mathrm{i} & (1+\mathrm{i}) \\ (1-\mathrm{i}) & \mathrm{i} \end{bmatrix} \tag{4.32a,b,c}$$

where the subscripts s, c and f refer the boundary conditions, respectively.

4.7 Spectral elements

Consider a semi-infinite uniform straight beam extending to $x = +\infty$. The dynamic stiffness matrix for the semi-infinite, or throw-off, beam is given by

$$\mathbf{D}^{+\infty} = -\mathbf{\Phi}^{+}\left(\mathbf{\Psi}^{+}\right)^{-1} \tag{4.33}$$

Substituting the displacement and internal force matrices given by equations (4.8a,c) into equation (4.33) gives

$$\mathbf{D}^{+\infty} = EI \begin{bmatrix} -(1-\mathrm{i})k_b^3 & \mathrm{i}k_b^2 \\ \mathrm{i}k_b^2 & (1+\mathrm{i})k_b \end{bmatrix} \tag{4.34}$$

The dynamic stiffness matrix $\mathbf{D}^{-\infty}$ for the semi-infinite uniform straight beam extending to $x=-\infty$ is the same as $\mathbf{D}^{+\infty}$, except for the sign changes of the (1,2) and (2,1) elements.

Consider now a finite uniform straight beam of length L. The dynamic stiffness matrix for the finite beam is given by

$$\mathbf{D}=\begin{bmatrix}-\mathbf{\Phi}^{+} & -\mathbf{\Phi}^{-}\mathbf{F}\\ \mathbf{\Phi}^{+}\mathbf{F} & \mathbf{\Phi}^{-}\end{bmatrix}\begin{bmatrix}\mathbf{\Psi}^{+} & \mathbf{\Psi}^{-}\mathbf{F}\\ \mathbf{\Psi}^{+}\mathbf{F} & \mathbf{\Psi}^{-}\end{bmatrix}^{-1} \tag{4.35}$$

Substituting equations (4.8) and (4.11) into equation (4.35) gives

$$\mathbf{D}=\frac{EIk_b^2}{\Delta}\begin{bmatrix}\mathbf{D}_{11} & \mathbf{D}_{12}\\ \mathbf{D}_{21} & \mathbf{D}_{22}\end{bmatrix} \tag{4.36}$$

where $\Delta=\cos k_bL\cosh k_bL-1$ and

$$\mathbf{D}_{11}=\begin{bmatrix}-k_b\left(\sinh k_bL\cos k_bL+\cosh k_bL\sin k_bL\right) & -\sin k_bL\sinh k_bL\\ -\sin k_bL\sinh k_bL & \dfrac{\sinh k_bL\cos k_bL-\cosh k_bL\sin k_bL}{k_b}\end{bmatrix},$$

$$\mathbf{D}_{22}=\begin{bmatrix}-k_b\left(\sinh k_bL\cos k_bL+\cosh k_bL\sin k_bL\right) & \sin k_bL\sinh k_bL\\ \sin k_bL\sinh k_bL & \dfrac{\sinh k_bL\cos k_bL-\cosh k_bL\sin k_bL}{k_b}\end{bmatrix},$$

$$\mathbf{D}_{12}=\begin{bmatrix}k_b\left(\sin k_bL+\sinh k_bL\right) & \cos k_bL-\cosh k_bL\\ -\left(\cos k_bL-\cosh k_bL\right) & \dfrac{1}{k_b}\left(\sin k_bL-\sinh k_bL\right)\end{bmatrix},$$

$$\mathbf{D}_{21}=\mathbf{D}_{12}^{T}$$

Note that the dynamic stiffness matrix is symmetric, i.e., $\mathbf{D}=\mathbf{D}^{T}$ because of reciprocity.

4.8 Energy flow

In section 2.9, the time-averaged power associated with waves in one-dimensional structures was given as

$$\Pi = \frac{1}{2}\mathbf{a}^H \mathbf{P}\,\mathbf{a} \tag{4.37}$$

where $\mathbf{a} = \left[\left(\mathbf{a}^+\right)^T \quad \left(\mathbf{a}^-\right)^T\right]^T$ and the power matrix $\mathbf{P}$ is

$$\mathbf{P} = \frac{\mathrm{i}\omega}{2}\left[\begin{bmatrix}\left(\Psi^+\right)^H\Phi^+ & \left(\Psi^+\right)^H\Phi^- \\ \left(\Psi^-\right)^H\Phi^+ & \left(\Psi^-\right)^H\Phi^-\end{bmatrix} - \begin{bmatrix}\left(\Phi^+\right)^H\Psi^+ & \left(\Phi^+\right)^H\Psi^- \\ \left(\Phi^-\right)^H\Psi^+ & \left(\Phi^-\right)^H\Psi^-\end{bmatrix}\right] \tag{4.38}$$

Substituting the displacement and internal force matrices for the uniform straight beams given by equation (4.8) into equation (4.38) yields

$$\mathbf{P} = 2\omega EIk_b^3\begin{bmatrix}1 & 0 & 0 & 0 \\ 0 & 0 & 0 & -\mathrm{i} \\ 0 & 0 & -1 & 0 \\ 0 & \mathrm{i} & 0 & 0\end{bmatrix} \tag{4.39}$$

Unlike that for axial vibration of bars, the power matrix is not diagonal. The presence of off-diagonal terms indicates that the energy can be transported by the interaction between nearfield waves. Suppose that there are two opposite-going nearfield waves with amplitudes a_N^+ and a_N^-, respectively, i.e., $\mathbf{a} = \begin{bmatrix}0 & a_N^+ & 0 & a_N^-\end{bmatrix}^T$. Then the time-averaged power associated with the nearfield waves is

$$\Pi = 2\omega EIk_b^3\,\mathrm{Re}\left(\mathrm{i}a_N^+\left(a_N^-\right)^*\right) \tag{4.40}$$

Equation (4.40) indicates that, if a_N^+ and a_N^- are not in phase and are not in counter-phase, the energy can be transported by interaction of the two opposite-going nearfield

waves, as indicated by Bobrovnitskii (1992). Note that the direction of energy flow is determined by the phase difference of the amplitudes, e.g., if a_N^+ leads in phase ahead of a_N^- by $\pi/2$, then the energy will propagate in the positive direction.

The power matrix in equation (4.39) also indicates that a propagating wave transports energy independent of all the other wave components. The time-averaged power associated with a positive-going propagating wave with amplitude a^+ is given by

$$\begin{aligned} \Pi &= \omega E I k_b^{\,3} \left|a^+\right|^2 \\ &= \frac{1}{2}\rho A \omega^2 \left|a^+\right|^2 c_g \end{aligned} \tag{4.41}$$

where $c_g = \mathrm{d}\omega/\mathrm{d}k$ is the group velocity for uniform straight beams. It can be seen that power is proportional to the group velocity times mass per unit length, i.e., energy is transported by the wave at that velocity. Similarly, the time-averaged power associated with a negative-going propagating wave with amplitude a^- is given by

$$\begin{aligned} \Pi &= -\omega E I k_b^{\,3} \left|a^-\right|^2 \\ &= -\frac{1}{2}\rho A \omega^2 \left|a^-\right|^2 c_g \end{aligned} \tag{4.42}$$

Note that the negative sign indicates the energy is transported in the negative direction.

In section 3.8, the power reflection coefficient ϱ and power transmission coefficient τ were introduced to indicate how much energy is reflected and transferred, e.g., at a discontinuity. They are given by

$$\varrho = -\frac{\Pi_r}{\Pi_i}, \qquad \tau = \frac{\Pi_t}{\Pi_i} \tag{4.43a,b}$$

where Π_i, Π_r and Π_t are the incident, reflected and transmitted powers, respectively. For example, suppose that a positive-going propagating wave with amplitude a^+ is incident on a point discontinuity and then reflected into negative-going waves with amplitudes a^- (propagating) and a_N^- (nearfield), and transmitted into waves with amplitudes d^+ and d_N^+. Note that, in this case, two opposite-going nearfield waves do not occur together so that no power is associated with the nearfield waves. Thus the power reflection and transmission coefficients are given by

$$\varrho = \frac{\left|a^-\right|^2}{\left|a^+\right|^2}, \qquad \tau = \frac{(EIk_b^{\,3})_2}{(EIk_b^{\,3})_1}\frac{\left|d^+\right|^2}{\left|a^+\right|^2} \tag{4.44a,b}$$

where the subscripts 1 and 2 refer to the left- and right-hand sides of the discontinuity, respectively.

4.9 Numerical examples

In this section, two numerical examples of application of the wave approach based on reflection, transmission, and propagation of waves are presented. The first is a uniform beam with two simple supports. It is shown that energy flow can be associated with the interaction of two opposite-going nearfield waves. Note that the approach based on the transfer matrix method cannot be applied to this case since the transfer matrix from the left-hand side of a simple support to the right-hand side cannot be defined. The second example is a beam where the cross-sectional area changes twice discontinuously. It is illustrated that the approach based on reflection, transmission and propagation of waves always provides well-conditioned numerical results while the

approach based on transfer matrix method may lead to numerical difficulties due to ill conditioning at high frequencies.

4.9.1 Reflection and transmission by two simple supports

Consider a uniform straight beam with two simple supports as shown in Figure 4-6 where the length between the two supports is denoted by L. Suppose that a propagating wave with amplitude a^+ is incident from the left-hand side of the left support, therefore, the incident wave vector $\mathbf{a}^+$ is

$$\mathbf{a}^+ = \begin{Bmatrix} a^+ \\ 0 \end{Bmatrix} \tag{4.45}$$

The reflection and transmission matrices for a simple support have been obtained as equation (4.25), namely,

$$\mathbf{R} = \frac{1}{1-\mathrm{i}}\begin{bmatrix} -1 & -1 \\ \mathrm{i} & \mathrm{i} \end{bmatrix}, \qquad \mathbf{T} = \frac{1}{1-\mathrm{i}}\begin{bmatrix} -\mathrm{i} & -1 \\ \mathrm{i} & 1 \end{bmatrix} \tag{4.46a,b}$$

which are valid when waves are incident from the right-hand side of the support as well as from the left-hand side of the support. The propagation matrix $\mathbf{F}$ between the two supports is

$$\mathbf{F} = \begin{bmatrix} \mathrm{e}^{-\mathrm{i}k_b L} & 0 \\ 0 & \mathrm{e}^{-k_b L} \end{bmatrix} \tag{4.47}$$

For two general discontinuities, the reflected waves $\mathbf{a}^-$ and the transmitted waves $\mathbf{d}^+$ were obtained as equation (2.35). In this case they are given by

$$\begin{aligned} \mathbf{a}^- &= \left(\mathbf{R} + \mathbf{TFRF}[\mathbf{I} - \mathbf{RFRF}]^{-1}\mathbf{T}\right)\mathbf{a}^+ \\ \mathbf{d}^+ &= \mathbf{TF}[\mathbf{I} - \mathbf{RFRF}]^{-1}\mathbf{T}\mathbf{a}^+ \end{aligned} \tag{4.48a,b}$$

Suppose that a^- and a_N^- are the amplitudes of the reflected propagating and nearfield waves, respectively, and d^+ and d_N^+ are the amplitudes of the transmitted propagating and nearfield waves, i.e., $\mathbf{a}^- = \begin{bmatrix} a^- & a_N^- \end{bmatrix}^T$ and $\mathbf{d}^+ = \begin{bmatrix} d^+ & d_N^+ \end{bmatrix}^T$. Since no opposite-going nearfield counterparts to the nearfield waves a_N^- and d_N^+ exist and the nearfield waves a_N^- and d_N^+ cannot carry energy alone, the power reflection and transmission coefficients, ϱ and τ, for the two supports are given by

$$\varrho = \frac{\left|a^-\right|^2}{\left|a^+\right|^2}, \qquad \tau = \frac{\left|d^+\right|^2}{\left|a^+\right|^2} \tag{4.49a,b}$$

Approximate values of the power reflection and transmission coefficients can be calculated by neglecting the nearfield waves set up in the intermediate region between two supports. Taking only the (1,1) elements of the matrices $\mathbf{R}$, $\mathbf{T}$, $\mathbf{F}$ and $\mathbf{I}$, the transmitted amplitude d^+ is given in this case by

$$d^+ = \frac{e^{ik_bL}}{1+2ie^{i2k_bL}}a^+ \tag{4.50}$$

The maximum value of the magnitude of d^+ is $\left|d^+\right|_{\max} = \left|a^+\right|$ and occurs when $e^{i2k_bL} = i$, i.e., when

$$k_bL = \left(n+\frac{1}{4}\right)\pi \tag{4.51}$$

where $n = 0, 1, 2, 3, \ldots$. Note that this maximum transmission occurs when the phase of the term **RFRF** equals a multiple of 2π. The minimum value of magnitude of d^+ is $\left|d^+\right|_{\min} = \frac{1}{3}\left|a^+\right|$ and occurs when $e^{i2k_bL} = -i$, i.e., when

$$k_b L = \left(n + \frac{3}{4} \right) \pi \tag{4.52}$$

Therefore the power transmission coefficients for maximum and minimum transmission are

$$\tau_{\max} = 1, \qquad \tau_{\min} = \frac{1}{9} \tag{4.53}$$

Since no energy dissipation is assumed in this case, the maximum and minimum values of the power reflection coefficient are 0 and $8/9$, respectively.

Figure 4-7 shows numerical results for the power reflection and transmission coefficients. The results, when nearfield waves in the region between the two supports are neglected and when they are included, are compared. It can be seen that discrepancies between the two results exist when $k_b L < \pi$. Thus it indicates that the influence of nearfield waves, which set up in the intermediate region between two supports, on the energy flow cannot be neglected if the length between two supports is less than half a wavelength. When $k_b L > \pi$, the results show good agreement with the approximate behaviour obtained when neglecting the nearfield waves.

The numerical results have been obtained using the wave approach based on reflection, transmission and propagation of waves. Note that the approach based on the transfer matrix method cannot be applied to this case since the point transfer matrix from the left-hand side of a simple support to the left-hand side cannot be defined. Generally, if the stiffness of an intermediate elastic support is very large compared to the bending stiffness of the beam, numerical difficulties may arise in using the approach based on transfer matrix method (Pestel and Leckie 1963).

4.9.2 Reflection and transmission by area changes

Consider a straight rectangular beam where the cross-sectional area changes discontinuously at two points such that $A_1 \to A_2 \to A_3$, as shown in Figure 4-8. The points, where the area changes and denoted by junction 1 and junction 2 in the figure, are by a distance L apart. In subsection 4.9.2.1, numerical results for the power transmission in this case are obtained using two approaches, one based on reflection, transmission and propagation of waves and the other based on the transfer matrix method. It is shown that a different kind of numerical difficulty, which is related to nearfield waves, may occur in using the approach based on the transfer matrix method. In subsection 4.9.2.2, reflection and transmission of waves under various conditions of the area change are studied.

4.9.2.1 Comparison of the two numerical methods

For the beam shown in Figure 4-8, assume that the width b is invariant but the thickness h changes such that $h \to 2h \to h$. A propagating wave with amplitude a^+ is incident from the left-hand side of junction 1, therefore, the incident wave vector $\mathbf{a}^+$ is

$$\mathbf{a}^+ = \begin{Bmatrix} a^+ \\ 0 \end{Bmatrix} \tag{4.54}$$

The reflection and transmission matrices for the discrete change in the geometric and material properties have been obtained as in equation (4.27). In this case, the reflection and transmission matrices for junction 1 are

$$\mathbf{R}_1 = \frac{1}{24+25\sqrt{2}}\begin{bmatrix} 8-\mathrm{i}9\sqrt{2} & -15(1+\mathrm{i})\sqrt{2} \\ -15(1-\mathrm{i})\sqrt{2} & 8+\mathrm{i}9\sqrt{2} \end{bmatrix},$$

$$\mathbf{T}_1 = \frac{1}{24+25\sqrt{2}}\begin{bmatrix} 10(2+\sqrt{2}) & 6(2-\mathrm{i}\sqrt{2}) \\ 6(2+\mathrm{i}\sqrt{2}) & 10(2+\sqrt{2}) \end{bmatrix},$$

$$\hat{\mathbf{R}}_1 = \frac{1}{24+25\sqrt{2}}\begin{bmatrix} -8-\mathrm{i}9\sqrt{2} & 15(1+\mathrm{i})\sqrt{2} \\ 15(1-\mathrm{i})\sqrt{2} & -8+\mathrm{i}9\sqrt{2} \end{bmatrix}, \qquad (4.55a,b,c,d)$$

$$\hat{\mathbf{T}}_1 = \frac{1}{24+25\sqrt{2}}\begin{bmatrix} 40(1+\sqrt{2}) & -24(1-\mathrm{i}\sqrt{2}) \\ -24(1+\mathrm{i}\sqrt{2}) & 40(1+\sqrt{2}) \end{bmatrix}$$

Note again that the elements of the matrices are independent of frequency. The matrices for junction 2 are

$$\mathbf{R}_2 = \hat{\mathbf{R}}_1, \qquad \mathbf{T}_2 = \hat{\mathbf{T}}_1,$$
$$\hat{\mathbf{R}}_2 = \mathbf{R}_1, \qquad \hat{\mathbf{T}}_2 = \mathbf{T}_1 \qquad (4.56a,b,c,d)$$

The propagation matrix between the two junctions is given by

$$\mathbf{F} = \begin{bmatrix} e^{-\mathrm{i}k_{b,2}L} & 0 \\ 0 & e^{-k_{b,2}L} \end{bmatrix} \qquad (4.57)$$

where $k_{b,2}$ is the wavenumber in the central region. Then the reflected and transmitted waves, $\mathbf{a}^-$ and $\mathbf{d}^+$, are obtained by

$$\mathbf{a}^- = \mathbf{R}_T\mathbf{a}^+; \qquad \mathbf{R}_T = \mathbf{R}_1 + \hat{\mathbf{T}}_1\mathbf{F}\hat{\mathbf{R}}_1\mathbf{F}[\mathbf{I}-\hat{\mathbf{R}}_1\mathbf{F}\hat{\mathbf{R}}_1\mathbf{F}]^{-1}\mathbf{T}_1$$
$$\mathbf{d}^+ = \mathbf{T}_T\mathbf{a}^+; \qquad \mathbf{T}_T = \hat{\mathbf{T}}_1\mathbf{F}[\mathbf{I}-\hat{\mathbf{R}}_1\mathbf{F}\hat{\mathbf{R}}_1\mathbf{F}]^{-1}\mathbf{T}_1 \qquad (4.58a,b)$$

where $\mathbf{R}_T$ and $\mathbf{T}_T$ are *global* reflection and transmission matrices for the case.

The reflected and transmitted waves have been obtained by using the wave approach based on reflection, transmission and propagation of waves. Now the waves are obtained by the approach based on the transfer matrix method. The relationships

between the waves at the left-hand side of junction 1 and the waves at the right-hand side of junction 2 are

$$\begin{Bmatrix} \mathbf{d}^+ \\ \mathbf{0} \end{Bmatrix} = \mathcal{T} \begin{Bmatrix} \mathbf{a}^+ \\ \mathbf{a}^- \end{Bmatrix}; \qquad \begin{Bmatrix} \mathbf{d}^+ \\ \mathbf{0} \end{Bmatrix} = \begin{bmatrix} \mathcal{T}_{11} & \mathcal{T}_{12} \\ \mathcal{T}_{21} & \mathcal{T}_{22} \end{bmatrix} \begin{Bmatrix} \mathbf{a}^+ \\ \mathbf{a}^- \end{Bmatrix} \tag{4.59}$$

where the transfer matrix $\mathcal{T}$ is given by

$$\mathcal{T} = \begin{bmatrix} \hat{\mathbf{T}}_1 - \mathbf{R}_1 \mathbf{T}_1^{-1} \hat{\mathbf{R}}_1 & \mathbf{R}_1 \mathbf{T}_1^{-1} \\ -\mathbf{T}_1^{-1} \hat{\mathbf{R}}_1 & \mathbf{T}_1^{-1} \end{bmatrix} \begin{bmatrix} \mathbf{F} & 0 \\ 0 & \mathbf{F}^{-1} \end{bmatrix} \begin{bmatrix} \mathbf{T}_1 - \hat{\mathbf{R}}_1 \hat{\mathbf{T}}_1^{-1} \mathbf{R}_1 & \hat{\mathbf{R}}_1 \hat{\mathbf{T}}_1^{-1} \\ -\hat{\mathbf{T}}_1^{-1} \mathbf{R}_1 & \hat{\mathbf{T}}_1^{-1} \end{bmatrix} \tag{4.60}$$

In equation (4.59), note the assumption that there are no negative-going waves in the right-hand side of junction 2. The reflected and the transmitted waves are then obtained by

$$\begin{aligned} \mathbf{a}^- &= \mathbf{R}_T \mathbf{a}^+; & \mathbf{R}_T &= -\mathcal{T}_{22}^{-1} \mathcal{T}_{21} \\ \mathbf{d}^+ &= \mathbf{T}_T \mathbf{a}^+; & \mathbf{T}_T &= \mathcal{T}_{11} - \mathcal{T}_{12} \mathcal{T}_{22}^{-1} \mathcal{T}_{21} \end{aligned} \tag{4.61a,b}$$

Substituting the reflection, transmission and propagation matrices given by equations (4.55), (4.56) and (4.57) into equation (4.60) gives the transfer matrix $\mathcal{T}$, and then the amplitudes of the reflected and transmitted waves are obtained by using equation (4.61). This is the approach based on the transfer matrix method.

Equations (4.58) and (4.61) should give the same results. However, there are some difficulties relating to nearfield waves when numerical calculations using the approach based on the transfer matrix method are performed. As shown in equation (4.60), the transfer matrix includes $\mathbf{F}^{-1}$ so that the element for the transfer of the nearfield wave, i.e, $e^{k_{b,2}L}$, will grow rapidly as $k_{b,2}L$ increases. For example, when $k_{b,2}L \approx 38$ (or, $L/\lambda_2 \approx 6$), the 2-norm condition number of $\mathbf{F}^{-1}$ is approximately 10^{16}. Thus important information contained in other small terms could be lost in the

computational process, e.g., a small value multiplied by $e^{k_{b,2}L}$ may be the rounded off when $k_{b,2}L$ is high (Pestel and Leckie 1963). This rounding off may lead to significant errors in the numerical results.

Figure 4-9 shows numerical results, obtained by the two approaches of the (1,1) elements of the *global* reflection and transmission matrices, $R_{T,11}$ and $T_{T,11}$. It can be seen that the approach based on the transfer matrix method fails to give a reasonable result when $k_{b,2}L$ (L/λ_2 in the figure) is high enough. However, the wave approach based on reflection, transmission and propagation of waves does not lead to such numerical errors, i.e., the numerical results are always well conditioned.

4.9.2.2 Effect of cross-section change

In this subsection, reflection and transmission of waves for various area changes are investigated. Figures 4-10(a) shows numerical results of the power transmission coefficients for the case where the width b of the rectangular beam changes but the thickness h is invariant. As shown in equation (4.28), the phase of the (1,1) element of $\mathbf{R}$ for the junction is $-\pi/2$. Thus, when neglecting nearfield waves, the maximum transmission occurs at frequencies such that

$$-\pi + 2k_{b,2}L = 2n\pi\ ; \qquad k_{b,2}L = \left(n + \frac{1}{2}\right)\pi \tag{4.62}$$

where $n = 0, 1, 2, \ldots$. It is seen in the figure that the frequencies, at which the maximum transmission occurs, agree well with equation (4.62) when $k_{b,2}L > \pi$. The frequencies are independent of the width change ratio. Discrepancies at low value of $k_{b,2}L$ can be attributed to the effects of nearfield waves.

Figure 4-10(b) shows numerical results for the power transmission coefficients for various thickness changes when the width is invariant. The values of $k_{b,2}L$, for which the maximum and minimum transmissions occur, depend on the specific thickness changes and tend to a limit when the change ratio becomes greater. The tendency can be understood by the fact that, as noted below equation (4.27), the phase of the (1,1) element of $\mathbf{R}$ for the junction tends to $-\pi/2$ as the thickness difference increases.

4.10 Summary

The bending motion of uniform, straight beams has been described in terms of waves and their reflection, transmission and propagation. The displacement, internal force and propagation matrices for the beams were defined and used for the systematic analysis of wave motion for various situations such as the wave generation by a force, the reflection and transmission of waves at discontinuities, the reflection of waves at boundaries, and the derivation of the spectral elements. The energy flow associated with waves was also described in matrix form. Energy can be transported by interaction between two opposite-going nearfield waves. The power depends on the relative phase of the nearfield components.

Two numerical examples, a beam where two points are simply supported and a beam where the area changes twice discontinuously, were presented. The first example showed explicitly the possibility that the energy flow could be associated with nearfield waves. The second example showed that the approach based on the transfer matrix method may lead to numerical difficulties related to nearfield waves while the wave approach based on reflection, transmission and propagation of waves always provides well-conditioned numerical results.

In chapter 3 and this chapter, the motion of uniform straight structures were studied by the wave approach based on reflection, transmission and propagation of waves. Examples included the longitudinal and bending motions, which are not coupled in this case, of the structures. In the following two chapters, the motion of deterministically varying structures is studied by the wave approach.

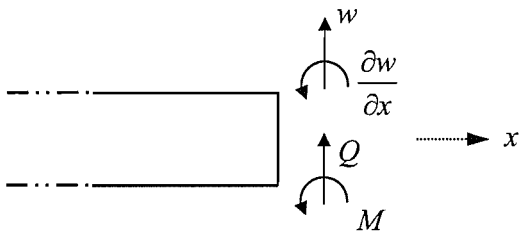

Figure 4-1. Sign convention of physical quantities for bending motion.

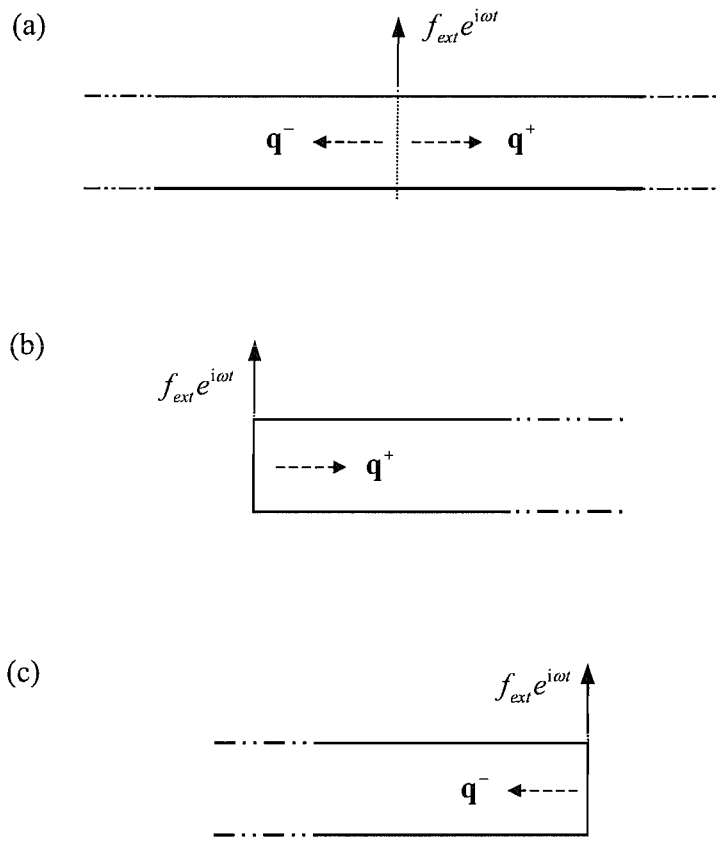

Figure 4-2. Wave generation in a uniform straight beam by a local harmonic force: (a) a point is excited, (b) the left-hand end is excited, (c) the right-hand end is excited.

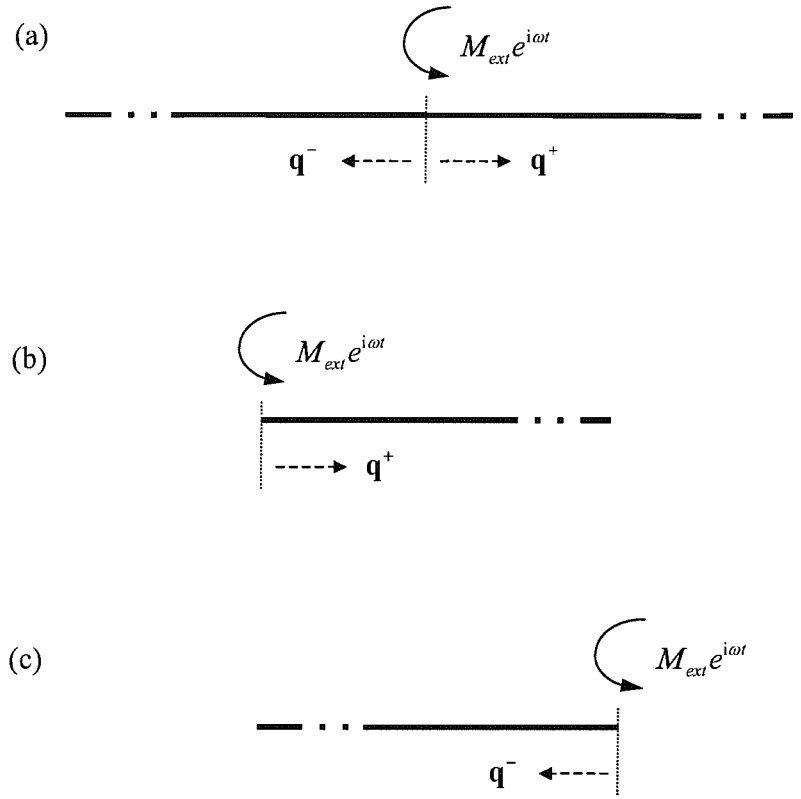

Figure 4-3. Generation of bending waves in a uniform straight beam by an external harmonic moment: (a) applied at a point, (b) applied at left-hand end, (c) applied at right-hand end.

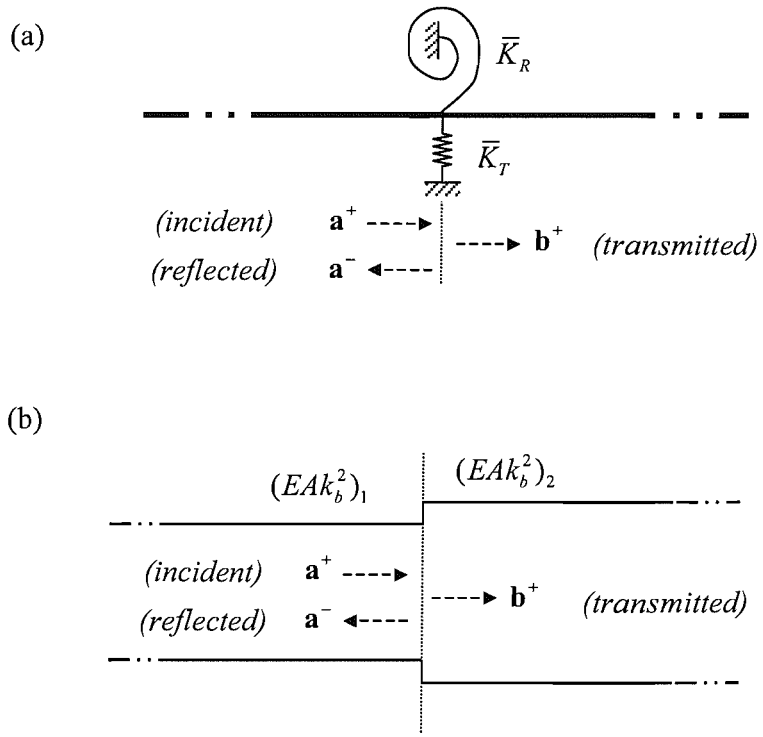

Figure 4-4. Reflection and transmission of bending waves: (a) at a point supported by translational and rotational dynamic stiffnesses, (b) at a junction of two different uniform straight beams directly connected.

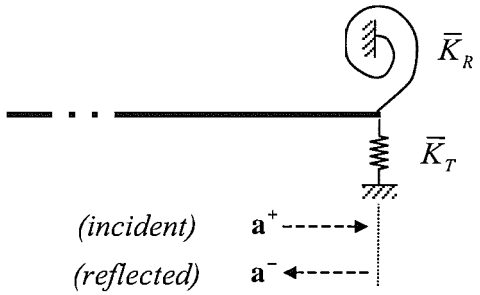

Figure 4-5. Reflection of bending waves at the right-hand end of a uniform straight beam supported by translational and rotational dynamic stiffnesses.

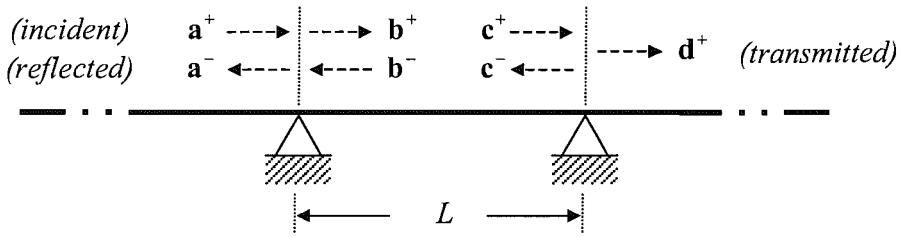

Figure 4-6. Reflection and transmission of bending waves in a uniform straight beam with two simple supports.

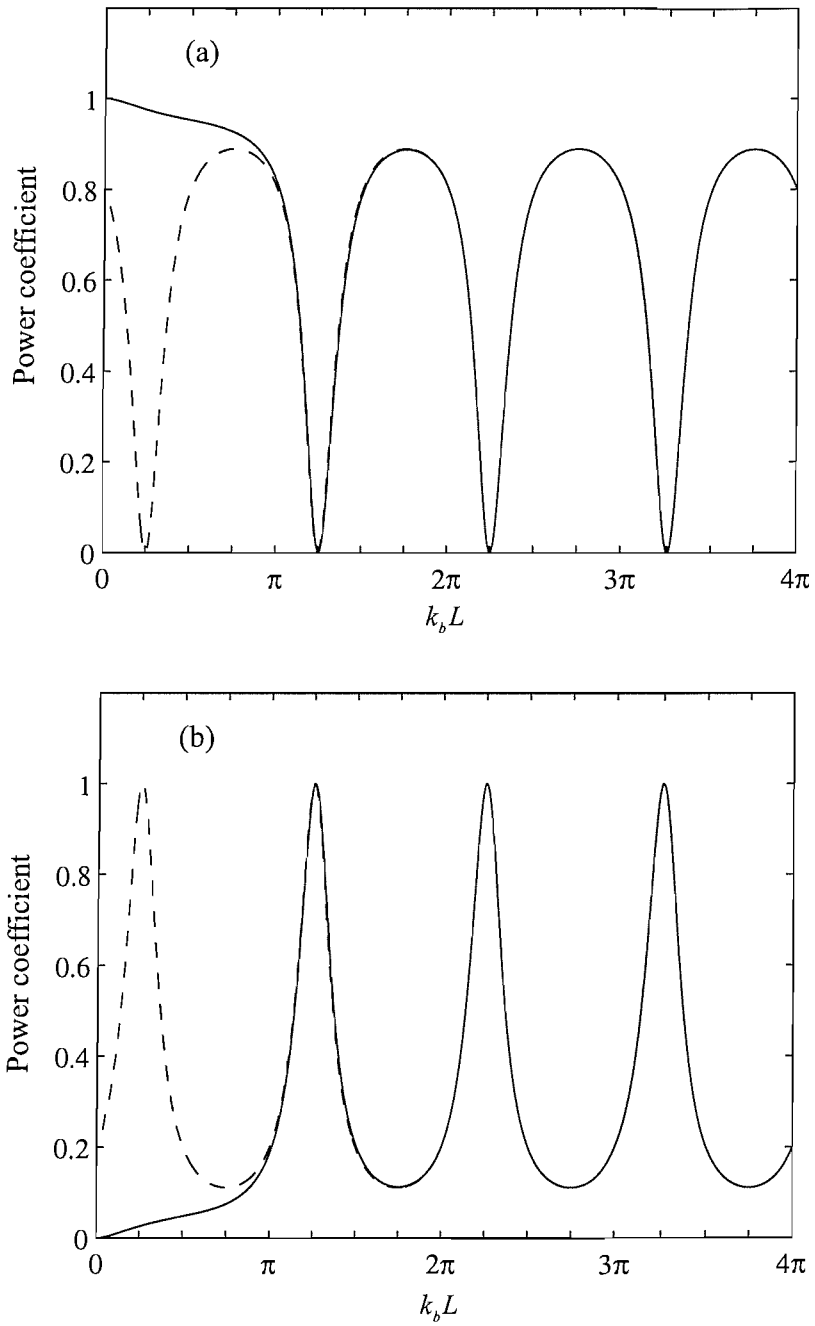

Figure 4-7. Power reflection and transmission coefficients of bending waves in a beam with two simple supports: (a) reflection coefficient, (b) transmission coefficient; ——, including nearfield wave components (exact), ------, excluding nearfield wave components (approximate).

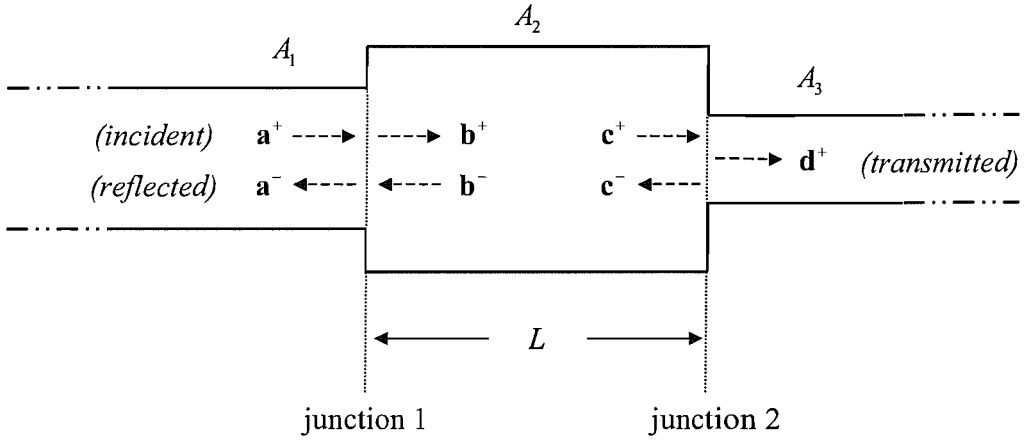

Figure 4-8. Reflection and transmission of bending waves in a straight beam where cross-section area changes twice discontinuously, $A_1 \to A_2 \to A_3$.

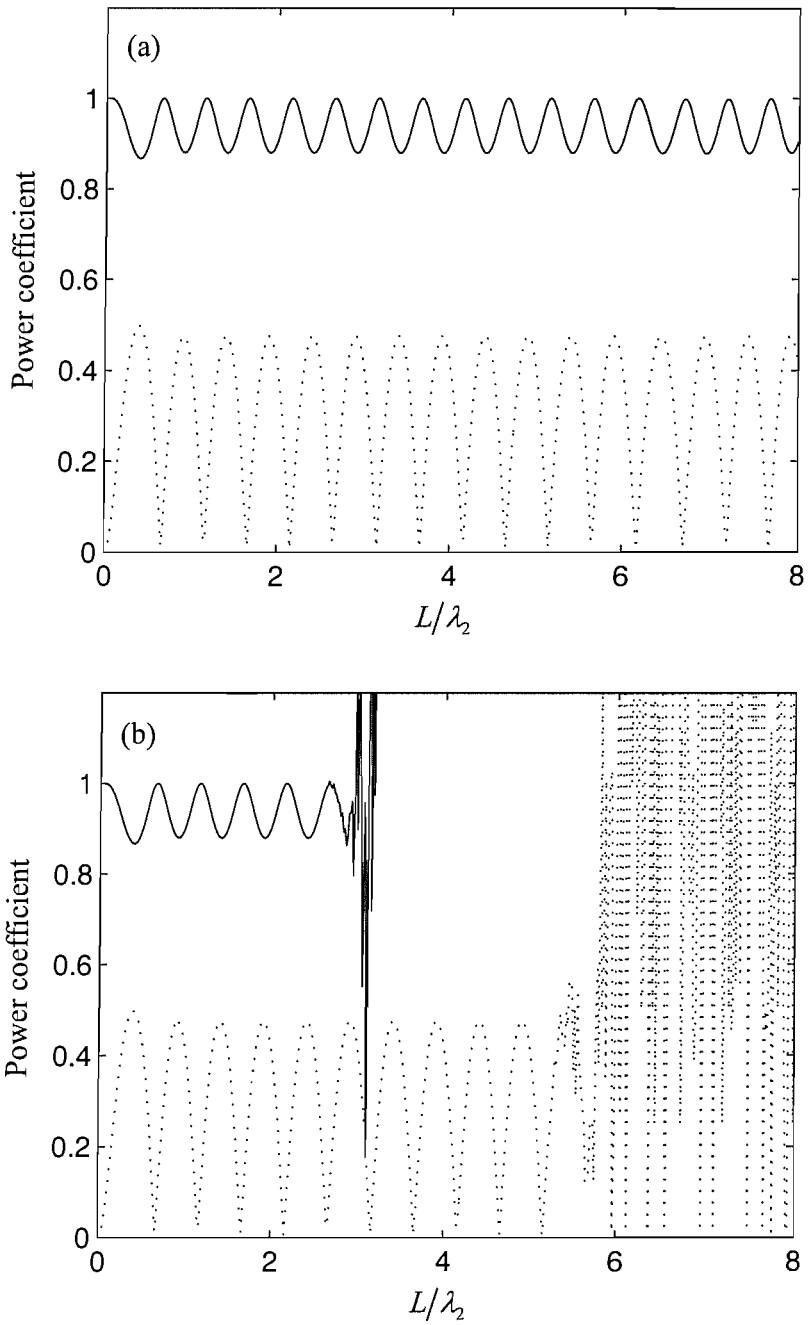

Figure 4-9. Reflection and transmission coefficients for thickness changes, $h \to 2h \to h$, obtained (a) by the approach based on reflection, transmission and propagation of waves, (b) by the approach based on transfer matrix method; ——— , $T_{T,11}$; ..... , $R_{T,11}$.

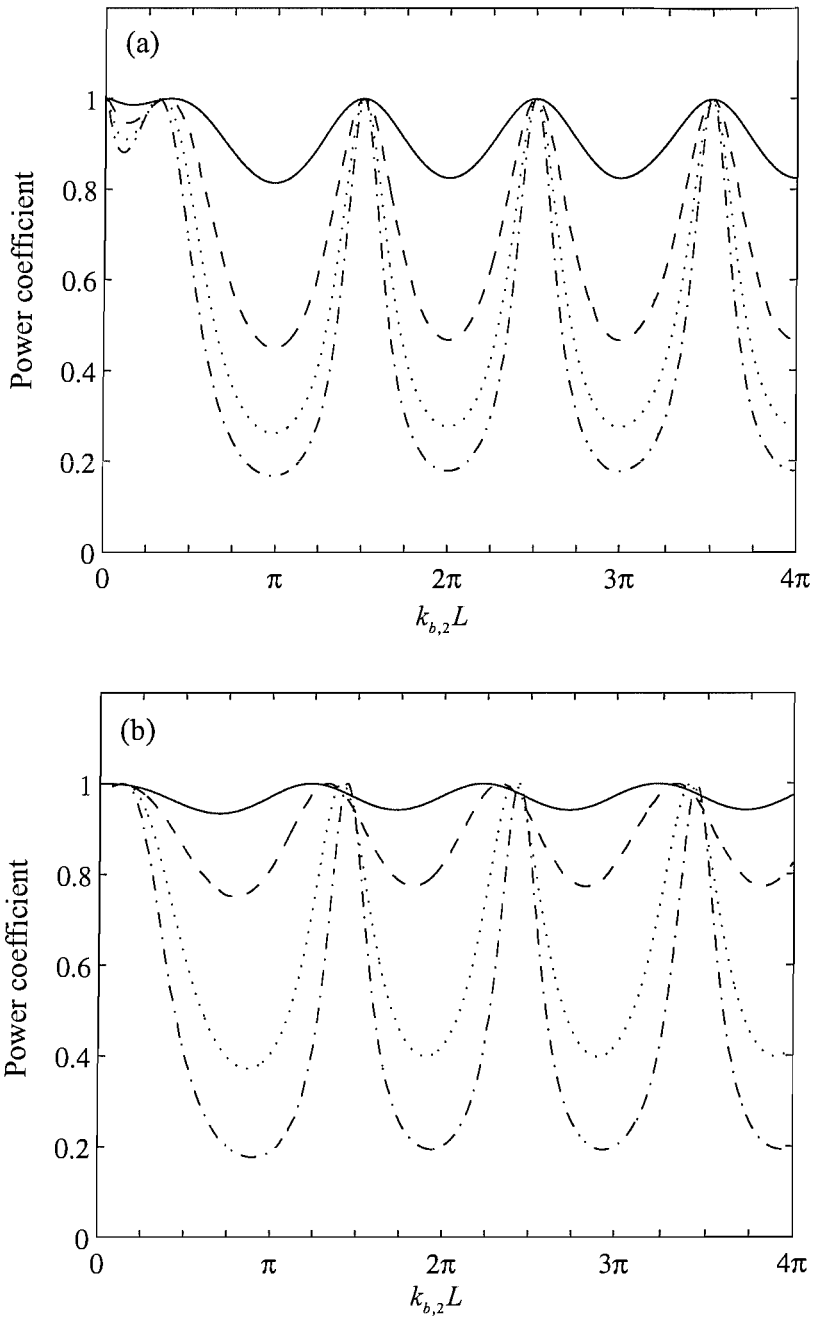

Figure 4-10. Power transmission coefficients (a) for various width changes; ——, $b \to 4b \to b$; ------, $b \to 8b \to b$; ·····, $b \to 12b \to b$; -·-·-·-, $b \to 16b \to b$; (b) for various thickness changes; ——, $h \to 1.5h \to h$; ------, $h \to 2h \to h$; ·····, $h \to 3h \to h$; -·-·-·-, $h \to 4h \to h$.

Chapter 5.

WAVE MOTION IN NON-UNIFORM, STRAIGHT BARS

5.1 Introduction

In the previous two chapters, the wave approach based on reflection, transmission and propagation of waves was applied to cases concerning uniform, straight structures. There is a class of waveguides, which are not uniform but in which waves can propagate without reflection as they do in uniform waveguides. This class was categorised as deterministically varying waveguides in chapter 1. Even though little work has been done previously on this subject, the wave approach can be applied to cases concerning deterministically varying waveguides in a same manner as that for uniform waveguides. In this chapter, one such deterministically varying waveguide is studied – a straight bar undergoing longitudinal motion where the cross-sectional area varies as $A(x) \propto x^{\mu}$ where μ is a non-negative constant. This is an example of a deterministically varying, one-mode system. In chapter 6, wave motion of a deterministically varying, two-mode system is described. Several other cases are listed in section 8.3 as well.

In section 5.2, the governing equation for a straight bar undergoing longitudinal motion is reviewed. If the area of the bar varies in a power-law manner, the motion can be expressed as a linear combination of Hankel functions of the first and second kinds. In section 5.3, the displacement, internal force and propagation matrices for the bar are

defined. Note again that the vectors and matrices for the longitudinal motion consist of only one element.

Using the matrix formulation, wave generation by a force, reflection and transmission of waves at discontinuities, reflection of waves at boundaries, and spectral elements are described in sections 5.4 to 5.7.

In sections 5.8 and 5.9, the energy flow associated with waves in the non-uniform bar is described. The energy transport velocity, which is generally different to the group velocity, for the non-uniform bar is derived exactly using the relationship between power and energy density.

In section 5.10, numerical results are presented for the transmission of longitudinal waves through a tapered connector.

5.2 Equation of motion

The axial displacement $u(x,t)$ for the free vibration of a straight bar at position x and time t is governed by

$$\frac{\partial}{\partial x}\left[EA\frac{\partial u}{\partial x}\right] = \rho A\frac{\partial^2 u}{\partial t^2} \tag{5.1}$$

In section 3.2, it was shown that the solution to equation (5.1) can be easily obtained when the bar is uniform. Now, assume that the material properties of the bar are constant again but, as shown in Figure 5-1, the cross-sectional area A varies as

$$A(x) = \alpha_A x^{\mu} \tag{5.2}$$

where $\alpha_A > 0$, $x > 0$ is the position from the apex (the point at which the area becomes zero when the bar is extended as shown in Figure 5-1), and $\mu \geq 0$ is the flaring index (μ can be negative but here attention is focused on the gradually increasing bars along

x). When $\mu = 0, 1, 2$, the bar could be uniform, linearly tapered in thickness, and conical, respectively. Assuming an $e^{i\omega t}$ time dependence but suppressing it here for clarity, substituting equation (5.2) into equation (5.1) gives

$$\frac{d^2u}{dx^2} + \frac{\mu}{x}\frac{du}{dx} + k_l^2 u = 0 \tag{5.3}$$

where $k_l = \sqrt{\rho\omega^2/E}$ is the longitudinal wavenumber. No damping is present here so that k_l is a positive-real constant.

Equation (5.3) is a form of Bessel's equation. The general solution can be expressed in terms of a linear combination of the Hankel functions of the first and second kinds of order $\nu = (\mu - 1)/2$ with argument $k_l x$, i.e. $H_\nu^{(1,2)}(k_l x)$ (McLachlan 1955). Since the terms $H_\nu^{(1,2)}(k_l x)$ can be considered to represent negative- and positive-going waves, respectively, the displacement is simply expressed as

$$u(x) = a^+(x) + a^-(x) \tag{5.4}$$

where a^+ and a^- are the amplitudes of the waves given by

$$a^+ = x^{-\nu} H_\nu^{(2)}(k_l x) C_1, \qquad a^- = x^{-\nu} H_\nu^{(1)}(k_l x) C_2 \tag{5.5a,b}$$

where C_1 and C_2 are arbitrary constants. The axial force P is then

$$P(x) = -EAk_l \frac{H_{\nu+1}^{(2)}(k_l x)}{H_\nu^{(2)}(k_l x)} a^+ - EAk_l \frac{H_{\nu+1}^{(1)}(k_l x)}{H_\nu^{(1)}(k_l x)} a^- \tag{5.6}$$

Note that the amplitude a is defined such that the displacement $u(x)$ is determined directly from $a^\pm$, i.e., the amplitude a represents the amplitude of a *displacement wave.*

5.3 The wave description

In this section, equations (5.4) and (5.6) are re-expressed in forms of the vectors and matrices introduced in equation (2.17). When $\mathbf{w} = \{u\}$, $\mathbf{f} = \{P\}$, $\mathbf{a}^+ = \{a^+\}$ and $\mathbf{a}^- = \{a^-\}$, the displacement and internal force matrices for the non-uniform bars are

$$\Psi^+ = [1], \qquad \Psi^- = [1],$$
$$\Phi^+ = \left[-EAk_l \frac{H_{\nu+1}^{(2)}(k_l x)}{H_\nu^{(2)}(k_l x)}\right], \qquad \Phi^- = \left[-EAk_l \frac{H_{\nu+1}^{(1)}(k_l x)}{H_\nu^{(1)}(k_l x)}\right] \tag{5.7a,b,c,d}$$

Note that the internal force matrices are function of x. When $k_l x >> 1$ (i.e. the frequency is high such that $x >> \lambda_l/2\pi$, where λ_l is the wavelength), the internal force matrices asymptote (see Appendix A) to those for the uniform bar, i.e.,

$$\Phi^+ \approx [-\mathrm{i}EAk_l], \qquad \Phi^- \approx [\mathrm{i}EAk_l] \tag{5.8a,b}$$

These matrices also satisfy

$$\begin{aligned} \left(\Psi^+\right)^T \Phi^+ &= \left(\Phi^+\right)^T \Psi^+, \\ \left(\Psi^-\right)^T \Phi^- &= \left(\Phi^-\right)^T \Psi^-, \\ \left(\Psi^+\right)^T \Phi^- - \left(\Phi^+\right)^T \Psi^- &= \Lambda \end{aligned} \tag{5.9a,b,c}$$

where the diagonal matrix Λ for this case is

$$\Lambda(x) = \left[\frac{\mathrm{i}4EA}{\pi x \left|H_\nu^{(2)}(k_l x)\right|^2}\right] \tag{5.10}$$

The propagation matrix $\mathbf{F}$ relating the amplitudes of waves at two points x and $x+L$ are defined as

$$\mathbf{a}^+(x+L) = \mathbf{F}^+\mathbf{a}^+(x), \qquad \mathbf{a}^-(x) = \mathbf{F}^-\mathbf{a}^-(x+L) \tag{5.11a,b}$$

Combined with equation (5.5), they are obtained as

$$\mathbf{F}^{+}=\left[\left(\frac{x}{x+L}\right)^{\nu}\frac{H_{\nu}^{(2)}(k_l x+k_l L)}{H_{\nu}^{(2)}(k_l x)}\right],\quad \mathbf{F}^{-}=\left[\left(\frac{x+L}{x}\right)^{\nu}\frac{H_{\nu}^{(1)}(k_l x)}{H_{\nu}^{(1)}(k_l x+k_l L)}\right] \tag{5.12a,b}$$

There is a simple relation between them such that

$$\mathbf{F}^{+}\mathbf{\Lambda}(x+L)=\mathbf{\Lambda}(x)\mathbf{F}^{-} \tag{5.13}$$

where $\mathbf{\Lambda}$ is given by equation (5.10). When $k_l x >> 1$, the matrices asymptote to

$$\mathbf{F}^{+}\approx\left(\frac{x}{x+L}\right)^{\frac{\mu}{2}}\left[e^{-ik_l L}\right],\quad \mathbf{F}^{-}\approx\left(\frac{x+L}{x}\right)^{\frac{\mu}{2}}\left[e^{-ik_l L}\right] \tag{5.14a,b}$$

This indicates that, at high frequencies or if the point x is far from the apex, waves in the non-uniform bars propagate as they do in the uniform bar with their amplitudes scaled by the square root of the ratio of the cross-sectional area (or generally the characteristic impedances defined by $A\sqrt{E\rho}$) at each end of the section.

5.4 Wave generation by local excitation

The displacement, internal force and propagation matrices for the non-uniform bars with a power-law variation in area were defined in the previous section. These matrices can be used in a systematic way for solving various problems concerning the bars. First, the response of the bars to a local external force is investigated in this section.

5.4.1 For bars of gradually increasing area

Consider a non-uniform bar with a power-law variation in cross-sectional area as equation (5.2). When the left-hand end is excited by the time-harmonic longitudinal force $f_{ext}e^{i\omega t}$ as shown in Figure 5-2(a), the equilibrium condition at the end is given by

$$-P(x)=f_{ext};\qquad -\mathbf{\Phi}^{+}\mathbf{q}^{+}=\{f_{ext}\} \tag{5.15}$$

where $\mathbf{q}^+$ is a vector of the amplitude of the induced wave. Substituting the internal force matrix given by equation (5.7c) into equation (5.15) gives

$$\mathbf{q}^+ = \left\{ \frac{1}{EAk_l} \frac{H_\nu^{(2)}(k_l x)}{H_{\nu+1}^{(2)}(k_l x)} \right\} f_{ext} \tag{5.16}$$

Specifically, when $\mu = 0$ (i.e., $\nu = -1/2$), $\mathbf{q}^+$ reduces to (see Appendix A)

$$\mathbf{q}^+ = \left\{ \frac{1}{\mathrm{i}EAk_l} \right\} f_{ext} \tag{5.17}$$

Note that the amplitude of the induced wave is identical to that of a uniform bar. When $\mu = 2$ (i.e., $\nu = 1/2$, a "conical" bar), equation (5.16) reduces to

$$\mathbf{q}^+ = \left\{ \frac{x}{EA} \frac{1}{\mathrm{i}k_l x + 1} \right\} f_{ext} \tag{5.18}$$

Compared to the case of the uniform bar where $\mathbf{q}^+ = f_{ext}/(\mathrm{i}EAk_l)$, the non-uniformity of the bar introduces a stiffness-like term EA/x as well as the damping-like term $\mathrm{i}EAk_l$. The stiffness term becomes dominant when $k_l x << 1$. When $k_l x >> 1$, the stiffness term becomes negligible and the amplitude asymptotes to that of the uniform bar.

5.4.2 For bars of gradually decreasing area

Now consider the case where the longitudinal force excites the right-hand end as shown in Figure 5-2(b), i.e., the response of the gradually decreasing bars to the external force. The equilibrium condition at the end is

$$P(x) = f_{ext}; \qquad \Phi^- \mathbf{q}^- = \{ f_{ext} \} \tag{5.19}$$

Substituting the internal force matrix given by equation (5.7d) into equation (5.19) gives

$$\mathbf{q}^- = \left\{ -\frac{1}{EAk_l} \frac{H_\nu^{(1)}(k_l x)}{H_{\nu+1}^{(1)}(k_l x)} \right\} f_{ext} \tag{5.20}$$

Note that reflection from the apex is ignored in the derivation of equation (5.20).

Specifically, when $\mu = 0$, $\mathbf{q}^-$ reduces to that of that of a uniform bar, i.e., $\mathbf{q}^- = f_{ext}/(\mathrm{i}EAk_l)$. When $\mu = 2$,

$$\mathbf{q}^- = \left\{ \frac{x}{EA} \frac{1}{\mathrm{i}k_l x - 1} \right\} f_{ext} \tag{5.21}$$

Compared to equation (5.18), the sign of the additional term EA/x due to the non-uniformity is now negative, which means that the mass-like behaviour is dominant at low frequencies in this case. Note that $\frac{EA}{x} = \frac{\rho A x \omega^2}{k_l^2 x^2}$.

5.4.3 When a section is excited

Now a point of the bar is excited by the force as shown in Figure 5-2(c). The continuity condition at the point makes the amplitudes of the positive- and negative-going waves induced by the force identical at the excitation point in this case, i.e.,

$$\mathbf{q}^+ = \mathbf{q}^- \tag{5.22}$$

The equilibrium condition at the point is given by

$$-\Phi^+ \mathbf{q}^+ + \Phi^- \mathbf{q}^- = f_{ext} \tag{5.23}$$

Substituting equation (5.22) into equation (5.23) gives

$$\mathbf{q}^+ = \left\{ \frac{\pi x}{\mathrm{i}2EA} \left| H_\nu^{(2)}(k_l x) \right|^2 \right\} \frac{f_{ext}}{2} \tag{5.24}$$

Note that the response is purely imaginary, which indicates that the reactive elements cancel each other and the response is governed by the damping term as with a uniform bar. When $\mu = 0$ and $\mu = 2$, the amplitude reduces to

$$\mathbf{q}^{+} = \left\{ \frac{1}{\mathrm{i}2EAk_l} \right\} f_{ext} \tag{5.25}$$

which is identical to that of a uniform bar.

5.4.4 Numerical results

Figures 5-3 and 5-4 show the amplitudes of the induced waves in the non-uniform bars when the left and right-hand ends of the bar are excited, respectively. The magnitude is normalised by the magnitude of the wave that would be induced in the uniform bar, i.e. f_{ext}/EAk_l. The magnitudes in the two cases are equal but the phases are symmetric about $-\pi/2$. When $k_l x << 1$, for the gradually increasing bar the phase asymptotes to zero (i.e. stiffness-dominated) while for the gradually decreasing bar the phase asymptotes to $-\pi$ (i.e. mass-dominated).

Figure 5-5 shows the amplitudes of the waves induced in the non-uniform bars when an internal point is excited. In the figure the magnitudes are normalised by $f_{ext}/2EAk_l$. The magnitude for the case of $\mu = 2$ (i.e., conical bar) is the same as that for the case of $\mu = 0$ (i.e., uniform bar) so that they cannot be distinguished. The response of the bar for which $\mu = 3$ is larger than that of the uniform bar. The phases for all cases are equal to $-\pi/2$ and are independent of frequency.

5.5 Reflection and transmission at discontinuities

Consider a case where two different non-uniform bars are directly connected as shown in Figure 5-6. The material properties of the two bars are the same. The area of the left-hand bar, indicated by bar A in the figure, varies as

$$A(x) = \alpha_a x^{\mu_a} \tag{5.26}$$

where the subscripts a denote bar A. The position of the junction from the apex is x_a so that the area A_a of bar A at the junction is $A_a = \alpha_a x_a^{\mu_a}$. Meanwhile the area of the right-hand bar, indicated by bar B in the figure, varies as

$$A(x) = \alpha_b x^{\mu_b} \tag{5.27}$$

where the subscripts b denote bar B. The position of the junction from the apex is x_b so that the area A_b of bar B at the junction is $A_b = \alpha_b x_b^{\mu_b}$. The two bars are generally different so that α_b, μ_b and x_b for bar A may be not equal to α_a, μ_a and x_a of bar B, respectively.

The axial displacement and internal force are continuous at the junction, namely,

$$\begin{aligned} \boldsymbol{\Psi}_a^{+}\mathbf{a}^{+} + \boldsymbol{\Psi}_a^{-}\mathbf{a}^{-} &= \boldsymbol{\Psi}_b^{+}\mathbf{b}^{+}, \\ \boldsymbol{\Phi}_a^{+}\mathbf{a}^{+} + \boldsymbol{\Phi}_a^{-}\mathbf{a}^{-} &= \boldsymbol{\Phi}_b^{+}\mathbf{b}^{+} \end{aligned} \tag{5.28a,b}$$

Combined with the displacement and internal force matrices given by equations (5.7), the reflection and transmission matrices for the junction are determined to be

$$\mathbf{R} = \begin{bmatrix} -\dfrac{\dfrac{A_b}{A_a}\dfrac{H_{\nu_b+1}^{(2)}(k_l x_b)}{H_{\nu_b}^{(2)}(k_l x_b)} - \dfrac{H_{\nu_a+1}^{(2)}(k_l x_a)}{H_{\nu_a}^{(2)}(k_l x_a)}}{\dfrac{A_b}{A_a}\dfrac{H_{\nu_b+1}^{(2)}(k_l x_b)}{H_{\nu_b}^{(2)}(k_l x_b)} - \dfrac{H_{\nu_a+1}^{(1)}(k_l x_a)}{H_{\nu_a}^{(1)}(k_l x_a)}} \end{bmatrix}, \quad \mathrm{T} = \begin{bmatrix} \dfrac{4\mathrm{i}}{\pi k_l x_a \left| H_{\nu_a}^{(2)}(k_l x_a) \right|^2} \\ \dfrac{A_b}{A_a}\dfrac{H_{\nu_b+1}^{(2)}(k_l x_b)}{H_{\nu_b}^{(2)}(k_l x_b)} - \dfrac{H_{\nu_a+1}^{(1)}(k_l x_a)}{H_{\nu_a}^{(1)}(k_l x_a)} \end{bmatrix} \tag{5.29a,b}$$

where $\nu_a = (\mu_a - 1)/2$ and $\nu_b = (\mu_b - 1)/2$. Similarly, the reflection and transmission matrices $\hat{\mathbf{R}}$ and $\hat{\mathrm{T}}$ for waves incident from the right-hand side of the junction are

$$\hat{\mathbf{R}} = \begin{bmatrix} -\dfrac{\dfrac{A_a}{A_b}\dfrac{H_{\nu_a+1}^{(1)}(k_l x_a)}{H_{\nu_a}^{(1)}(k_l x_a)} - \dfrac{H_{\nu_b+1}^{(1)}(k_l x_b)}{H_{\nu_b}^{(1)}(k_l x_b)}}{\dfrac{A_a}{A_b}\dfrac{H_{\nu_a+1}^{(1)}(k_l x_a)}{H_{\nu_a}^{(1)}(k_l x_a)} - \dfrac{H_{\nu_b+1}^{(2)}(k_l x_b)}{H_{\nu_b}^{(2)}(k_l x_b)}} \end{bmatrix}, \quad \hat{\mathrm{T}} = \begin{bmatrix} -\dfrac{4\mathrm{i}}{\pi k_l x_b \left| H_{\nu_b}^{(2)}(k_l x_b) \right|^2} \\ \dfrac{A_a}{A_b}\dfrac{H_{\nu_a+1}^{(1)}(k_l x_a)}{H_{\nu_a}^{(1)}(k_l x_a)} - \dfrac{H_{\nu_b+1}^{(2)}(k_l x_b)}{H_{\nu_b}^{(2)}(k_l x_b)} \end{bmatrix} \tag{5.30a,b}$$

For a case where $\mu_a = \mu_b = 2$ and $A_a = A_b$ (i.e., they are conical bars and the areas at the junction are equal), $\mathbf{R}$ and $\mathbf{T}$ reduce to

$$\mathbf{R} = \left[\frac{\mathrm{i}\xi}{1-\mathrm{i}\xi}\right], \qquad \mathbf{T} = \left[\frac{1}{1-\mathrm{i}\xi}\right] \tag{5.31a,b}$$

where the dimensionless parameter ξ is given by

$$\xi = \frac{1}{2k_l}\left(\frac{1}{x_b} - \frac{1}{x_a}\right) \tag{5.32}$$

Since $A_a = \alpha_a x_a^2$, $A_b = \alpha_b x_b^2$ and $A_a = A_b$, equation (5.32) can be written as

$$\xi = \frac{1}{2k_l x_a}\left(\sqrt{\frac{\alpha_b}{\alpha_a}} - 1\right) \tag{5.33}$$

Note that the reflection and transmission of waves depend on the position (i.e., x_a in equation (5.33)), as well as the ratio of the taper rates. Note also that, when one of the two bars is uniform rather than conical, the reflection and transmission matrices can be obtained by assuming $x_a \to \infty$ or $x_b \to \infty$ in equation (5.32).

5.6 Reflection at boundaries

Consider a boundary of a non-uniform bar supported by a translational dynamic stiffness $\bar{K}_T$ as shown in Figure 5-7. The area of the non-uniform bar varies in a power-law manner as equation (5.2). The equilibrium condition at the right-hand boundary is

$$\mathbf{\Phi}^+\mathbf{a}^+ + \mathbf{\Phi}^-\mathbf{a}^- = -\bar{K}_T\left(\mathbf{\Psi}^+\mathbf{a}^+ + \mathbf{\Psi}^-\mathbf{a}^-\right) \tag{5.34}$$

Thus the reflection matrix $\mathbf{R}$ for the boundary is given by

$$\mathbf{R} = \left[-\frac{K_T - \dfrac{H_{\nu+1}^{(2)}(k_l x)}{H_{\nu}^{(2)}(k_l x)}}{K_T - \dfrac{H_{\nu+1}^{(1)}(k_l x)}{H_{\nu}^{(1)}(k_l x)}} \right] \tag{5.35}$$

where the dimensionless dynamic stiffness $K_T = \bar{\bar{K}}_T / EAk_l$. Since no damping is present, the magnitude of $\mathbf{R}$ is unity. Similarly, the reflection matrix $\hat{\mathbf{R}}$ for the left-hand boundary can be obtained.

If $K_T = \infty$ (i.e., clamped boundary), the reflection matrix is

$$\mathbf{R}_c = [-1] \tag{5.36}$$

Equation (5.36) indicates that the non-uniformity of the bar has no effect on the reflection of waves at a clamped boundary.

When $K_T = 0$ and $\mu = 2$ (i.e., free boundary for a conical bar), the reflection matrix reduces to

$$\mathbf{R}_f = -\left[\frac{1 + ik_l x}{1 - ik_l x} \right] \tag{5.37}$$

Figure 5-8 shows the phase of the reflection coefficient for a free boundary (i.e., $K_T = 0$) of a non-uniform bar for different values of μ. It is seen that the phase for a left-hand case is the opposite of that for the right-hand case, i.e., $\mathbf{R}_f = \hat{\mathbf{R}}_f^*$ where the superscript * denotes complex conjugate.

5.7 Spectral elements

In section 2.10.2 the dynamic stiffness matrix for an element was defined in terms of the displacement and internal force matrices. Then the dynamic stiffness matrices of the semi-infinite elements extending to $x = +\infty$ or $x = -\infty$ were given by

$$\mathbf{D}^{+\infty} = -\Phi^{+}\left(\Psi^{+}\right)^{-1}, \qquad \mathbf{D}^{-\infty} = \Phi^{-}\left(\Psi^{-}\right)^{-1} \tag{5.38a,b}$$

Substituting equation (5.7) into equation (5.38) gives

$$\mathbf{D}^{+\infty} = \left[EAk_l \frac{H_{\nu+1}^{(2)}(k_l x)}{H_{\nu}^{(2)}(k_l x)}\right], \qquad \mathbf{D}^{-\infty} = \left[-EAk_l \frac{H_{\nu+1}^{(1)}(k_l x)}{H_{\nu}^{(1)}(k_l x)}\right] \tag{5.39a,b}$$

Similarly, the dynamic stiffness matrix for a finite non-uniform bar can be obtained by substituting equations (5.7) and (5.12) into equation (2.66) to give the result, which has been obtained by Banerjee and Williams (1985).

5.8 Energy flow

In section 2.9, the time-averaged power associated with waves in one-dimensional structures was expressed as

$$\Pi = \frac{1}{2}\mathbf{a}^{H}\mathbf{P}\,\mathbf{a} \tag{5.40}$$

where the power matrix $\mathbf{P}$ is

$$\mathbf{P} = \frac{i\omega}{2}\left[\begin{bmatrix} \left(\Psi^{+}\right)^{H}\Phi^{+} & \left(\Psi^{+}\right)^{H}\Phi^{-} \\ \left(\Psi^{-}\right)^{H}\Phi^{+} & \left(\Psi^{-}\right)^{H}\Phi^{-} \end{bmatrix} - \begin{bmatrix} \left(\Phi^{+}\right)^{H}\Psi^{+} & \left(\Phi^{+}\right)^{H}\Psi^{-} \\ \left(\Phi^{-}\right)^{H}\Psi^{+} & \left(\Phi^{-}\right)^{H}\Psi^{-} \end{bmatrix}\right] \tag{5.41}$$

Substituting the displacement and internal force matrices given by equation (5.7) into equation (5.41) yields

$$\mathbf{P} = \frac{2\omega EA}{\pi x\left|H_{\nu}^{(2)}(k_l x)\right|^2}\begin{bmatrix} 1 & 0 \\ 0 & -1 \end{bmatrix} \tag{5.42}$$

In this case, the power matrix is diagonal so that energy is transported independently by each single wave component and there is no energy transported through the interaction

between the positive- and negative-going components. Thus the time-averaged power associated with a positive-going wave with amplitude a^+ is

$$\Pi = \rho A \omega^2 \left|a^+\right|^2 \frac{c_l}{\pi k_l x} \left|H_\nu^{(2)}(k_l x)\right|^{-2} \tag{5.43}$$

where $c_l = \omega / k_l$ is the phase velocity of the longitudinal wave. Noting that a^+ is given by equation (5.5a), it follows that the power is constant along the bar. This is of course obvious from conservation of energy considerations. Similarly, the time-averaged power associated with a negative-going wave with amplitude a^- is

$$\Pi = -\rho A \omega^2 \left|a^-\right|^2 \frac{c_l}{\pi k_l x} \left|H_\nu^{(1)}(k_l x)\right|^{-2} \tag{5.44}$$

The negative sign indicates that the energy is propagated in the negative direction.

5.9 Energy transport velocity

For uniform bars, the energy transport velocity is equal to the phase velocity. This is generally not true for non-uniform bars. In this section, the energy transport velocity for non-uniform bars with a power-law variation in area is derived.

The kinetic and potential energies per unit length (i.e. the energy densities), $\mathcal{T}$ and $\mathcal{V}$ respectively, for longitudinal motion of a bar are given by (Cremer *et al.* 1973)

$$\mathcal{T} = \frac{1}{2} \rho A \left\{ \mathrm{Re}\left(\frac{\partial u}{\partial t} \right) \right\}^2, \qquad \mathcal{V} = \frac{1}{2} EA \left\{ \mathrm{Re}\left(\frac{\partial u}{\partial x} \right) \right\}^2 \tag{5.45a,b}$$

where $\mathrm{Re}(\cdot)$ denotes the real part of the quantity. If there is only a positive-going wave with amplitude a^+ in the non-uniform bar, the displacement of the bar will be $u(x) = a^+$. For time harmonic motion, the time-averaged energy densities associated with the wave are then

$$\langle \mathcal{T} \rangle = \frac{1}{4}\rho A\omega^2 \left|a^+\right|^2$$
$$\langle \mathcal{V} \rangle = \frac{1}{4}\rho A\omega^2 \left|a^+\right|^2 \left|\frac{H_{\nu+1}^{(2)}(k_l x)}{H_{\nu}^{(2)}(k_l x)}\right|^2 \qquad (5.46a,b)$$

where $\langle \cdot \rangle$ indicates a time-averaged quantity. The total energy density is given by $\mathcal{E} = \langle \mathcal{T} \rangle + \langle \mathcal{V} \rangle$, therefore

$$\mathcal{E} = \frac{1}{4}\rho A\omega^2 \left|a^+\right|^2 \frac{\left|H_{\nu}^{(2)}(k_l x)\right|^2 + \left|H_{\nu+1}^{(2)}(k_l x)\right|^2}{\left|H_{\nu}^{(2)}(k_l x)\right|^2} \qquad (5.47)$$

Figure 5-9 shows the time-averaged kinetic and potential energy densities, normalised by the total energy density, associated with the longitudinal wave in the non-uniform bars with four different values of μ. When $\mu = 0$ (i.e., uniform bar), the kinetic and potential energy densities are the same but, for the other cases, it is seen that $\langle \mathcal{V} \rangle > \langle \mathcal{T} \rangle$ in the region of $k_l x < \pi$. As $k_l x$ increases, the energy densities become the same.

In terms of the total energy density and the power, the energy transport velocity c^E is defined by (Lighthill 1978)

$$c^E = \frac{\Pi}{\mathcal{E}} \qquad (5.48)$$

This energy transport velocity is generally different to the group velocity, which is formally defined by $c_g = \mathrm{d}\omega/\mathrm{d}k$ (for real wavenumbers). Note that, for uniform bars, $c_g = c_l$. Substituting equations (5.47) and (5.43) into equation (5.48) gives

$$c_l^E = \frac{4c_l}{\pi k_l x}\left(\left|H_{\nu}^{(2)}(k_l x)\right|^2 + \left|H_{\nu+1}^{(2)}(k_l x)\right|^2\right)^{-1} \qquad (5.49)$$

The energy transport velocity associated with the negative-going wave is the same as that associated with the positive-going wave as would be expected from physical consideration. Specifically, when $\mu = 2$, equation (5.49) reduces to

$$c_l^E = \frac{c_l}{1+\left(\sqrt{2}k_l x\right)^{-2}} \tag{5.50}$$

Figure 5-10 shows the energy transport velocity, normalized by the longitudinal velocity c_l, for a non-uniform bar. It can be seen that the velocity decreases as μ increases, i.e. as the degree of non-uniformity increases. When $k_l x << 1$, the velocity is approximately proportional to $\left(k_l x\right)^{\mu}$. The velocity increases as $k_l x$ increases and finally asymptotes to that of a uniform bar.

5.10 Numerical examples

Consider a tapered bar of length L connecting two uniform rectangular bars with the same width but different thicknesses, h_1 and h_2, as shown in Figure 5-11. The thickness of the connector varies with x (measured from the apex) as

$$h(x) = h_1 x / x_1 \tag{5.51}$$

where $x_1 = h_1 L/\left(h_2 - h_1\right)$ is the position of junction 1 from the apex. Note that the connector is the non-uniform bar of $\mu = 1$. For simplicity, the material properties of the connector and the bars are assumed to be the same.

Now consider waves $\mathbf{a}^+$ incident on the connector from the left-hand uniform bar. When the relevant waves at the junctions are denoted by $\mathbf{b}^{\pm}$, $\mathbf{c}^{\pm}$ and $\mathbf{d}^+$, the relationships among the waves are

$$
\begin{aligned}
\mathbf{b}^{+} &= \mathbf{T}_1\mathbf{a}^{+} + \hat{\mathbf{R}}_1\mathbf{b}^{-}, \\
\mathbf{c}^{+} &= \mathbf{F}^{+}\mathbf{b}^{+}, \\
\mathbf{c}^{-} &= \mathbf{R}_2\mathbf{c}^{+}, \\
\mathbf{b}^{-} &= \mathbf{F}^{-}\mathbf{c}^{-} \\
\mathbf{a}^{-} &= \mathbf{R}_1\mathbf{a}^{+} + \hat{\mathbf{T}}_1\mathbf{b}^{-}, \\
\mathbf{d}^{+} &= \mathbf{T}_2\mathbf{c}^{+}
\end{aligned}
\qquad (5.52a,b,c,d,e,f)
$$

where $\mathbf{R}_1$, $\mathbf{T}_1$ etc., are the reflection and transmission matrices at the junctions, and $\mathbf{F}^{+}$ and $\mathbf{F}^{-}$ are the propagation matrices between the junctions. The reflection and transmission matrices are obtained in a systematic way by using equation (5.7) with $\nu = 0$ for the connector and equation (3.9) for the uniform bar, as required. The propagation matrices $\mathbf{F}^{+}$ and $\mathbf{F}^{-}$ are given by equation (5.12) with $x = x_1$. Rearranging equations (5.52) in terms of the incident waves $\mathbf{a}^{+}$ yields

$$
\begin{aligned}
\mathbf{a}^{-} &= \left[\mathbf{R}_1 + \hat{\mathbf{T}}_1\mathbf{F}^{-}\mathbf{R}_2\mathbf{F}^{+}[\mathbf{I} - \hat{\mathbf{R}}_1\mathbf{F}^{-}\mathbf{R}_2\mathbf{F}^{+}]^{-1}\mathbf{T}_1\right]\mathbf{a}^{+}, \\
\mathbf{d}^{+} &= \left[\mathbf{T}_2\mathbf{F}^{+}[\mathbf{I} - \hat{\mathbf{R}}_1\mathbf{F}^{-}\mathbf{R}_2\mathbf{F}^{+}]^{-1}\mathbf{T}_1\right]\mathbf{a}^{+}
\end{aligned}
\qquad (5.53a,b)
$$

where $\mathbf{I}$ is the identity matrix.

Figure 5-12 shows the transmission coefficients for the connector when a propagating wave component $\mathbf{a}^{+} = \{a^{+}\}$ is incident. When $k_l L >> 1$, the power transmission coefficient $\tau \to 1$, i.e. the power incident on the connector is totally transmitted when the frequency or length increases. The phase difference θ between the propagating components a^{+} and d^{+} then asymptotes to $-k_l L$. When $k_l L << 1$, the results asymptote to those of the case where the two uniform bars are directly connected without the connector. As the ratio of thickness increases, less power can transmit through the connector.

5.11 Summary

The wave approach based on reflection, transmission and propagation of waves has been applied to one example of deterministically varying waveguides: straight bars undergoing longitudinal motion where the cross-sectional area varies as $A(x) \propto x^{\mu}$ where μ is a non-negative constant. The displacement, internal force and propagation matrices for the bars were defined and used for the systematic analysis of wave motion for various situations such as the wave generation by a force, the reflection and transmission of waves at discontinuities, the reflection of waves at boundaries, and the derivation of the spectral elements.

The effect of non-uniformity becomes larger as the frequency decreases or as the position moves closer to the apex. For example, the response of the gradually increasing bar to the external force exhibits stiffness-dominated behaviour while the response of the gradually decreasing bar exhibits mass-dominated behaviour near the apex. These reactive elements cancel each other when a point is excited: thus the response exhibits damping-like behaviour as with a uniform bar.

The energy transport velocity of the non-uniform bars was also derived. In contrast to that of uniform bars, it is not equal to the phase velocity, and depends on position as well as frequency. It was shown that it decreases as the position moves toward the apex

Finally numerical results were presented for the transmission of longitudinal waves through a tapered connector. It was demonstrated that the approach can predict the dynamic response of cases concerning deterministically varying waveguides without approximation errors, irrespective of frequency.

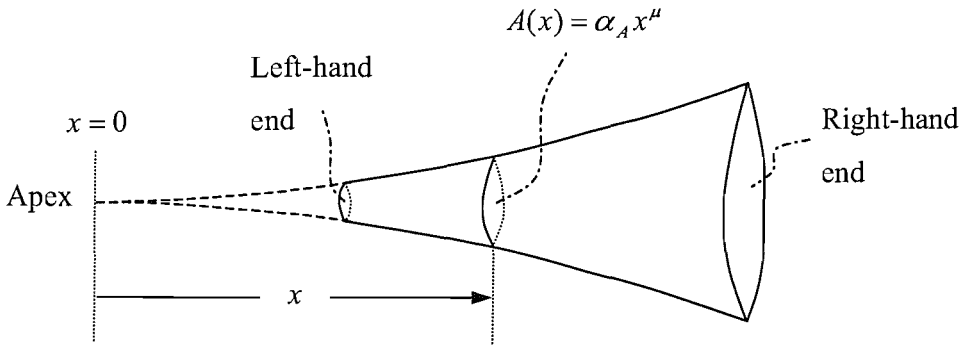

Figure 5-1. A non-uniform, straight bar where the area varies as $A(x) = \alpha_A x^{\mu}$.

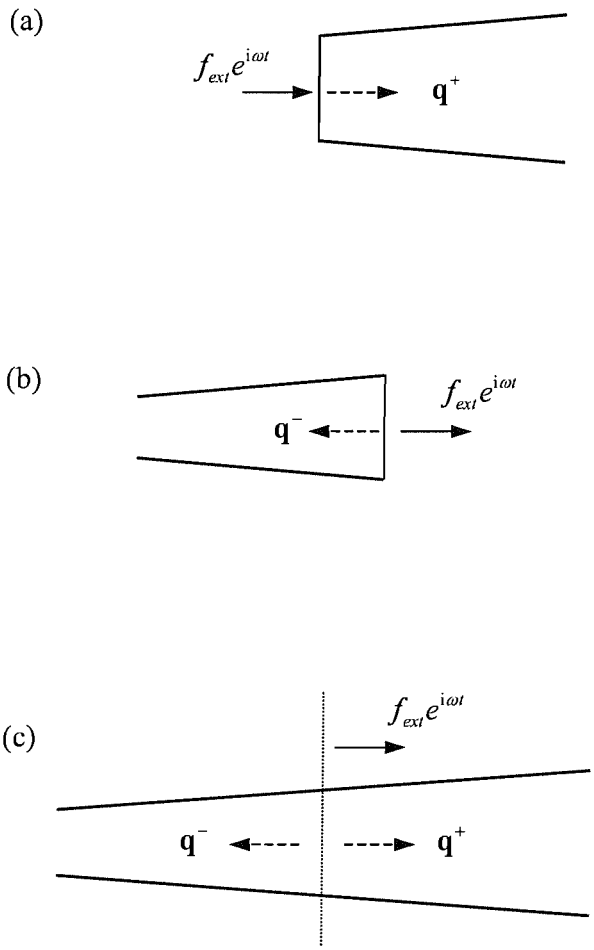

Figure 5-2. Wave generation in a non-uniform bar by a local harmonic force: (a) the left-hand end is excited, (b) the right-hand end is excited, (c) a cross-section is excited.

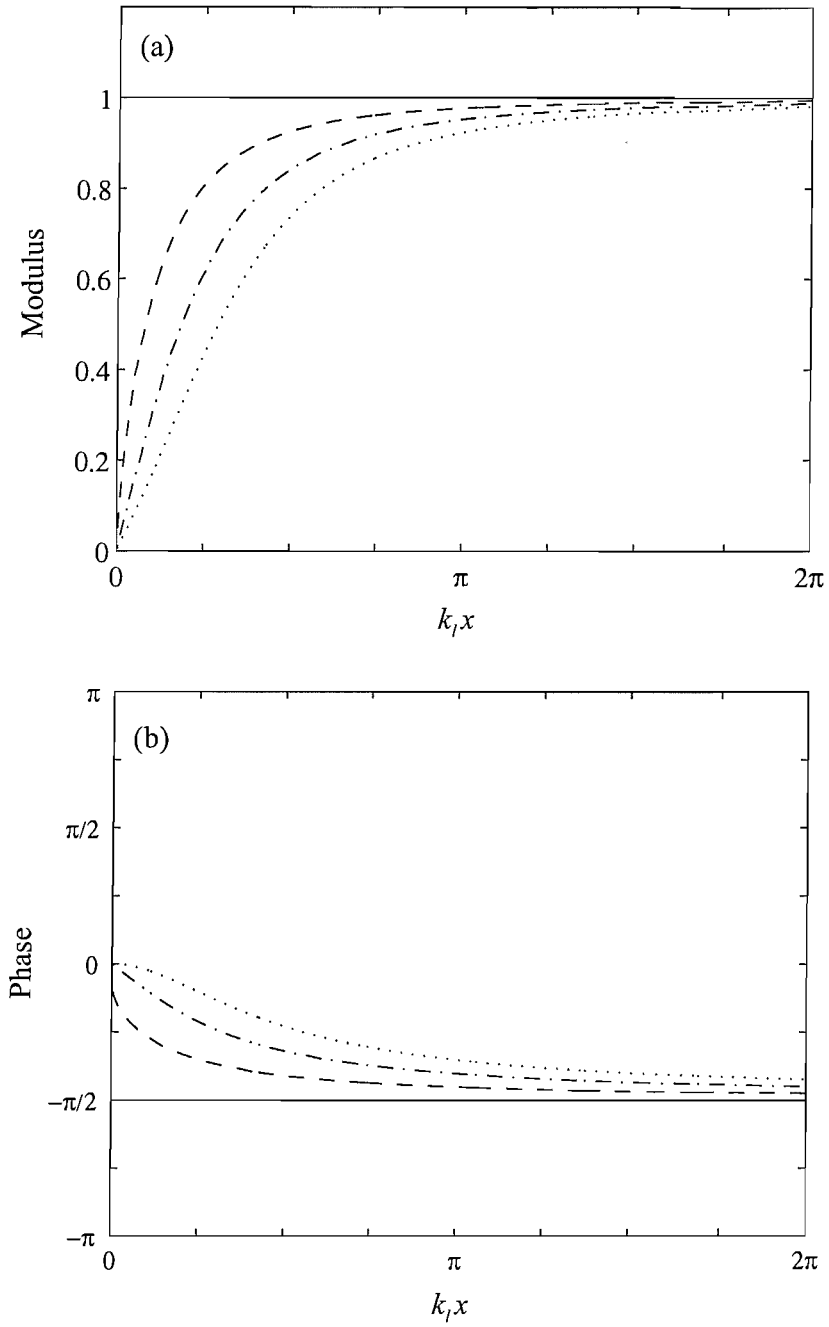

Figure 5-3. Wave generation at the left-hand end of a non-uniform bar with a power-law variation in area as equation (5.2): (a) the magnitude of induced wave, normalised by that in the uniform bar, (b) the phase of induced wave; ——— , $\mu = 0$; ------ , $\mu = 1$; -·-·-· , $\mu = 2$; ····· , $\mu = 3$.

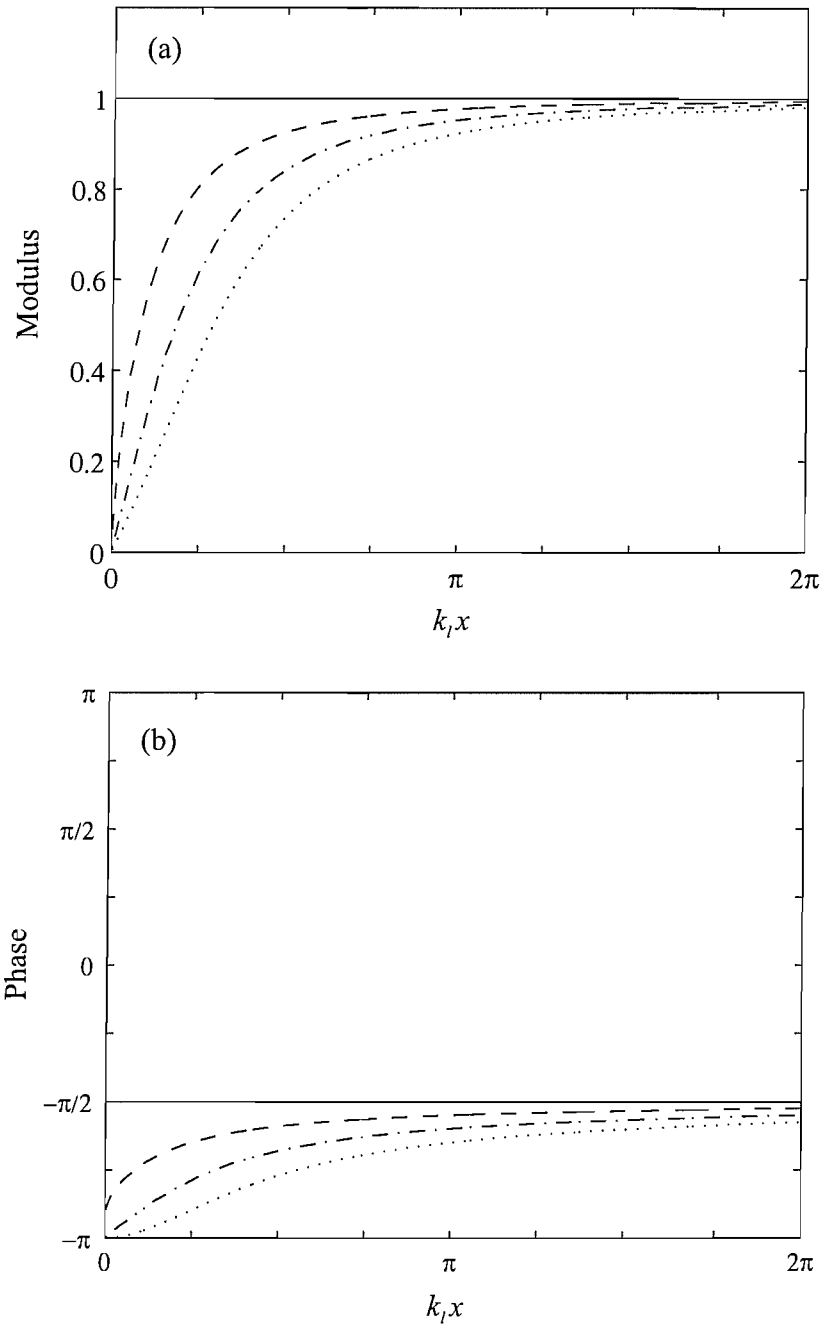

Figure 5-4. Wave generation at the right-hand end of a non-uniform bar with a power-law variation in area as equation (5.2): (a) the amplitude of induced wave, normalised by that in the uniform bar, (b) the phase of induced wave;
——— , $\mu = 0$; ------ , $\mu = 1$; -·-·-·- , $\mu = 2$; ····· , $\mu = 3$.

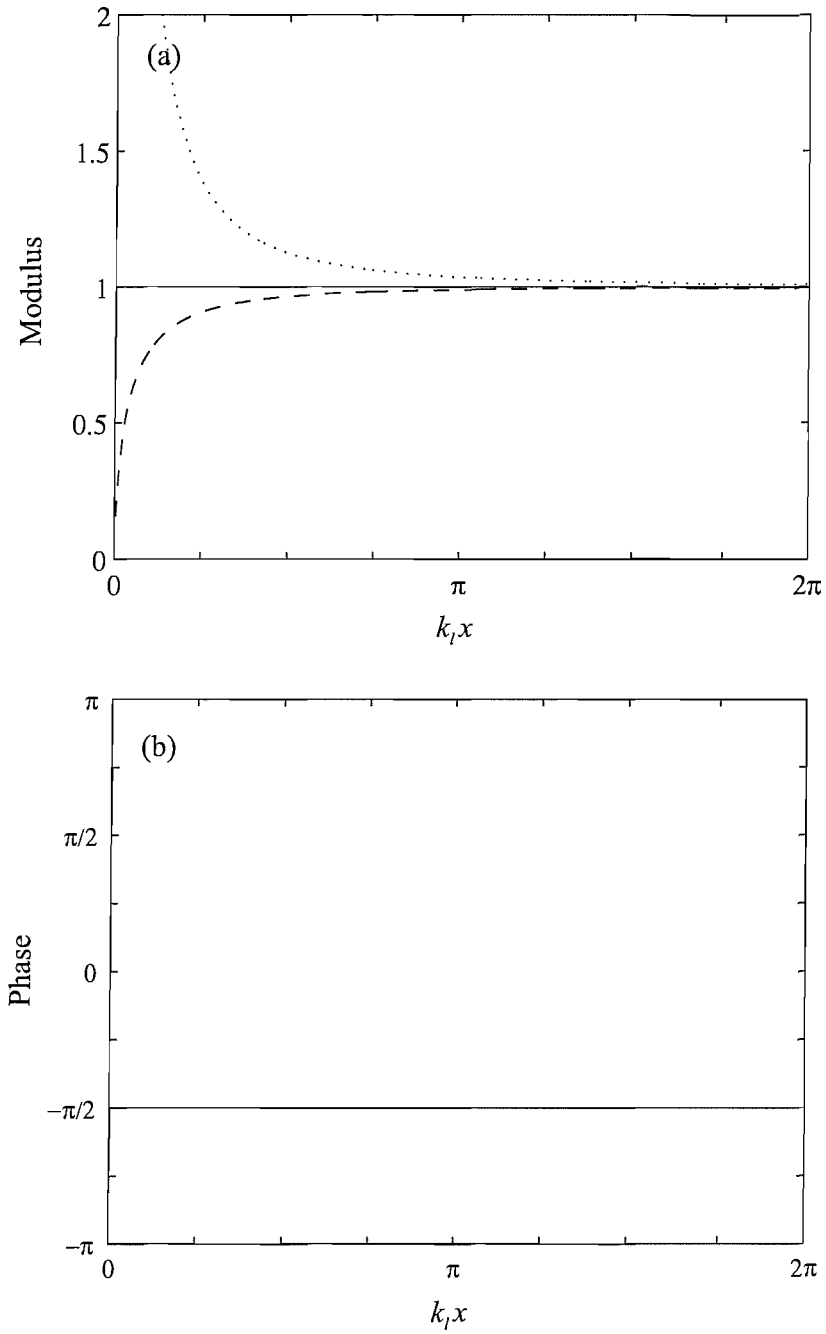

Figure 5-5. Wave generation at the right-hand end of a non-uniform bar with a power-law variation in area as equation (5.2): (a) the amplitude of induced wave normalized by that in the uniform bar, (b) the phase of induced wave; ——— , $\mu = 0$; ------ , $\mu = 1$; -·-·-·- , $\mu = 2$; ····· , $\mu = 3$.

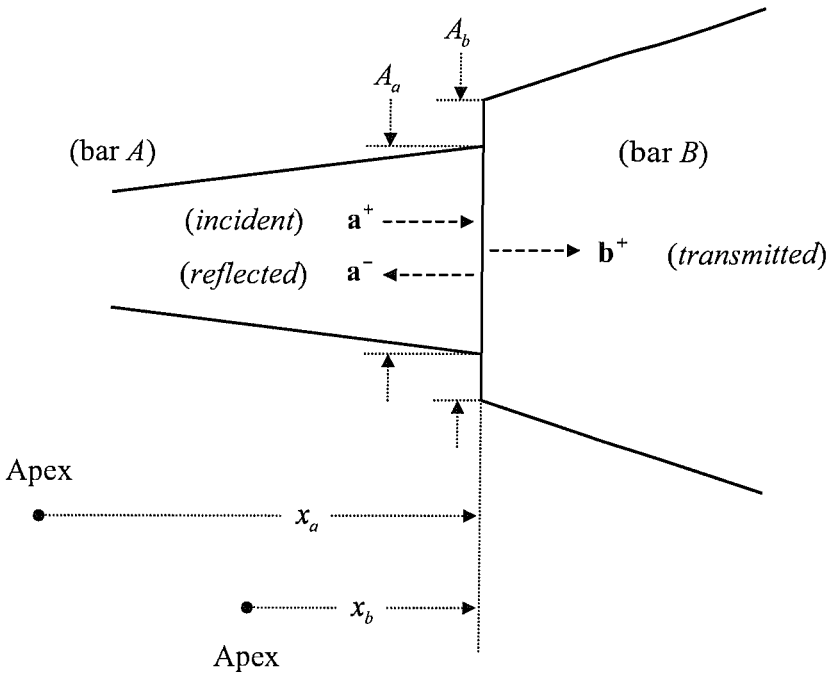

Figure 5-6. Reflection and transmission of waves at a junction between two different non-uniform straight bars.

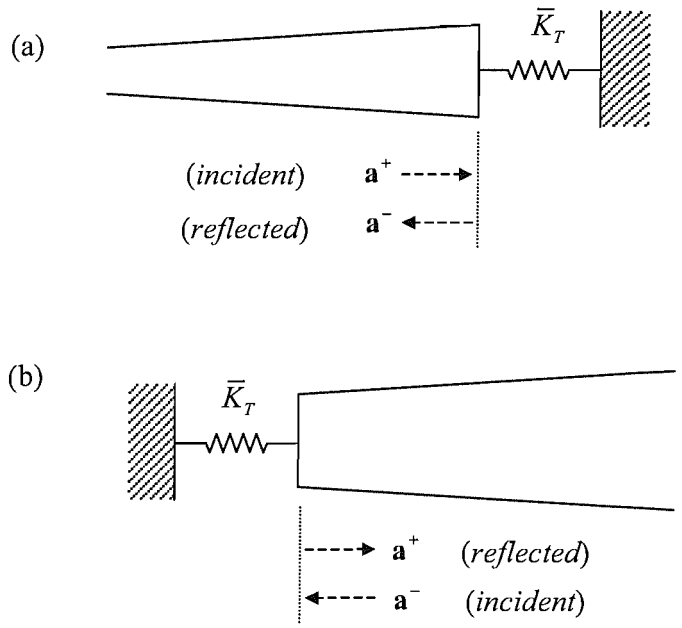

Figure 5-7. Reflection of waves at a boundary of a non-uniform bar supported by a translational dynamic stiffness: (a) right-hand boundary, (b) left-hand boundary.

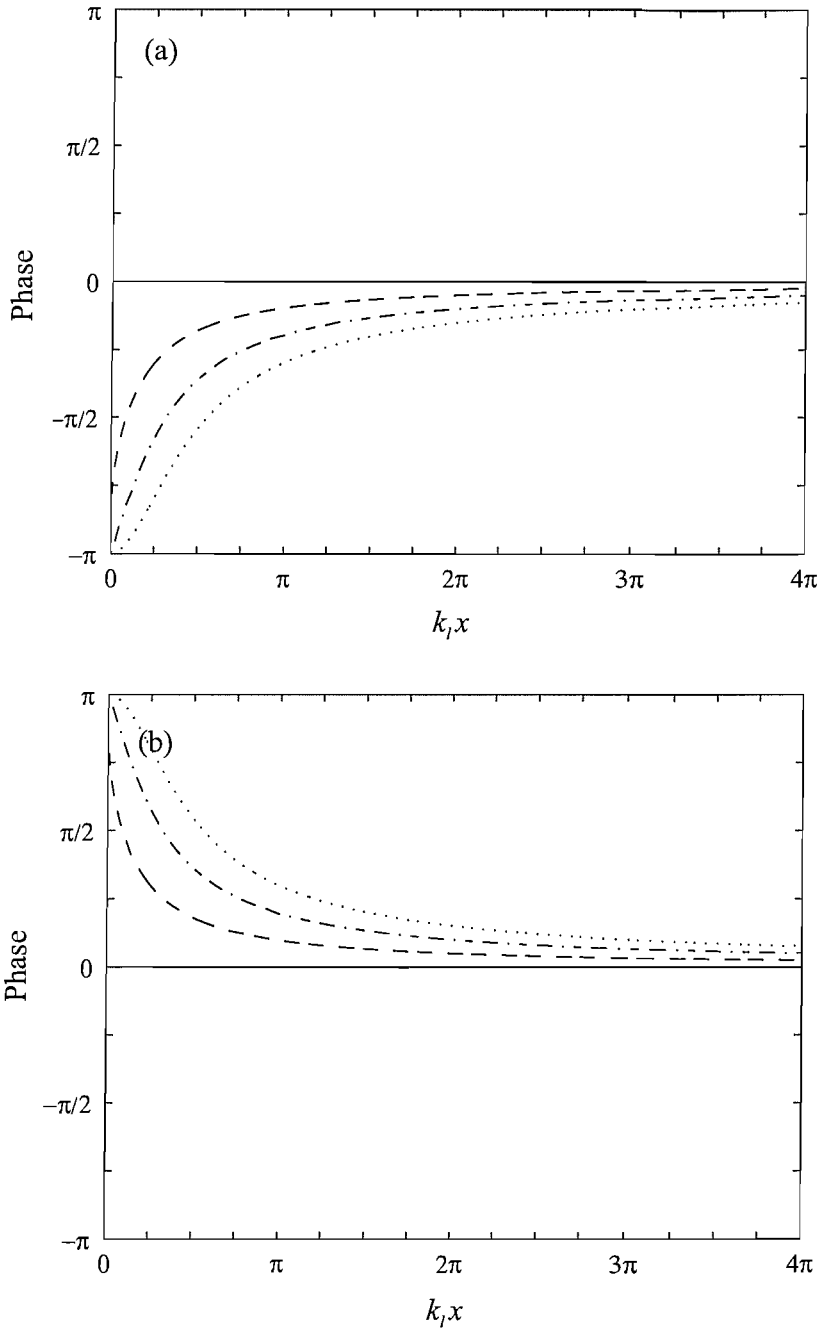

Figure 5-8. Phase of the reflection coefficient for free boundary of a non-uniform bar with a power-law variation in area as in equation (5.2): (a) right-hand boundary, (b) left-hand boundary; ——, $\mu = 0$; - - - - - -, $\mu = 1$; -·-·-·-, $\mu = 2$; ·····, $\mu = 3$.

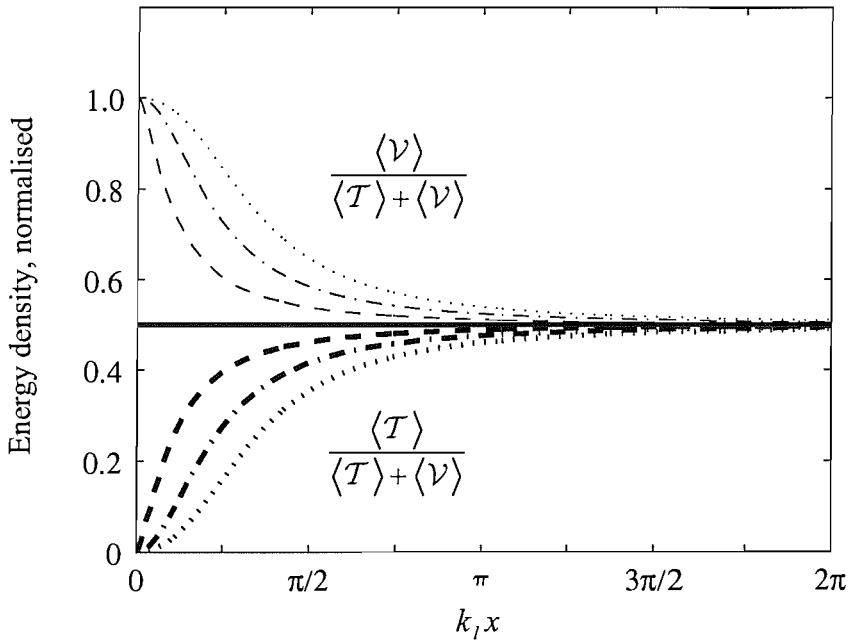

Figure 5-9. Time-averaged kinetic and potential energy densities, normalised by the total energy density, associated with a longitudinal wave in a non-uniform bar with a power-law variation in area as in equation (5.2): ——— , $\mu = 0$; ------ , $\mu = 1$; -·-·-·- , $\mu = 2$; ····· , $\mu = 3$; thin lines are for $\langle \mathcal{V} \rangle / (\langle \mathcal{T} \rangle + \langle \mathcal{V} \rangle)$ and thick lines are for $\langle \mathcal{T} \rangle / (\langle \mathcal{T} \rangle + \langle \mathcal{V} \rangle)$. Note that, when $\mu = 0$ (i.e., uniform bar), the kinetic and potential energy densities are the same.

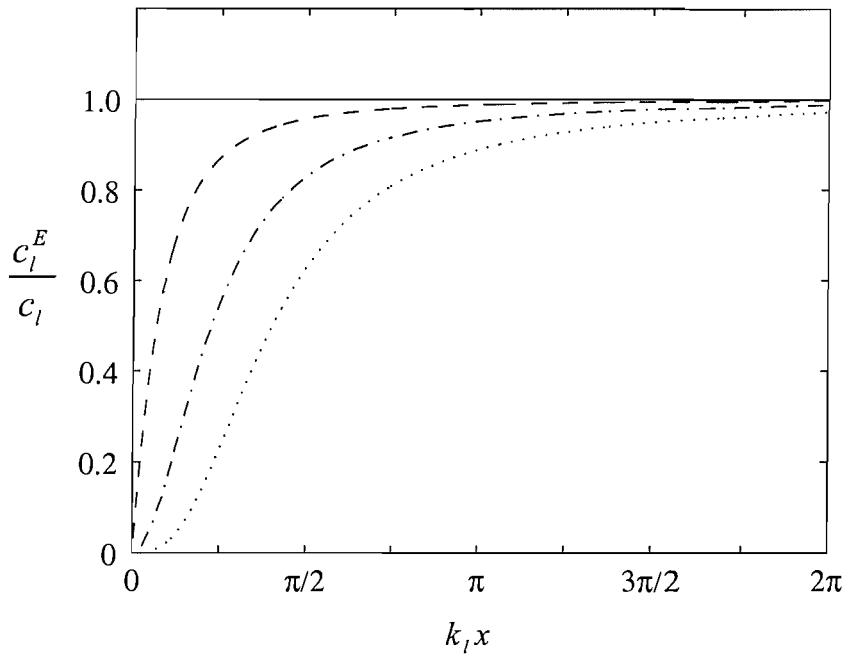

Figure 5-10. Energy transport velocity, normalised by the phase velocity c_l, associated with the longitudinal wave in a non-uniform bar with a power-law variation in area as in equation (5.2): ——— , $\mu = 0$; ------ , $\mu = 1$; -·-·-·- , $\mu = 2$; ····· , $\mu = 3$.

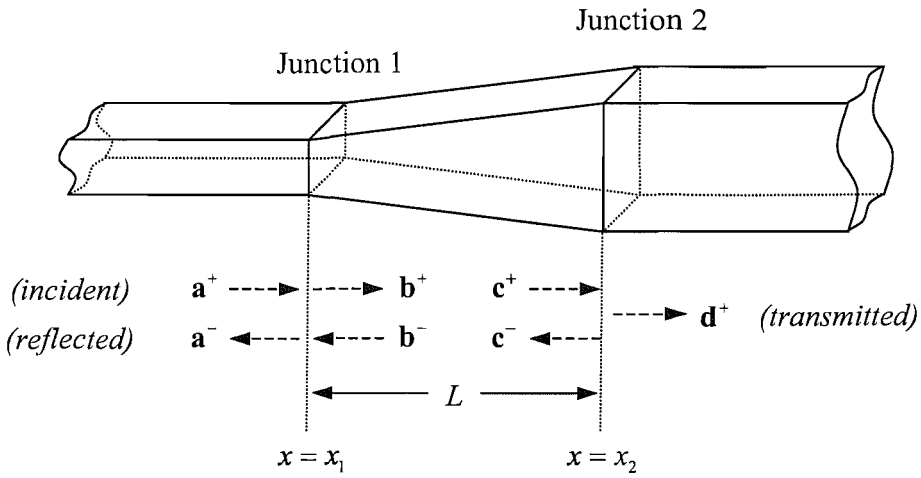

Figure 5-11. A rectangular, non-uniform bar connecting two uniform bars.

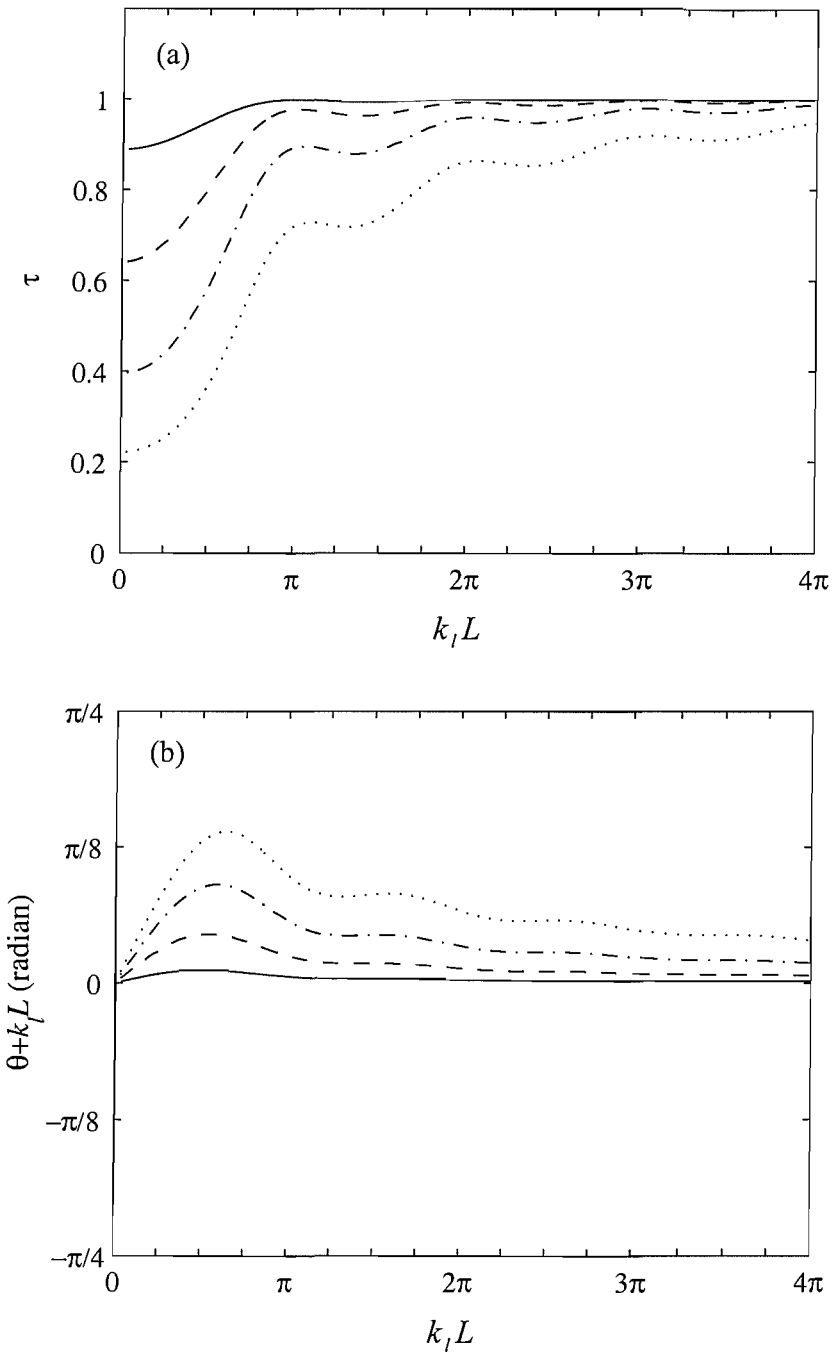

Figure 5-12. Transmission of a longitudinal wave through the connector: (a) the power transmission coefficient τ, (b) phase difference θ between a^+ and d^+, added by $k_l L$; ——, $h_2/h_1 = 2$; - - - - -, $h_2/h_1 = 4$; - · - · -, $h_2/h_1 = 8$; ·····, $h_2/h_1 = 16$.

Chapter 6.

WAVE MOTION IN NON-UNIFORM, STRAIGHT BEAMS

6.1 Introduction

In chapter 5, the wave approach based on reflection, transmission and propagation of waves was applied to one class of deterministically varying waveguides: straight bars with a power-law variation in area, which are a one-mode system. In this chapter, a two-mode deterministically varying waveguide is studied: straight beams where the area and second moment of area vary respectively as powers of x. The systematic formulation is useful since solving the problem explicitly is difficult in these two-mode systems. Note also that, as illustrated in chapter 4, the wave approach provides a well-conditioned computation for these cases.

The development of this chapter is similar to that of chapter 5 for non-uniform bars. In section 6.2, the governing equation for a non-uniform, straight beam is reviewed. The motion is based on Euler-Bernoulli theory. If the cross-sectional area and the second moment of area vary as $A(x) \propto x^{\mu}$ and $I(x) \propto x^{\mu+2}$ where μ is a non-negative constant, the motion can be expressed as a linear combination of Hankel functions of the first and second kinds and the modified Bessel functions. In section 6.3, the displacement, internal force and propagation matrices for the beam are defined. Since the beams are a two-mode system, the matrices are now 2×2.

Wave generation by a force and spectral elements are studied in sections 6.4 to 6.5. As illustrated so far, other problems such as the reflection and transmission of

waves at a discontinuity or boundary can also be solved in a systematic way using the displacement, internal force and propagation matrices. However, since the expressions are too complicated to state explicitly, they are not described here.

In sections 6.6 and 6.7, energy flow associated with bending waves in the non-uniform beam is described. The energy transport velocity, which is generally different from the group velocity, associated with bending waves in the non-uniform beam is derived exactly using the relationship between power and energy density.

In section 6.8, numerical results are presented for the transmission of bending waves through a tapered connector.

6.2 Equation of motion

Consider an Euler-Bernoulli beam undergoing bending motion. The lateral displacement $w(x,t)$ for the free vibration of the beam is governed by

$$\frac{\partial^2}{\partial x^2}\left[EI\frac{\partial^2 w}{\partial x^2}\right]+\rho A\frac{\partial^2 w}{\partial t^2}=0 \tag{6.1}$$

In section 4.2, it was shown that the solution to equation (6.1) can be easily obtained when the beam is uniform. Now, assume that the material properties are constant again but, as shown in Figure 6-1, the cross-sectional area and the second moment of area vary as

$$A(x)=\alpha_A x^{\mu}, \qquad I(x)=\alpha_I x^{\mu+2} \tag{6.2a,b}$$

where $\alpha_A>0$, $\alpha_I>0$, $x>0$ is the position from the apex (the point at which the area and the second moment of area become zero when the beam is extended as shown in Figure 6-1), and $\mu\geq 0$ is the flaring index (μ can be negative but here attention is focused on the gradually increasing beams along x). When $\mu=1$ and the cross-sectional

shape of the beam is rectangular, the beam has linearly varying thickness and constant width. Assuming an $e^{i\omega t}$ time dependence, substituting equation (6.2) into equation (6.1) gives

$$x^2\frac{\mathrm{d}^4 w}{\mathrm{d}x^4}+2(\mu+2)x\frac{\mathrm{d}^3 w}{\mathrm{d}x^3}+(\mu+1)(\mu+2)\frac{\mathrm{d}^2 w}{\mathrm{d}x^2}-k_b^4 x^2 w=0 \tag{6.3}$$

where $k_b=\sqrt[4]{\rho A(x)\omega^2/EI(x)}$ is the flexural wavenumber at position x. In contrast to that for uniform beams, the bending wavenumber k_b now depends on the position as well as frequency, i.e., $k_b(x)\propto\sqrt{\omega/x}$. Hereafter, if there is no specific indication, k_b means the wavenumber $k_b(x)$ at position x.

Equation (6.3) can be factorised into the product of the Bessel equation and the modified Bessel equation (Cranch and Aldler 1956) so that the general solution can be expressed by a linear combination of Hankel functions of order μ with argument $2k_b x$, $H_\mu^{(1,2)}(2k_b x)$, and modified Bessel functions, $K_\mu(2k_b x)$ and $I_\mu(2k_b x)$. The terms $H_\mu^{(1,2)}$ represent negative- and positive-going propagating waves, respectively, and the terms K_μ and I_μ positive- and negative-going nearfield waves, respectively. Thus the solution of equation (6.3) is given by

$$w(x)=a^+ + a_N^+ + a^- + a_N^- \tag{6.4}$$

where a^+, a_N^+, a^-, a_N^- are the amplitudes of the four waves at position x given by

$$\begin{aligned} a^+ &= x^{-\frac{\mu}{2}}H_\mu^{(2)}(2k_b x)C_1, \qquad & a_N^+ &= x^{-\frac{\mu}{2}}K_\mu(2k_b x)C_2, \\ a^- &= x^{-\frac{\mu}{2}}H_\mu^{(1)}(2k_b x)C_3, \qquad & a_N^- &= x^{-\frac{\mu}{2}}I_\mu(2k_b x)C_4, \end{aligned} \tag{6.5,a,b,c,d}$$

where $C_{1,2,3,4}$ are arbitrary constants. The slope $\partial w/\partial x$ and the internal forces defined by equations (4.2) can also be expressed in terms of the amplitudes of the waves, straightforwardly.

6.3 The wave description

Noting that $\mathbf{w}=\left[w \quad \mathrm{d}w/\mathrm{d}x\right]^T$, $\mathbf{f}=\left[Q \quad M\right]^T$, $\mathbf{a}^+=\left[a^+ \quad a_N^+\right]^T$ and $\mathbf{a}^-=\left[a^- \quad a_N^-\right]^T$, the displacement and internal force matrices for the non-uniform beam are given by

$$
\begin{aligned}
\boldsymbol{\Psi}^+ &= \begin{bmatrix} 1 & 1 \\ -k_b \dfrac{H_{\mu+1}^{(2)}(2k_bx)}{H_\mu^{(2)}(2k_bx)} & -k_b \dfrac{K_{\mu+1}(2k_bx)}{K_\mu(2k_bx)} \end{bmatrix}, \\
\boldsymbol{\Psi}^- &= \begin{bmatrix} 1 & 1 \\ -k_b \dfrac{H_{\mu+1}^{(1)}(2k_bx)}{H_\mu^{(1)}(2k_bx)} & k_b \dfrac{I_{\mu+1}(2k_bx)}{I_\mu(2k_bx)} \end{bmatrix}, \\
\boldsymbol{\Phi}^+ &= EI \begin{bmatrix} -k_b^3 \dfrac{H_{\mu+1}^{(2)}(2k_bx)}{H_\mu^{(2)}(2k_bx)} & k_b^3 \dfrac{K_{\mu+1}(2k_bx)}{K_\mu(2k_bx)} \\ k_b^2 \dfrac{H_{\mu+2}^{(2)}(2k_bx)}{H_\mu^{(2)}(2k_bx)} & k_b^2 \dfrac{K_{\mu+2}(2k_bx)}{K_\mu(2k_bx)} \end{bmatrix}, \\
\boldsymbol{\Phi}^- &= EI \begin{bmatrix} -k_b^3 \dfrac{H_{\mu+1}^{(1)}(2k_bx)}{H_\mu^{(1)}(2k_bx)} & -k_b^3 \dfrac{I_{\mu+1}(2k_bx)}{I_\mu(2k_bx)} \\ k_b^2 \dfrac{H_{\mu+2}^{(1)}(2k_bx)}{H_\mu^{(1)}(2k_bx)} & k_b^2 \dfrac{I_{\mu+2}(2k_bx)}{I_\mu(2k_bx)} \end{bmatrix}
\end{aligned}
\qquad (6.6a,b,c,d)
$$

These matrices satisfy

$$
\begin{aligned}
\left(\boldsymbol{\Psi}^+\right)^T \boldsymbol{\Phi}^+ &= \left(\boldsymbol{\Phi}^+\right)^T \boldsymbol{\Psi}^+, \\
\left(\boldsymbol{\Psi}^-\right)^T \boldsymbol{\Phi}^- &= \left(\boldsymbol{\Phi}^-\right)^T \boldsymbol{\Psi}^-, \\
\left(\boldsymbol{\Psi}^+\right)^T \boldsymbol{\Phi}^- - \left(\boldsymbol{\Phi}^+\right)^T \boldsymbol{\Psi}^- &= \boldsymbol{\Lambda}
\end{aligned}
\qquad (6.7a,b,c)
$$

where the diagonal matrix $\mathbf{\Lambda}$ is

$$\mathbf{\Lambda}(x) = EIk_b^2 \begin{bmatrix} \dfrac{4\mathrm{i}}{\pi x} \dfrac{1}{\left|H_\mu^{(2)}(2k_b x)\right|^2} & 0 \\ 0 & -\dfrac{1}{x} \dfrac{1}{I_\mu(2k_b x)K_\mu(2k_b x)} \end{bmatrix} \tag{6.8}$$

When $2k_b x >> 1$, these matrices asymptote to those for the uniform beams given by equation (4.8), respectively.

The propagation matrix $\mathbf{F}$ relating the amplitudes of waves at two points x and $x+L$ are defined as

$$\mathbf{a}^+(x+L) = \mathbf{F}^+\mathbf{a}^+(x), \qquad \mathbf{a}^-(x) = \mathbf{F}^-\mathbf{a}^-(x+L) \tag{6.9a,b}$$

Combined with equation (6.5), they are found to be

$$\mathbf{F}^+ = \left(\frac{x}{x+L}\right)^{\frac{\mu}{2}} \begin{bmatrix} \dfrac{H_\mu^{(2)}\left(2k_b\sqrt{x(x+L)}\right)}{H_\mu^{(2)}\left(2k_b x\right)} & 0 \\ 0 & \dfrac{K_\mu\left(2k_b\sqrt{x(x+L)}\right)}{K_\mu\left(2k_b x\right)} \end{bmatrix},$$

$$\mathbf{F}^- = \left(\frac{x+L}{x}\right)^{\frac{\mu}{2}} \begin{bmatrix} \dfrac{H_\mu^{(1)}\left(2k_b x\right)}{H_\mu^{(1)}\left(2k_b\sqrt{x(x+L)}\right)} & 0 \\ 0 & \dfrac{I_\mu\left(2k_b x\right)}{I_\mu\left(2k_b\sqrt{x(x+L)}\right)} \end{bmatrix} \tag{6.10a,b}$$

There is a simple relation between them such that

$$\mathbf{F}^+\mathbf{\Lambda}(x+L) = \mathbf{\Lambda}(x)\mathbf{F}^- \tag{6.11}$$

where $\mathbf{\Lambda}$ is given by equation (6.8). When $2k_b x >> 1$, the propagation matrices asymptote to

$$\mathbf{F}^{+} \approx \left(\frac{x}{x+L}\right)^{\left(\frac{\mu}{2}+\frac{1}{4}\right)} \begin{bmatrix} e^{-ik_{b,m}L} & 0 \\ 0 & e^{-k_{b,m}L} \end{bmatrix},$$
$$\mathbf{F}^{-} \approx \left(\frac{x+L}{x}\right)^{\left(\frac{\mu}{2}+\frac{1}{4}\right)} \begin{bmatrix} e^{-ik_{b,m}L} & 0 \\ 0 & e^{-k_{b,m}L} \end{bmatrix} \qquad (6.12a, b)$$

where $k_{b,m}$ is given by

$$\frac{1}{k_{b,m}} = \frac{1}{2}\left(\frac{1}{k_b(x)} + \frac{1}{k_b(x+L)}\right) \qquad (6.13)$$

The wavenumber $k_{b,m}$ is the *effective* wavenumber, the inverse of which is equal to the average of the inverse of the wavenumbers $k_b(x)$ and $k_b(x+L)$. In other words, the *effective* wavelength between the two points is given by the average of the wavelengths at these points. Equations (6.12) indicate that, at high frequencies or when the position is far away from the apex, waves propagate as they do in a uniform beam with the effective wavenumber and their amplitudes are scaled by the square root of the ratio of $A\sqrt{x}$ (or generally the characteristic impedances defined by $2EIk_b^3/\omega$) at each end of the section.

6.4 Wave generation by local excitation

The displacement, internal force and propagation matrices for the non-uniform beams where the geometric properties vary as in equation (6.2) have been defined. These matrices can be used in a systematic way for solving various problems concerning beams. First, the response of beams to a local force is investigated in this section.

6.4.1 For beams of gradually increasing area

Consider a non-uniform beam where the area and second moment of area vary as equation (6.2). When the left-hand end is excited by the time-harmonic lateral force $f_{ext}e^{i\omega t}$ as shown in Figure 6-2(a), the equilibrium condition at the end is given by

$$-\mathbf{\Phi}^{+}\mathbf{q}^{+}=\mathbf{f}_{ext} \tag{6.14}$$

where $\mathbf{f}_{ext}=\begin{bmatrix} f_{ext} & 0 \end{bmatrix}^{T}$. Even though force-only excitation is described here, moment excitation or their combination can also be handled by simply changing the force vector $\mathbf{f}_{ext}$ into, e.g., $\mathbf{f}_{ext}=\begin{bmatrix} 0 & M_{ext} \end{bmatrix}^{T}$, where M_{ext} is the amplitude of the time-harmonic moment. Substituting the internal force matrix given by equation (6.6c) into equation (6.14) gives

$$\mathbf{q}^{+}=\frac{k_b^2}{\mathrm{Det}\left(\mathbf{\Phi}^{+}\right)}\begin{Bmatrix} -\dfrac{K_{\mu+2}\left(2k_bx\right)}{K_{\mu}\left(2k_bx\right)} \\ \dfrac{H_{\mu+2}^{(2)}\left(2k_bx\right)}{H_{\mu}^{(2)}\left(2k_bx\right)} \end{Bmatrix} f_{ext} \tag{6.15}$$

where

$$\mathrm{Det}\left(\mathbf{\Phi}^{+}\right)=-EIk_b^5\frac{H_{\mu+1}^{(2)}\left(2k_bx\right)K_{\mu+2}\left(2k_bx\right)+H_{\mu+2}^{(2)}\left(2k_bx\right)K_{\mu+1}\left(2k_bx\right)}{H_{\mu}^{(2)}\left(2k_bx\right)K_{\mu}\left(2k_bx\right)} \tag{6.16}$$

When $\mu=1$ and $2k_bx<<1$, referring to the asymptotic behaviour of Bessel functions given in Appendix A, equation (6.15) asymptotes to

$$\mathbf{q}^{+}\approx\frac{x}{EIk_b^2}\begin{Bmatrix} 1 \\ -1 \end{Bmatrix}\frac{f_{ext}}{2} \tag{6.17}$$

It can be seen that the propagating and nearfield components represent frequency dependent stiffness- and mass-like responses, respectively, with equal magnitude. For

the displacement, higher order terms are required since the two first order terms cancel out. Considering the higher order terms, the displacement induced by the lateral force asymptotes to

$$w \approx -\frac{x^3}{EI}\left\{ \mathrm{i}\frac{\pi}{2} + 2\left(\ln\left(k_b x\right) + \gamma - \frac{1}{4} \right) \right\} f_{ext} \tag{6.18}$$

which is consistent with the results for the point mobility obtained by Petersson and Nijman (1998).

6.4.2 For beams of gradually decreasing area

Now consider the case where the lateral force excites the right-hand end as shown in Figure 6-2(b), i.e., the response of gradually decreasing beams to external force. The equilibrium condition at the end is

$$\mathbf{\Phi}^{-}\mathbf{q}^{-} = \mathbf{f}_{ext} \tag{6.19}$$

Substituting $\mathbf{\Phi}^{-}$ given by equation (6.6c) into equation (6.19) gives $\mathbf{q}^{-}$. When $\mu = 1$ and $2k_b x << 1$,

$$\mathbf{q}^{-} \approx \frac{1}{EIk_b^3}\begin{Bmatrix} \left(k_b x\right)^3/6 \\ -2/\left(k_b x\right) \end{Bmatrix} f_{ext} \tag{6.20}$$

The propagating component is negligible compared to the nearfield component and the response exhibits rigid body motion with a mass equal to $\rho Ax/2$.

6.4.3 When a section is excited

Now a point of the beam is excited by the lateral force as shown in Figure 6-2(c). The continuity and equilibrium conditions at the point are

$$\begin{aligned} \Psi^{+}\mathbf{q}^{+} &= \Psi^{-}\mathbf{q}^{-}, \\ -\Phi^{+}\mathbf{q}^{+} + \Phi^{-}\mathbf{q}^{-} &= \mathbf{f}_{ext} \end{aligned} \tag{6.21}$$

Combined with equation (6.6), $\mathbf{q}^{+}$ is found to be

$$\mathbf{q}^{+} = -\frac{x}{EIk_b^2}\begin{Bmatrix} \mathrm{i}\pi\left|H_{\mu}^{(2)}(2k_bx)\right|^2 \\ 4K_{\mu}(2k_bx)I_{\mu}(2k_bx) \end{Bmatrix}\frac{f_{ext}}{4} \tag{6.22}$$

and

$$\mathbf{q}^{-} = \mathbf{q}^{+} \tag{6.23}$$

The propagating component is now purely imaginary, representing damping-like behaviour, while the nearfield component is negative-real, representing mass-like behaviour.

6.4.4 Numerical results

Figures 6-3 and 6-4 show the amplitudes of waves induced by the lateral force when the left- and right-hand ends of the non-uniform beam are excited, respectively. In the figures the magnitudes are normalised by $f_{ext}/\sqrt{2}EIk_b^3$. Note that the horizontal axis k_bx is proportional to $\sqrt{\omega x}$. When the right-hand end is excited, the response shows the rigid body motion if $2k_bx << 1$, which leads to very large values of the magnitude of the nearfield component. When $2k_bx << 1$, the phase of the propagating component tends to zero while the phase of the nearfield component tends to $-\pi$. When $2k_bx >> 1$, the behaviour asymptotes to that of the uniform beam. It is seen from Figures 6-3 (A.b) and 6-4 (A.b) that the phase of the propagating wave component in the former case changes from 0 to $-3\pi/4$ (counter-clockwise) but the phase in the latter case changes

from 0 to $5\pi/4$ (clockwise). Also note that Figures 6-3 (B.b) and 6-4 (B.b) are similar but not the same.

Figure 6-5 shows the amplitudes of waves induced by the lateral force when a point of the non-uniform beam is excited. In the figure the magnitudes are normalised by $f_{ext}/4EIk_b^3$. The phases are not presented here since the phase of the propagating component is $-\pi/2$ and the phase of the nearfield component is $-\pi$ at all frequencies as shown in equation (6.22).

6.5 Spectral elements

Substituting equations (6.6a,c) into equation (2.67a) gives the dynamic stiffness matrix at the boundary for the semi-infinite gradually increasing beam such that

$$\mathbf{D}^{+\infty} = \frac{EI}{\Delta}\begin{bmatrix} \hat{D}_{11} & \hat{D}_{12} \\ \hat{D}_{21} & \hat{D}_{22} \end{bmatrix} \tag{6.24}$$

where

$$\begin{aligned} \Delta &= H_{\mu+1}^{(2)}(2k_bx)K_\mu(2k_bx) - K_{\mu+1}(2k_bx)H_\mu^{(2)}(2k_bx) \\ \hat{D}_{11} &= -2k_b^3 H_{\mu+1}^{(2)}(2k_bx)K_{\mu+1}(2k_bx), \\ \hat{D}_{12} &= \hat{D}_{21} = -k_b^2\left\{H_{\mu+1}^{(2)}(2k_bx)K_\mu(2k_bx) + K_{\mu+1}(2k_bx)H_\mu^{(2)}(2k_bx)\right\}, \\ \hat{D}_{22} &= k_b\left\{H_{\mu+2}^{(2)}(2k_bx)K_\mu(2k_bx) - K_{\mu+2}(2k_bx)H_\mu^{(2)}(2k_bx)\right\} \end{aligned} \tag{6.25a,b,c,d}$$

When $2k_bx >> 1$, the matrix asymptotes to that of the semi-infinite uniform beam, i.e.

$$\mathbf{D} \approx EI\begin{bmatrix} -(1-\mathrm{i})k_b^3 & \mathrm{i}k_b^2 \\ \mathrm{i}k_b^2 & (1+\mathrm{i})k_b \end{bmatrix} \tag{6.26}$$

The dynamic stiffness matrix for the finite non-uniform beam can be also obtained by substituting equations (6.6) and (6.10) into equation (2.66) to give the result, which has been obtained by Banerjee and Williams (1985).

6.6 Energy flow

In section 2.9, the time-averaged power associated with waves in one-dimensional structures was expressed as

$$\Pi = \frac{1}{2}\mathbf{a}^H \mathbf{P}\,\mathbf{a} \tag{6.27}$$

where the power matrix $\mathbf{P}$ is

$$\mathbf{P} = \frac{i\omega}{2}\left[\begin{bmatrix} \left(\Psi^+\right)^H \Phi^+ & \left(\Psi^+\right)^H \Phi^- \\ \left(\Psi^-\right)^H \Phi^+ & \left(\Psi^-\right)^H \Phi^- \end{bmatrix} - \begin{bmatrix} \left(\Phi^+\right)^H \Psi^+ & \left(\Phi^+\right)^H \Psi^- \\ \left(\Phi^-\right)^H \Psi^+ & \left(\Phi^-\right)^H \Psi^- \end{bmatrix}\right] \tag{6.28}$$

Substituting the displacement and internal force matrices given by equation (6.6) into equation (6.28) yields

$$\mathbf{P} = 2\omega EIk_b^3 \begin{bmatrix} g_1 & 0 & 0 & 0 \\ 0 & 0 & 0 & -ig_2 \\ 0 & 0 & -g_1 & 0 \\ 0 & ig_2 & 0 & 0 \end{bmatrix} \tag{6.29}$$

where

$$g_1 = \frac{1}{\pi k_b x}\frac{1}{\left|H_\mu^{(2)}(2k_b x)\right|^2}, \qquad g_2 = \frac{1}{4k_b x}\frac{1}{I_\mu(2k_b x)K_\mu(2k_b x)} \tag{6.30a,b}$$

Unlike that of axial vibration of bars, the power matrix is not diagonal. The presence of off-diagonal terms indicates that the energy can be transported by the interaction between nearfield waves. Suppose that there are two opposite-going nearfield waves with amplitudes a_N^+ and a_N^-, respectively, i.e., $\mathbf{a} = \begin{bmatrix} 0 & a_N^+ & 0 & a_N^- \end{bmatrix}^T$. Then the time-averaged power associated with the nearfield waves is

$$\Pi = 2\omega EIk_b^3 g_2 \,\mathrm{Re}\left(ia_N^+ \left(a_N^-\right)^*\right) \tag{6.31}$$

Equation (6.31) indicates that, if a_N^+ and a_N^- are not in phase and are not in counter-phase, energy can be transported by interaction of the two opposite-going nearfield waves, as indicated by Bobrovnitskii (1992). Note that the direction of energy flow is determined by the phase difference of the wave amplitudes, e.g., if a_N^+ leads a_N^- by $\pi/2$, then the energy will be propagated in the positive direction and *vice versa.*

The power matrix in equation (6.29) also indicates that a propagating wave transports energy independent of all the other wave components. The time-averaged power associated with a positive-going propagating wave with amplitude a^+ is given by

$$\Pi = \rho A \omega^2 \left| a^+ \right|^2 c_b g_1 \tag{6.32}$$

where $c_b = \omega / k_b$ is the phase velocity. Noting that a^+ is given by equation (6.5a), it follows that the power is constant along the beam. This is of course obvious from conservation of energy considerations. Similarly, the time-averaged power associated with a negative-going wave with amplitude a^- is

$$\Pi = -\rho A \omega^2 \left| a^- \right|^2 c_b g_1 \tag{6.33}$$

The negative sign indicates that the energy is propagated in the negative direction.

6.7 Energy transport velocity

For uniform beams, the energy transport velocity is equal to the group velocity defined by $c_g = \mathrm{d}\omega / \mathrm{d}k_b$. It is generally not true for non-uniform beams. In this section, the energy transport velocity for non-uniform beams with power-law variations in area and the second moment of area is found.

The kinetic and potential energies per unit length (i.e. the energy densities), $\mathcal{T}$ and $\mathcal{V}$ respectively, for bending motion of a beam are given by (Cremer *et al.* 1973)

$$\mathcal{T} = \frac{1}{2}\rho A\left\{\mathrm{Re}\left(\frac{\partial w}{\partial t}\right)\right\}^2, \qquad \mathcal{V} = \frac{1}{2}EI\left\{\mathrm{Re}\left(\frac{\partial^2 w}{\partial x^2}\right)\right\}^2 \tag{6.34a,b}$$

If there is only the positive-going propagating wave in the non-uniform beam, i.e. $\mathbf{a}^+ = \begin{bmatrix} a^+ & 0 \end{bmatrix}^T$, the displacement of the beam will be $w(x) = a^+$. For time harmonic motion, the time-averaged energy densities associated with this component are

$$\langle \mathcal{T} \rangle = \frac{1}{4}\rho A\omega^2 \left|a^+\right|^2, \qquad \langle \mathcal{V} \rangle = \frac{1}{4}\rho A\omega^2 \left|a^+\right|^2 \frac{\left|H_{\mu+2}^{(2)}(2k_b x)\right|^2}{\left|H_{\mu}^{(2)}(2k_b x)\right|^2} \tag{6.35a,b}$$

where $\langle \cdot \rangle$ indicates a time averaged quantity. Note that these are not equal. Indeed, for a bar with increasing cross-sectional area in the direction of the wave propagation, $\langle \mathcal{V} \rangle > \langle \mathcal{T} \rangle$. The total energy density is given by $\mathcal{E} = \langle \mathcal{T} \rangle + \langle \mathcal{V} \rangle$, therefore

$$\mathcal{E} = \frac{1}{4}\rho A\omega^2 \left|a^+\right|^2 \frac{\left|H_{\mu}^{(2)}(2k_b x)\right|^2 + \left|H_{\mu+2}^{(2)}(2k_b x)\right|^2}{\left|H_{\mu}^{(2)}(2k_b x)\right|^2} \tag{6.36}$$

Figure 6-6 shows the time-averaged kinetic and potential energy densities, normalised by the total energy density, associated with the propagating bending in the non-uniform beams with four different values of μ. It is seen that $\langle \mathcal{V} \rangle > \langle \mathcal{T} \rangle$ but, as $k_b x$ increases, the energy densities become the same.

In terms of the total energy density and the power, the energy transport velocity c^E is defined by (Lighthill 1978)

$$c^E = \frac{\Pi}{\mathcal{E}} \tag{6.37}$$

This energy transport velocity is generally different from the group velocity, which is formally defined by $c_g = \mathrm{d}\omega/\mathrm{d}k$ (for real wavenumbers). Note that, for uniform beams, $c_g = 2c_b$. Substituting equations (6.32) and (6.36) into equation (6.37) gives

$$c_b^E = \frac{4c_b}{\pi k_b x}\left(\left|H_\mu^{(2)}(2k_b x)\right|^2 + \left|H_{\mu+2}^{(2)}(2k_b x)\right|^2\right)^{-1} \tag{6.38}$$

The energy transport velocity associated with the propagating component of the positive-going wave is the same as that associated with the negative-going wave.

Figure 6-6 shows the energy transport velocity, normalised with respect to c_b, for the non-uniform beam with four different values of μ. The behaviour is similar to that of the longitudinal wave described in section 5.9. When $2k_b x << 1$, the velocity is approximately proportional to $(k_b x)^{2\mu+4}$, i.e., $(\omega x)^{\mu+2}$. When $2k_b x >> 1$, the velocity asymptotes to the group velocity of the uniform beam, i.e. $c_b^E = 2c_b$.

6.8 Numerical examples

Consider the tapered connector of length L, introduced in section 5.10. The situation is the same as before but, here, the structure is undergoing bending motion instead of longitudinal motion. The relationships between the waves derived in section 5.10 are still valid for this case. Thus the reflected and transmitted waves are

$$\begin{aligned} \mathbf{a}^- &= \left[\mathbf{R}_1 + \hat{\mathbf{T}}_1\mathbf{F}^-\mathbf{R}_2\mathbf{F}^+[\mathbf{I} - \hat{\mathbf{R}}_1\mathbf{F}^-\mathbf{R}_2\mathbf{F}^+]^{-1}\mathbf{T}_1\right]\mathbf{a}^+, \\ \mathbf{d}^+ &= \left[\mathbf{T}_2\mathbf{F}^+[\mathbf{I} - \hat{\mathbf{R}}_1\mathbf{F}^-\mathbf{R}_2\mathbf{F}^+]^{-1}\mathbf{T}_1\right]\mathbf{a}^+ \end{aligned} \tag{6.39a,b}$$

In equation (6.39), the reflection and transmission matrices are obtained in a systematic way by using equation (6.6) with $\mu = 1$ for the connector and equation (4.8) for the

uniform beam, as required. The propagation matrices $\mathbf{F}^+$ and $\mathbf{F}^-$ are given by equation (6.10) with $x = x_1$.

Figure 6-7 shows the transmission coefficients for the connector when a propagating bending wave is incident, i.e. $\mathbf{a}^+ = \begin{bmatrix} a^+ & 0 \end{bmatrix}^T$. Note that the abscissa is $k_{b,m}L$, where $k_{b,m}$ is the effective wavenumber for the connector defined by equation (6.13). When $k_{b,m}L >> 1$, the power transmission coefficient τ tends to 1, i.e. the power incident on the connector is totally transmitted when the frequency or length increases. The phase difference θ between the propagating components a^+ and d^+ then asymptotes to $-k_{b,m}L$. When $k_{b,m}L << 1$, the results asymptote to those of the case where the two uniform beams are directly connected without the tapered connector.

6.9 Summary

The wave approach based on reflection, transmission and propagation of waves has been applied for a two-mode deterministically varying waveguide: non-uniform straight beams where $A(x) \propto x^{\mu}$ and $I(x) \propto x^{\mu+2}$. The displacement, internal force and propagation matrices were defined for the beams, and then the response to external excitation and the spectral element were described in a systematic way using the matrices.

The effect of non-uniformity becomes larger as the frequency decreases or as the position moves closer to the apex. The propagating and nearfield components represent frequency dependent stiffness- and mass-like responses, respectively, due to the non-uniformity in the region.

The energy transport velocity of the non-uniform beams was derived exactly. In contrast to that of uniform beams, it is not equal to twice the phase velocity, and depends on position as well as frequency. It was shown that the velocity decreases as the position moves toward to the apex.

Finally numerical results were presented for the transmission of bending waves through a tapered connector. The results are exact, irrespective of frequency, since no approximations are imposed, other than those involved in the derivation of the equation of motion. The results obtained by the wave approach are also well-conditioned even in the existence of nearfield waves.

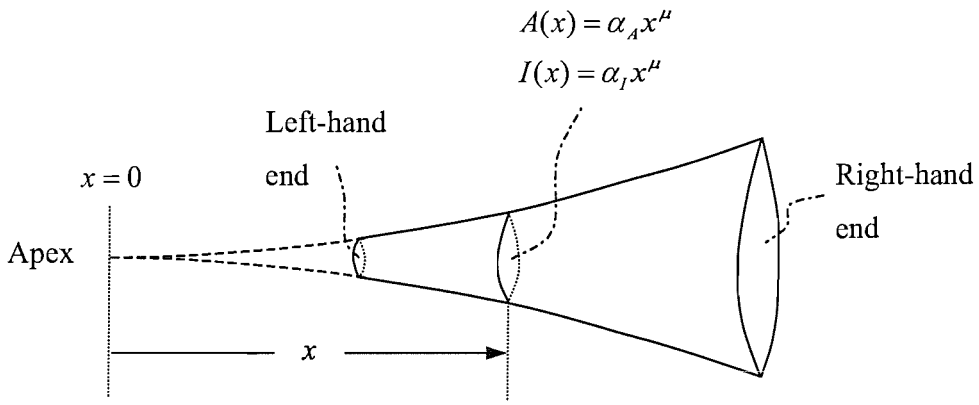

Figure 6-1. A non-uniform, straight beam where the area and second moment of area vary as $A(x) = \alpha_A x^\mu$ and $I(x) = \alpha_I x^{\mu+2}$.

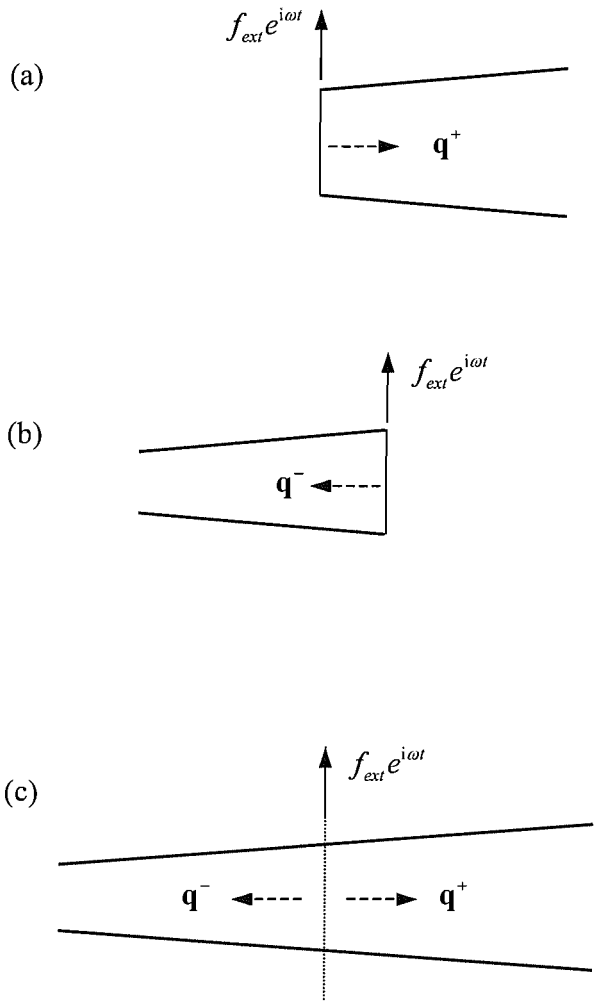

Figure 6-2. Wave generation in a non-uniform beam by a local harmonic force: (a) when the left-hand end is excited, (b) when the right-hand end is excited, (c) when a cross-section is excited.

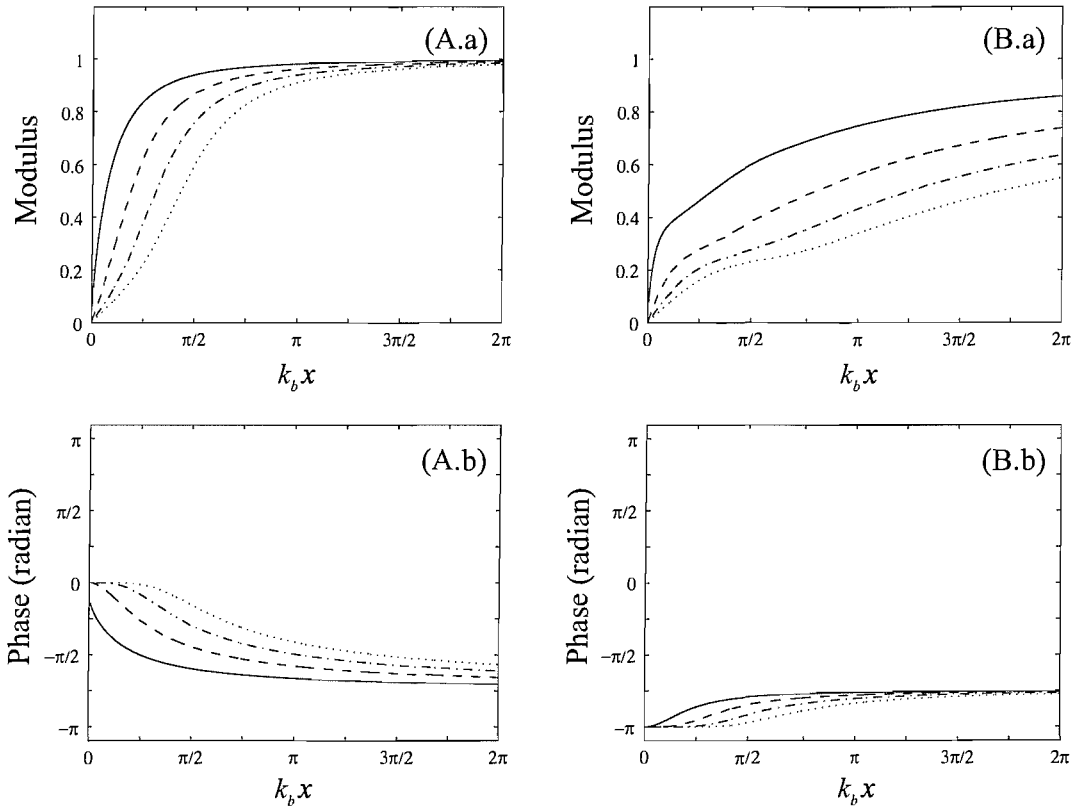

Figure 6-3. Wave generation at the left-hand end of a non-uniform beam described by equation (6.2): (A) propagating component, (B) nearfield component: (a) magnitude normalised by that in the uniform beam, (b) phase; ——— , $\mu = 0$; ------ , $\mu = 1$; -·-·-·- , $\mu = 2$; ····· , $\mu = 3$.

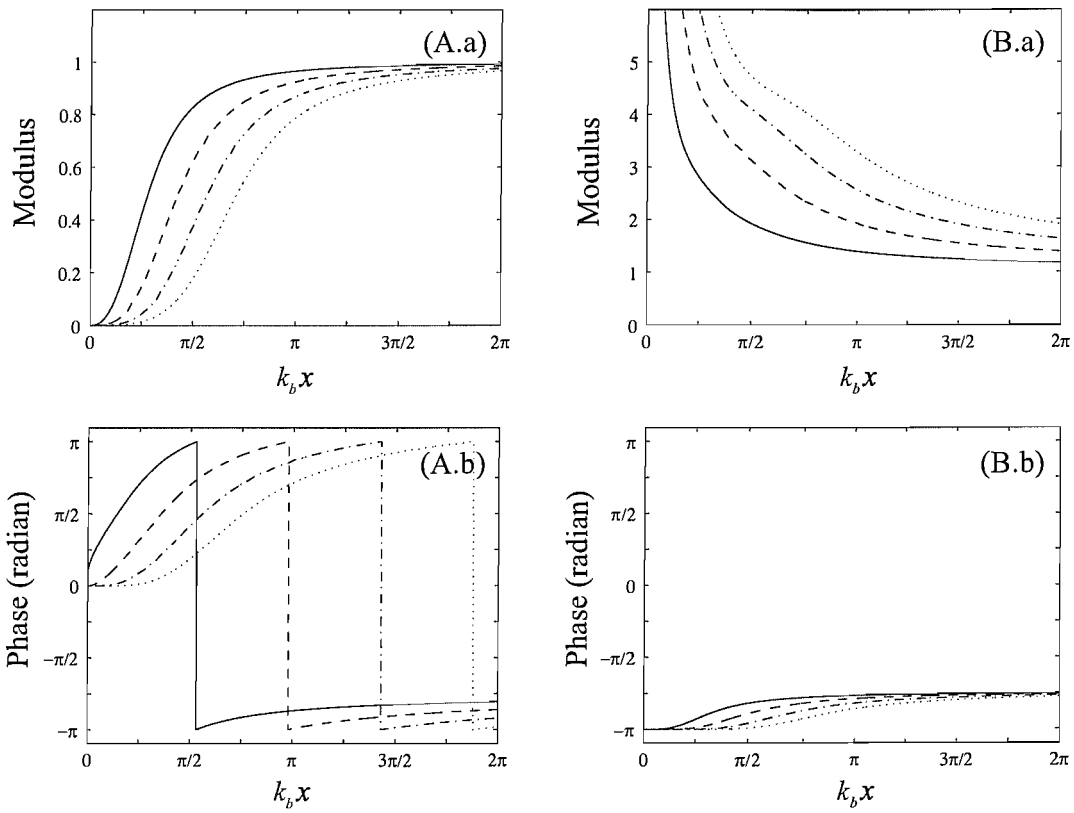

Figure 6-4. Wave generation at the right-hand end of a non-uniform beam described by equation (6.2): (A) propagating component, (B) nearfield component: (a) magnitude normalised by that in the uniform beam, (b) phase; ——— , $\mu = 0$; ------ , $\mu = 1$; -·-·-·- , $\mu = 2$; ····· , $\mu = 3$.

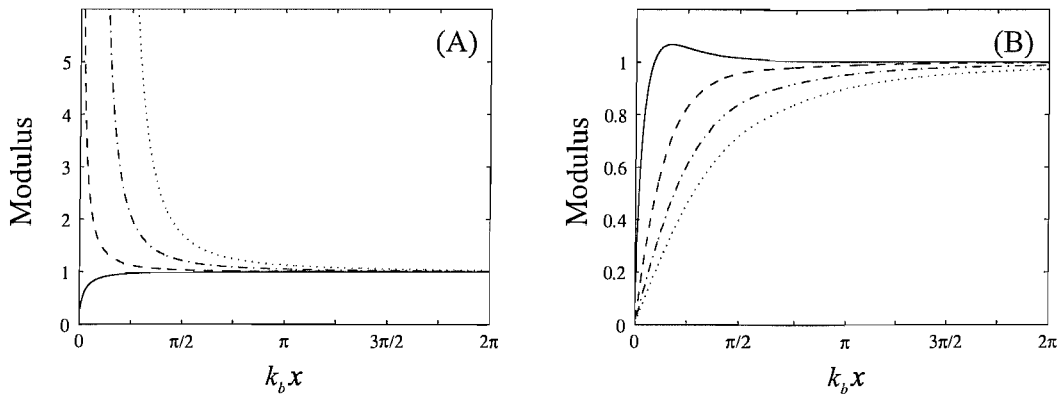

Figure 6-5. Wave generation at a point of a non-uniform beam described by equation (6.2): magnitude, normalised by that in the uniform beam, of (A) propagating component and (B) nearfield component; ——— , $\mu = 0$; ------ , $\mu = 1$; -·-·-·- , $\mu = 2$; ····· , $\mu = 3$.

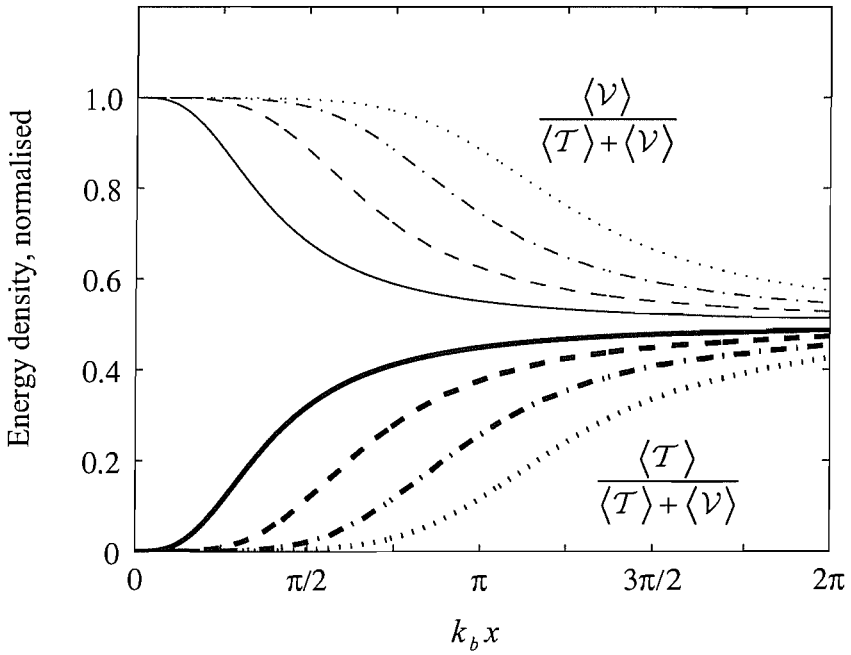

Figure 6-6. Time-averaged kinetic and potential energy densities, normalised by the total energy density, associated with a propagating bending wave in a non-uniform beam described by equation (6.2): ——— , $\mu = 0$; ------ , $\mu = 1$; -·-·-·- , $\mu = 2$; ····· , $\mu = 3$; thin lines are for $\langle \mathcal{V} \rangle / (\langle \mathcal{T} \rangle + \langle \mathcal{V} \rangle)$ and thick lines are for $\langle \mathcal{T} \rangle / (\langle \mathcal{T} \rangle + \langle \mathcal{V} \rangle)$.

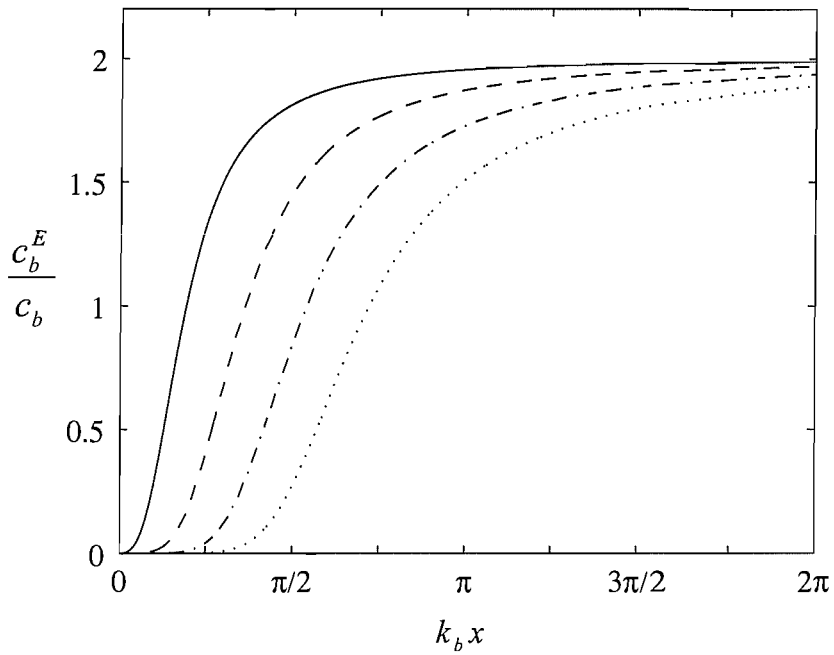

Figure 6-7. Energy transport velocity, normalised by the phase velocity c_b, associated with a propagating bending wave in a non-uniform beam described by equation (6.2): ——— , $\mu = 0$; - - - - - - , $\mu = 1$; - · - · - · , $\mu = 2$; ····· , $\mu = 3$.

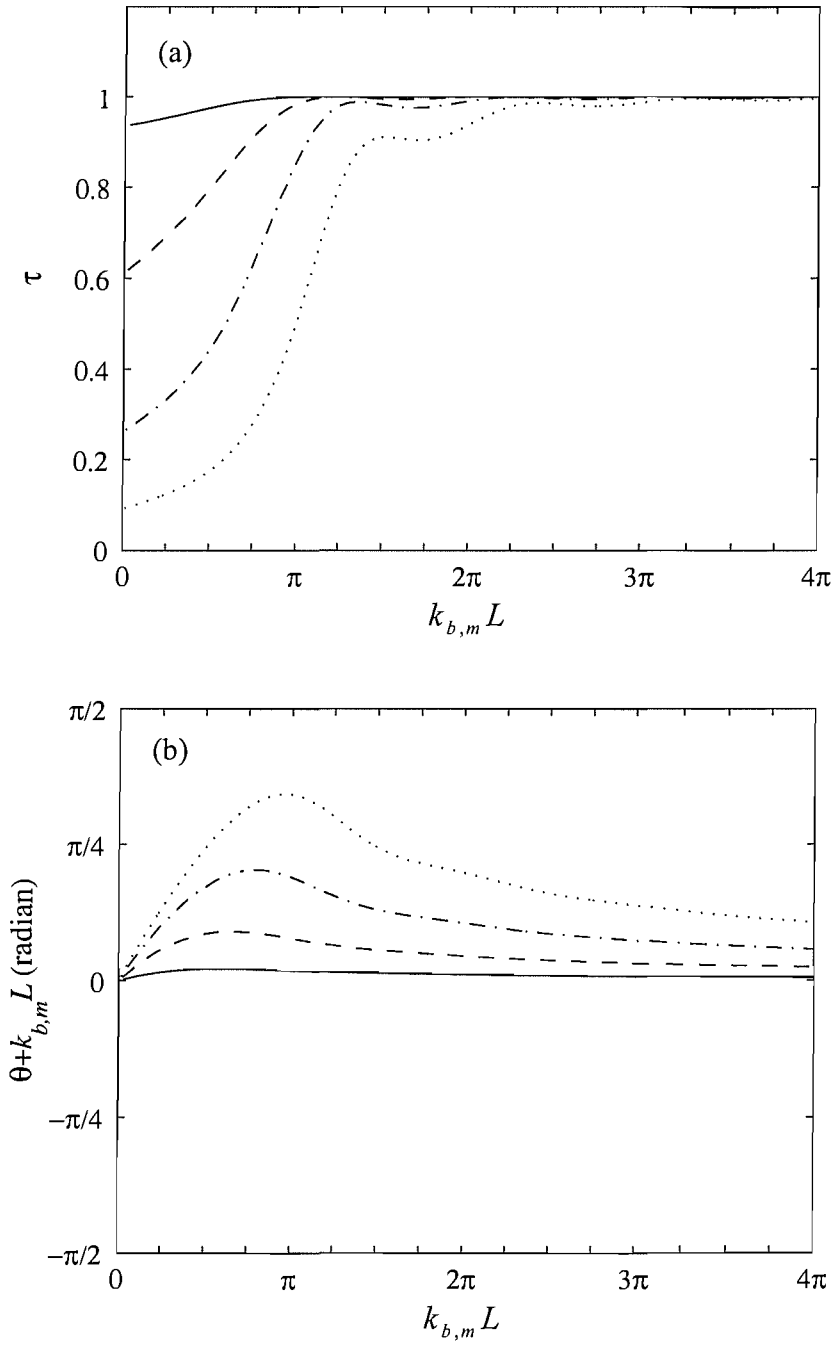

Figure 6-8. Transmission of a propagating bending wave through the connector: (a) power transmission coefficient τ, (b) phase difference θ between a^+ and d^+, added by $k_{b,m}L$; ——, $h_2/h_1 = 2$; - - - -, $h_2/h_1 = 4$; - · - · -, $h_2/h_1 = 8$; ·····, $h_2/h_1 = 16$.

Chapter 7.

WAVE MOTION IN UNIFORM, CURVED BEAMS

7.1 Introduction

In this chapter, the wave approach is applied to cases concerning a thin, uniform, curved beam with constant curvature. Attention is focused only on the in-plane motion of the beam, i.e., the motion in the plane formed by the centreline of the undeformed beam. The radial and tangential displacements of the beam are coupled in this case, which does not occur in the straight structures of the last four chapters.

In section 7.2, the in-plane motion of thin, uniform, curved beams is reviewed. The motion is based on the four assumptions, known as Love's first approximation. The strain-displacement relation of Flügge is used for the equations of motion. The effects of rotary inertia, shear deformations and damping are ignored as before.

In section 7.3, the characteristic equation is derived assuming time harmonic motion. The equation is of 6^{th} order in wavenumber so that there are six wavenumbers satisfying the equation. A criterion to define the direction of propagation of each component is suggested: the imaginary value of the wavenumber of a positive-going wave should be negative and the energy transport velocity associated with a positive-going wave should be positive. Using this criterion, the dispersion relation for each wave component is defined.

As a measure of the coupling of the displacements, the ratio of the tangential displacement to the radial displacement is considered in section 7.4. If the magnitude of this ratio is much higher than unity or much lower than unity, it will mean that the coupling is weak and the motion in one direction is dominant compared to the other.

In section 7.5, the displacement, internal force and propagation matrices for the curved beams are defined. The propagation matrix is diagonal in this case so that, even though the displacements are coupled together, the wave components are not coupled at all. Thus the problem can be simplified in the wave domain.

These matrices can be used in a systematic manner for various problems such as wave generation by external excitation, reflection and transmission of waves at discontinuities, and derivation of spectral elements. However, such examples are not specifically presented because wave motion of the curved beams is too complex to present full analytical expressions for these cases.

In section 7.6, the energy flow associated with waves is described. The power matrix for the curved beam is defined and the elements of the power matrix are obtained explicitly in terms of wavenumbers. Their values are classified according to the different conditions for the wavenumbers. Using the results, in section 7.7, the power associated with waves is determined for a given frequency.

In section 7.8, numerical results for the power transmission and reflection through a U-shaped structure are presented.

7.2 Equations of motion

Based on Flügge's theory, the equations of the in-plane motion of a curved beam with constant curvature are presented. The cross-section is uniform and symmetric

about the plane defined by the centreline of the beam, and the material is linearly elastic, homogeneous, isotropic and continuous across the cross-section. The in-plane and out-of-plane motions of the beam uncouple in this case. Indeed it is assumed here that out-of-plane motion does not occur, i.e. the beam supports only circumferential stress along the centreline. This beam provides coupling between the radial and tangential displacements, which were treated separately in the previous chapters since they are not coupled in the straight beams.

Consider a small segment, subtending an angle $d\theta$ at the centre of curvature, of a thin curved beam as shown in Figure 7-1. In the figure the centreline is defined as the locus of centroids of each cross-sectional segment. The circumferential coordinate along the centreline is denoted by s and the coordinate along the normal to the centreline is z. The displacements of the centreline in the radial and tangential directions are denoted by w and u, respectively. The arc length ds of the section is $ds = Rd\theta$ where R is radius of curvature of the centreline. The sign convention for the internal forces is also indicated in the figure.

When the effects of rotary inertia are neglected, the equations of motion in the radial and tangential directions are

$$\begin{aligned} \frac{\partial Q}{\partial s} - \frac{N}{R} &= \rho A \frac{\partial^2 w}{\partial t^2} \\ \frac{\partial N}{\partial s} + \frac{Q}{R} &= \rho A \frac{\partial^2 u}{\partial t^2} \\ \frac{\partial M}{\partial s} + Q &= 0 \end{aligned} \qquad (7.1a,b,c)$$

Using equation (7.1c), eliminating the shear force Q in equations (7.1a) and (7.1b) gives

$$-\frac{\partial^2 M}{\partial s^2}-\frac{N}{R}=\rho A\frac{\partial^2 w}{\partial t^2},$$
$$\frac{\partial N}{\partial s}-\frac{1}{R}\frac{\partial M}{\partial s}=\rho A\frac{\partial^2 u}{\partial t^2} \qquad (7.2a,b)$$

No constraint has been made on R in deriving equation (7.2). Thus equation (7.2) is valid for the motion of curved beams where R is constant or a function of s.

The four assumptions, following Love's first approximation in the classical thin shell theory (Leissa 1977), are now made:

(i) The thickness of the beam in the plane of curvature is thin enough, typically, the ratio of the thickness to the smallest radius of curvature is less than about 0.1.

(ii) Strains and displacements are sufficiently small so that the quantities of second- and higher-order magnitude in the strain-displacement relations may be neglected in comparison with the first-order terms.

(iii) Compared to the circumferential normal stress and strain, the other normal stresses and strains are small enough to be neglected.

(iv) Normals to the centreline of the beam remain straight and normal to the deformed centreline and suffer no extension, i.e, all shear strains and stresses are neglected. However, the radial shear force Q, given as the integral of the radial shear stress, is supposed to not be zero.

Displacement components in the radial and tangential direction at a point on the curved beam are denoted by $W(r,s,t)$ and $U(r,s,t)$ where $r=R+z$. Considering the fourth assumption, expanding the displacement components in a Taylor series about the centreline gives (Doyle 1997)

$$W(r,s,t)\approx w(R,s,t), \qquad U(r,s,t)\approx u(R,s,t)-z\varphi(R,s,t) \qquad (7.3a,b)$$

where φ is rotation of the normal to the centreline in the counter-clockwise direction and is given by

$$\varphi = -\frac{u}{R} + \frac{\partial w}{\partial s} \tag{7.4}$$

Equation (7.3a), where W is independent of r, implies that the radial strain is zero, and equation (7.3b) implies that the radial shear strain is zero. The only nonzero component is the circumferential strain e_s and is given by (Walsh and White 2000)

$$e_s(z) = \frac{1}{1 + z/R}\left(\varepsilon_s - z\beta_s\right) \tag{7.5}$$

where ε_s is the extensional strain at the centreline due to stretching of the beam and β_s is the change in curvature of the centreline due to the bending deformation of the beam. They are related to the displacement components at the centreline by

$$\varepsilon_s = \frac{w}{R} + \frac{\partial u}{\partial s}, \qquad \beta_s = \frac{\partial}{\partial s}\left(-\frac{u}{R} + \frac{\partial w}{\partial s}\right) \tag{7.6a,b}$$

Equation (7.5) is the strain-displacement equation used by Flügge. It implies that the circumferential strain e_s does not vary linearly with z. In Love's theory, the strain-displacement relationship is obtained by neglecting the term z/R with respect to unity in the denominator in equation (7.5), i.e., the strain varies linearly with z as in the straight beam.

The extensional stress σ_s corresponding to the total strain is given from Hooke's law, and therefore (Walsh and White 2000)

$$\sigma_s = E e_s \tag{7.7}$$

Utilizing the assumption that $z/R << 1$, the total strain e_s of equation (7.5) can be expressed as a power series in z/R. If the series is truncated from the third-order terms in R and substituted into equation (7.7), it gives

$$\sigma_s \approx E\left(\varepsilon_s - \frac{z}{R}\varepsilon_s + \frac{z^2}{R^2}\varepsilon_s - z\beta_s - \frac{z^2}{R}\beta_s\right) \tag{7.8}$$

The normal force N and bending moment M at a cross-section are then obtained by integration of the extensional stress, i.e.,

$$N = \int_A \sigma_s \, dA, \qquad M = -\int_A \sigma_s z \, dA \tag{7.9a,b}$$

Substituting equation (7.8) into equations (7.9) and integrating give

$$N = EA\varepsilon_s + \frac{EI}{R}\left(\frac{\varepsilon_s}{R} + \beta_s\right), \qquad M = EI\left(\frac{\varepsilon_s}{R} + \beta_s\right) \tag{7.10a,b}$$

Finally substituting equation (7.10) into equation (7.2) gives the equations of motion for curved beams where EA, EI and R could vary with s.

Henceforth attention is restricted to uniform curved beams where EA, EI and R are constant along the beam. The normal force N and bending moment M for the curved beam are then given from equations (7.10) and (7.6) by

$$\begin{aligned} N &= EA\left(\frac{w}{R} + \frac{\partial u}{\partial s}\right) + \frac{EI}{R}\left(\frac{w}{R^2} + \frac{\partial^2 w}{\partial s^2}\right) \\ M &= EI\left(\frac{w}{R^2} + \frac{\partial^2 w}{\partial s^2}\right) \end{aligned} \tag{7.11a,b}$$

The shear force Q is obtained by substituting equation (7.11b) into equation (7.1c), therefore,

$$Q = -EI\left(\frac{1}{R^2}\frac{\partial w}{\partial s} + \frac{\partial^3 w}{\partial s^3}\right) \tag{7.12}$$

Now substituting equation (7.11) into equation (7.2) gives (Walsh and White 2000)

$$-EI\left(\frac{\partial^4 w}{\partial s^4}+\frac{2}{R^2}\frac{\partial^2 w}{\partial s^2}+\frac{w}{R^4}\right)-\frac{EA}{R}\left(\frac{w}{R}+\frac{\partial u}{\partial s}\right)=\rho A\frac{\partial^2 w}{\partial t^2},$$
$$EA\left(\frac{\partial^2 u}{\partial s^2}+\frac{1}{R}\frac{\partial w}{\partial s}\right)=\rho A\frac{\partial^2 u}{\partial t^2} \qquad (7.13a,b)$$

These are the equations of motion for thin, uniform, curved beams with constant curvature based on Flügge theory. When R tends to infinity, the radial and tangential displacements decouple and the equations become those for the uniform, straight beams.

7.3 Dispersion relation

The radial and tangential displacements satisfying equation (7.13) are assumed to be of exponential form such that

$$w(s,t)=C_w e^{\mathrm{i}(\omega t-ks)}, \qquad u(s,t)=C_u e^{\mathrm{i}(\omega t-ks)} \qquad (7.14a,b)$$

where C_w and C_u are arbitrary constants, and k is wavenumber for the curved beam. Substituting equation (7.14) into equation (7.13) gives

$$\begin{bmatrix} \frac{I}{AR^2}\left(k^2R^2-1\right)^2+1-\frac{\rho}{E}R^2\omega^2 & -\mathrm{i}kR \\ \mathrm{i}kR & k^2R^2-\frac{\rho}{E}R^2\omega^2 \end{bmatrix}\begin{Bmatrix} C_w \\ C_u \end{Bmatrix}=0 \qquad (7.15)$$

For non-trivial solutions, the determinant of the matrix in equation (7.15) should be zero so that

$$k^6-\left(\frac{\rho\omega^2}{E}+\frac{2}{R^2}\right)k^4+\left(\frac{1}{R^4}-\frac{\rho A\omega^2}{EI}+\frac{2\rho\omega^2}{ER^2}\right)k^2-\frac{\rho\omega^2}{E}\left(\frac{1}{R^4}+\frac{A}{IR^2}-\frac{\rho A\omega^2}{EI}\right)=0 \qquad (7.16)$$

If k_l and k_b denote the longitudinal and bending wavenumbers for the straight beam, equation (7.16) can be written as

$$k^6-\left(k_l^2+2\kappa^2\right)k^4+\left(\kappa^4-k_b^4+2\kappa^2k_l^2\right)k^2-\left(\kappa^4k_l^2+\kappa^2k_b^4-k_l^2k_b^4\right)=0 \qquad (7.17)$$

where $\kappa=1/R$ is the curvature. Equation (7.17) is the dispersion relation. Since it is a cubic equation with respect to k^2, there are three pairs of k satisfying equation (7.17) at a given frequency, three for positive-going waves and three for negative-going waves.

Before obtaining solutions to equation (7.17), it is worthwhile investigating their asymptotic values in certain limits. When κ is small enough such that the terms involving κ can be neglected, equation (7.17) reduces to

$$\left(k^4-k_b^4\right)\left(k^2-k_l^2\right)=0 \qquad (7.18)$$

i.e., four wavenumbers asymptote to the bending wavenumber and two wavenumbers asymptote to the longitudinal wavenumber as expected. This is the "straight beam limit".

Unlike the straight beams, there exists a cut-off frequency ω_c in the curved beam. Letting $k=0$ in equation (7.17) gives

$$\kappa^4k_l^2+\kappa^2k_b^4-k_l^2k_b^4=0 \qquad (7.19)$$

From this it follows that

$$\omega_c=\frac{c_l}{R}\sqrt{1+\frac{I}{AR^2}} \qquad (7.20)$$

where c_l is the longitudinal phase velocity for a uniform straight bar. The frequency ω_c is called as the "ring frequency" of the beam. Note that this ring frequency, based on Flügge theory, slightly differs from that obtained on Love's theory by the term I/AR^2.

However this difference is likely to be negligible since I/AR^2 (or h/R for a rectangular beam) should be small for the thin beam assumption to be valid.

When $\omega \to 0$, equation (7.17) reduces to

$$k^2\left(k^2-\kappa^2\right)^2=0 \tag{7.21}$$

The wavenumber for one mode tends to zero but the other two modes are such that $k^2=\kappa^2$, i.e., the wavelength asymptotes to $2\pi R$ (the beam is simply displaced in a rigid-body motion).

The asymptotic behaviour of the wavenumbers for the curved beam in certain limits has been discussed. Exact solution of equation (7.17) can be obtained by noting that equation (7.17) is a cubic equation in $z=k^2$. The solution for a cubic equation can be found in the work of Abramowitz and Stegun (1965). Substituting $k^2=z$, equation (7.17) becomes

$$z^3+a_2z^2+a_1z+a_0=0 \tag{7.22}$$

where a_2 a_1 and a_0 are the corresponding coefficients of equation (7.17). Now let

$$r=(2a_2^3-9a_2a_1+27a_0)/54, \qquad q=(a_2^2-3a_1)/9 \tag{7.23a,b}$$

and

$$s_1=-\left(r+\sqrt{r^2-q^3}\right)^{1/3}, \qquad s_2=\frac{-q}{\left(r+\sqrt{r^2-q^3}\right)^{1/3}} \tag{7.24a,b}$$

The three roots z_1, z_2 and z_3 of the cubic equation (7.22) are

$$z_1 = (s_1 + s_2) - \frac{1}{3}a_2$$
$$z_2 = -\frac{1}{2}(s_1 + s_2) - \frac{1}{3}a_2 + \mathrm{i}\frac{\sqrt{3}}{2}(s_1 - s_2) \qquad (7.25a,b,c)$$
$$z_3 = -\frac{1}{2}(s_1 + s_2) - \frac{1}{3}a_2 - \mathrm{i}\frac{\sqrt{3}}{2}(s_1 - s_2)$$

Finally, the six solutions of equation (7.17) are $k = \pm\sqrt{z_i}$, $i = 1,2,3$. Here note that the three roots z_1, z_2 and z_3 satisfy

$$\begin{aligned} z_1 + z_2 + z_3 &= -a_2, \\ z_1 z_2 + z_2 z_3 + z_3 z_1 &= a_1, \\ z_1 z_2 z_3 &= -a_0 \end{aligned} \qquad (7.26a,b,c)$$

which are used later for discussion of power associated with waves in section 7.6.

Figure 7-2 shows a typical dispersion relation for a curved beam with constant curvature. Here, for clarity, dimensionless parameters for the radius of gyration χ, wavenumber k and angular frequency ω are introduced such that

$$\overline{\chi} = \sqrt{\frac{I}{AR^2}}, \qquad \xi = kR, \qquad \Omega = \frac{\omega R}{c_l} \qquad (7.27)$$

Then equation (7.17) can be re-written in terms of the dimensionless parameters as

$$\left\{\overline{\chi}^2\left(\xi^2 - 1\right)^2 + 1 - \Omega^2\right\}\left(\xi^2 - \Omega^2\right) - \xi^2 = 0 \qquad (7.28)$$

In the figure, the wavenumbers are shown for the beam with $\overline{\chi}^2 = 1/1200$, which implies that $h/R = 0.1$ if the beam is rectangular. The frequency range concerned here is far below the cross-over frequency, where predominant bending and extensional wave modes have the same wavenumber, $\Omega = 1/\overline{\chi} \approx 34.6$ (i.e., the longitudinal wavelength λ_l is $\lambda_l = 2\pi\overline{\chi}$) (Walsh and White 2000). There are five branch points as a whole. The

lowest two branch points are located near the frequency $\Omega_1 = \overline{\chi}/3 \approx 10^{-2}$. The next two points are located near the frequency $\Omega_2 = 4\overline{\chi} \approx 0.16$ where the bending wavelength λ_b is $\lambda_b = \pi R$. The highest branch point is at the ring frequency $\Omega_3 = 1$, i.e., $\lambda_l = 2\pi R$.

The existence of these branch points may cause difficulties in deciding the direction of propagation associated with each solution for k. These difficulties cannot be removed by adding damping as for the quadratic case - for example, bending motion of a straight uniform beam on an elastic foundation (Doyle 1997). A criterion suggested here is that the wavenumber of a positive-going wave should satisfy

$$\mathrm{Im}\{k\} \le 0, \qquad \mathrm{Re}\{\partial k/\partial \omega\} > 0 \text{ if } \mathrm{Im}\{k\} = 0 \qquad (7.29a,b)$$

Equation (7.29a) indicates that imaginary value of the wavenumber of a positive-going wave should not be positive. If non-zero, the amplitude of the wave thus decays in the positive x direction. If the imaginary value is zero, equation (7.29b) is used: the slope of the dispersion curve for the real part of the wavenumber of a positive-going wave should be positive (more precisely, the energy transport velocity associated with a positive-going wave should be positive). Figure 7-3 shows the dispersion relation for the three positive-going waves when this criterion is applied. The wavenumbers of the three negative-going waves are the negatives of those of the positive-going waves.

In Figure 7-3, the frequency range is divided into 4 regions separated by the branch points. In region I, the wavenumbers for the three modes are all purely real so that all the wave modes propagate along the curved beam. One interesting feature is that the real wavenumbers for the third mode ξ_3^+ are negative in this region. Thus the phase velocity of the mode is negative while the energy is transported in the positive x direction (i.e., a wave transports energy in the direction opposite to the direction of the

phase velocity). In region II, ξ_2 is complex, which represents a decaying but oscillating wave. Since $\xi_2 = -(\xi_3)^*$, a spatially decaying standing wave can be set up. Only the first mode can propagate. In region III also, only the first mode propagates. The other wave modes are both evanescent, i.e., they decay without a change in phase. In region IV, ξ_3 becomes purely real. In this region the waves are broadly analogous to bending and extensional waves in a straight beam.

7.4 Displacement ratio

The radial and tangential displacements of the curved beam are not independent of each other. From equation (7.15), the ratio $\alpha = C_u/C_w$ of these displacements is obtained by

$$\alpha = \frac{\mathrm{i}\kappa k}{k_l^2 - k^2} \tag{7.30}$$

If the magnitude of α is greater than unity, the tangential motion will be larger than the radial motion, and *vice versa.*

There are six wave components associated with the motion of the curved beam as described in section 7.3. For clarity, the direction of wave motion is no longer explicitly specified using the subscripts '+' and '−'. Instead the wave components are now denoted by subscript i where $i = 1, 2, \ldots, 6$, where $i = 1, 2, 3$ denote the three positive-going components, respectively, and $i = 4, 5, 6$ denote the corresponding negative-going components, respectively. Then the ratio α_i for a wave component i is given by replacing k with k_i in equation (7.30), and therefore,

$$\alpha_i = \frac{\mathrm{i}\kappa k_i}{k_l^2 - k_i^2}; \qquad i = 1, 2, \ldots, 6 \tag{7.31}$$

Note that $\alpha_{4,5,6} = -\alpha_{1,2,3}$, respectively, since $k_{4,5,6} = -k_{1,2,3}$, respectively.

Figure 7-4 shows the ratio for the three positive-going wave components for the curved beam with $\bar{\chi}^2 = 1/1200$. The four regions shown in Figure 7-3 are not marked again in this figure for clarity. They can be inferred from the discontinuous behaviour of the results. First it is seen that the radial displacement is dominant for the first wave mode since the magnitude of α_1 is less than unity in the whole frequency range. In region II, the magnitude of α_2 is the same as that of α_3. In regions III and IV, the radial motion is dominant for the second mode. Near the ring frequency $\Omega = 1$, the radial motion is dominant for the third mode (see the magnitude of α_3 tends to zero at the ring frequency) but, as frequency goes up, the tangential motion becomes dominant. The phase difference between the amplitudes is between $\pi/2$ and $-\pi/2$.

7.5 The wave description

In this section the displacement, internal force and propagation matrices for the uniform curved beam are presented. Since the curved beam is a three-mode system, the relevant vectors and matrices are now defined of order 3×1 and 3×3, respectively.

Assuming the displacements to be of the exponential form given by equation (7.14), the radial and tangential displacements of the beam are given by

$$\begin{aligned} w(s) &= C_1 e^{-\mathrm{i}k_1 s} + C_2 e^{-\mathrm{i}k_2 s} + C_3 e^{-\mathrm{i}k_3 s} + C_4 e^{-\mathrm{i}k_4 s} + C_5 e^{-\mathrm{i}k_5 s} + C_6 e^{-\mathrm{i}k_6 s} \\ u(s) &= \alpha_1 C_1 e^{-\mathrm{i}k_1 s} + \alpha_2 C_2 e^{-\mathrm{i}k_2 s} + \alpha_3 C_3 e^{-\mathrm{i}k_3 s} + \alpha_4 C_4 e^{-\mathrm{i}k_4 s} + \alpha_5 C_5 e^{-\mathrm{i}k_5 s} + \alpha_6 C_6 e^{-\mathrm{i}k_6 s} \end{aligned} \tag{7.32a,b}$$

where C's are arbitrary constants. Note again that $k_{4,5,6} = -k_{1,2,3}$ and $\alpha_{4,5,6} = -\alpha_{1,2,3}$.

Even though equation (7.32) is simple, it is not in a suitable form for later development since, at high frequencies (where the radial and tangential displacements decouple), α_3 and α_6 tend to infinity. Instead, the radial and tangential displacements are expressed as

$$\begin{aligned} w(s) &= C_1 e^{-ik_1 s} + C_2 e^{-ik_2 s} + (\alpha_3)^{-1} C_3 e^{-ik_3 s} + C_4 e^{-ik_4 s} + C_5 e^{-ik_5 s} + (\alpha_6)^{-1} C_6 e^{-ik_6 s} \\ u(s) &= \alpha_1 C_1 e^{-ik_1 s} + \alpha_2 C_2 e^{-ik_2 s} + C_3 e^{-ik_3 s} + \alpha_4 C_4 e^{-ik_4 s} + \alpha_5 C_5 e^{-ik_5 s} + C_6 e^{-ik_6 s} \end{aligned} \quad (7.33a,b)$$

Now, at high frequencies, all the coefficients $\alpha_{1,2,4,5}$ and $(\alpha_{3,6})^{-1}$ tend to zero.

The physical vectors $\mathbf{w}$ and $\mathbf{f}$, consisting of the generalized displacements and corresponding internal forces, are defined as

$$\mathbf{w} = \begin{Bmatrix} w \\ \varphi \\ u \end{Bmatrix}, \qquad \mathbf{f} = \begin{Bmatrix} Q \\ M \\ N \end{Bmatrix} \quad (7.34a,b)$$

Note that the rotation φ and the internal forces Q, M and N are obtained by substituting equation (7.33) into equations (7.4), (7.12), (7.11b) and (7.11a), respectively. The wave vectors consisting of wave amplitudes are defined as

$$\mathbf{a}^+(s) = \begin{Bmatrix} C_1 e^{-ik_1 s} \\ C_2 e^{-ik_2 s} \\ C_3 e^{-ik_3 s} \end{Bmatrix}, \qquad \mathbf{a}^-(s) = \begin{Bmatrix} C_4 e^{-ik_4 s} \\ C_5 e^{-ik_5 s} \\ C_6 e^{-ik_6 s} \end{Bmatrix} \quad (7.35a,b)$$

Then the matrices Ψ and Φ for the transformation from the wave domain to the physical domain are given by

$$\begin{aligned} \Psi^+ &= \begin{bmatrix} \psi_1 & \psi_2 & \psi_3 \end{bmatrix}, & \Psi^- &= \begin{bmatrix} \psi_4 & \psi_5 & \psi_6 \end{bmatrix}, \\ \Phi^+ &= \begin{bmatrix} \phi_1 & \phi_2 & \phi_3 \end{bmatrix}, & \Phi^- &= \begin{bmatrix} \phi_4 & \phi_5 & \phi_6 \end{bmatrix} \end{aligned} \quad (7.36a,b,c,d)$$

where the column vectors ψ_i and ϕ_i for $i = 1, 2, 4, 5$ are

$$\psi_i = \begin{Bmatrix} 1 \\ -(\kappa\alpha_i + \mathrm{i}k_i) \\ \alpha_i \end{Bmatrix}, \qquad \phi_i = \begin{Bmatrix} \mathrm{i}EIk_i\left(\kappa^2 - k_i^2\right) \\ EI\left(\kappa^2 - k_i^2\right) \\ EA\left(\kappa - \mathrm{i}k_i\alpha_i\right) + EI\kappa\left(\kappa^2 - k_i^2\right) \end{Bmatrix} \tag{7.37a,b}$$

and ψ_i and ϕ_i for $i = 3, 6$ are

$$\psi_i = \frac{1}{\alpha_i}\begin{Bmatrix} 1 \\ -(\kappa\alpha_i + \mathrm{i}k_i) \\ \alpha_i \end{Bmatrix}, \qquad \phi_i = \frac{1}{\alpha_i}\begin{Bmatrix} \mathrm{i}EIk_i\left(\kappa^2 - k_i^2\right) \\ EI\left(\kappa^2 - k_i^2\right) \\ EA\left(\kappa - \mathrm{i}k_i\alpha_i\right) + EI\kappa\left(\kappa^2 - k_i^2\right) \end{Bmatrix} \tag{7.38a,b}$$

When $\Omega >> 1$, when the radial and tangential displacements decouple, the matrices Ψ^+ and Φ^+ asymptote to

$$\Psi^+ \approx \begin{bmatrix} 1 & 1 & 0 \\ -\mathrm{i}k_b & -k_b & 0 \\ 0 & 0 & 1 \end{bmatrix}, \qquad \Phi^+ \approx \begin{bmatrix} -\mathrm{i}EIk_b^3 & EIk_b^3 & 0 \\ -EIk_b^2 & EIk_b^2 & 0 \\ 0 & 0 & -\mathrm{i}EAk_l \end{bmatrix} \tag{7.39a,b}$$

i.e., the matrices are composed of those of the uniform straight beam and the uniform straight bar, and the other elements are zero, as expected.

The propagation matrix $\mathbf{F}$ describing propagation of waves over length L along the curved beam is given by

$$\mathbf{F}(L) = \begin{bmatrix} e^{-\mathrm{i}k_1 L} & 0 & 0 \\ 0 & e^{-\mathrm{i}k_2 L} & 0 \\ 0 & 0 & e^{-\mathrm{i}k_3 L} \end{bmatrix} \tag{7.40}$$

The positive and negative propagation matrices are the same in this case as expected.

The displacement, internal force and propagation matrices for the curved beam have been defined in equations (7.36) and (7.40). As illustrated so far, these matrices can be used in a systematic manner for various problems such as wave generation by external excitation, reflection and transmission of waves at discontinuities, and

derivation of spectral elements. However, such examples are not specifically presented because wave motion of the curved beams is too complex to present full analytical expressions for these cases. In section 7.8, a numerical example is presented. Before doing this, the energy flow associated with waves in the curved beam is studied first in the following two sections.

7.6 Energy flow

In section 2.9, the time-averaged power associated with waves in one-dimensional structures was expressed as

$$\Pi = \frac{1}{2}\mathbf{a}^H \mathbf{P}\,\mathbf{a} \tag{7.41}$$

where $\mathbf{a} = \left[\left(\mathbf{a}^+\right)^T \quad \left(\mathbf{a}^-\right)^T\right]^T$ and the matrix $\mathbf{P}$ is given by

$$\mathbf{P} = \frac{\mathrm{i}\omega}{2}\left[\begin{bmatrix} \left(\Psi^+\right)^H \Phi^+ & \left(\Psi^+\right)^H \Phi^- \\ \left(\Psi^-\right)^H \Phi^+ & \left(\Psi^-\right)^H \Phi^- \end{bmatrix} - \begin{bmatrix} \left(\Phi^+\right)^H \Psi^+ & \left(\Phi^+\right)^H \Psi^- \\ \left(\Phi^-\right)^H \Psi^+ & \left(\Phi^-\right)^H \Psi^- \end{bmatrix}\right] \tag{7.42}$$

Substituting equation (7.36) into equation (7.42) gives the power matrix $\mathbf{P}$ for the curved beam with constant curvature. Then the (m, n) element of the matrix for $m = 1, \ldots, 6$ and $n = 1, \ldots, 6$ is

$$P_{mn} = \frac{\mathrm{i}\omega}{2}\left(\psi_m^H \phi_n - \phi_m^H \psi_n\right) \tag{7.43}$$

In section 7.5, ψ_i and ϕ_i for $i = 3, 6$ were not defined in the same form as ψ_i and ϕ_i for $i = 1, 2, 4, 5$ for the reason stated there. However using the definition will make the following discussion lengthy. Thus, for the time being, ψ_i and ϕ_i for $i = 3, 6$ are assumed to be given in the same form as equation (7.37). Indeed this assumption will

not affect the qualitative investigation of P_{mn} since the difference only comes from dividing by the displacement ratio α_3 or α_6. Under this assumption, equation (7.43) is given by

$$P_{mn} = \frac{\omega}{2}\left\{EI\left(k_n + k_m^*\right)\left(k_n^2 + \left(k_m^*\right)^2 - 2\kappa^2\right) + EA\left(k_n + k_m^*\right)\alpha_n\alpha_m^* - \mathrm{i}EA\kappa\left(\alpha_n - \alpha_m^*\right)\right\} \quad (7.44)$$

Finally substituting equation (7.31) for the displacement ratio into equation (7.44) gives

$$P_{mn} = \frac{\omega EI\left(k_n + k_m^*\right)}{2}\left\{k_n^2 + \left(k_m^*\right)^2 - 2\kappa^2 + \frac{k_b^4\kappa^2}{\left(k_l^2 - k_n^2\right)\left(k_l^2 - \left(k_m^*\right)^2\right)}\right\} \quad (7.45)$$

Note again that equation (7.45) is only true for $P_{m,n}$ for $m = 1, 2, 4, 5$ and $n = 1, 2, 4, 5$, respectively. When the components of the third mode are concerned (i.e. m or n is 3 or 6, respectively), it should be divided again by α_3, α_6, or their self or cross product as required.

Equation (7.45) indicates the energy flow associated with the six wave components in the curved beam. Three cases are discussed separately in the next three subsections: the energy carried by a single wave component in subsection 7.6.1, the energy carried by interaction between the positive-going and negative-going components of one mode in subsection 7.6.2, and the energy carried by interaction between the components from two different modes in subsection 7.6.3.

7.6.1 Energy flow due to a single wave component

The diagonal elements of the matrix $\mathbf{P}$ are related to the power carried by a single wave component. When $n = m$, equation (7.45) becomes

$$P_{mm} = \frac{\omega EI\left(k_m + k_m^*\right)}{2}\left\{k_m^2 + \left(k_m^*\right)^2 - 2\kappa^2 + \frac{k_b^4\kappa^2}{\left(k_l^2 - k_m^2\right)\left(k_l^2 - \left(k_m^*\right)^2\right)}\right\} \tag{7.46}$$

Now P_{mm} is investigated for three cases for the wavenumber k_m as follows:

(i) Purely imaginary wavenumber: The first parenthesized term in equation (7.46) indicates that, if k_m is purely imaginary (i.e., the wave mode is evanescent), the element will be zero. Thus power carried by the wave components of the second mode will be zero in regions III and IV, i.e. $P_{22} = P_{44} = 0$ in these regions.

(ii) Purely real wavenumber: If k_m is purely real (i.e. $k_m^* = k_m$), equation (7.46) reduces to

$$P_{mm} = \omega EIk_m\left\{2\left(k_m^2 - \kappa^2\right) + \frac{k_b^4\kappa^2}{\left(k_l^2 - k_m^2\right)^2}\right\} \tag{7.47}$$

Equation (7.47) holds for wave components $m = 1, 2, 4, 5$. For the third mode (i.e. $m = 3, 6$), it becomes

$$\begin{aligned} P_{mm} &= \frac{\omega EIk_m}{|\alpha_m|^2}\left\{2\left(k_m^2 - \kappa^2\right) + \frac{k_b^4\kappa^2}{\left(k_l^2 - k_m^2\right)^2}\right\} \\ &= \omega EA\frac{k_l^2}{k_m}\left\{1 + \frac{2\left(k_m^2 - \kappa^2\right)\left(k_l^2 - k_m^2\right)^2}{k_b^4\kappa^2}\right\} \end{aligned} \tag{7.48}$$

When κ is small so that the terms involving κ can be neglected with respect to k_m and k_m asymptotes to the wavenumbers of the straight beam and bar, equation (7.47) asymptotes to that for the straight beam and equation (7.48) asymptotes to that of the straight bar as expected.

(iii) Complex wavenumber: Now assume k_m is not purely real or purely imaginary. Since k_m satisfies the characteristic equation (7.17),

$$k_m^6 + a_2 k_m^4 + a_1 k_m^2 + a_0 = 0 \tag{7.49}$$

the complex conjugate of k_m also satisfies the characteristic equation, i.e,

$$\left(k_m^*\right)^6 + a_2\left(k_m^*\right)^4 + a_1\left(k_m^*\right)^2 + a_0 = 0 \tag{7.50}$$

Subtracting equation (7.49) from equation (7.50) gives

$$\left\{k_m^2 - \left(k_m^*\right)^2\right\}\left\{k_m^4 + k_m^2\left(k_m^*\right)^2 + \left(k_m^*\right)^4 + a_2\left(k_m^2 + \left(k_m^*\right)^2\right) + a_1\right\} = 0 \tag{7.51}$$

Since the first bracketed term in equation (7.51) will not be zero if k_m is not purely real or purely imaginary, it follows that

$$k_m^4 + k_m^2\left(k_m^*\right)^2 + \left(k_m^*\right)^4 + a_2\left(k_m^2 + \left(k_m^*\right)^2\right) + a_1 = 0 \tag{7.52}$$

Using equation (7.52) it can be shown that the bracketed term in equation (7.46) is zero for complex k_m.

According to the discussion above, a single wave component can transport energy only when the wavenumber is purely real, as expected.

7.6.2 Energy flow due to two opposite-going waves of one mode

The non-diagonal elements of **P** are related to the power carried by the interaction between two different wave components. First consider the case that a positive-going wave component of one mode interacts with the negative-going component of the same mode, or *vice versa*. Six elements of the power matrix are relevant to this case, i.e. P_{14}, P_{25}, P_{36}, P_{41}, P_{52} and P_{63}. The power matrix is Hermitian

so that the first three elements are complex conjugates of the latter three elements. Since $k_n = -k_m$ in this case, equation (7.45) becomes

$$P_{mn} = \frac{\omega EI\left(-k_m + k_m^*\right)}{2}\left\{k_m^2 + \left(k_m^*\right)^2 - 2\kappa^2 + \frac{k_b^4\kappa^2}{\left(k_l^2 - k_m^2\right)\left(k_l^2 - \left(k_m^*\right)^2\right)}\right\} \tag{7.53}$$

Equation (7.53) is the same as equation (7.46) except for the first parenthesized term. Thus the interaction between two opposite-going wave components of one mode can transport energy only when the wavenumber is purely imaginary: if k_m is real, the first parenthesized term is zero, and, if k_m is complex, the bracketed term is zero. Therefore $P_{14} = P_{41} = 0$ in the whole frequency range, P_{25} and P_{52} are non-zero in regions III and IV, and P_{36} and P_{63} are non-zero in region III. The non-zero element P_{25} is

$$P_{25} = -\omega EIk_2\left\{2\left(k_2^2 - \kappa^2\right) + \frac{k_b^4\kappa^2}{\left(k_l^2 - k_2^2\right)^2}\right\} \tag{7.54}$$

and the non-zero element P_{36}, after allowing for the normalisation with respect to α_3 and α_6, is

$$P_{36} = -\omega EA\frac{k_l^2}{k_3}\left\{1 + \frac{2\left(k_3^2 - \kappa^2\right)\left(k_l^2 - k_3^2\right)^2}{k_b^4\kappa^2}\right\} \tag{7.55}$$

Note again that the counterpart elements P_{52} and P_{63} are the complex conjugates of P_{25} and P_{36}, respectively.

7.6.3 Energy flow due to two different wave modes

Now consider the case that a wave component of one mode interacts with a component of another mode. The elements P_{12}, P_{13}, P_{15}, P_{16}, etc of the power matrix are relevant to this case. Since k_m and k_n in equation (7.45) are independent wavenumbers for different modes, it follows from equation (7.26) that

$$\left(k_l^2 - k_m^2\right)\left(k_l^2 - k_n^2\right)\left(k_m^2 + k_n^2 - 2\kappa^2\right) + k_b^4\kappa^2 = 0 \tag{7.56}$$

Substituting $k_b^4\kappa^2$ from equation (7.56) into equation (7.45) yields

$$P_{mn} = \frac{\omega EI\left(k_n + k_m^*\right)\left\{k_m^2 - \left(k_m^*\right)^2\right\}\left\{k_m^2 + \left(k_m^*\right)^2 + k_n^2 - k_l^2 - 2\kappa^2\right\}}{2\left(k_l^2 - \left(k_m^*\right)^2\right)} \tag{7.57}$$

Using the wavenumber k_o for the third mode, which is related through equation (7.26a) to k_m and k_n, equation (7.57) reduces to

$$P_{mn} = \frac{\omega EI\left(k_n + k_m^*\right)\left\{k_m^2 - \left(k_m^*\right)^2\right\}\left\{\left(k_m^*\right)^2 - k_o^2\right\}}{2\left(k_l^2 - \left(k_m^*\right)^2\right)} \tag{7.58}$$

(i) The first bracketed term in the numerator of equation (7.58) indicates that the interaction of the two components cannot transport power if the wavenumber for one of the two interacting waves is purely real or purely imaginary. Thus $P_{12} = P_{13} = P_{15} = P_{16} = 0$, $P_{42} = P_{43} = 0$, and $P_{54} = P_{64} = 0$ in the whole frequency range.

(ii) Only P_{23}, P_{26} and P_{35} (and their counterparts) in the matrix **P** have not been considered yet. These elements are related to energy transported by interaction between a wave component of the second mode and a wave component of the

third mode. Since at least one wavenumber for the two modes is purely real or purely imaginary in the whole frequency range except region II, P_{23}, P_{26} and P_{35} are zero over most of the frequency range. The first parenthesized term in the numerator of equation (7.58) indicates that, even in region II, P_{23} is zero since $k_3 = -k_2^*$. As a result, P_{26} and P_{35} are non-zero in region II. Since $k_6 = k_2^*$ in region II, the non-zero P_{26} in the region is, after allowing for the normalisation with respect to α_6, given by

$$P_{26} = -\frac{\mathrm{i}\omega EI}{\kappa}\left(k_2^2 - \left(k_2^*\right)^2\right)\left(\left(k_2^*\right)^2 - k_1^2\right) \tag{7.59}$$

The non-zero P_{35} in region II is $P_{35} = P_{26}^*$.

7.6.4 Summary of section 7.6

The elements of the power matrix for the curved beam with constant curvature have been expressed explicitly in terms of wavenumbers, and their values were classified according to different conditions for the wavenumbers. It was shown that energy flow is associated with three cases:

- a single wave with purely real wavenumber (i.e., a propagating wave)
- interaction between two opposite-going waves of one mode, for which the wavenumber is purely imaginary (i.e., two opposite-going nearfield waves)
- interaction between two opposite-going waves from different modes, for which the wavenumbers are a complex conjugate pair

In the next section, these results are used to find the power associated with waves when the frequency is given.

7.7 Energy flow at a single frequency

To help to clarify the energy flow in the curved beam, the results of section 7.6 are described here again from a somewhat different viewpoint: when the frequency is given, the energy flow paths (carriers) are identified at that frequency as follows:

(i) In region I: all waves are propagating and the wavenumbers are real in this frequency range. The power matrix becomes diagonal and is given by

$$\mathbf{P}=\begin{bmatrix} P_{11} & 0 & 0 & 0 & 0 & 0 \\ 0 & P_{22} & 0 & 0 & 0 & 0 \\ 0 & 0 & P_{33} & 0 & 0 & 0 \\ 0 & 0 & 0 & -P_{11} & 0 & 0 \\ 0 & 0 & 0 & 0 & -P_{22} & 0 \\ 0 & 0 & 0 & 0 & 0 & -P_{33} \end{bmatrix} \tag{7.60}$$

where the diagonal elements are

$$\begin{aligned} P_{11} &= \omega E I k_1 \left\{ 2\left(k_1^2-\kappa^2\right)+\frac{k_b^4\kappa^2}{\left(k_l^2-k_1^2\right)^2} \right\}, \\ P_{22} &= \omega E I k_2 \left\{ 2\left(k_2^2-\kappa^2\right)+\frac{k_b^4\kappa^2}{\left(k_l^2-k_2^2\right)^2} \right\}, \\ P_{33} &= \omega E A \frac{k_l^2}{k_3}\left\{ 1+\frac{2\left(k_3^2-\kappa^2\right)\left(k_l^2-k_3^2\right)^2}{k_b^4\kappa^2} \right\} \end{aligned} \tag{7.61a,b,c}$$

Note that the net power due to waves in vector $\mathbf{a}$ is given by

$$\Pi=\frac{1}{2}\mathbf{a}^H\mathbf{P}\,\mathbf{a} \tag{7.62}$$

For example, if there are two opposite-going waves of the first mode, i.e., $\mathbf{a}=\begin{bmatrix} a_1 & 0 & 0 & a_4 & 0 & 0 \end{bmatrix}^T$, the net power is given by

$$\Pi = \frac{1}{2} P_{11} \left(|a_1|^2 - |a_4|^2 \right) \tag{7.63}$$

(ii) In region II: the non-zero elements are P_{11}, P_{26}, P_{35} and their counterparts P_{44}, P_{62} and P_{53}. In the case, $P_{26} = P_{62}^* = P_{35}^* = P_{53}$. Thus the power matrix is given by

$$\mathbf{P} = \begin{bmatrix} P_{11} & 0 & 0 & 0 & 0 & 0 \\ 0 & 0 & 0 & 0 & 0 & P_{26} \\ 0 & 0 & 0 & 0 & P_{26}^* & 0 \\ 0 & 0 & 0 & -P_{11} & 0 & 0 \\ 0 & 0 & P_{26} & 0 & 0 & 0 \\ 0 & P_{26}^* & 0 & 0 & 0 & 0 \end{bmatrix} \tag{7.64}$$

where the element P_{11} is the same as equation (7.61a) and

$$P_{26} = -\frac{i\omega EI}{\kappa} \left(k_2^2 - \left(k_2^* \right)^2 \right) \left(\left(k_2^* \right)^2 - k_1^2 \right) \tag{7.65}$$

For example, for the case where $\mathbf{a} = \begin{bmatrix} 0 & a_2 & 0 & 0 & 0 & a_6 \end{bmatrix}^T$, the power associated with the waves is given by

$$\Pi = \mathrm{Re} \left(P_{26} \left(a_2 \right)^* a_6 \right) \tag{7.66}$$

where $\mathrm{Re}(\cdot)$ denotes the real part of the quantity. The direction of energy flow depends on the sum of the phases of P_{26}, $\left(a_2 \right)^*$ and a_6.

The power matrix is not diagonal in this region, which may lead to further transformation to a basis, so-called power wave basis, where power is transported independently only by a single component. The matrices **V** and **E** of the eigenvalues and eigenvectors, respectively, of the power matrix for the transformation are

$$\mathbf{V} = \begin{bmatrix} P_{11} & 0 & 0 & 0 & 0 & 0 \\ 0 & |P_{26}| & 0 & 0 & 0 & 0 \\ 0 & 0 & |P_{26}| & 0 & 0 & 0 \\ 0 & 0 & 0 & -P_{11} & 0 & 0 \\ 0 & 0 & 0 & 0 & -|P_{26}| & 0 \\ 0 & 0 & 0 & 0 & 0 & -|P_{26}| \end{bmatrix},$$

$$\mathbf{E} = \begin{bmatrix} 1 & 0 & 0 & 0 & 0 & 0 \\ 0 & \frac{1}{\sqrt{2}} & 0 & 0 & 0 & \frac{\phi}{\sqrt{2}} \\ 0 & 0 & \frac{1}{\sqrt{2}} & 0 & \frac{\phi^*}{\sqrt{2}} & 0 \\ 0 & 0 & 0 & 1 & 0 & 0 \\ 0 & 0 & \frac{\phi}{\sqrt{2}} & 0 & -\frac{1}{\sqrt{2}} & 0 \\ 0 & \frac{\phi^*}{\sqrt{2}} & 0 & 0 & 0 & -\frac{1}{\sqrt{2}} \end{bmatrix} \qquad (7.67a,b)$$

where $\phi = \dfrac{P_{26}}{|P_{26}|}$. Note that P_{26} is complex in this region.

(iii) In region III: the power matrix is given by

$$\mathbf{P} = \begin{bmatrix} P_{11} & 0 & 0 & 0 & 0 & 0 \\ 0 & 0 & 0 & 0 & P_{25} & 0 \\ 0 & 0 & 0 & 0 & 0 & P_{36} \\ 0 & 0 & 0 & -P_{11} & 0 & 0 \\ 0 & P_{25}^* & 0 & 0 & 0 & 0 \\ 0 & 0 & P_{36}^* & 0 & 0 & 0 \end{bmatrix} \qquad (7.68)$$

where the element P_{11} is the same as equation (7.61a) and

$$P_{25} = -\omega E I k_2 \left\{ 2\left(k_2^2 - \kappa^2\right) + \frac{k_b^4 \kappa^2}{\left(k_1^2 - k_2^2\right)^2} \right\},$$

$$P_{36} = -\omega E A \frac{k_1^2}{k_3} \left\{ 1 + \frac{2\left(k_3^2 - \kappa^2\right)\left(k_1^2 - k_3^2\right)^2}{k_b^4 \kappa^2} \right\} \qquad (7.69a,b)$$

The elements P_{25} and P_{36} are negative-imaginary in this region so that the eigenvalues and eigenvectors are

$$\mathbf{V} = \begin{bmatrix} P_{11} & 0 & 0 & 0 & 0 & 0 \\ 0 & |P_{25}| & 0 & 0 & 0 & 0 \\ 0 & 0 & |P_{36}| & 0 & 0 & 0 \\ 0 & 0 & 0 & -P_{11} & 0 & 0 \\ 0 & 0 & 0 & 0 & -|P_{25}| & 0 \\ 0 & 0 & 0 & 0 & 0 & -|P_{36}| \end{bmatrix},$$

$$\mathbf{E} = \begin{bmatrix} 1 & 0 & 0 & 0 & 0 & 0 \\ 0 & \frac{1}{\sqrt{2}} & 0 & 0 & -\frac{\mathrm{i}}{\sqrt{2}} & 0 \\ 0 & 0 & \frac{1}{\sqrt{2}} & 0 & 0 & -\frac{\mathrm{i}}{\sqrt{2}} \\ 0 & 0 & 0 & 1 & 0 & 0 \\ 0 & \frac{\mathrm{i}}{\sqrt{2}} & 0 & 0 & -\frac{1}{\sqrt{2}} & 0 \\ 0 & 0 & \frac{\mathrm{i}}{\sqrt{2}} & 0 & 0 & -\frac{1}{\sqrt{2}} \end{bmatrix} \qquad (7.70a,b)$$

(iv) <u>In region IV</u>: the power matrix is given by

$$\mathbf{P} = \begin{bmatrix} P_{11} & 0 & 0 & 0 & 0 & 0 \\ 0 & 0 & 0 & 0 & P_{25} & 0 \\ 0 & 0 & P_{33} & 0 & 0 & 0 \\ 0 & 0 & 0 & -P_{11} & 0 & 0 \\ 0 & P_{25}^{*} & 0 & 0 & 0 & 0 \\ 0 & 0 & 0 & 0 & 0 & -P_{33} \end{bmatrix} \qquad (7.71)$$

where the elements P_{11}, P_{33} and P_{25} are the same as equations (7.61a), (7.61c) and (7.69a), respectively. The element P_{25} is negative-imaginary in this region so that the eigenvalues and eigenvectors are

$$\mathbf{V}=\begin{bmatrix} P_{11} & 0 & 0 & 0 & 0 & 0 \\ 0 & |P_{25}| & 0 & 0 & 0 & 0 \\ 0 & 0 & P_{33} & 0 & 0 & 0 \\ 0 & 0 & 0 & -P_{11} & 0 & 0 \\ 0 & 0 & 0 & 0 & -|P_{25}| & 0 \\ 0 & 0 & 0 & 0 & 0 & -P_{33} \end{bmatrix},$$

$$\mathbf{E}=\begin{bmatrix} 1 & 0 & 0 & 0 & 0 & 0 \\ 0 & \frac{1}{\sqrt{2}} & 0 & 0 & -\frac{\mathrm{i}}{\sqrt{2}} & 0 \\ 0 & 0 & 1 & 0 & 0 & 0 \\ 0 & 0 & 0 & 1 & 0 & 0 \\ 0 & \frac{\mathrm{i}}{\sqrt{2}} & 0 & 0 & -\frac{1}{\sqrt{2}} & 0 \\ 0 & 0 & 0 & 0 & 0 & 1 \end{bmatrix} \qquad (7.72a,b)$$

Figure 7-5 shows the magnitudes of the elements of **P** for the curved beam with $\bar{\chi}^2 = 1/1200$ as a function of a frequency. In the figure the magnitudes of P_{33} and P_{36} are normalised with respect to ωEAk_l and the others are normalised with respect to $2\omega EIk_b^3$. It is seen that there are always three energy transport paths at any frequency given. It means that, including the counterparts not shown in the figure (e.g., in region I, P_{44}, P_{55} and P_{66} associated with the negative-going waves), there are six energy transport paths as expected. It is also seen that, at high frequencies, the powers associated with the waves tend to those in the straight beam (i.e., P_{11}, P_{25} and P_{36} tends to unity above the ring frequency $\Omega = 1$).

7.8 Numerical examples

In section 7.5, the displacement, internal force and propagation matrices for the curved beams were defined as equations (7.36) and (7.40). These matrices can be used

in a systematic manner for various problems concerning the motion of the curved beam In this section, a numerical example is given for illustration of the approach based on reflection, transmission and propagation of waves.

Consider a structure where two parallel straight beams are connected by a curved beam with constant curvature subtending angle π as shown in Figure 7-6. The beams are made of the same material, and the cross-sections are all rectangular in shape of thickness h and width b. The vector of amplitudes of waves incident from the left-hand side of junction 1 is $\mathbf{a}^+$, that of reflected waves is $\mathbf{a}^-$, and that of transmitted waves is $\mathbf{d}^+$.

The physical quantities are continuous at the two junctions, respectively. At junction 1, the continuity conditions are

$$\begin{aligned} \mathbf{w}_a &= \mathbf{w}_b \\ \mathbf{f}_a &= \mathbf{f}_b \end{aligned} \tag{7.73a,b}$$

where $\mathbf{w} = \begin{bmatrix} w & \varphi & u \end{bmatrix}^T$, $\mathbf{f} = \begin{bmatrix} Q & M & N \end{bmatrix}^T$, and the subscripts a and b denote the left- and right-hand sides of junction 1, respectively. Assuming that, at the right-hand side of junction 1, the amplitudes of positive-going waves are given in a vector $\mathbf{b}^+$ but there are no negative-going waves at this moment, equation (7.73) is re-written as

$$\begin{aligned} \Psi_a^{\ +}\mathbf{a}^+ + \Psi_a^{\ -}\mathbf{a}^- &= \Psi_b^{\ +}\mathbf{b}^+, \\ \Phi_a^{\ +}\mathbf{a}^+ + \Phi_a^{\ -}\mathbf{a}^- &= \Phi_b^{\ +}\mathbf{b}^+ \end{aligned} \tag{7.74a,b}$$

where the matrices for the straight beam are

$$\Psi_a^+ = \begin{bmatrix} 1 & 1 & 0 \\ -\mathrm{i}k_b & -k_b & 0 \\ 0 & 0 & 1 \end{bmatrix}, \qquad \Phi_a^+ = \begin{bmatrix} -\mathrm{i}EIk_b^3 & EIk_b^3 & 0 \\ -EIk_b^2 & EIk_b^2 & 0 \\ 0 & 0 & -\mathrm{i}EAk_l \end{bmatrix},$$

$$\Psi_a^- = \begin{bmatrix} 1 & 1 & 0 \\ \mathrm{i}k_b & k_b & 0 \\ 0 & 0 & 1 \end{bmatrix}, \qquad \Phi_a^- = \begin{bmatrix} \mathrm{i}EIk_b^3 & -EIk_b^3 & 0 \\ -EIk_b^2 & EIk_b^2 & 0 \\ 0 & 0 & \mathrm{i}EAk_l \end{bmatrix} \qquad (7.75a,b,c,d)$$

and the matrices Ψ_b^+ and Φ_b^+ for the curved beam are given by equation (7.36a,c). Note in equation (7.74) that the wave vectors $\mathbf{a}^{\pm}$ in the straight beam are 3×1, the first and second elements are the propagating and nearfield waves relating to bending motion, respectively, and the third element is the propagating wave relating to longitudinal motion. From equation (7.74), the reflection and transmission matrices $\mathbf{R}_1$ and $\mathbf{T}_1$ for waves incident from the left-hand side of junction 1 are given by

$$\mathbf{R}_1 = \left[\Phi_b^+ \left(\Psi_b^+\right)^{-1} \Psi_a^- - \Phi_a^-\right]^{-1} \left[-\Phi_b^+ \left(\Psi_b^+\right)^{-1} \Psi_a^+ + \Phi_a^+\right],$$

$$\mathbf{T}_1 = \left[\Phi_a^- \left(\Psi_a^-\right)^{-1} \Psi_b^+ - \Phi_b^+\right]^{-1} \left[\Phi_a^- \left(\Psi_a^-\right)^{-1} \Psi_a^+ - \Phi_a^+\right] \qquad (7.76a,b)$$

The other reflection and transmission matrices $\hat{\mathbf{R}}_1$, $\hat{\mathbf{T}}_1$, $\mathbf{R}_2$, $\mathbf{T}_2$ $\hat{\mathbf{R}}_2$ and $\hat{\mathbf{T}}_2$ can be obtained in a similar way. The propagation matrix $\mathbf{F}$ between the junctions is given by equation (7.40). Using the reflection, transmission and propagation matrices, the reflected and transmitted waves for the case are obtained as

$$\mathbf{a}^- = \mathbf{R}_T \mathbf{a}^+; \qquad \mathbf{R}_T = \mathbf{R}_1 + \hat{\mathbf{T}}_1 \mathbf{F} \hat{\mathbf{R}}_1 \mathbf{F} [\mathbf{I} - \hat{\mathbf{R}}_1 \mathbf{F} \hat{\mathbf{R}}_1 \mathbf{F}]^{-1} \mathbf{T}_1$$

$$\mathbf{d}^+ = \mathbf{T}_T \mathbf{a}^+; \qquad \mathbf{T}_T = \hat{\mathbf{T}}_1 \mathbf{F} [\mathbf{I} - \hat{\mathbf{R}}_1 \mathbf{F} \hat{\mathbf{R}}_1 \mathbf{F}]^{-1} \mathbf{T}_1 \qquad (7.77a, b)$$

where $\mathbf{R}_T$ and $\mathbf{T}_T$ are *global* reflection and transmission matrices for the junctions.

Suppose that the incident waves are $\mathbf{a}^+ = \begin{bmatrix} a_1^+ & 0 & 0 \end{bmatrix}^T$, i.e., only the propagating bending wave component of amplitude a^+ impinges from the left-hand side of junction 1. Then the input power into the curved connector is

$$\Pi_i = \omega E I k_b^{\,3} \left| a_1^+ \right|^2 \tag{7.78}$$

If the amplitudes of the reflected waves are $\mathbf{a}^- = \begin{bmatrix} a_1^- & a_2^- & a_3^- \end{bmatrix}^T$, the reflected power is

$$\Pi_r = -\omega E I k_b^{\,3} \left| a_1^- \right|^2 - \frac{1}{2} \omega E A k_l \left| a_3^- \right|^2 \tag{7.79}$$

Thus the power reflection coefficient $\varrho = -\Pi_r / \Pi_i$ is given by

$$\varrho = \varrho_{BB} + \varrho_{BL} \tag{7.80}$$

where ϱ_{BB} and ϱ_{BL} are

$$\varrho_{BB} = \frac{\left| a_1^- \right|^2}{\left| a_1^+ \right|^2}, \qquad \varrho_{BL} = \frac{k_b}{2k_l} \frac{\left| a_3^- \right|^2}{\left| a_1^+ \right|^2} \tag{7.81a,b}$$

Note that ϱ_{BB} is the coefficient related to bending-to-bending reflection and ϱ_{BL} is the coefficient related to bending-to-longitudinal reflection. Similarly, for transmitted waves $\mathbf{d}^+ = \begin{bmatrix} d_1^+ & d_2^+ & d_3^+ \end{bmatrix}^T$, the power transmission coefficient $\tau = \Pi_t / \Pi_i$ is given by

$$\tau = \tau_{BB} + \tau_{BL} \tag{7.82}$$

where the coefficients τ_{BB} and τ_{BL} are

$$\tau_{BB} = \frac{\left| d_1^+ \right|^2}{\left| a_1^+ \right|^2}, \qquad \tau_{BL} = \frac{k_b}{2k_l} \frac{\left| d_3^+ \right|^2}{\left| a_1^+ \right|^2} \tag{7.83}$$

Note that the sum of the coefficients is unity for a conservative system, i.e.,

$$\varrho + \tau = \varrho_{BB} + \varrho_{BL} + \tau_{BB} + \tau_{BL} = 1 \tag{7.84}$$

Suppose now that the incident waves are $\mathbf{a}^+ = \begin{bmatrix} 0 & 0 & a_3^+ \end{bmatrix}^T$, i.e., a propagating longitudinal wave of amplitude a_3^+ impinges from the left-hand side of junction 1. In this case the input power into the curved beam is

$$\Pi_i = \frac{1}{2}\omega EAk_l \left|a_3^+\right|^2 \tag{7.85}$$

Then the power reflection and transmission coefficients ϱ and τ for this case are

$$\varrho = \varrho_{LB} + \varrho_{LL}, \qquad \tau = \tau_{LB} + \tau_{LL}$$

where the coefficients are

$$\varrho_{LB} = \frac{2k_l}{k_b}\frac{\left|a_1^-\right|^2}{\left|a_3^+\right|^2}, \quad \varrho_{LL} = \frac{\left|a_3^-\right|^2}{\left|a_3^+\right|^2}, \quad \tau_{LB} = \frac{2k_l}{k_b}\frac{\left|d_1^+\right|^2}{\left|a_3^+\right|^2}, \quad \tau_{LL} = \frac{\left|d_3^+\right|^2}{\left|a_3^+\right|^2} \tag{7.86a,b,c,d}$$

For a conservative system, the sum of these four coefficients is unity.

Figure 7-7(a) shows numerical examples of the power coefficients for the cases where a propagating bending wave is incident on junction 1 from the left-hand side, i.e., $\mathbf{a}^+ = \begin{bmatrix} a_1^+ & 0 & 0 \end{bmatrix}^T$ while Figure 7-7(b) shows those where a propagating longitudinal wave is incident, i.e., $\mathbf{a}^+ = \begin{bmatrix} 0 & 0 & a_3^+ \end{bmatrix}^T$. Although it is not shown in the figure, the sum of the four coefficients is unity. It is seen that $\tau_{BL} = \tau_{LB}$ and $\varrho_{BL} = \varrho_{LB}$ due to reciprocity. Above the ring frequency $\Omega = 1$, τ_{BB} and τ_{LL} are approximately equal to unity, i.e. the incident waves can pass through the junctions and the curved beam freely without scattering or conversion into the other wave type. Below the ring frequency, the bending wave is substantially transmitted but the longitudinal wave is mainly reflected backwards as a longitudinal wave. For a frequency $\Omega < 10^{-2}$, it is seen that $\tau_{BL} = \varrho_{BL}$

and $\tau_{LB} = \varrho_{LB}$. Although it is not shown in the figure (b), it holds that $\varrho = \varrho_{LB} + \varrho_{LL} = 0.5$ (thus $\tau = \tau_{LB} + \tau_{LL} = 0.5$) at the ring frequency $\Omega = 1$, i.e., half the energy carried by the longitudinal wave is reflected and the other half is transmitted.

7.9 Summary

The equations of in-plane motion of thin, uniform, curved beams have been derived based on Flügge theory. The radial and tangential displacements of the curved beam are coupled together due to curvature. This coupling will be negligible when the curvature becomes smaller and/or frequencies increase. The dispersion relation for constant curvature has been obtained when time harmonic motion was assumed. The equation is of 6^{th} order in k so that six wave components are associated with the motion of the curved beam, three positive-going components and the other three negative-going components: the curved beam is a three wave mode system.

An ambiguity may occur in defining each branch of the dispersion curve for the six wave components. In this thesis, a criterion has been suggested to remove the ambiguity: the wavenumber of a positive-going wave should satisfy

$$\mathrm{Im}\{k\} \le 0, \qquad \mathrm{Re}\{\partial k/\partial \omega\} > 0 \text{ if } \mathrm{Im}\{k\} = 0 \tag{7.87a,b}$$

i.e., the imaginary value of the wavenumber of a positive-going wave should be negative and the energy transport velocity (the slope of the dispersion curve of the real wavenumber in this case) associated with a positive-going wave should be positive. Using this criterion, the dispersion curve for each component was well defined. The first and second modes are predominantly related to the propagating and nearfield waves of bending deformation. The third mode is predominantly related to the longitudinal

motion. Above the ring frequency, where the longitudinal wavelength is equal to the circumference of the complete ring, the wavenumber of the third mode becomes purely real. It was seen that energy is transported by the second mode in the direction opposite to the direction of the disturbance propagation, at low frequencies.

After specifying each branch of the dispersion relation in this manner, the wave motion of the curved beams was described in a systematic way. The displacement, internal force and propagation matrices for the curved beams were defined. The propagation matrix is diagonal in this case so that, even though the displacements are coupled together, the wave components are not coupled at all. Thus the problem could be simplified in the wave domain.

The time-averaged power associated with waves was expressed explicitly in terms of wavenumbers. It was shown that energy flow is associated with three cases:

- a single wave with purely real wavenumber (i.e., a propagating wave)
- interaction between two opposite-going waves of one mode, for which the wavenumber is purely imaginary (i.e., two opposite-going nearfield waves)
- interaction between two opposite-going waves from different modes, for which the wavenumbers are a complex conjugate pair

Using these results the power associated with waves in the curved beam was determined when the frequency is given.

Numerical results for the power transmission and reflection through a U-shaped structure are presented using the wave approach based on reflection, transmission and propagation of waves. It was shown that, above the ring frequency, the energy associated with the propagating waves can be transmitted through the curved section

with negligible reflection. At the ring frequency, half the energy carried by the longitudinal wave is reflected and the other half is transmitted.

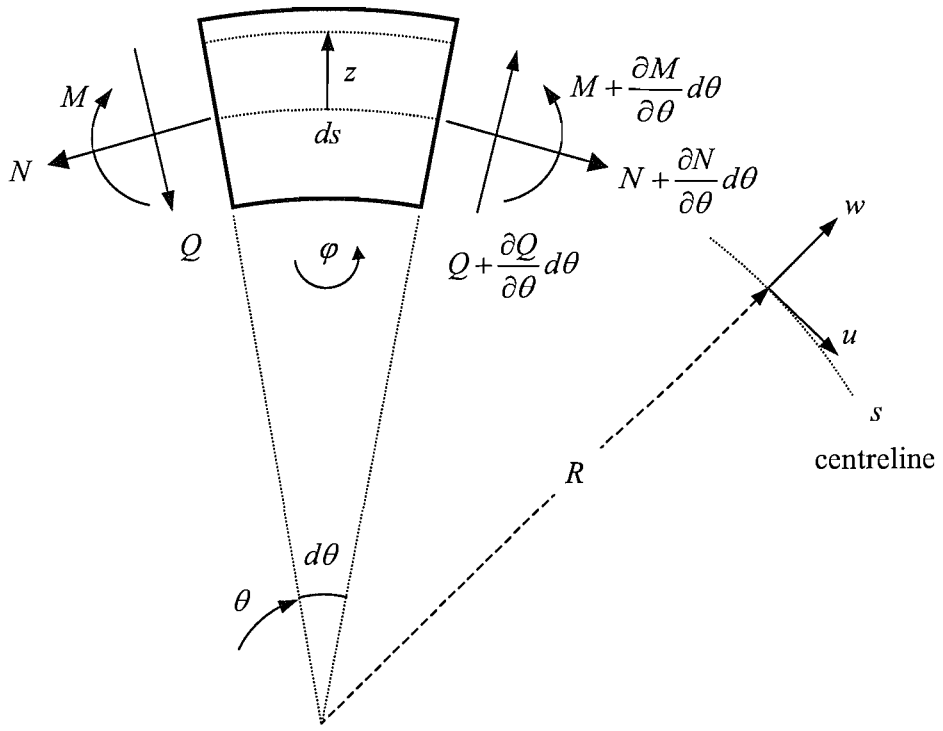

Figure 7-1. Differential element of a thin, curved beam and sign convention of physical quantities.

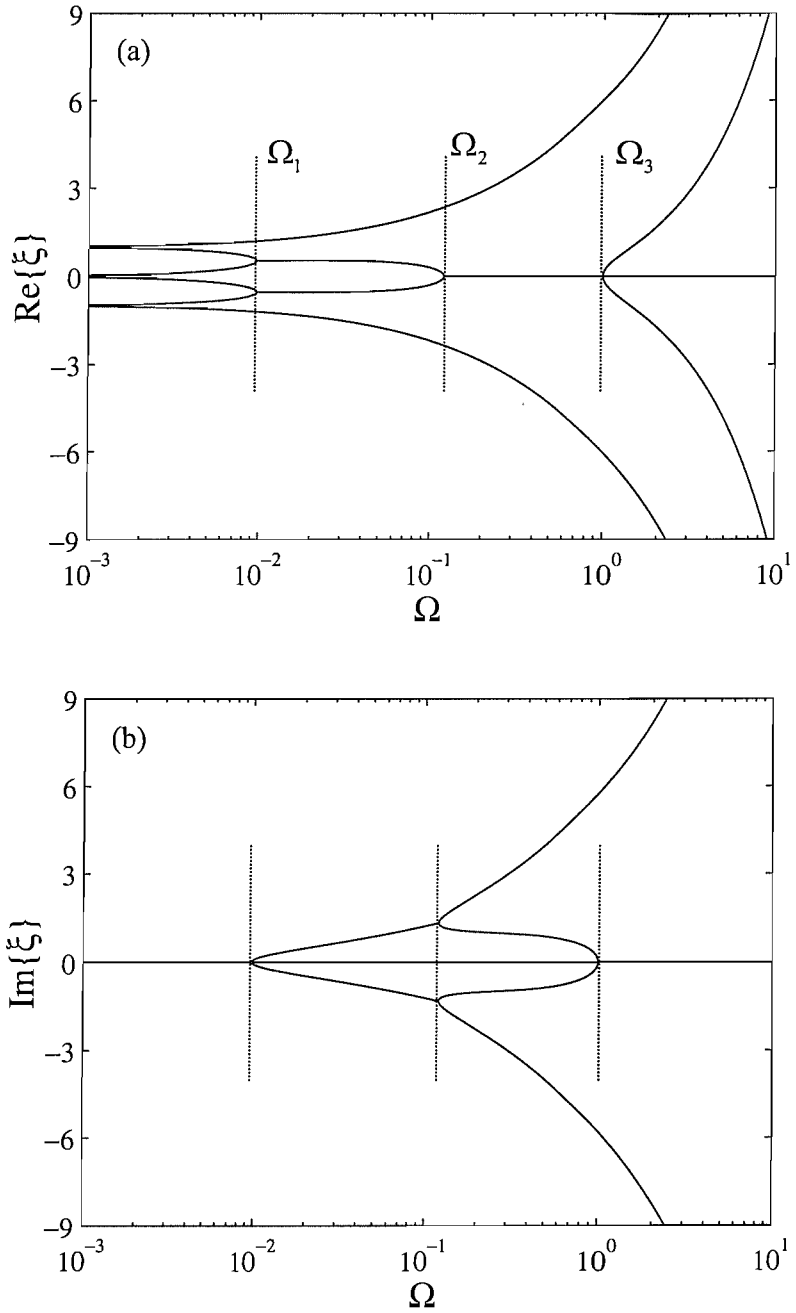

Figure 7-2. Dispersion relations for wave modes in the curved beam with $\overline{\chi}^2 = 1/1200$.

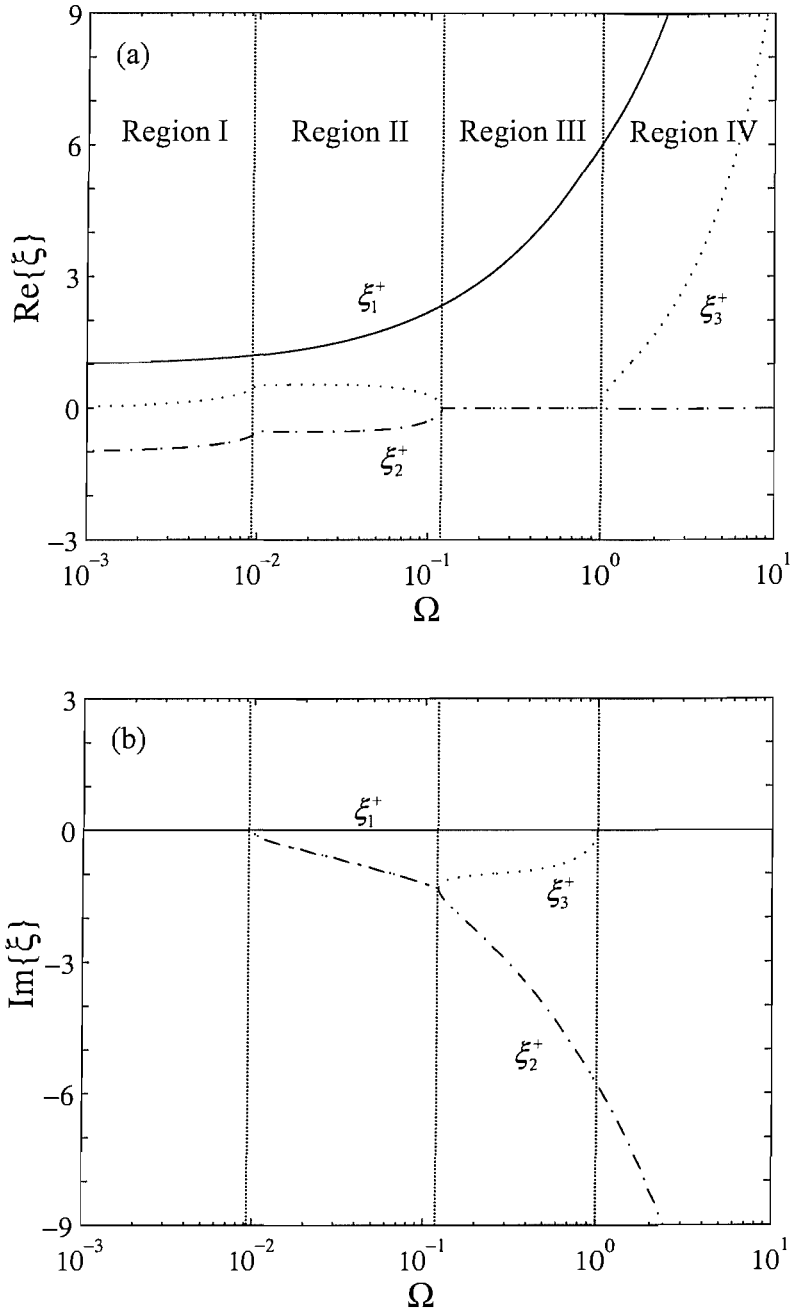

Figure 7-3. Dispersion relations for positive-going waves in the curved beam with $\bar{\chi}^2 = 1/1200$.

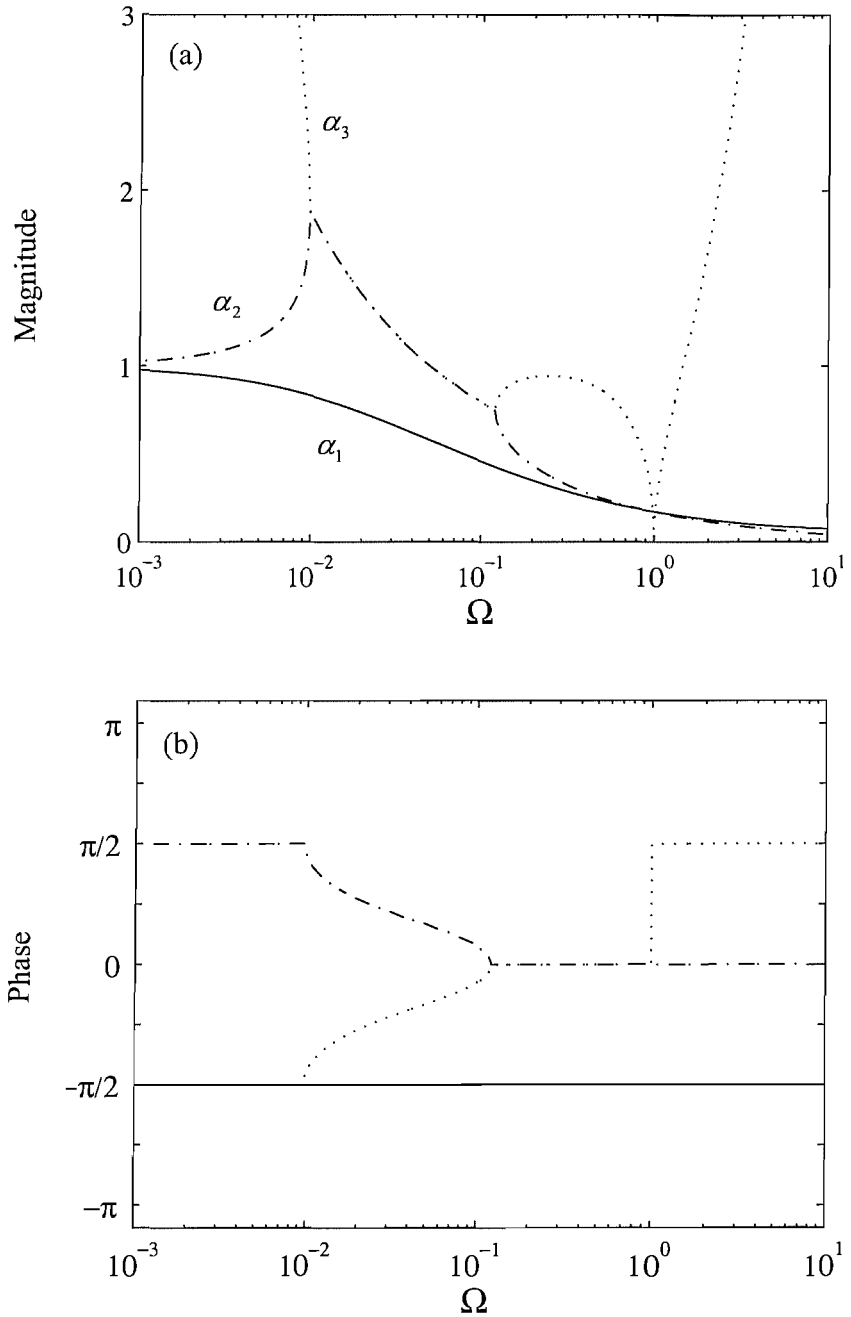

Figure 7-4. Ratio of the tangential displacement to the radial displacement, $\alpha = C_u/C_w$, for the curved beam with $\bar{\chi}^2 = 1/1200$.

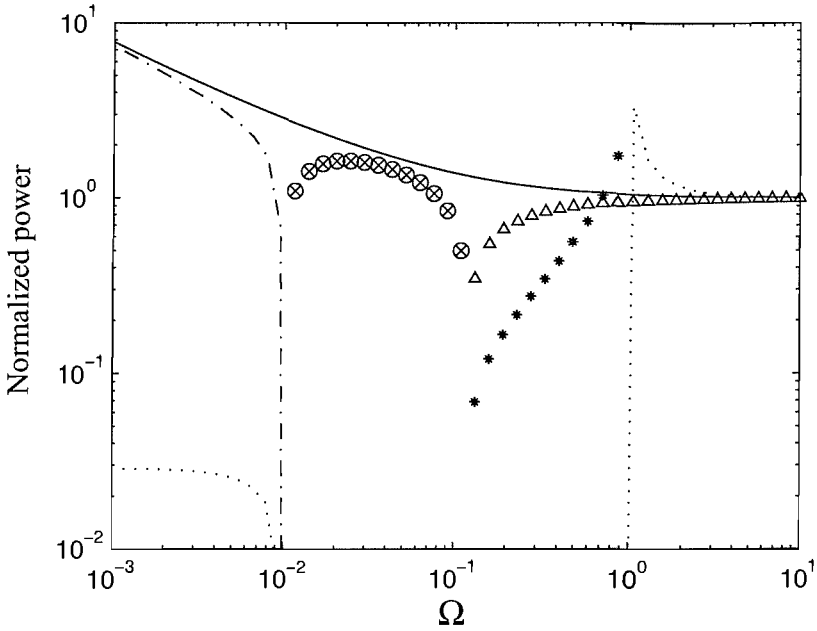

Figure 7-5. Elements of power matrix for the curved beam with $\bar{\chi}^2 = 1/1200$: ——, P_{11}; -·-·-, P_{22}; ·····, P_{33}; ○, P_{26}; ×, P_{35}; △, P_{25}; *, P_{36}. In the figure the magnitudes of P_{33} and P_{36} are normalised with respect to ωEAk_l and the others are normalised with respect to $2\omega EIk_b^3$.

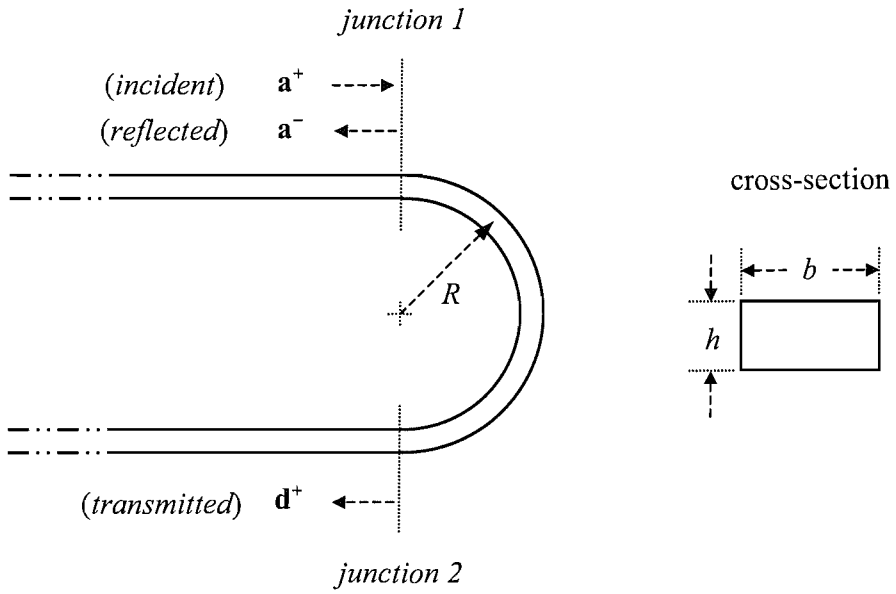

Figure 7-6. Reflection and transmission of waves through a curved beam with constant curvature.

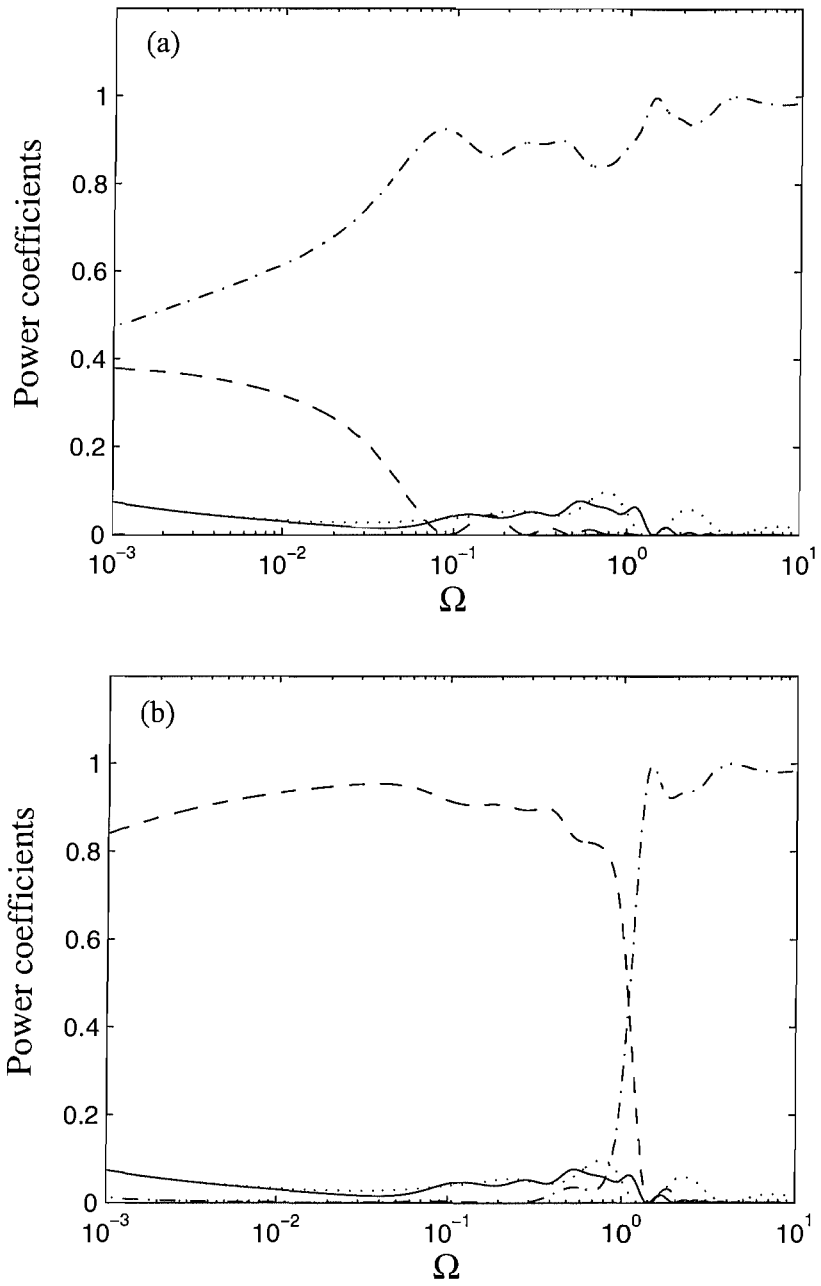

Figure 7-7. Power transmission and reflection coefficients for the half-circular beam (a) when the propagating bending wave is incident; -·-·-·- , τ_{BB}; ····· , τ_{BL}; ------ , ϱ_{BB}; ——— , ϱ_{BL}; (b) when the propagating axial wave is incident; ····· , τ_{LB}; -·-·-·- , τ_{LL}; ——— , ϱ_{LB}; ------, ϱ_{LL}.

Chapter 8.

APPLICATIONS

8.1 Introduction

A generalised wave approach based on reflection, transmission and propagation of waves has been developed and applied to cases concerning uniform and deterministically varying structures in previous chapters. Attention was paid especially to longitudinal and bending motions of the structures. As would be expected, there are plenty of other cases where the wave approach can be used as an efficient and well-conditioned method. For example, torsional motion of structures is expressed in the same mathematical form as longitudinal motion. Thus the results obtained in chapters 3 and 5 can be directly used for the structures undergoing torsion rather than longitudinal motion by replacing relevant parameters and variables. Table 8.1 lists the motions sharing the same mathematical form and relationships of the parameters.

The objective of this chapter is to illustrate further possible application of the wave approach by presenting several other cases, which have not been dealt with to date. First, in section 8.2, application of the wave approach to higher-order uniform waveguides is briefly discussed. The displacement, internal force and propagation matrices for the longitudinal wave motion based on Love theory and for the bending wave motion based on Timoshenko theory are presented, respectively. One thing, which may be noted, is that it is always possible to use the wave approach for the motion of uniform waveguides where the coefficients of the governing equations are constant.

Even at high frequencies, the wave approach will provide an efficient and well-conditioned computational approach.

In section 8.3, several different kinds of deterministically varying waveguides are presented. The displacement, internal force and propagation matrices for waveguides with an exponential, rather than power-law, variation in the geometric properties are presented. The longitudinal power transmission through an exponential connector is investigated using the matrices.

In section 8.4, the wave approach is applied for the motion of arbitrarily varying waveguides where the properties vary in a complex manner so that exact solution to the motion is difficult or impossible to obtain. In the application, the arbitrarily varying waveguide is divided into a series of small segments, and then each segment is modelled by a known structural element - a piecewise approach. Several different schemes in developing a piecewise model by using uniform elements and deterministically varying elements are described. The numerical efficiency relating to each model is then investigated.

In section 8.5, as a final example for the application of the wave approach, the motion of finite structures is studied. A general procedure for obtaining the natural frequencies and mode shapes is described and numerical results for the modal behaviour of a tapered, curved beam are presented.

8.2 Higher-order uniform waveguides

Even though the interest of this thesis has been confined to cases based on elementary theories such as Euler-Bernoulli beam theory, the wave approach can equally be applied to the motion of uniform structures based on higher-order theories.

These higher-order theories, such as Love's bar theory and Timoshenko's beam theory, provide more accurate description of the motion at high frequencies than elementary theories. Since the wave approach does not suffer numerical difficulties due to ill-conditioning at high frequencies, in contrast to other methods such as the transfer matrix method, no drawback will occur in applying the wave approach.

8.2.1 Straight bar based on Love's theory

The longitudinal wave motion in uniform straight bars, described in chapter 3, is based on the elementary theory assuming constant longitudinal strain across the cross-section and neglecting the transverse deflection. The real deformation is more complex so that the elementary theory is not adequate for the motion at high frequencies. Higher-order theories such as Love, Mindlin-Herrmann and three-mode theories can be considered in this case. In this subsection, the displacement, internal force and propagation matrices for the longitudinal wave motion based on Love's theory are presented.

As a bar deforms axially, it also contracts transversly due to the Poisson effect. Assume that the kinetic energy is affected by this transverse deformation but the strain energy remains unchanged. Then the axial displacement $u(x,t)$ for the free vibration is governed by (Doyle 1997)

$$EA\frac{\partial^2 u}{\partial x^2}+\nu^2\rho J\frac{\partial^2}{\partial x^2}\left(\frac{\partial^2 u}{\partial t^2}\right)-\rho A\frac{\partial^2 u}{\partial t^2}=0 \tag{8.1}$$

where ν is the Poisson ratio and J is the polar moment of area. The axial force P is then defined as

$$P = EA\frac{\partial u}{\partial x} + \nu^2 \rho J \frac{\partial}{\partial x}\left(\frac{\partial^2 u}{\partial t^2}\right) \tag{8.2}$$

For time harmonic motion, the solution to equation (8.1) is found to be

$$u(x) = C_1 e^{-\mathrm{i}\beta x} + C_2 e^{\mathrm{i}\beta x} \tag{8.3}$$

where the wavenumber β is

$$\beta = \omega\sqrt{\frac{\rho A}{EA - \nu^2 \rho J \omega^2}} \tag{8.4}$$

Note that, above the frequency $\omega = \sqrt{EA/(\nu^2 \rho J)}$, the wavenumber is purely imaginary. At such frequencies the assumptions made break down.

The displacement and internal force matrices for the longitudinal motion based on Love's theory are

$$\begin{aligned} \Psi^+ &= [1], & \Psi^- &= [1], \\ \Phi^+ &= \left[-\mathrm{i}\left(EA - \nu^2 \rho J \omega^2\right)\beta\right], & \Phi^- &= \left[\mathrm{i}\left(EA - \nu^2 \rho J \omega^2\right)\beta\right] \end{aligned} \tag{8.5a,b,c,d}$$

The propagation matrix $\mathbf{F}$ for propagation of waves between two points, a distance L apart, in the bar is

$$\mathbf{F} = \left[e^{-\mathrm{i}\beta L}\right] \tag{8.6}$$

8.2.2 Straight beams based on Timoshenko's theory

The bending wave motion in uniform straight beams, described in chapter 4, is based on Euler-Bernoulli theory neglecting the effects of rotary inertia and transverse shear deformation. In this subsection, the displacement, internal force and propagation matrices for the bending wave motion based on Timoshenko's theory accounting for the two effects are presented.

The equations of motion for a uniform, straight beam based on Timoshenko's theory are given by (Graff 1975)

$$\begin{aligned} GAK\left(\frac{\partial\varphi}{\partial x}-\frac{\partial^2 w}{\partial x^2}\right)+\rho A\frac{\partial^2 w}{\partial t^2}&=0,\\ EI\frac{\partial^2\varphi}{\partial x^2}+GAK\left(\frac{\partial w}{\partial x}-\varphi\right)-\rho I\frac{\partial^2 w}{\partial t^2}&=0 \end{aligned} \qquad (8.7a,b)$$

where φ is the slope due to bending, G is shear modulus and K is the Timoshenko shear coefficient. The shear coefficient K is less than 1 and $K \approx 0.83$ for a rectangular cross-section. The shear force Q and bending moment M are given by

$$Q = GAK\left(\frac{\partial w}{\partial x}-\varphi\right), \qquad M = EI\frac{\partial\varphi}{\partial x} \qquad (8.8a,b)$$

Equations (8.7a) and (8.7b) are coupled through w and φ. The terms including GAK of equation (8.7) are due to the shear deformation and the term including ρI is due to the effect of rotary inertia.

Assume that the solutions to equation (8.7) are of the exponential form as

$$w(x,t) = C_w e^{\mathrm{i}(\omega t-\beta x)}, \qquad \varphi(x,t) = \alpha C_w e^{\mathrm{i}(\omega t-\beta x)} \qquad (8.9a,b)$$

where C_w is a arbitrary constant and α is a constant relating to the dependence between the lateral displacement and slope. Substituting equation (8.9) into equation (8.7) gives

$$\begin{bmatrix} GAK\beta^2-\rho A\omega^2 & -\mathrm{i}\beta GAK \\ \mathrm{i}\beta GAK & EI\beta^2+GAK-\rho I\omega^2 \end{bmatrix}\begin{Bmatrix} C_w \\ \alpha C_w \end{Bmatrix} = 0 \qquad (8.10)$$

For non-trivial solutions, the determinant of the matrix in equation (8.10) should be zero so that

$$\beta^4-\left(k_l^2+k_s^2\right)\beta^2+\left(k_s^2k_l^2-k_b^4\right)=0 \qquad (8.11)$$

where

$$k_l = \sqrt{\frac{\rho\omega^2}{E}}, \quad k_s = \sqrt{\frac{\rho\omega^2}{GK}}, \quad k_b = \left(\frac{\rho A\omega^2}{EI}\right)^{\frac{1}{4}} \tag{8.12a,b,c}$$

At low frequencies, equation (8.11) tends to

$$\beta^4 - k_b^4 = 0 \tag{8.13}$$

i.e., the wavenumbers asymptote to those of Euler-Bernoulli beam theory. At high frequencies, it tends to

$$\left(\beta^2 - k_l^2\right)\left(\beta^2 - k_s^2\right) = 0 \tag{8.14}$$

i.e., one pair of the wavenumbers asymptotes to the longitudinal wavenumbers while the other pair asymptotes to the shear wavenumbers. Note also that there is a cut-off frequency ω_c: letting $\beta = 0$ in equation (8.11) gives

$$k_s^2 k_l^2 = k_b^4; \quad \omega = \sqrt{\frac{GAK}{\rho I}} \tag{8.15}$$

Since equation (8.11) is quadratic in β^2, there are four roots, β_1, β_2, $-\beta_1$ and $-\beta_2$ where

$$\begin{aligned} \beta_1 &= \frac{1}{\sqrt{2}}\left\{\left(k_l^2 + k_s^2\right) + \sqrt{4k_b^4 + \left(k_l^2 - k_s^2\right)^2}\right\}^{\frac{1}{2}}, \\ \beta_2 &= \frac{1}{\sqrt{2}}\left\{\left(k_l^2 + k_s^2\right) - \sqrt{4k_b^4 + \left(k_l^2 - k_s^2\right)^2}\right\}^{\frac{1}{2}} \end{aligned} \tag{8.16a,b}$$

For curved beams, a criterion to distinguish the wavenumber for a positive-going wave was introduced in chapter 7: the imaginary value of the wavenumber is negative and the energy transport velocity is positive. It can also be applied to this case. Here β_1 and β_2 represent positive-going waves, and $-\beta_1$ and $-\beta_2$ negative-going waves. If no damping is present, β_1 is positive-real while β_2 is negative-imaginary below the cut-off

frequency and positive-real above that frequency. They asymptote to the shear and longitudinal wavenumbers, respectively, at high frequency. The plot of the dispersion relation for these wavenumbers is found in the work of Doyle (1997). For each wave component, the ratio α of the slope to the lateral displacement is found from equation (8.10) to be α_1, α_2, $-\alpha_1$ and $-\alpha_2$ where

$$\alpha_1 = \frac{\mathrm{i}}{\beta_1}\left(k_s^2 - \beta_1^2\right), \quad \alpha_2 = \frac{\mathrm{i}}{\beta_2}\left(k_s^2 - \beta_2^2\right) \tag{8.17a,b}$$

Thus the general solution to equation (8.7) is given by

$$\begin{aligned} w(x) &= C_1 e^{-\mathrm{i}\beta_1 x} + C_2 e^{-\mathrm{i}\beta_2 x} + C_3 e^{\mathrm{i}\beta_1 x} + C_4 e^{\mathrm{i}\beta_2 x}, \\ \varphi(x) &= \alpha_1 C_1 e^{-\mathrm{i}\beta_1 x} + \alpha_2 C_2 e^{-\mathrm{i}\beta_2 x} - \alpha_1 C_3 e^{\mathrm{i}\beta_1 x} - \alpha_2 C_4 e^{\mathrm{i}\beta_2 x} \end{aligned} \tag{8.18a,b}$$

The shear force and moment can then be obtained by substituting equation (8.18) into equations (8.8).

Thus the displacement and internal force matrices for the positive-going waves in Timoshenko beams are obtained by

$$\boldsymbol{\Psi}^+ = \begin{bmatrix} 1 & 1 \\ \alpha_1 & \alpha_2 \end{bmatrix}, \qquad \boldsymbol{\Phi}^+ = \begin{bmatrix} -GAK\left(\mathrm{i}\beta_1 + \alpha_1\right) & -GAK\left(\mathrm{i}\beta_2 + \alpha_2\right) \\ -\mathrm{i}EI\beta_1\alpha_1 & -\mathrm{i}EI\beta_2\alpha_2 \end{bmatrix} \tag{8.19a,b}$$

The matrices for the negative-going waves are obtained by replacing β with $-\beta$ (consequently also replacing α with $-\alpha$). The propagation matrix $\mathbf{F}$ between two points, a distance L apart, in the beam is

$$\mathbf{F} = \begin{bmatrix} e^{-\mathrm{i}\beta_1 L} & 0 \\ 0 & e^{-\mathrm{i}\beta_2 L} \end{bmatrix} \tag{8.20}$$

These matrices can be used for the systematic wave analysis of problems concerning Timoshenko beams.

8.3 Deterministically varying waveguides

In chapters 5 and 6, the wave approach was applied to non-uniform waveguides where the geometric properties vary as a power of x. The wave approach can also be applied to the motion of different types of non-uniform waveguides, where exact solutions can be found. In subsection 8.3.1, those undergoing longitudinal motion are described briefly and, in subsection 8.3.2, those undergoing bending motion are described. Numerical results, which are used in section 8.4, for the power transmission through an exponential connector are presented in subsection 8.3.3.

8.3.1 Non-uniform, straight bars

Consider again a non-uniform, straight bar undergoing longitudinal motion. The axial displacement $u(x,t)$ for the free vibration is governed by

$$\frac{\partial}{\partial x}\left[EA\frac{\partial u}{\partial x}\right]=\rho A\frac{\partial^2 u}{\partial t^2} \tag{8.21}$$

Equation (8.21) can be rewritten as

$$\left\{\frac{\partial^2}{\partial x^2}+\frac{1}{4A^2}[(A')^2-2AA'']-\frac{\rho}{E}\frac{\partial^2}{\partial t^2}\right\}A^{1/2}u=0 \tag{8.22}$$

where the primes denote differentiation with respect to x. It can be easily solved for the case where the coefficient $(1/4A^2)[(A')^2-2AA'']$ is constant. For example, suppose that the cross-sectional area A varies in a exponential manner such that

$$A(x)=A_0e^{2\alpha x} \tag{8.23}$$

where α is a real number. Assuming a time dependence of the form $e^{i\omega t}$ but suppressing it here for clarity, substituting equation (8.23) into equation (8.22) gives

$$\left\{\frac{\mathrm{d}^2}{\mathrm{d}x^2}+\left(k_l^2-\alpha^2\right)\right\}A^{1/2}u=0 \tag{8.24}$$

where $k_l=\sqrt{\rho\omega^2/E}$. The solution to equation (8.24) is found to be

$$u(x)=C_1e^{-\mathrm{i}\beta x}e^{-\alpha x}+C_2e^{\mathrm{i}\beta x}e^{-\alpha x} \tag{8.25}$$

where

$$\beta=\sqrt{k_l^2-\alpha^2} \tag{8.26}$$

Note that there is a cut-off frequency $k_l=\alpha$, below which β is imaginary, i.e., waves cannot propagate.

The displacement and internal force matrices for this bar with exponential variation in the area are defined as

$$\begin{aligned}\boldsymbol{\Psi}^+&=\left[e^{-\alpha x}\right], & \boldsymbol{\Psi}^-&=\left[e^{-\alpha x}\right],\\ \boldsymbol{\Phi}^+&=\left[-EA\left(\mathrm{i}\beta+\alpha\right)e^{-\alpha x}\right], & \boldsymbol{\Phi}^-&=\left[EA\left(\mathrm{i}\beta-\alpha\right)e^{-\alpha x}\right]\end{aligned} \tag{8.27a,b,c,d}$$

The propagation matrix $\mathbf{F}$ for propagation of waves between two points, a distance L apart, in the bar is given by

$$\mathbf{F}=\left[e^{-\mathrm{i}\beta L}\right] \tag{8.28}$$

Non-uniform bars including the exponential bar, where the cross-sectional area $A(x)$ varies such that the coefficient $(1/4A^2)[(A')^2-2AA'']$ is constant, are listed in Table 8.2. The displacement and internal force matrices for positive-going waves are presented for the bars. The matrices for negative-going waves can be obtained by replacing the wavenumber β with $-\beta$ in the matrices. The propagation matrices for these non-uniform bars are the same as equation (8.28) so that they are not stated in the table.

8.3.2 Non-uniform, straight beams

In chapter 6, the wave approach was applied to bending motion of non-uniform Euler-Bernoulli beams where $A(x) \propto x^{\mu}$ and $I(x) \propto x^{\mu+2}$. Similar analysis can be followed for bending motion of non-uniform beams where $A(x) \propto x^{\mu}$ and $I(x) \propto x^{\mu+4}$, where $A(x) \propto x^{\mu}$ and $I(x) \propto x^{\mu+6}$, and where $A(x) \propto x^{\mu}$ and $I(x) \propto x^{(\mu+8)/3}$. The solutions for these beams are expressed in terms of Bessel functions as shown by Cranch and Adler (1956).

Besides these power-law-type non-uniform beams, exact solutions for the wave motion in beams with exponential variation can be found as well. Consider again a non-uniform, straight beam undergoing bending motion. The bending displacement $w(x,t)$ for the free vibration of a beam is governed by

$$\frac{\partial^2}{\partial x^2}\left[EI\frac{\partial^2 w}{\partial x^2}\right]+\rho A\frac{\partial^2 w}{\partial t^2}=0 \tag{8.29}$$

Suppose that the geometric properties vary in an exponential manner such that

$$A(x)=A_0e^{2\alpha x}, \quad I(x)=I_0e^{2\alpha x} \tag{8.30a,b}$$

Rectangular beams with exponential variation in width but constant thickness satisfy equation (8.30). For time harmonic motion, combining equation (8.30) with equation (8.29) gives

$$\left(\frac{\mathrm{d}^2}{\mathrm{d}x^2}+2\alpha\frac{\mathrm{d}}{\mathrm{d}x}-k_{b,0}^2\right)\left(\frac{\mathrm{d}^2}{\mathrm{d}x^2}+2\alpha\frac{\mathrm{d}}{\mathrm{d}x}+k_{b,0}^2\right)w=0 \tag{8.31}$$

where $k_{b,0}^4=\dfrac{\rho A_0\omega^2}{EI_0}$. Thus the solution to equation (8.31) is

$$w(x)=e^{-\alpha x}\left(C_1e^{-\mathrm{i}\beta_1 x}+C_2e^{-\beta_2 x}+C_3e^{\mathrm{i}\beta_1 x}+C_4e^{\beta_2 x}\right) \tag{8.32}$$

where

$$\beta_1 = \sqrt{k_{b,0}^2 - \alpha^2}\,, \qquad \beta_2 = \sqrt{k_{b,0}^2 + \alpha^2} \tag{8.33a,b}$$

Note that, below the frequency $k_{b,0} = \alpha$, the wavenumber β_1 is imaginary: no wave can propagate.

The displacement and internal force matrices for the positive-going waves in the exponential beam are

$$\begin{aligned} \boldsymbol{\Psi}^+ &= e^{-\alpha x}\begin{bmatrix} 1 & 1 \\ -\mathrm{i}\beta_1 - \alpha & -\beta_2 - \alpha \end{bmatrix}, \\ \boldsymbol{\Phi}^+ &= e^{-\alpha x} EI \begin{bmatrix} -\mathrm{i}\beta_1^3 - \alpha\beta_1^2 - \mathrm{i}\alpha^2\beta_1 - \alpha^3 & \beta_2^3 + \alpha\beta_2^2 - \alpha^2\beta_2 - \alpha^3 \\ -\beta_1^2 + \mathrm{i}2\alpha\beta_1 + \alpha^2 & \beta_2^2 + 2\alpha\beta_2 + \alpha^2 \end{bmatrix} \end{aligned} \tag{8.34a,b}$$

The matrices for the negative-going waves are obtained by replacing β with $-\beta$. The propagation matrix $\mathbf{F}$ between two points, a distance L apart, in the beam is

$$\mathbf{F} = \begin{bmatrix} e^{-\mathrm{i}\beta_1 L} & 0 \\ 0 & e^{-\beta_2 L} \end{bmatrix} \tag{8.35}$$

These matrices can be used for the systematic wave analysis of problems concerning the exponential beam.

8.3.3 Longitudinal power transmission through an exponential connector

The power transmission through an exponential bar of length L connecting two uniform bars, as shown in Figure 8.1, is studied here. Results are used further in section 8.4 where various approximate solutions are considered. The areas of the uniform bars are A_0 and A_L, respectively, and the area of the exponential bar varies as

$$A(x) = A_0 e^{2\alpha x} \tag{8.36}$$

Note that the parameter α is determined to be

$$\alpha = \frac{1}{2L}\ln\left(\frac{A_L}{A_0}\right) \tag{8.37}$$

The displacement, internal force and propagation matrices for the exponential bar were derived in subsection 8.3.1. Using these matrices and the matrices for the uniform bars, the wave analysis for this case can be conducted in a systematic way. Since similar work has been done for many examples so far, results are given here without details.

The power transmission coefficient τ for longitudinal wave transmission through the exponential bar is given by

$$\tau = \frac{k_l^2 - \alpha^2}{k_l^2 - \alpha^2 \cos^2\left(\sqrt{k_l^2 L^2 - \alpha^2 L^2}\right)} \tag{8.38}$$

Figure 8.2 shows τ for three cases: $A_L = 1.1A_0$, $A_L = 2A_0$, and $A_L = 5A_0$. When $k_l L << \frac{1}{2}\ln\left(\frac{A_L}{A_0}\right)$, the coefficient asymptotes that of the case where two uniform bars are connected directly, i.e., $\tau = \frac{2A_0A_L}{(A_0 + A_L)^2}$. When $k_l L >> \frac{1}{2}\ln\left(\frac{A_L}{A_0}\right)$, $\tau \to 1$ as would be expected.

8.4 Arbitrarily varying waveguides: a piecewise approach

So far this thesis has been concerned with cases where the problems can be solved exactly. However, most real non-uniform structures are too complicated to analyse exactly. Consider now non-uniform structures where the properties vary in a complex manner so that the exact solution is difficult or impossible to obtain. These structures were categorised as arbitrarily varying waveguides in chapter 1.

One approximate approach for the motion of arbitrarily varying structures is a piecewise representation where the structure is divided into small segments. Each segment is then modelled by an element, for which the solution is known, such as uniform elements. The motion of the original structure is then predicted by combining the behaviour of the elements and properties of the joints between the elements. In subsections 8.4.1 to 8.4.3, four different piecewise models for an exponential connector are presented. It is seen that employment of a deterministically varying element, rather than a uniform element, for modelling the segment can lead to rapid convergence at low computational cost.

8.4.1 Modelling of a section: using uniform elements

Consider again the exponential connector of length L as shown in Figure 8-1. In subsection 8.3.3 the exact results for the longitudinal power transmission through the connector were presented. Here the exponential connector is approximated by a series of uniform elements of length Δx. Although it is possible and may be recommendable to divide a structure irregularly, here the interval Δx is chosen to be constant. Figure 8-3 shows two different schemes in the piecewise modelling of the exponential connector. One uses the uniform element with the smallest area of each segment and the other uses the uniform element with the geometric-mean area of each segment.

Figure 8-4 shows the longitudinal power transmission coefficients through the connector estimated by the two piecewise models when $A_L = 5A_0$. The exact results, obtained earlier in subsection 8.3.3, are shown as well. Figure 8-4(a) is the result when the connector was modelled by a series of three uniform elements (i.e., $\Delta x = L/3$). It seems that there is no substantial advantage using the geometric-mean area instead of

the smallest area in this case. When the piecewise model is refined (here increasing the number of elements to 10), it gives better approximate results as seen in Figure 8-4(b).

8.4.2 Modelling of a section: using deterministically varying elements

In the previous subsection, the exponential connector was approximated by a series of uniform elements. Now the connector is approximated by a series of non-uniform elements where the area is given by

$$A(x) = A_0\left(1+\frac{x}{x_0}\right)^{\mu} \tag{8.39}$$

where x_0 is the distance from the apex to the end. Recall that these non-uniform elements were studied in chapter 5. Figure 8-5 shows two different schemes in modelling the connector as a series of the non-uniform elements. One employs the non-uniform element with $\mu = 1$ while the other employs the non-uniform element with $\mu = 2$. Note that, when A_0 and A_L is fixed and $\mu \to \infty$, the area change becomes exponential:

$$\lim_{\mu\to\infty}\frac{\mu}{x_0} = \lim_{\mu\to\infty}\frac{\mu}{L}\left\{\left(\frac{A_L}{A_0}\right)^{\frac{1}{\mu}}-1\right\} = \frac{1}{L}\ln\left(\frac{A_L}{A_0}\right) = 2\alpha \tag{8.40}$$

Thus

$$\lim_{\mu\to\infty} A_0\left(1+\frac{x}{x_0}\right)^{\mu} = \lim_{\mu\to\infty} A_0\left(1+\frac{2\alpha x}{\mu}\right)^{\mu} = A_0 e^{2\alpha x} \tag{8.41}$$

First the connector is approximated by only a single non-uniform element. Figure 8-6(a) shows the longitudinal power transmission coefficients through the connector

estimated in this case. The model using the non-uniform element with $\mu = 2$ is better in the accuracy than the model using the non-uniform element with $\mu = 1$. Next the connector is approximated by a series of three non-uniform elements. As seen in Figure 8-6(b), the estimation results are nearly the same as the exact results. When compared to the results shown in Figure 8-4(a), it is seen that these models using the non-uniform elements give much better estimation than the models using the uniform elements, if the numbers of the piecewise elements are the same.

8.4.3 Numerical efficiency

Four different schemes in piecewise modelling have been illustrated in the previous two subsections. At this stage, a question may occur as to how many segments the structure should be divided into, and what element should be used for the segment. The answer is a compromise between the computational cost and the accuracy: the numerical procedures should have sufficient accuracy but not excessive accuracy, as this increases significantly the cost of computation. In this subsection, such a compromise in applying the piecewise approach is discussed in relation to the previous example, the longitudinal power transmission through the exponential connector.

Figure 8-7(a) shows the computational time, taken in estimating the power transmission through the exponential connector by using the piecewise models, versus the number of elements used for the models. Since no substantial difference occurs between the two uniform models – one with the smallest area and the other with the geometric mean area, only the uniform model with the smallest area is used here. There is no difference in the computing time between the piecewise models using the non-uniform element with $\mu = 1$ and $\mu = 2$ (the results for the model of $\mu = 2$ are almost

identical to those for the model of $\mu = 1$). It is seen that a longer time is required by the models using the non-uniform element than the model using the uniform element. However, as seen in Figure 8-7(b), the models using the non-uniform element provide more accurate estimates than the model using the uniform element. The model using the non-uniform element with $\mu = 2$ is better in the accuracy than the model using the non-uniform element with $\mu = 1$. Note that the rapid drop in the estimation error when the number of elements increases from 6 to 7 is related to the finite frequency range, which cannot be infinite, fixed for the error calculation.

Rearranging the results of Figure 8-7, a plot of the computational time versus the estimation error is obtained as shown in Figure 8-8. It is seen that the convergence of the model using the uniform elements is slower than the others. From this plot, one can compare the numerical efficiency of each model and decide which one is the best when considering the computational environment given and the estimation accuracy required. In general cases the same situation is expected. A piecewise model using deterministically varying elements, instead of uniform elements, could provide rapid convergence to the exact results at low computational cost, especially when non-uniformity of the waveguide is severe.

8.5 Finite waveguides: natural frequencies and mode shapes

The numerical examples, which have been presented until now, are related to infinite structures where no boundary conditions are imposed. As a final example, the vibration of finite structures is investigated using the wave approach in this section. In subsections 8.5.1, the natural frequencies of a uniform, curved beam under various boundary conditions are obtained. Kang *et al.* (2003) studied the same cases.

Comparison to their results is made for validation of the present work. In subsections 8.5.2 and 8.5.3, the natural frequencies and mode shapes of non-uniform, curved beams are presented.

8.5.1 Natural frequencies of a uniform, curved beam

Consider a uniform, curved beam subtending an angle θ_L, as shown in Figure 8-9(a), where the radius of curvature of the centreline, R, is constant. The amplitudes of waves at the ends are related by

$$\begin{aligned} \mathbf{d}^+ &= \mathbf{F}\mathbf{a}^+, \\ \mathbf{d}^- &= \mathbf{R}_L\mathbf{d}^+, \\ \mathbf{a}^- &= \mathbf{F}\mathbf{d}^-, \\ \mathbf{a}^+ &= \mathbf{R}_0\mathbf{a}^- \end{aligned} \qquad (8.42a,b,c,d)$$

where $\mathbf{R}_0$ and $\mathbf{R}_L$ are reflection matrices at the ends ($\theta = 0$ and $\theta = \theta_L$), respectively, and $\mathbf{F}$ is the propagation matrix for the curved beam given by equation (7.40). Rearranging equation (8.42) gives

$$\left[\mathbf{R}_0\mathbf{F}\mathbf{R}_L\mathbf{F} - \mathbf{I}\right]\mathbf{a}^+ = 0 \qquad (8.43)$$

Let $C(\omega)$ be the determinant of the term in the bracket, i.e.,

$$C(\omega) = \left|\mathbf{R}_0\mathbf{F}\mathbf{R}_L\mathbf{F} - \mathbf{I}\right| \qquad (8.44)$$

The frequencies at which $C(\omega) = 0$ are the natural frequencies of the beam. Since the reflection and propagation matrices are given exactly, this will give the exact natural frequencies for the case.

Besides the exact results, approximate results by using a piecewise approach are obtained. In the approach the curved beam is modelled by a series of n uniform, straight elements as shown in Figure 8-9(b). Each element has the same length $ds = R\Delta\theta$,

where $\Delta\theta = \theta_L / n$ is the angle subtended by one element. The local co-ordinate system changes for each element. Thus the continuity conditions at a junction between the jth element and (j+1)th element are

$$\begin{aligned} \mathbf{w}_j &= \mathbf{A}\mathbf{w}_{j+1}, \\ \mathbf{f}_j &= \mathbf{A}\mathbf{f}_{j+1} \end{aligned} \tag{8.45a,b}$$

where $\mathbf{w} = \begin{bmatrix} w & \varphi & u \end{bmatrix}^T$ and $\mathbf{f} = \begin{bmatrix} Q & M & N \end{bmatrix}^T$ with the subscripts j or (j+1) denoting the element, and

$$\mathbf{A} = \begin{bmatrix} \cos(\Delta\theta) & 0 & \sin(\Delta\theta) \\ 0 & 1 & 0 \\ -\sin(\Delta\theta) & 0 & \cos(\Delta\theta) \end{bmatrix} \tag{8.46}$$

One can establish the relationships between the waves in this piecewise model by considering the reflection and transmission at each junction and the propagation in each element, and finally derive the same form as equation (8.42) such that

$$\begin{aligned} \mathbf{b}^+ &= \mathbf{F}_{0,L}\mathbf{a}^+, \\ \mathbf{b}^- &= \mathbf{R}_L\mathbf{b}^+, \\ \mathbf{a}^- &= \mathbf{F}_{L,0}\mathbf{b}^-, \\ \mathbf{a}^+ &= \mathbf{R}_0\mathbf{a}^- \end{aligned} \tag{8.47a,b,c,d}$$

where $\mathbf{F}_{0,L}$ and $\mathbf{F}_{L,0}$ are not the diagonal propagation matrices but the matrices defining the relationships between the waves at the ends. Rearranging equation (8.47) gives

$$\left[\mathbf{R}_0\mathbf{F}_{L,0}\mathbf{R}_L\mathbf{F}_{0,L} - \mathbf{I}\right]\mathbf{a}^+ = 0 \tag{8.48}$$

The frequencies at which the determinant of the term in the bracket is zero are the natural frequencies estimated by the piecewise model.

Figures 8.10 shows the plot of the determinant $C(\omega)$ for a uniform curved beam with clamped-clamped ends for $\overline{\chi}^2 = 1/1200$ and $\theta_L = 5^\circ$. The non-dimensional frequency Ω' is introduced, for comparison to the previous results, as

$$\Omega' = \omega R^2 \sqrt{\frac{\rho A}{EI}} \tag{8.49}$$

Note that $\Omega' = \Omega/\overline{\chi}$. The frequencies at which the real and imaginary values of $C(\Omega')$ are both zero are indicated in the plot and are the natural frequencies. It is seen that the natural frequencies obtained by a piecewise approach using 60 straight elements agree well with the exact result. Further comments regarding the third frequency Ω_3' are made in the next paragraph. Note here that the real and imaginary parts of the determinant are zero at Ω_3'. Figure 8.11 shows the determinant $C(\Omega')$ when the subtended angle is $\theta_L = 180^\circ$. Figure 8-11(a) was already presented by Kang *et al.* (2003): Figure 7 in their work. Even though Kang *et al.* obtained it based on Love's theory and the present work obtains it based on Flügge 's theory, the two results are very similar. One distinct difference, which does not affect the determination of the natural frequencies, is that the present results do not show the abrupt change in the slope of $C(\Omega')$ near $\Omega' = 4.164$. It seems due to the differences in determining the dispersion relation of a curved beam.

Table 8.3 shows the first four non-dimensional natural frequencies Ω' of the uniform curved beam for $\overline{\chi}^2 = 1/1200$. The results are compared to those obtained by Kang *et al.* (2003). It seems that the third frequency Ω_3' of the clamped-clamped beam of $\theta_L = 5^\circ$ is missing in the results of Kang *et al.* Rather than the results by the exact model using the single curved element, the results by the piecewise model using 60

uniform elements are much closer to those of Kang *et al.* It seems to be because the curved model of the present work is based on Flügge 's theory instead of Love's theory.

8.5.2 Natural frequencies of a linearly tapered, curved beam

Consider again a curved beam subtending an angle θ_L but now the beam is non-uniform as shown in Figure 8-12. The cross-sectional shape of this curved beam is rectangular, where the width is constant but the thickness h varies linearly along the angle θ as

$$h(\theta) = h_{L/2}\left[1+\alpha\left(2\frac{\theta}{\theta_L}-1\right)\right] \tag{8.50}$$

where α is a constant (note that the thickness ratio at the ends of the beam is given by $(1+\alpha)/(1-\alpha)$) and $h_{L/2}$ is the thickness at angle $\theta_L/2$. The thickness of the beam is uniform if $\alpha = 0$ while, if $\alpha > 0$, it gets gradually thicker in the direction of θ. The boundary conditions are imposed such that the slender end of the beam is free and the thick end is clamped. No exact solution for the motion of this non-uniform curved beam seems to exist so that natural frequencies of the beam are here obtained by a piecewise approach. The curved beam is equally partitioned into n segments so that each segment subtends the same angle $\Delta\theta = \theta_L/n$. Each segment is then modelled as a uniform, curved element.

A question may occur as to how to define the thickness of the curved element and how many elements should be used for obtaining adequate accuracy. In order to investigate it numerically, three different models are developed: in the first the element's thickness is taken to be the smallest thickness of the segment, in the second it is the largest thickness, and in the third it is the geometric mean of the smallest and

largest thickness. The first is called here the *thinner* model, the second the *thicker* model, and the third the *mean* model. Thus, in the thinner model, the thickness h_j^s of the jth element is given by

$$h_j^s = h_{L/2}\left[1+\alpha\left(2\frac{\theta_{j-1}}{\theta_L}-1\right)\right] \tag{8.51}$$

where $\theta_{j-1} = (j-1)\Delta\theta$ for $j = 1, 2, \ldots, n$. In the thicker model, the thickness h_j^b of the jth element is given by

$$h_j^b = h_{L/2}\left[1+\alpha\left(2\frac{\theta_j}{\theta_L}-1\right)\right] \tag{8.52}$$

where $\theta_j = j\Delta\theta$ for $j = 1, 2, \ldots, n$. In the mean model, the thickness h_j^m of the jth element is given by

$$h_j^m = \sqrt{h_j^s h_j^b} \tag{8.53}$$

Figures 8-13 to 8-15 show the first four natural frequencies of the free-clamped beam subtending angles $\theta_L = 1°$, $\theta_L = 20°$ and $\theta_L = 40°$, respectively. In this case $h_{L/2}/R = 0.1$ and the constant α in equation (8.50) is $\alpha = 0.9$. The number of elements increases in increments of 5 starting from 5 elements. In the figure, the non-dimensional frequency Ω'' is defined by using the properties at angle $\theta_L/2$ as

$$\Omega'' = \omega\left(R\theta_L\right)^2\left(\sqrt{\frac{\rho A}{EI}}\right)_{L/2} \tag{8.54}$$

Note that this non-dimensional frequency is different to the previous frequency defined as equation (8.49).

In general the thinner and thicker models do not guarantee upper and lower bounds, respectively, on the frequency since the modelling underestimates or overestimates both the mass and the stiffness. However, in the present case, the results of the two models tend to decrease or increase monotonically after a sufficient number of elements (e.g., 40) is used so that the true natural frequencies seem *likely* to be bounded by the results of the thinner and thicker models. The geometric mean model seems to provide the compromise between the thinner and thicker models, and provide quicker and better estimation.

It is commonly seen that the estimates become approximately constant after the number of elements becomes greater than 40. In order to obtain an adequate number of elements quantitatively, from the results presented in Figures 8-13 to 8-15, the change rate δ as a percentage is calculated as shown in Figure 8-16. The rate δ is defined as

$$\delta = \frac{|f' - f|}{f} \times 100 \tag{8.55}$$

where f and f' are the estimated frequencies before and after refining the model using more elements, respectively. If $\delta < 1$, the frequency obtained by the next-step refinement differs within 1% of the current frequency (i.e., the improvement in estimating the frequency by next-step refinement is expected to be less than 1% of the current estimate). It is seen that, after 40 elements, δ becomes less than 0.5%. Thus the following numerical results for the case are obtained by using 40 elements.

Figure 8-17 shows the first five natural frequencies versus the angle subtended by the beam. Figure 8-17(a) is the plot for the uniform, curved beam ($\alpha = 0$) and Figure 8-17(b) is the plot for the tapered, curved beam with $\alpha = 0.9$. It should be noted that, in the tapered beam, the taper rate (i.e., non-uniformity) becomes smaller as the angle

increases. In the figure some trends can be noticed: in some regions the natural frequencies hardly change while in other regions they change linearly as the angle increases.

In order to explain these behaviours closely, Figure 8-17(a) is drawn again as Figure 8-18(a) where 6 further lines are added. The horizontal lines are the natural frequencies of the beam undergoing pure bending (or inextensional) motion while the diagonal lines are the frequencies of the beam undergoing pure extensional motion (see the section below where the mode shapes for each natural frequency are given). The results indicate that the mode sequences will change as the angle increases, even for the uniform curved beam: for example, when $\theta_L < 4^\circ$ the first mode of the uniform beam is related to the pure extensional motion but when $\theta_L > 4^\circ$ the first mode is related to the pure bending motion.

In order to get a clearer view of the change of natural frequencies when the beam becomes tapered, Figures 8-17(a) and 8-17(b) are combined as shown in Figure 8-18(b). It is seen that the first and second horizontal lines move up while the third and the fourth lines move down. The slopes of the lines relating to the pure extensional motion become larger but, as modes get higher, the changes become smaller (e.g., for the 4^{th} extensional lines, it is seen that they are almost same).

8.5.3 Mode shapes of a linearly tapered, curved beam

Once the natural frequencies are known, the mode shapes for each natural frequency can be obtained. The shapes can be easily obtained in some cases, e.g., a uniform structure where waves do not suffer reflection in the region between the ends, but it could be cumbersome in other cases, e.g., where there are many discontinuities. In

this section, the relationships are derived for a general case and then the mode shapes of the non-uniform curved beam of the previous subsection are presented.

Figure 8-19 shows a piecewise model consisting of n elements, or a finite structure with $(n-1)$ discontinuities between the ends. The relationships between waves can be found the following procedure:

Step 1: obtain individual matrix at each point

(i) reflection matrices at the ends: $\hat{\mathbf{R}}_1$, $\mathbf{R}_{n+1}$

(ii) reflection matrices at discontinuities: $\mathbf{R}_2$, $\mathbf{R}_3$, ..., $\mathbf{R}_n$, $\hat{\mathbf{R}}_2$, $\hat{\mathbf{R}}_3$, ..., $\hat{\mathbf{R}}_n$

(iii) transmission matrices at discontinuities: $\mathbf{T}_2$, $\mathbf{T}_3$, ..., $\mathbf{T}_n$, $\hat{\mathbf{T}}_2$, $\hat{\mathbf{T}}_3$, ..., $\hat{\mathbf{T}}_n$

(iv) propagation matrices for an element: $\mathbf{F}_1^+$, $\mathbf{F}_2^+$, ..., $\mathbf{F}_n^+$, $\mathbf{F}_1^-$, $\mathbf{F}_2^-$, ..., $\mathbf{F}_n^-$

Step 2: obtain *global* matrix between two points

(i) reflection matrices: $\hat{\mathbf{R}}_{1\sim2}$, $\hat{\mathbf{R}}_{1\sim3}$, ..., $\hat{\mathbf{R}}_{1\sim n}$, where the subscript $1\sim n$ denotes point 1 and point n.

(ii) transmission matrices: $\mathbf{T}_{1\sim2}$, $\mathbf{T}_{1\sim3}$, ..., $\mathbf{T}_{1\sim n}$

Step 3: obtain the relationships between waves in an iterative manner (This is one example. The relationships can also be established in other ways as would be expected)

(i) First obtain the amplitudes of waves in the nth element (i.e., the rightmost element). The relationships between wave in the nth element are

$$\begin{aligned}
\mathbf{a}_n^+ &= \mathbf{T}_{1\sim n}\mathbf{a}_1^+ + \hat{\mathbf{R}}_{1\sim n}\mathbf{a}_n^-, \\
\mathbf{a}_{n+1}^+ &= \mathbf{F}_n^+\mathbf{a}_n^+, \\
\mathbf{a}_{n+1}^- &= \mathbf{R}_{n+1}\mathbf{a}_{n+1}^+, \\
\mathbf{a}_n^- &= \mathbf{F}_n^-\mathbf{a}_{n+1}^-
\end{aligned} \qquad (8.56a,b,c,d)$$

Rearranging these relationships gives

$$\begin{aligned}
\mathbf{a}_{n+1}^{+} &= \left[\mathbf{I}-\mathbf{F}_n^{+}\hat{\mathbf{R}}_{1\sim n}\mathbf{F}_n^{-}\mathbf{R}_{n+1}\right]^{-1}\mathbf{F}_n^{+}\mathbf{T}_{1\sim n}\mathbf{a}_1^{+},\\
\mathbf{a}_{n+1}^{-} &= \mathbf{R}_{n+1}\mathbf{a}_{n+1}^{+},\\
\mathbf{a}_n^{-} &= \mathbf{F}_n^{-}\mathbf{a}_{n+1}^{-},\\
\mathbf{a}_n^{+} &= \mathbf{T}_{1\sim n}\mathbf{a}_1^{+}+\hat{\mathbf{R}}_{1\sim n}\mathbf{a}_n^{-}
\end{aligned} \qquad (8.57a,b,c,d)$$

Equation (8.57) indicates that $\mathbf{a}_{n+1}^{+}$, $\mathbf{a}_{n+1}^{-}$, $\mathbf{a}_n^{-}$ and $\mathbf{a}_n^{+}$ can be obtained in sequence from given $\mathbf{a}_1^{+}$.

(ii) Obtain the amplitudes of waves in the mth element. The amplitudes, $\mathbf{a}_{n-1}^{-}$ and $\mathbf{a}_{n-1}^{+}$, of waves at the point (n-1) can be obtained as

$$\begin{aligned}
\mathbf{a}_{n-1}^{-} &= \left[\mathbf{I}-\mathbf{F}_{n-1}^{-}\mathbf{R}_n\mathbf{F}_{n-1}^{+}\hat{\mathbf{R}}_{1\sim(n-1)}\right]^{-1}\left\{\mathbf{F}_{n-1}^{-}\mathbf{R}_n\mathbf{F}_{n-1}^{+}\mathbf{T}_{1\sim(n-1)}\mathbf{a}_1^{+}+\mathbf{F}_{n-1}^{-}\hat{\mathbf{T}}_n\mathbf{a}_n^{-}\right\},\\
\mathbf{a}_{n-1}^{+} &= \mathbf{T}_{1\sim(n-1)}\mathbf{a}_1^{+}+\hat{\mathbf{R}}_{1\sim(n-1)}\mathbf{a}_{n-1}^{-}
\end{aligned} \qquad (8.58a,b)$$

Equation (8.58) indicates that $\mathbf{a}_{n-1}^{-}$ and $\mathbf{a}_{n-1}^{+}$ can be obtained from $\mathbf{a}_1^{+}$ and $\mathbf{a}_n^{-}$ given. In general equation (8.58) can be written as

$$\begin{aligned}
\mathbf{a}_m^{-} &= \left[\mathbf{I}-\mathbf{F}_m^{-}\mathbf{R}_{m+1}\mathbf{F}_m^{+}\hat{\mathbf{R}}_{1\sim m}\right]^{-1}\left\{\mathbf{F}_m^{-}\mathbf{R}_{m+1}\mathbf{F}_m^{+}\mathbf{T}_{1\sim m}\mathbf{a}_1^{+}+\mathbf{F}_m^{-}\hat{\mathbf{T}}_{m+1}\mathbf{a}_{m+1}^{-}\right\},\\
\mathbf{a}_m^{+} &= \mathbf{T}_{1\sim m}\mathbf{a}_1^{+}+\hat{\mathbf{R}}_{1\sim m}\mathbf{a}_m^{-}
\end{aligned} \qquad (8.59a,b)$$

Equation (8.59) indicates that the amplitudes of waves at the point m are obtained from $\mathbf{a}_1^{+}$ and $\mathbf{a}_{m+1}^{-}$: the amplitudes can be obtained in an iterative manner for $m=n-1,n-2,\ldots,2$.

(iii) Obtain the amplitudes of waves in the first element (i.e., leftmost element). Finally $\mathbf{a}_1^{-}$ is obtained as

$$\mathbf{a}_1^{-}=\mathbf{F}_1^{-}\mathbf{R}_2\mathbf{F}_1^{+}\mathbf{a}_1^{+}+\mathbf{F}_1^{-}\hat{\mathbf{T}}_2\mathbf{a}_2^{-} \qquad (8.60)$$

It has been shown how the relationships between the waves in a piecewise model consisting of many elements or a finite structure with many discontinuities can be derived. In the procedure, waves at the right boundary are first identified and, then, waves at other positions are identified progressively along the structure until the left boundary is reached. As would be expected, the relationships can be established in other ways.

When relationships between the waves have been established, the physical behaviour of the structure is obtained by transformation from the wave domain to the physical domain. The physical quantities at the jth point are

$$\begin{Bmatrix} \mathbf{w} \\ \mathbf{f} \end{Bmatrix}_j = \begin{bmatrix} \boldsymbol{\Psi}^+ & \boldsymbol{\Psi}^- \\ \boldsymbol{\Phi}^+ & \boldsymbol{\Phi}^- \end{bmatrix}_j \begin{Bmatrix} \mathbf{a}^+ \\ \mathbf{a}^- \end{Bmatrix}_j \tag{8.61}$$

where $j = 1, 2, ..., n+1$.

Figure 8-20 shows the first five mode shapes of the tapered, curved beam of $\alpha = 0.9$ and $\theta_L = 15^\circ$. It is seen that the first, third and fifth modes are substantially related to the radial motion rather than the tangential motion (the shapes are the typical 1st, 2nd and 3rd of clamped-free straight beams). In contrast, the second and fourth modes are substantially related to the tangential motion. This behaviour is in good agreement with the previous interpretation of the natural frequencies. Consult again Figure 8-17(b). It can be seen in the figure that, when $\theta_L = 15^\circ$, the first, third and fifth natural frequencies are located close to the pure bending lines but the second and fourth natural frequencies are located close to the pure extensional lines.

From Figures 8-17(b) and 8-20, the modal behaviour of the tapered beam can be predicted when the length of the beam changes. For example, when $\theta_L = 5^\circ$, the first

natural frequency is on the first pure extensional line. Thus the mode shape is similar to the second, rather than the first, mode shape of $\theta_L = 15^\circ$.

8.6 Summary

The wave approach based on reflection, transmission and propagation of waves is a general method for the wave analysis for one-dimensional structures. It can always be applied to uniform waveguides where the coefficients of the governing equation are constant. The displacement, internal force and propagation matrices for the longitudinal wave motion based on Love theory and for the bending wave motion based on Timoshenko theory were presented. Since the wave approach always provides well-conditioned numerical results, no drawback will occur in applying the wave approach at high frequencies.

The displacement, internal force and propagation matrices for non-uniform waveguides with an exponential, rather than power-law, variation in the geometric properties were presented. These matrices can be used in a systematic way for further study of the motion of the exponential waveguides. The exact results for the longitudinal power transmission through an exponential connector were presented.

In conjunction with the piecewise approach, the wave approach can be applied to the motion of arbitrarily varying waveguides where the properties vary in a complex manner so that exact solution to the motion is difficult or impossible to obtain. Different schemes in developing a piecewise model were described and the corresponding numerical efficiency were investigated. It was seen that a piecewise model using deterministically varying elements, rather than uniform elements, could provide rapid convergence at low computational cost.

Consideration was then given to the motion of finite structures. A general procedure to obtain the natural frequencies and mode shapes was described and was validated by comparison to the existing work. Subsequently the modal behaviours of a linearly tapered curved beam with the clamped-free boundaries were studied when the length of the beam changed. This tapered curved beam is of similar shape to the bead part of a tyre. The tendencies of pure bending and pure extensional motions in the behaviour were revealed.

Table 8.1. Three cases equivalent to the longitudinal vibration of bars and relevant parameters.

Longitudinal vibration of bars	Axial displacement $u(x)$	$EA(x)$	$\rho A(x)$
Torsional vibration of rods	Rotation $\theta(x)$	For modulus of rigidity G and polar moment of inertia J, $GJ(x)$	$\rho J(x)$
Vibration of strings	Lateral displacement $w(x)$	Tension $\tau(x)$	Mass per unit length $\sigma(x)$
Acoustic wave motion in ducts	Pressure $p(x)$	$A(x)$	For speed of sound c, $\frac{A(x)}{c^2}$

Table 8-2. Non-uniform bars and their displacement and internal force matrices for the wave approach.

Cross-sectional area $A(x)$	Wavenumber β	Displacement matrix Ψ^+	Internal force matrix Φ^+
$A_0 e^{2\alpha x}$	$\sqrt{k_l^2 - \alpha^2}$	$e^{-\alpha x}$	$-EA(\mathrm{i}\beta + \alpha)e^{-\alpha x}$
$A_0 (\sin \alpha x)^2$	$\sqrt{k_l^2 + \alpha^2}$	$1/\sin \alpha x$	$-EA\left(\mathrm{i}\beta + \alpha \dfrac{\cos \alpha x}{\sin \alpha x}\right)\dfrac{1}{\sin \alpha x}$
$A_0 (\cos \alpha x)^2$	$\sqrt{k_l^2 + \alpha^2}$	$1/\cos \alpha x$	$-EA\left(\mathrm{i}\beta - \alpha \dfrac{\sin \alpha x}{\cos \alpha x}\right)\dfrac{1}{\cos \alpha x}$
$A_0 (\sinh \alpha x)^2$	$\sqrt{k_l^2 - \alpha^2}$	$1/\sinh \alpha x$	$-EA\left(\mathrm{i}\beta + \alpha \dfrac{\cosh \alpha x}{\sinh \alpha x}\right)\dfrac{1}{\sinh \alpha x}$
$A_0 (\cosh \alpha x)^2$	$\sqrt{k_l^2 - \alpha^2}$	$1/\cosh \alpha x$	$-EA\left(\mathrm{i}\beta + \alpha \dfrac{\sinh \alpha x}{\cosh \alpha x}\right)\dfrac{1}{\cosh \alpha x}$

Table 8.3. Non-dimensional natural frequencies $\bar{\omega}$ of a uniform, circular beam for $\bar{\chi}^2 = 1/1200$.

Span angle θ_L	B.C.	Mode	Kang *et al.* (2003)	Using a single circular element (exact)	Using 60 straight elements
5°	Clamped-Clamped	1	1247.5675	1247.0700	1247.5671
		2	2489.7481	2493.9590	2489.7522
		3	-	2937.7038	2942.5757
		4	3740.4334	3741.2092	3740.4345
	Free-Free	1	1247.1131	1247.4466	1247.1132
		2	2493.9771	2494.2896	2493.9773
		3	2937.7679	2937.2384	2937.7678
		4	3741.4749	3741.4112	3741.4752
180°	Clamped-Clamped	1	4.3694551	4.3721593	4.3699451
		2	9.4982704	9.5078102	9.4992769
		3	17.704014	17.722215	17.705837
		4	25.641709	25.668470	25.643747
	Free-Free	1	1.8363460	1.8371547	1.8365554
		2	5.3028579	5.3078041	5.3034600
		3	11.099972	11.111971	11.101225
		4	18.988464	19.010617	18.9905925

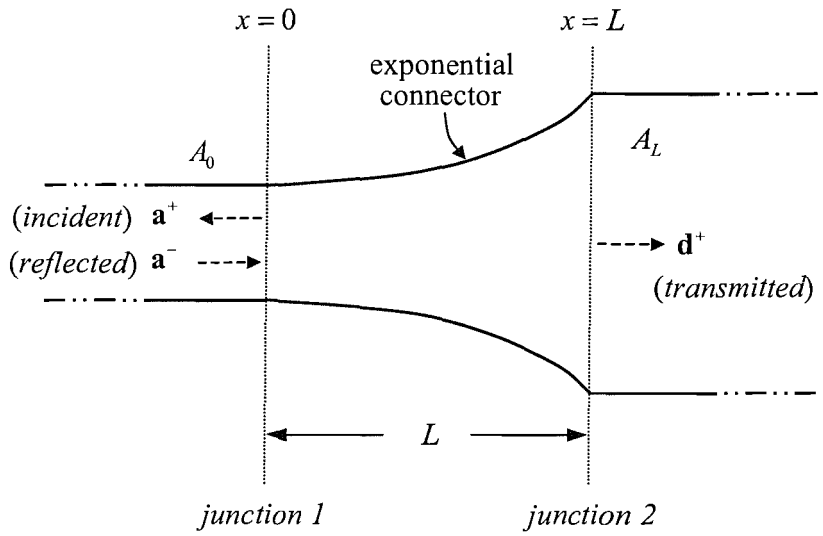

Figure 8-1. Reflection and transmission of waves through a connector of length L with exponential variation in area between two uniform bars with areas A_0 and A_L, respectively.

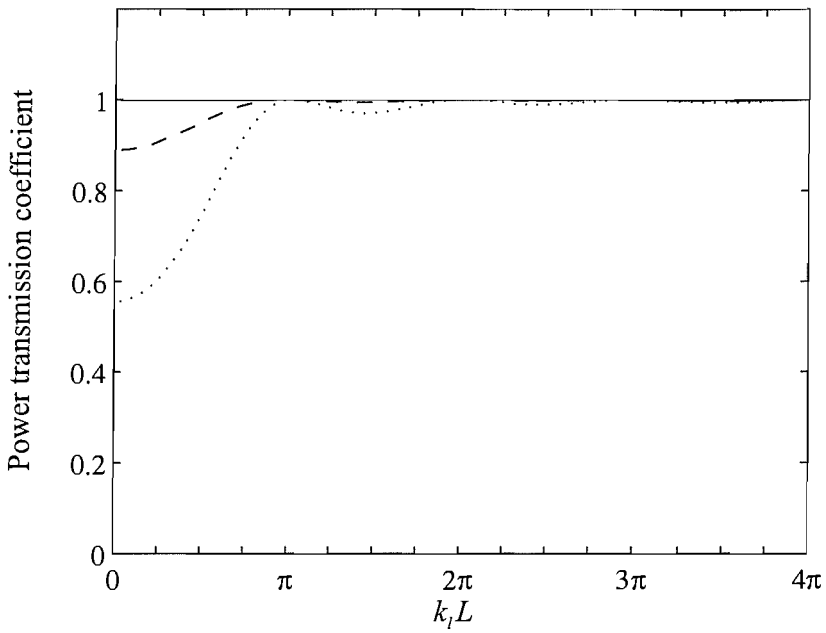

Figure 8-2. The longitudinal power transmission through the exponential connector of length L between two uniform bars with areas A_0 and A_L, respectively; —— , $A_L = 1.1A_0$; ---- , $A_L = 2A_0$; ····· , $A_L = 5A_0$.

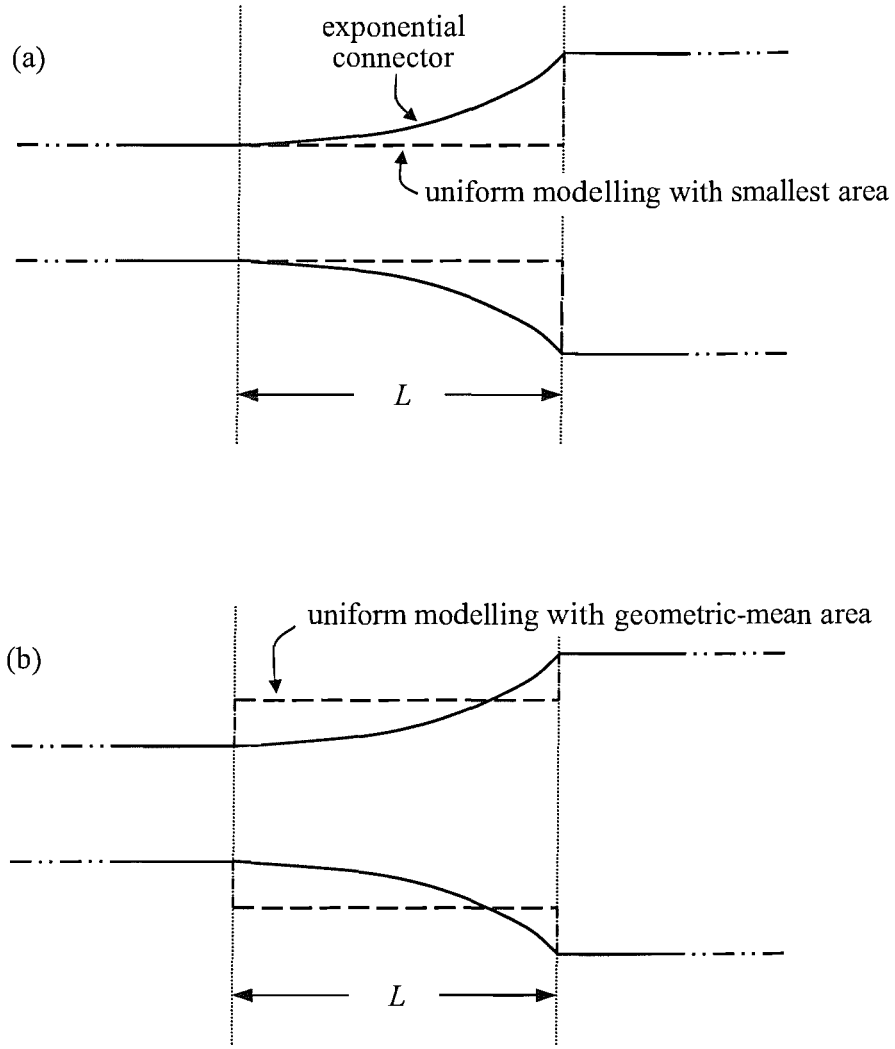

Figure 8-3. Two different schemes in piecewise modelling of the exponential connector: employment of uniform elements with (a) the smallest area and (b) the geometric-mean area.

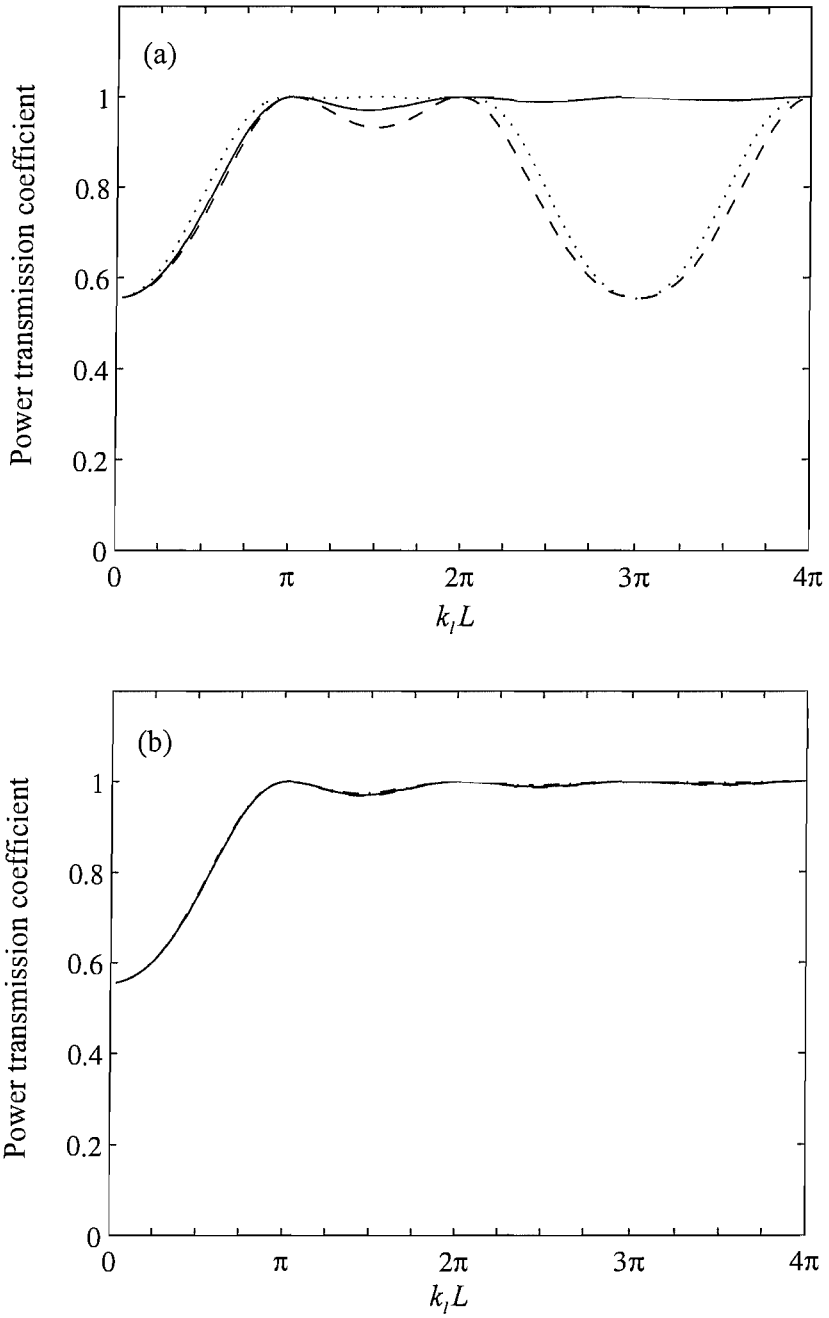

Figure 8-4. Estimation of the longitudinal power transmission coefficient for the exponential connector by modelling the connector as a series of (a) three uniform elements ($\Delta x = L/3$), (b) ten uniform elements ($\Delta x = L/10$): —— , exact; ---- , using the smallest area of each segment; ····· , using the geometric-mean area of each segment.

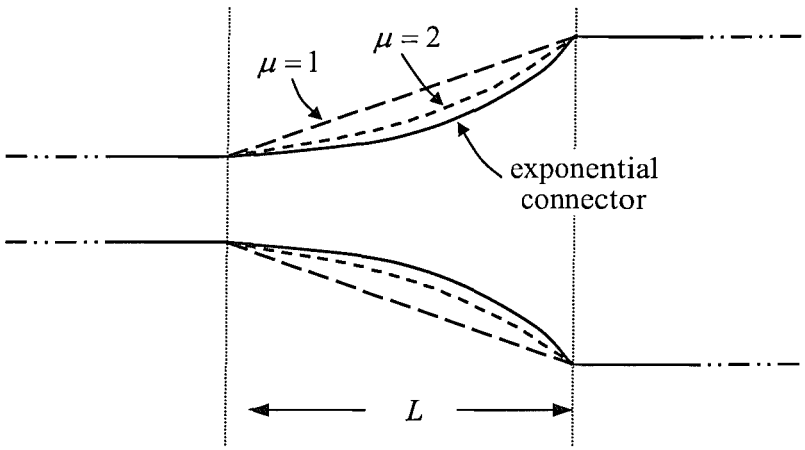

Figure 8-5. Modelling the exponential connector as a non-uniform element where the area varies as $A(x) \propto x^{\mu}$ with $\mu = 1$ and $\mu = 2$, respectively.

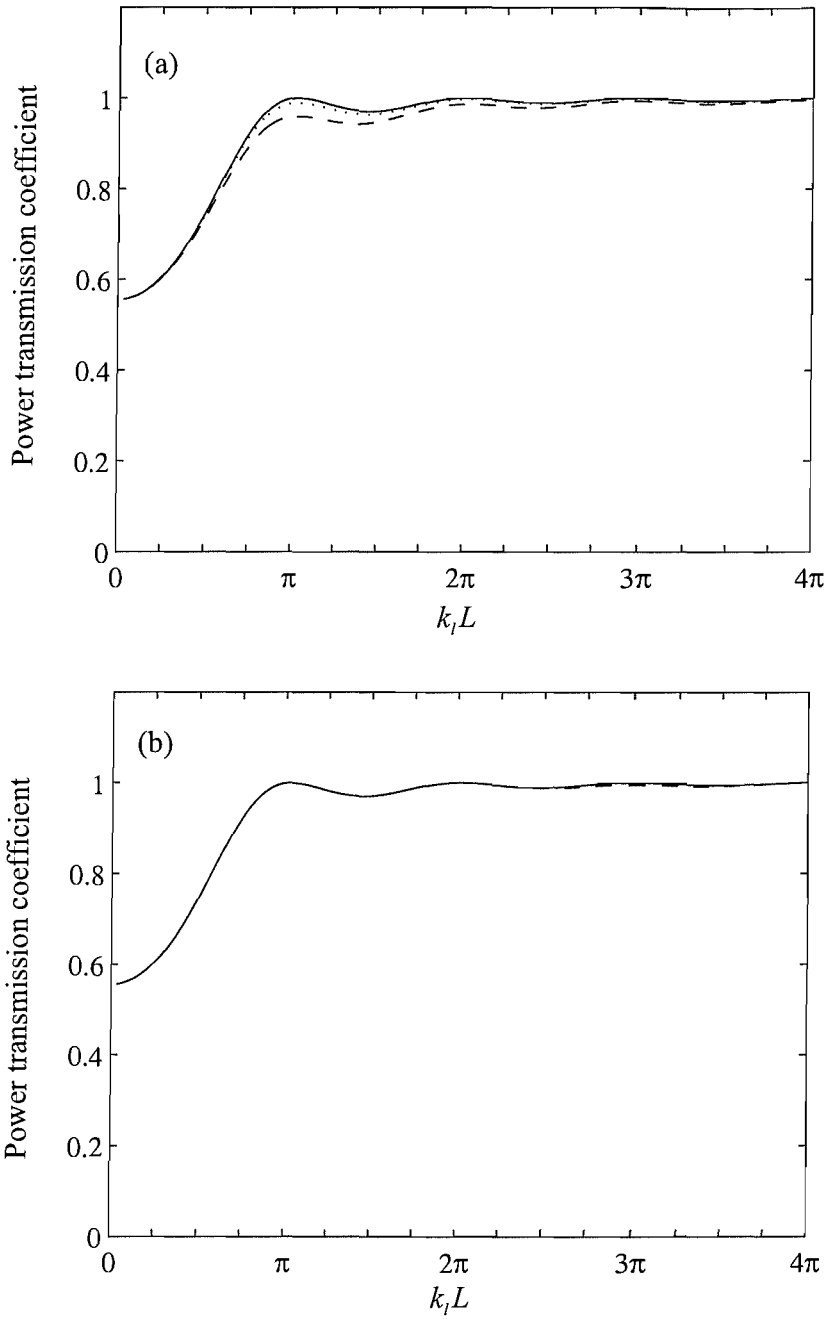

Figure 8-6. Estimation of the longitudinal power transmission coefficient for the exponential connector by modelling the connector as (a) a single non-uniform element ($\Delta x = L$), (b) a series of three non-uniform elements ($\Delta x = L/3$): —— , exact; ---- , using the non-uniform element with $\mu = 1$; ..... , using the non-uniform element with $\mu = 2$.

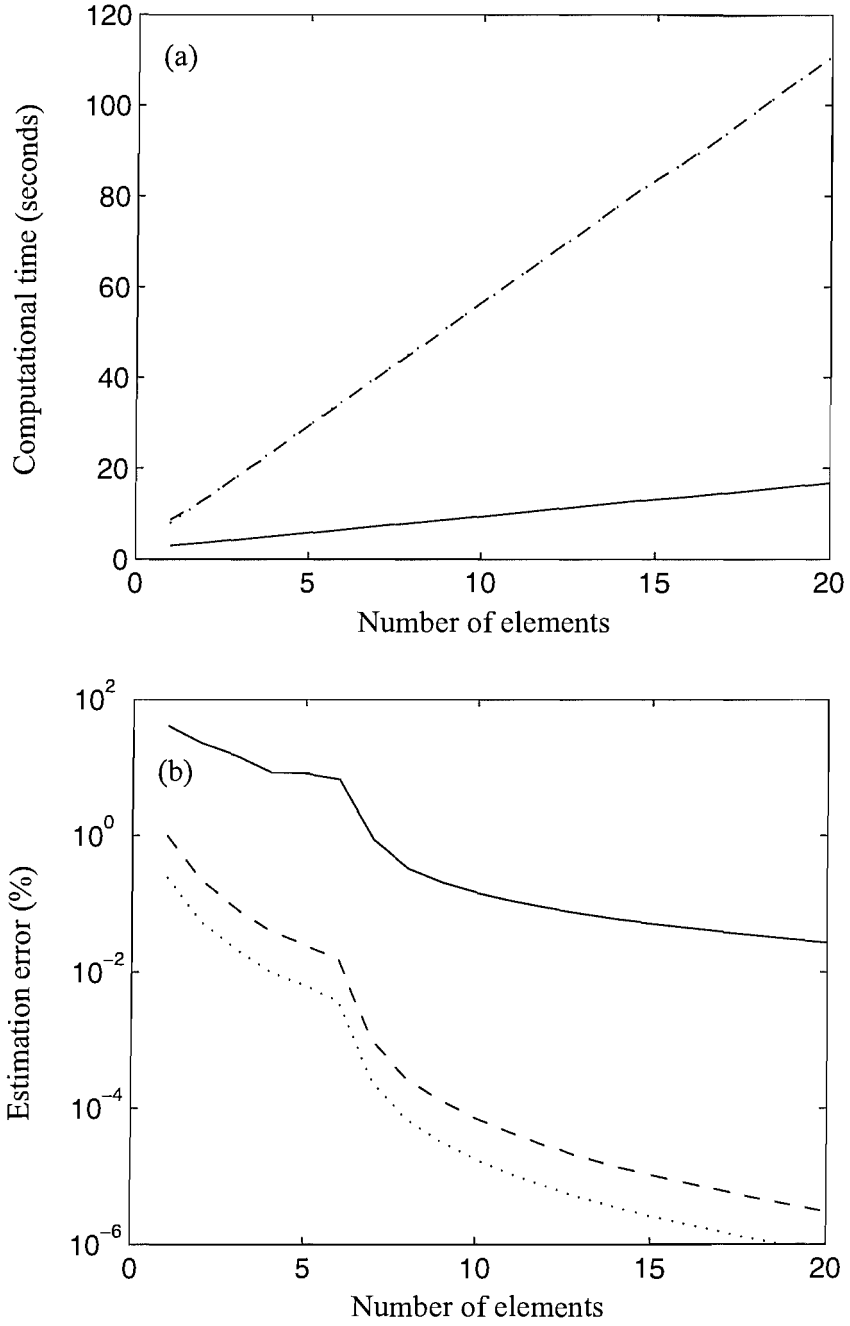

Figure 8-7. (a) The computational time versus the number of elements, (b) the estimation error versus the number of elements; —— , the model using the uniform elements; ---- , the model using the non-uniform elements with $\mu = 1$; ..... , the model using the non-uniform elements with $\mu = 2$.

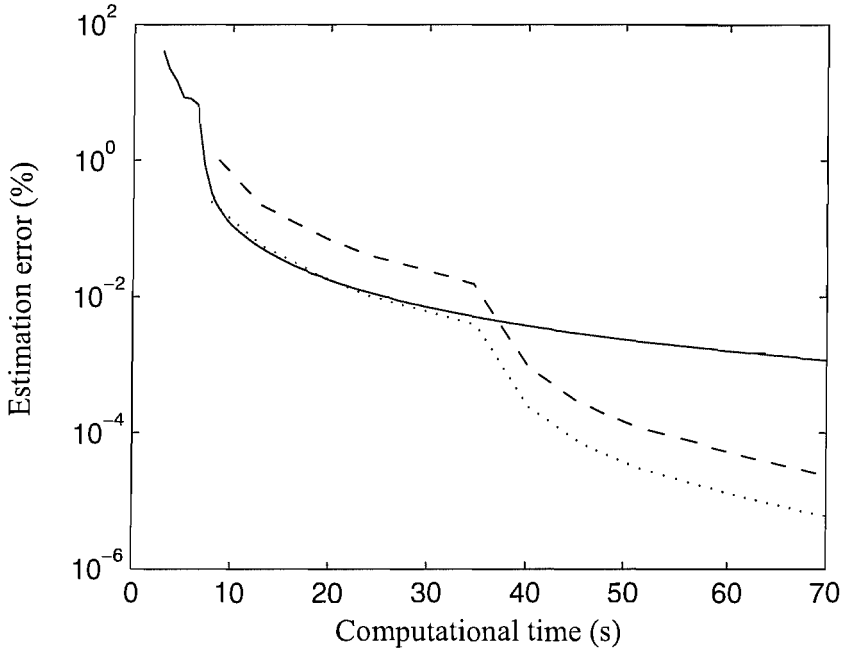

Figure 8-8. Computational time versus estimation error in using piecewise models; —— , the model using the uniform elements; ----- , the model using the non-uniform elements with $\mu = 1$; ..... , the model using the non-uniform elements with $\mu = 2$.

(a)

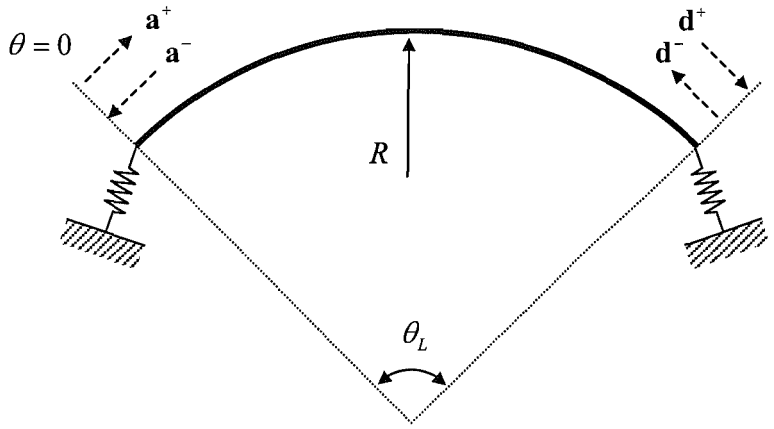

(b)

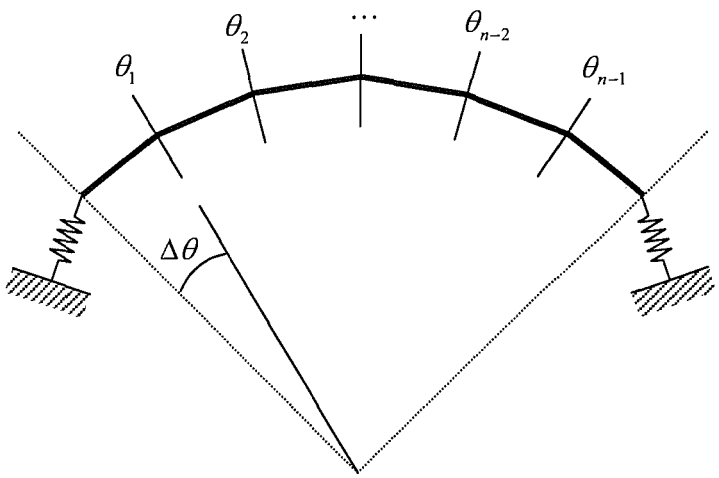

Figure 8-9. A finite uniform curved beam with constant curvature: (a) modelling with a single-span curved element, (b) piecewise representation of the circular beam with a series of straight elements.

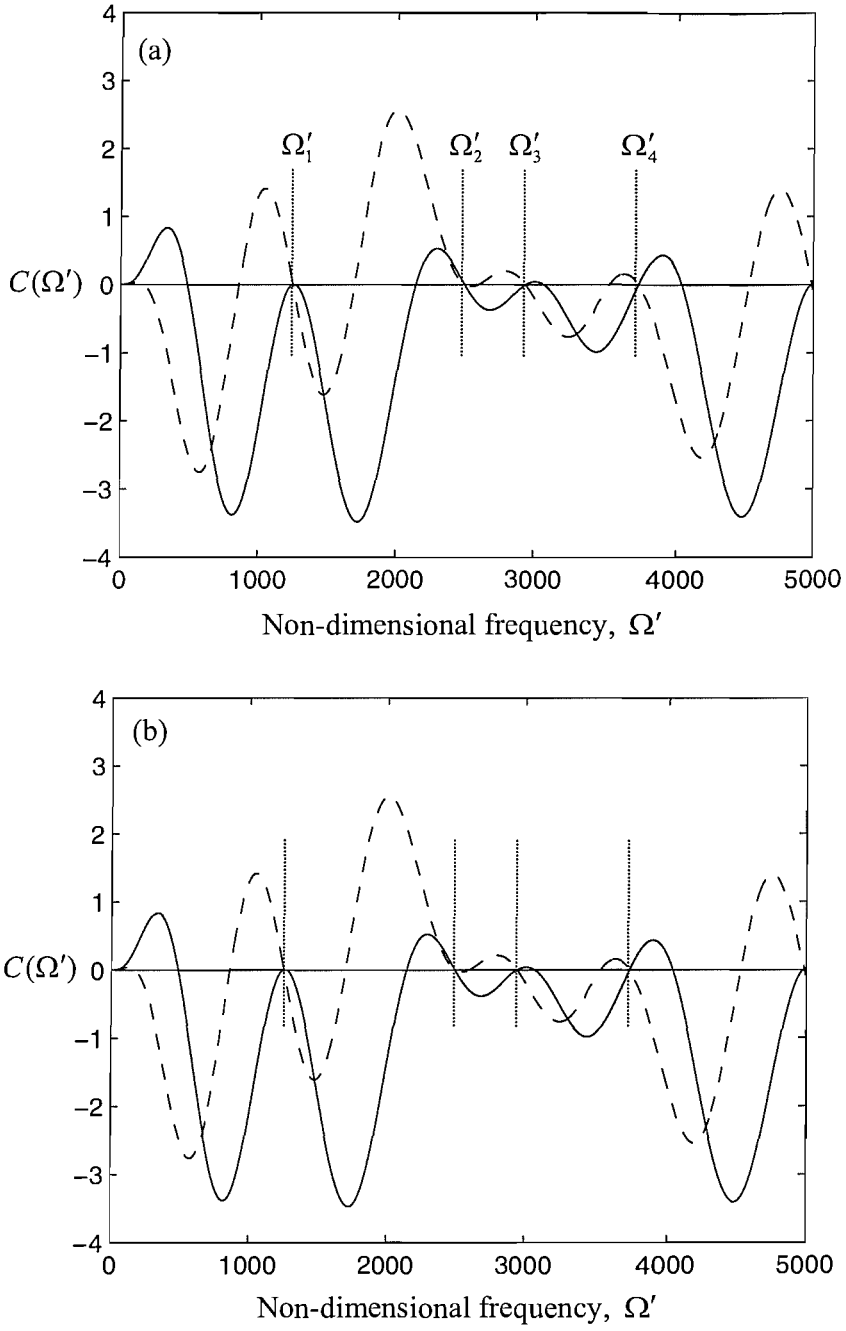

Figure 8-10. Results for a uniform circular beam with clamped-clamped ends for $\bar{\chi}^2 = 1/1200$ and $\theta_L = 5°$: obtained by (a) the exact, (b) the piecewise model using 60 straight elements; ——, $\mathrm{Re}\left[C(\Omega')\right]$; ---- , $\mathrm{Im}\left[C(\Omega')\right]$.

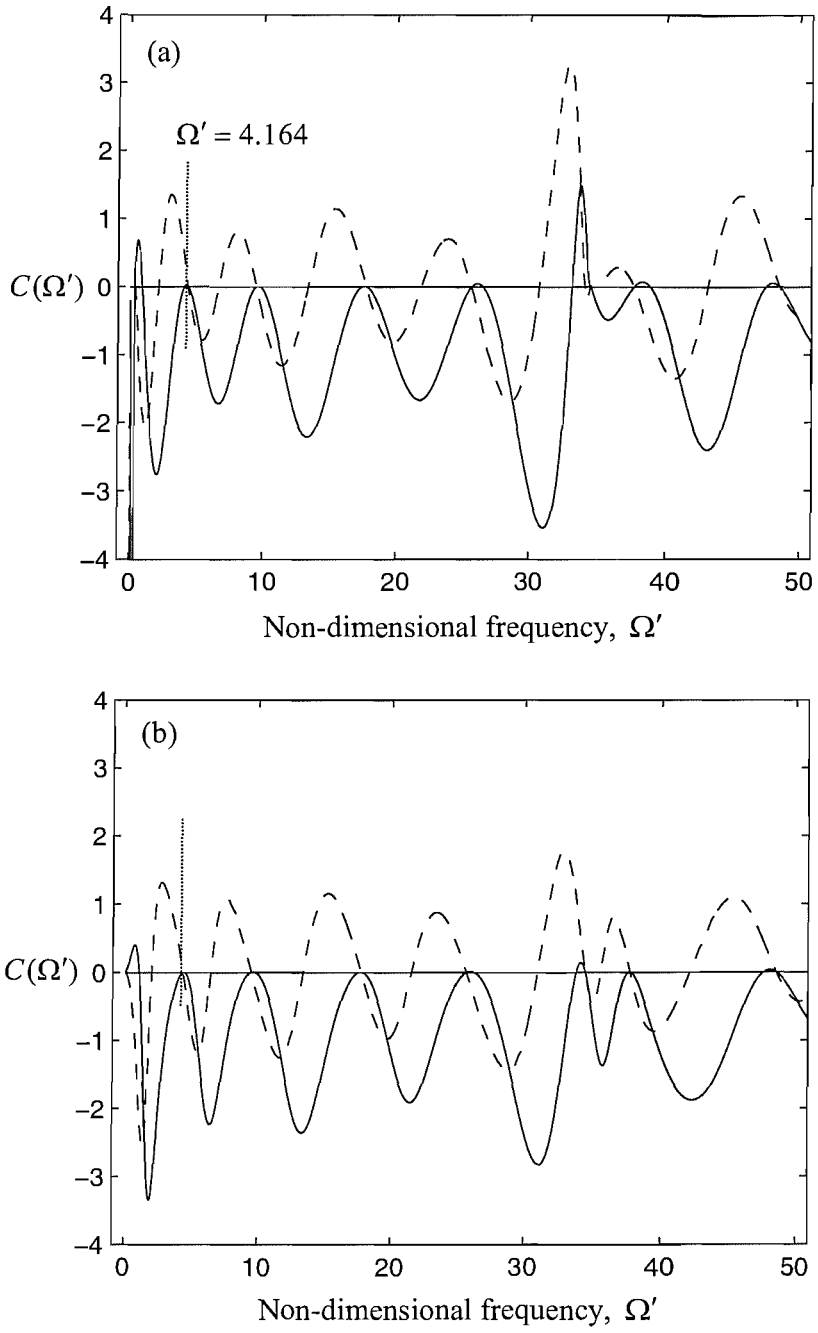

Figure 8-11. Results for a uniform circular beam with clamped-clamped ends for $\overline{\chi}^2 = 1/1200$ and $\theta_L = 180^\circ$: obtained by (a) the exact (b) the piecewise model using 60 straight elements. ——, $\mathrm{Re}\left[C(\Omega')\right]$; ----, $\mathrm{Im}\left[C(\Omega')\right]$.

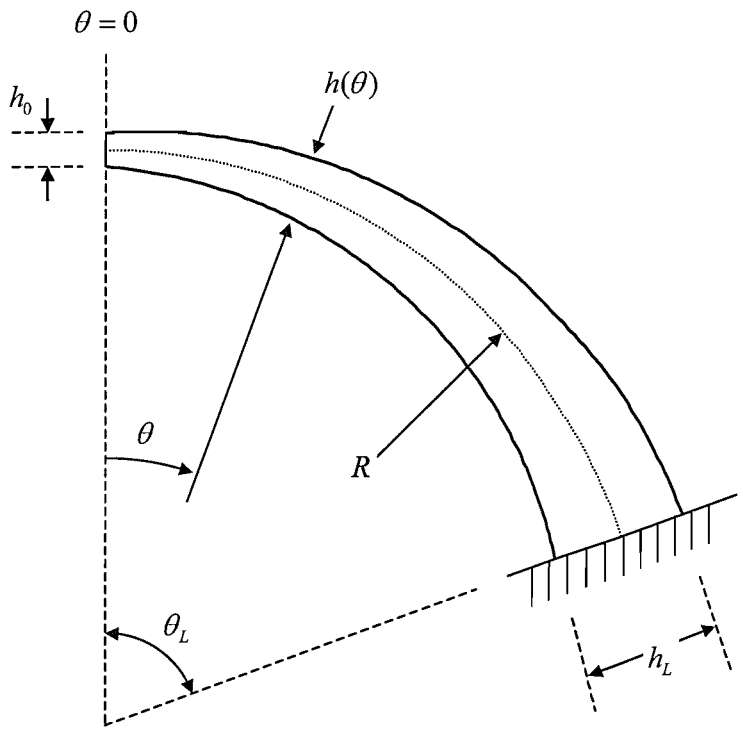

Figure 8-12. A circular beam with thickness varying linearly along the length.

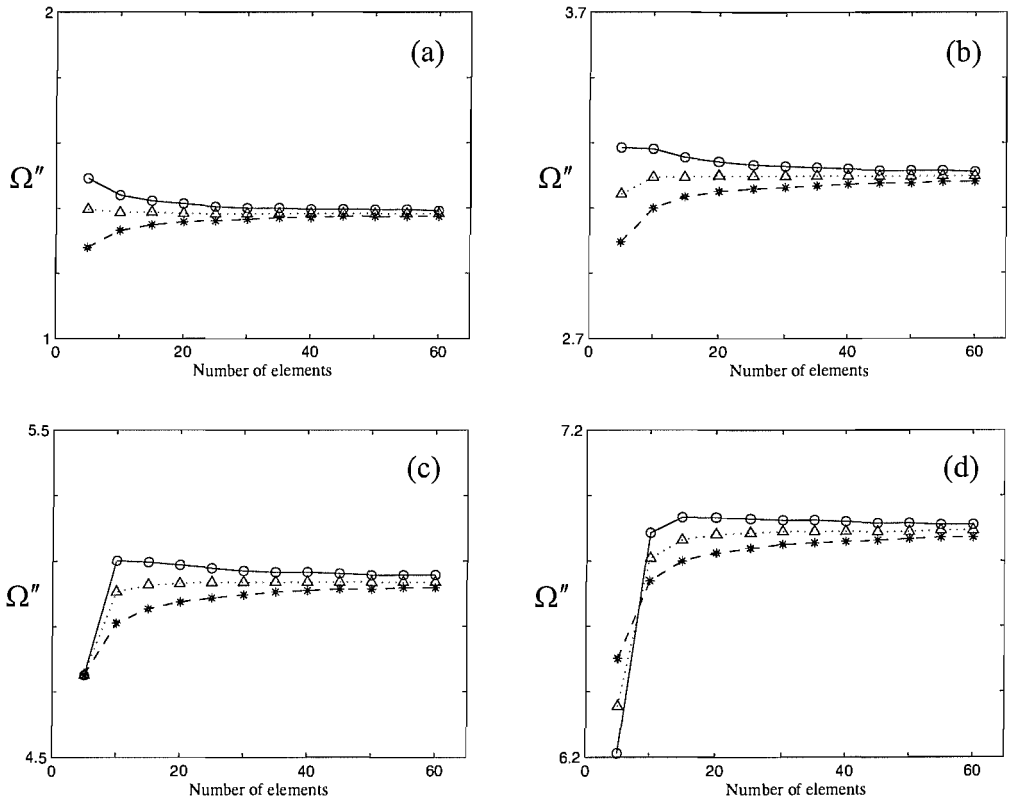

Figure 8-13. Natural frequencies of the free-clamped tapered curved beam of $h_{L/2}/R_0 = 0.1$, $\alpha = 0.9$ and $\theta_L = 1^\circ$: (a) first, (b) second, (c) third and (d) fourth frequencies; estimated by the thinner model (—o—), the thicker model (--*--), and the mean model (·····Δ·····). In the figure Ω'' is given by equation (8.54).

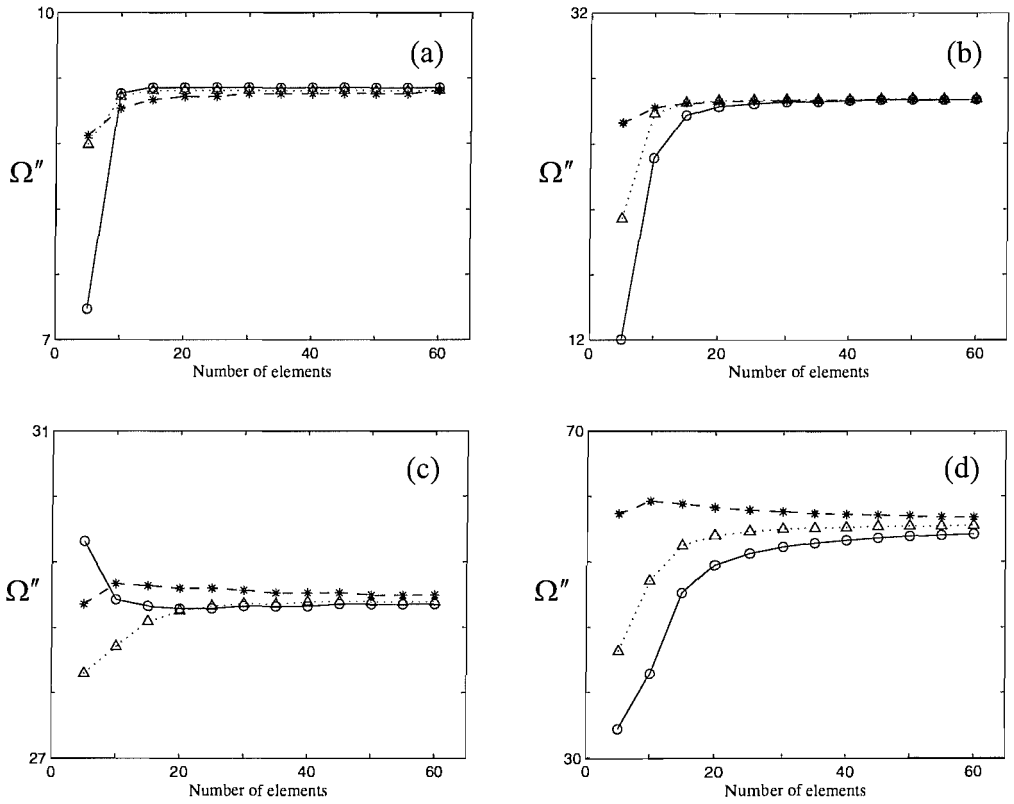

Figure 8-14. Natural frequencies of the free-clamped tapered curved beam of $h_{L/2}/R_0 = 0.1$, $\alpha = 0.9$ and $\theta_L = 20^\circ$: (a) first, (b) second, (c) third and (d) fourth frequencies; estimated by the thinner model (—o—), the thicker model (--*--), and the mean model (·····Δ·····). In the figure Ω'' is given by equation (8.54).

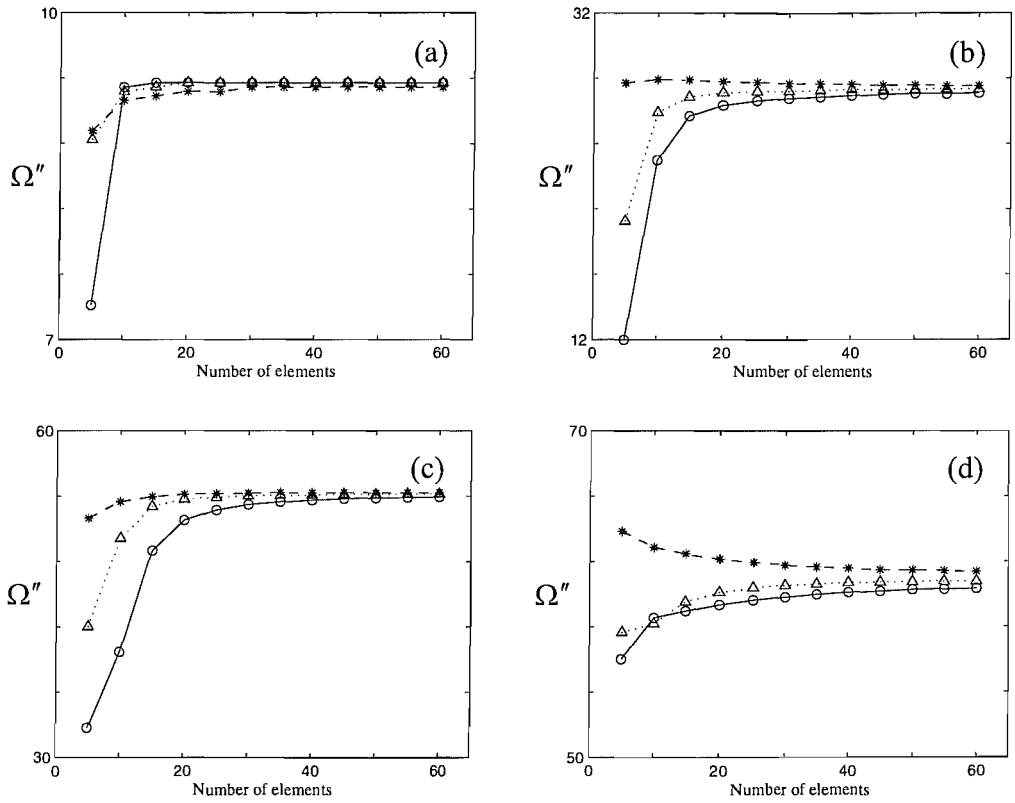

Figure 8-15. Natural frequencies of the free-clamped tapered curved beam of $h_{L/2}/R_0 = 0.1$, $\alpha = 0.9$ and $\theta_L = 40^\circ$: (a) first, (b) second, (c) third and (d) fourth frequencies; estimated by the thinner model (—o—), the thicker model (--*--), and the mean model (····Δ····). In the figure Ω'' is given by equation (8.54).

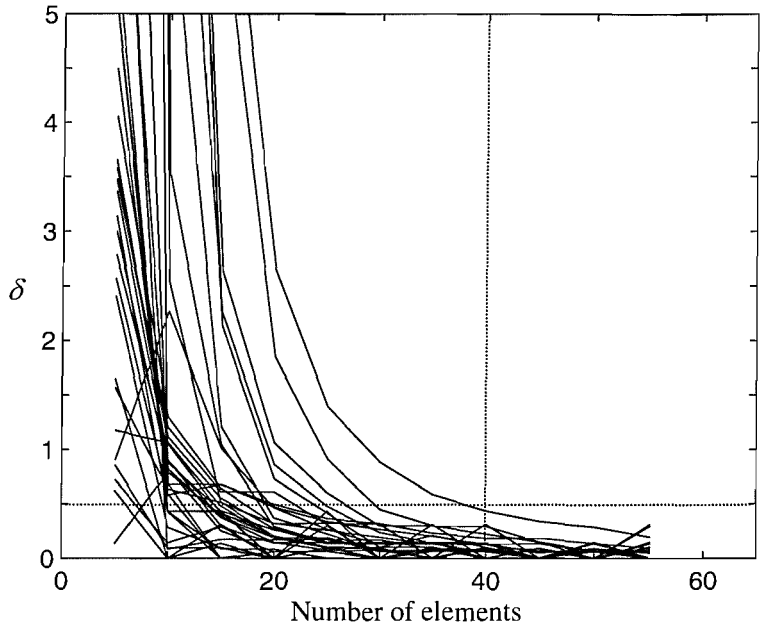

Figure 8-16. The percentage change of estimated natural frequencies versus the number of elements

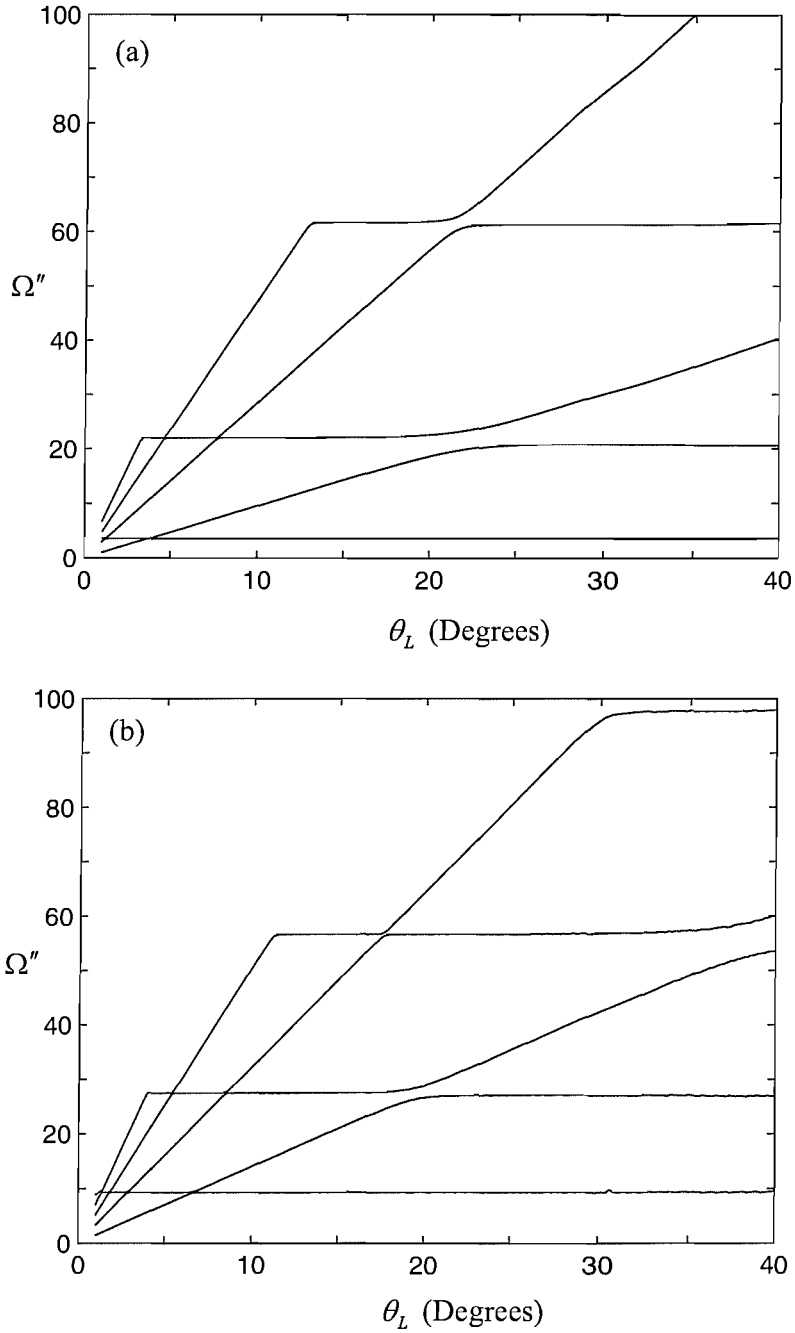

Figure 8-17. Non-dimensional natural frequency for clamped-free curved beams with $\bar{\chi}^2 = 1/1200$: (a) uniform beam, i.e., $\alpha = 0$, (b) non-uniform beam with $\alpha = 0.9$. In the figure Ω'' is given by equation (8.54) and θ_L is the arc subtended by the beam.

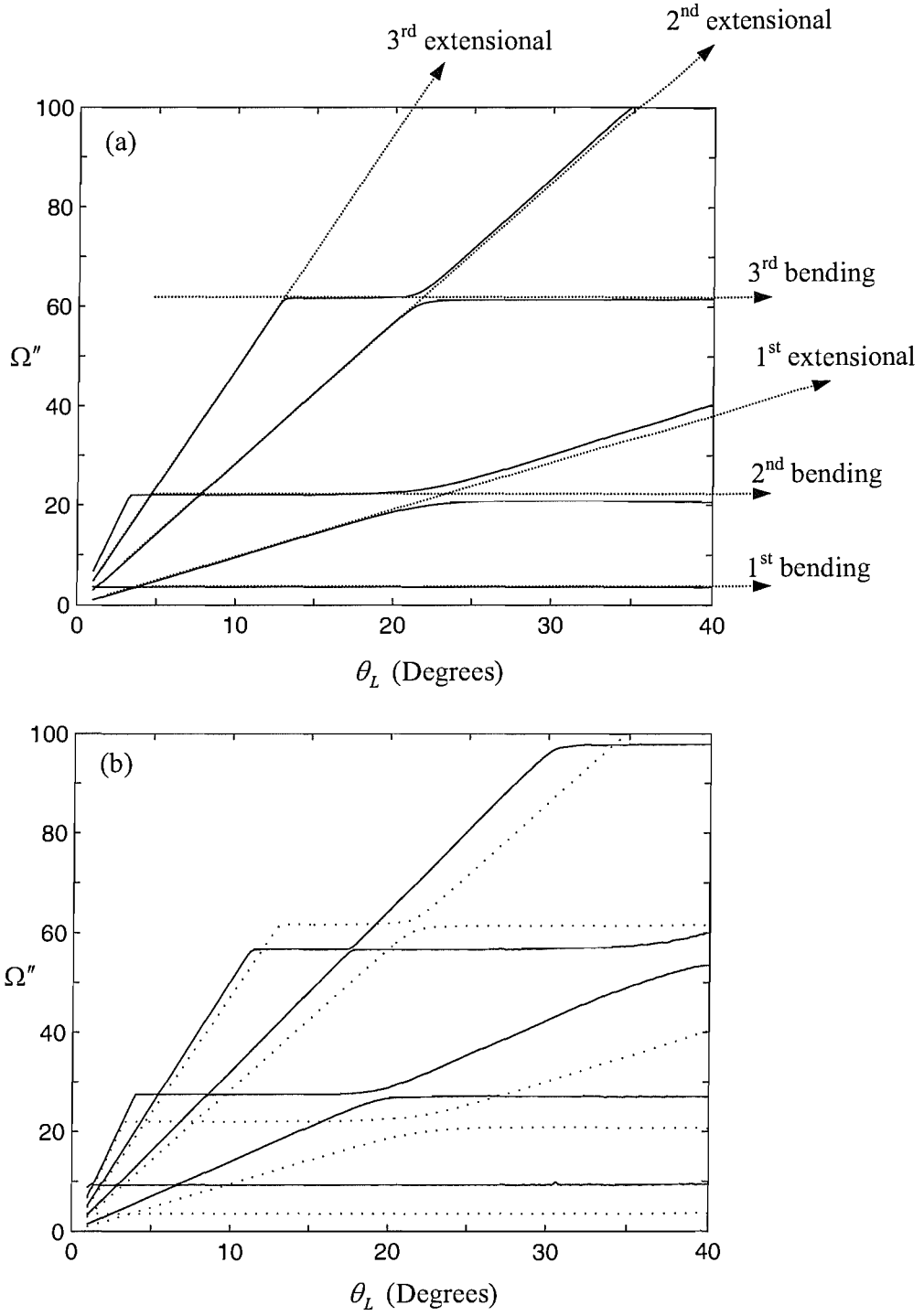

Figure 8-18. Re-drawing of Figure 8-17: (a) the natural frequencies of the uniform beam (solid lines) and their asymptotic behaviour (dotted lines with arrows), (b) the frequencies of the tapered beam (solid lines) versus those of the uniform beam (dotted lines).

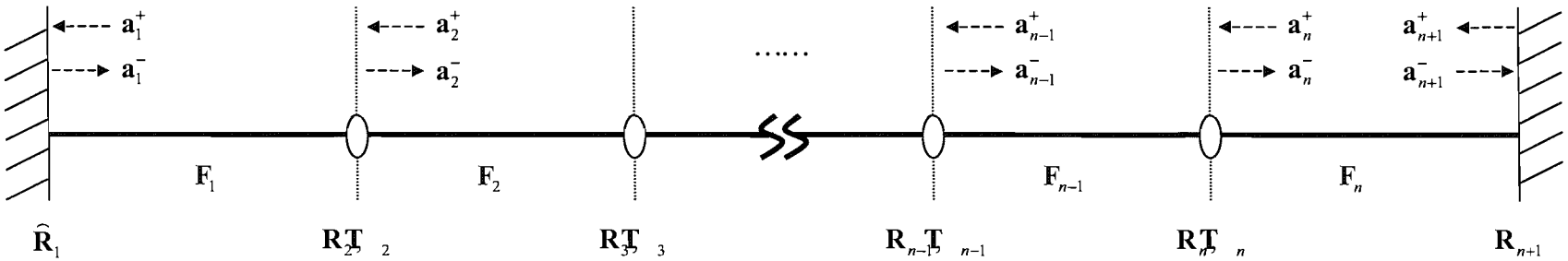

Figure 8-19. Reflection and transmission of waves in a finite structure.

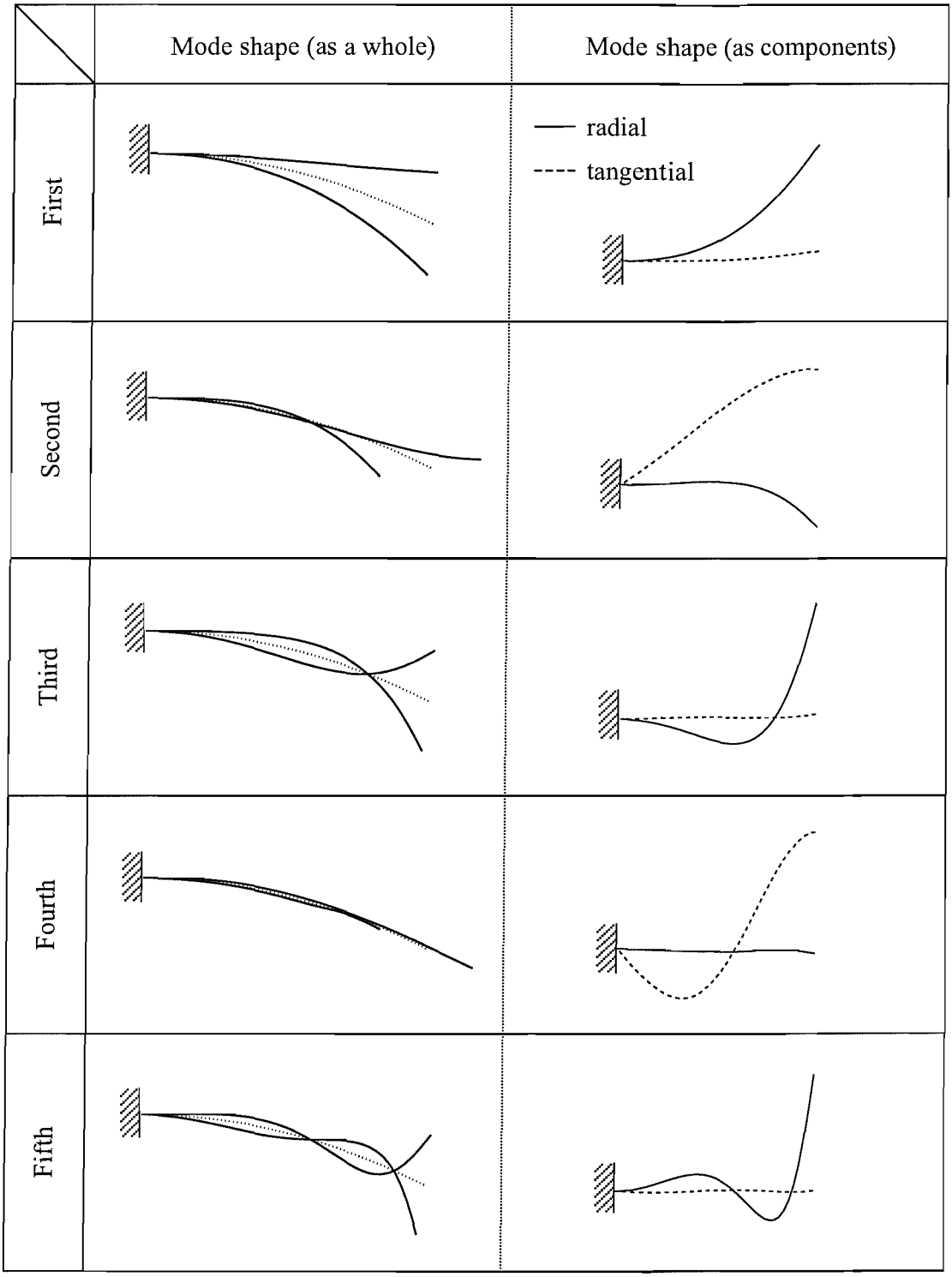

Figure 8-20. Mode shape of the free-clamped, circular beam with $h_{L/2}/R = 0.1$, $\alpha = 0.9$ and $\theta_L = 15^\circ$.

Chapter 9.

CONCLUSIONS

9.1 Summary of present work

This thesis provides a general overview and gives specific examples of a wave approach based on reflection, transmission and propagation of waves for one-dimensional structures. One-dimensional structures, the properties of which are linearly elastic and are prescribed by known functions, were categorised as in Figure 1-1. Among the categories, the present work was concerned with uniform structures and non-periodic non-uniform structures.

A generalised wave approach based on reflection, transmission and propagation of waves was developed in a systematic way. The physical quantities for the motion of one-dimensional structures were grouped into a vector and the governing equations were expressed as first order differential equations. The solution of the governing equations defines the transfer matrix in the physical domain, which is symplectic for a reciprocal system and K-unitary for a conservative system. The state vector in the physical domain was transformed to the wave domain using the eigenvectors of the transfer matrix and the general forms for the properties of the transfer matrix were obtained in the wave domain. If waves are not coupled to each other, the transfer matrix is diagonal. The positive- and negative-going waves were then separated and the amplitudes at one point were related to those at another point according to their propagation direction. This is one distinctive feature of the wave approach. In the wave

approach, all computations are conducted in the direction of wave propagation so that the associated numerical results are always well conditioned. For a systematic application of the wave approach, the displacement, internal force and propagation matrices were introduced. The response to external excitation, reflection and transmission of waves at a point discontinuity, reflection of waves at boundaries, the spectral elements and the energy flow associated with waves were described using the matrices. The general forms for the properties of the reflection, transmission and propagation matrices were given for a reciprocal system.

The wave approach provides exact and efficient computation, irrespective of the frequency, for the motion of uniform waveguides where the coefficients of the governing equations are constant. In chapter 3, the wave approach was applied to cases concerning straight uniform bars undergoing longitudinal motion, which are a single-mode system. These examples gave a simple, clear demonstration of the application of the wave approach. In chapter 4, the wave approach was applied to cases concerning straight uniform beams undergoing bending motion based on Euler-Bernoulli theory. The beams are a two-mode system, where two propagating waves and two nearfield waves ocurr. It was shown explicitly that the transfer method may lead to numerical difficulties related to nearfield waves at high frequencies while the wave approach does not suffer such difficulties. The energy flow associated with the interaction two opposite-going nearfield waves was studied as well. The wave approach to the motion of uniform structures based on higher-order theories, rather than elementary theories, was briefly studied in section 8.2.

There is a class of waveguides, which are not uniform but in which waves can propagate without reflection as they do in uniform waveguides. This class was

categorised as deterministically varying waveguides in this thesis. In chapters 5 and 6, the wave approach to the deterministically varying structures was described. Examples were cases concerning straight bars where the area varies as a power of x, and straight beams where the area and second moment of area vary as powers of x respectively. The response of the non-uniform structures to external forces was investigated and the reactive behaviour due to non-uniformity was revealed. It was shown that the wave approach can be applied equivalently as for uniform structures without drawbacks. It was seen that the potential energy per unit length associated with a propagating wave component is greater than the kinetic energy per unit length. The energy transport velocity, the velocity at which energy is carried by waves, was also derived using the relationship between power and energy. In contrast to that of uniform bars, it is not equal to the group velocity, which is formally defined by $c_g = \mathrm{d}\omega/\mathrm{d}k$ (for real wavenumbers). The velocity depends on position - it decreases as waves approach the apex - as well as frequency. The exponential types of deterministically varying waveguides were briefly studied in section 8.3.

In chapter 7, the wave approach was applied to cases concerning thin, uniform, curved beams with constant curvature, the motion of which was based on Flügge theory. The beams provide coupling of the radial and tangential displacements, which does not occur in the examples of the previous four chapters. However, in the wave domain, the waves are not coupled so that the problem could be simplified. The dispersion relation for each wave was defined by using a criterion: the imaginary value of the wavenumber of a positive-going wave should be negative and the energy transport velocity associated with a positive-going wave should be positive. The energy

flow associated with waves in the curved beam was revealed explicitly in terms of wavenumbers. Numerical results for the power transmission through a U-shaped structure were presented.

In conjunction with the piecewise modelling, the wave approach can be applied to arbitrarily varying structures. In the approach, the arbitrarily varying structure is divided into a series of small segments, and then each segment is modelled by a known structural element. It was illustrated that a piecewise model using deterministically varying elements could provide rapid convergence to the exact at low computational cost. The approach was also applied to the motion of finite systems. A general procedure for obtaining the natural frequencies and mode shapes was described. The modal behaviour of a linearly tapered curved beam with clamped-free boundaries was studied when the length of the beam changed. Its asymptotic behaviour was revealed to be related to the pure bending and pure extensional motions.

9.2 Proposals for future research

The wave approach based on reflection, transmission and propagation of waves presented in this thesis is a general method for the wave analysis for one-dimensional structures. Thus it can be applied in an equivalent way to cases beyond the current interest. The cases may be listed as:

- Application to non-conservative waveguides: the present work was concerned with conservative systems. Damping destroys the conservative nature. Since the wave approach provides well-conditioned numerical computation, it can be applied equivalently to heavily damped structures where all wavenumbers are

complex. The energy flow associated with waves may also be of interest since all wave components can in principle interact to transmit energy.

- Application to non-reciprocal waveguides: the present work was concerned with reciprocal systems. It can be destroyed in cases such as waveguides where the medium is moving. In this case, the symmetry between the positive-going and negative-going wave motions is not assured, i.e., the symmetry condition of the reflection, transmission and propagation matrices does not hold.
- Application to higher-order waveguides: some examples such as bars based on Love's theory and beams based on Timoshenko theory were briefly described. The higher-order theories provide more accurate description of the motion at high frequencies than elementary theories. In contrast to other methods such as the transfer matrix method, the wave approach always provides well-conditioned computation even at high frequencies.
- Application to multi-dimensional waveguides: interest can also be expanded to two- or three-dimensional structures where the problem is reducible to one-dimension, i.e., all the field quantities depend on only the x-axis. For example, the motion of thin uniform rectangular plates, where the state of cross-section is modelled by using admissible functions, can be solved using the wave approach.
- Application to industrial structures: eventually, the wave approach can be used for the motion of built-up structures. The computational efficiency and numerical conditioning problems in using the wave approach, rather than other methods, for such problems may be interesting. Combination of the wave approach with finite element method can also be attempted for complex structures.

REFERENCES

Abramowitz, M. and Stegun, I.A. (1965) *Handbook of Mathematical Functions with Formulas, Graphs, and Mathematical Tables* (New York: Dover Publications).

Abrate, S. (1995) Vibration of non-uniform rods and beams. *Journal of Sound and Vibration* **185**, 703-716.

Auciello, N.M. and Nole, G. (1998) Vibrations of a cantilever tapered beam with varying section properties and carrying a mass at the free end. *Journal of Sound and Vibration*, **214**, 105-119.

Banerjee, J.R. and Williams, F.W. (1985) Exact Euler-Bernoulli dynamic stiffness matrix for a range of tapered beams. *International Journal for Numerical Methods in Engineering*, **21**, 2289-2302.

Beale, L.S. and Accorsi, M.L. (1995) Power flow in two- and three-dimensional frame structures. *Journal of Sound and Vibration*, **185**, 685-702.

Bobrovnitskii, Y.I. (1992) On the energy flow in evanescent waves. *Journal of Sound and Vibration*, **152**, 175-176.

Burr, K.P., Triantafyllou, M.S. and Yue, D.K.P. (2001) Asymptotic governing equation for wave propagation along weakly non-uniform Euler-Bernoulli Beams. *Journal of Sound and Vibration*, **247**, 577-613.

Chidamparam, P. and Leissa, A.W. (1993) Vibrations of planar curved beams, rings and arches. *Applied Mechanics Reviews*, **46**, 467-483.

Conway, H.D., Becker, E.C.H. and Dubil, J.F. (1964) Vibration frequencies of tapered bars and circular plates. *Journal of Applied Mechanics*, **31**, 329-331.

Cranch, E.T. and Adler, A.A. (1956) Bending vibrations of variable section beams. *Journal of Applied Mechanics*, **23**, 103-108.

Craver, W.L. and Jampala, P. (1993) Transverse vibrations of a linearly tapered

cantilever beam with constraining springs. *Journal of Sound and Vibration*, **166**, 521-529.

Cremer, L., Heckl, M. and Ungar, E.E. (1973) *Structure-borne Sound* (Berlin: Springer-Verlag).

Doyle, J.F. (1997) *Wave Propagation in Structures: Spectral Analysis using Fast Discrete Fourier Transforms* (New York: Springer-Verlag).

Easwaran, V., Gupta, V.H. and Munjal, M.L. (1993) Relationship between the impedance matrix and the transfer matrix with specific reference to symmetrical, reciprocal and conservative systems. *Journal of Sound and Vibration*, **161**, 515-525.

Eisenberger, M. (1990) Exact static and dynamic stiffness matrices for general variable cross section members. *AIAA Journal*, **28**, 1105-1109.

Gallagher, R.H. and Lee, C.-H. (1970) Matrix dynamic and instability analysis with non-uniform elements. *International Journal for Numerical Methods in Engineering*, **2**, 265-275.

Goel, R.P. (1976) Transverse vibrations of tapered beams. *Journal of Sound and Vibration*, **47**, 1-7.

Gopalakrishnan, S. and Doyle, J.F. (1994) Wave propagation in connected waveguides of varying cross-section. *Journal of Sound and Vibration*, **175**, 347-363.

Graff, K.F. (1975) *Wave Motion in Elastic Solids* (Oxford: Clarenden Press).

Harland, N.R., Mace, B.R. and Jones, R.W. (2001) Wave propagation, reflection and transmission in tunable fluid-filled beams. *Journal of Sound and Vibration*, **241**, 735-754.

Hodges, D.H., Chung, Y.Y. and Shang, X.Y. (1994) Discrete transfer matric method for non-uniform rotating beams. *Journal of Sound and Vibration*, **169**, 276-283.

Kang, B., Riedel, C. H. and Tan, C. A. (2003) Free vibration analysis of planar curved beams by wave propagation. *Journal of Sound and Vibration*, **260**, 19-44.

Karabalis, D.L. and Beskos, D.E. (1983) Static, dynamic and stability analysis of

structures composed of tapered beams. *Computers & Structures*, **16**, 731-748.

Krylov, V.V. and Tilman, F.J.B.S. (2004) Acoustic 'black holes' for flexural waves as effective vibration dampers. *Journal of Sound and Vibration*, **274**, 605-619.

Kumar, B.M. and Sujith, R.I. (1997) Exact solutions for the longitudinal vibration of non-uniform rods. *Journal of Sound and Vibration*, **207**, 721-729.

Langley, R.S. (1996) A transfer matrix analysis of the energetics of structural wave motion and harmonic vibration. *Proceedings of the Royal Society of London A*, **452**, 1631-1648.

Langley, R.S. (1999) Wave evolution, reflection, and transmission along inhomogeneous waveguides. *Journal of Sound and Vibration*, **227**, 131-158.

Leissa, A. W. (1977) *Vibrations of shells*. NASA SP-288 (Washington, DC).

Lighthill, M.J. (1978) *Waves in Fluids* (Cambridge: Cambridge University Press).

Lin, Y. K. and Donaldson, B. K. (1969) A brief survey of transfer matrix techniques with special reference to the analysis of aircraft panels. *Journal of Sound and Vibration*, **10**, 103-143.

Mabie, H.H. and Rogers, C.B. (1968) Transverse vibrations of tapered cantilever beams with end support. *Journal of the Acoustical Society of America*, **44**, 1739-1741.

Mabie, H.H. and Rogers, C.B. (1974) Transverse vibrations of double-tapered cantilever beams with end support and with end mass. *Journal of the Acoustical Society of America*, **55**, 986-991.

Mace, B.R. (1984) Wave reflection and transmission in beams. *Journal of Sound and Vibration*, **97**, 237-246.

Mace, B.R. (1992) Reciprocity, conservation of energy and some properties of reflection and transmission coefficients. *Journal of Sound and Vibration*, **155**, 375-381.

McLachlan, N.W. (1955) *Bessel Functions for Engineers* (2nd ed., London: Oxford University Press).

Mead, D.J. (1994) Waves and modes in finite beams: application of the phase-closure

principle. *Journal of Sound and Vibration*, **171**, 695-702.

Mead, D.J. (1996) Wave propagation in continuous periodic structures: research contribution from Southampton, 1964–1995. *Journal of Sound and Vibration*, **190**, 495-524.

Meirovitch, M (1997) *Principles and techniques of vibrations* (Prentice-Hall International).

Miller, D.W. and von Flotow, A. (1989) A travelling wave approach to power flow in structural networks. *Journal of Sound and Vibration*, **128**, 145-162.

Milne, H.K. (1987) A note on beam reflection matrices and reciprocity. *Journal of Sound and Vibration*, **114**, 149-151.

Nagarkar, B.N. and Finch, R.D. (1971) Sinusoidal horns. *Journal of the Acoustical Society of America*, **50**, 23-31.

Pease, M.C. (1965) *Methods of Matrix Algebra* (New York: Academic Press).

Pestel, E.C. and Leckie, F.A. (1963) *Matrix Methods in Elastomechanics* (New York: McGraw-Hill).

Petersson, B.A.T. and Nijman, E.J.M. (1998) The one-dimensional bending wave counterpart to the acoustic horn and the semi-infinite wedge. *Journal of Sound and Vibration*, **211**, 95-121.

Pierce, A.D. (1981) *Acoustics: An Introduction to Its Physical Principles and Applications* (New York: McGraw-Hill).

Scott, J.F.M. and Woodhouse, J. (1992) Vibration of an elastic strip with varying curvature. *Philosophical Transactions: Physical Sciences and Engineering*, **339**, 587-625.

Suppiger, E.D. and Taleb, N.J. (1956) Free lateral vibration of beams of variable cross section. *ZAMP*, **7**, 501-520.

Tarnopolskaya, T., de Hoog, F., Fletcher, N.H. and Thwaites, S. (1996) Asymptotic analysis of the free in-plane vibrations of beams with arbitrarily varying curvature and cross-section. *Journal of Sound and Vibration*, **196**, 659-680.

Tarnopolskaya, T., de Hoog, F. and Fletcher, N.H. (1999) Low-frequency mode transition in the free in-plane vibration of curved beams. *Journal of Sound and Vibration*, **228**, 69-90.

Walsh, S.J. and White, R.G. (2000) Vibrational power transmission in curved beams. *Journal of Sound and Vibration*, **233**, 455-488.

Wang, H.C. (1968) Generalized hypergeometric function solutions on transverse vibrations of a class of nonuniform beams. *Journal of Applied Mechanics*, **34**, 702-708.

Wu, C.M. and Lundberg, B. (1996) Reflection and transmission of the energy of harmonic elastic waves in a bent bar. *Journal of Sound and Vibration*, **190**, 645-659.

Yong, Y. and Lin, Y. K. (1989) Propagation of decaying waves in periodic and piecewise periodic structures of finite length. *Journal of Sound and Vibration*, **129**, 99-118.

Zhong, W.X. and Williams, F.W. (1992) Wave problems for repetitive structures and sympletic mathematics. *Proceedings of the Instituition of Mechanical Engineers Part C*, **206**, 371-379.

Zhong, W.X. and Williams, F.W. (1995) On the direct solution of wave propagation for repetitive structures. *Journal of Sound and Vibration*, **181**, 485-501.

Appendix A.

BESSEL FUNCTIONS

A.1 Introduction

In this appendix some properties of Bessel functions are summarized. They relate to various forms of Bessel's equation and their solutions, the recurrence relations and the limiting behaviour. Further details can be found in references (McLachlan 1955, Abramowitz and Stegun 1965).

A.2 Bessel's equation

Many differential equations are transformable into Bessel's equation. One of the very useful general forms of Bessel's equation is (Doyle 1997)

$$z^2\frac{d^2\psi}{dz^2}+(1+2\alpha)z\frac{d\psi}{dz}+(\beta^2z^{2\gamma}+\delta^2)\psi=0 \tag{A.1}$$

The solution to equation (A.1) is given by

$$\psi=z^{-\alpha}\left[C_1H_\nu^{(1)}\left(\frac{\beta z^\gamma}{\gamma}\right)+C_2H_\nu^{(2)}\left(\frac{\beta z^\gamma}{\gamma}\right)\right] \tag{A.2}$$

where C_1 and C_2 represent arbitrary constants, and

$$\nu=\frac{\sqrt{\alpha^2-\delta^2}}{\gamma} \tag{A.3}$$

In equation (A.2), Hankel functions of the first and second kinds of order ν, $H_\nu^{(1)}(z)$ and $H_\nu^{(2)}(z)$ represent waves travelling toward the negative and positive z-directions, respectively.

Similarly, the general form of the differential equation for the modified Bessel functions is

$$z^2\frac{d^2\psi}{dz^2}+(1+2\alpha)z\frac{d\psi}{dz}+(-\beta^2z^{2\gamma}+\delta^2)\psi=0 \tag{A.4}$$

The solution to equation (A.4) is given by

$$\psi=z^{-\alpha}\left\{C_1I_\nu\left(\frac{\beta z^\gamma}{\gamma}\right)+C_2K_\nu\left(\frac{\beta z^\gamma}{\gamma}\right)\right\} \tag{A.5}$$

where $I_\nu(z)$ and $K_\nu(z)$ are the modified Bessel functions.

Specifically, several forms of Bessel's equation and their solutions are

$$\frac{d^2\psi}{dz^2}+\frac{(1+2\nu)}{z}\frac{d\psi}{dz}+k^2\psi=0,\quad \psi=z^{-\nu}\left\{C_1H_\nu^{(1)}(kz)+C_2H_\nu^{(2)}(kz)\right\} \tag{A.6a,b}$$

$$z\frac{d^2\psi}{dz^2}+(1+\nu)\frac{d\psi}{dz}+k^2\psi=0,\quad \psi=z^{-\nu/2}\left\{C_1H_\nu^{(1)}\left(2k\sqrt{z}\right)+C_2H_\nu^{(2)}\left(2k\sqrt{z}\right)\right\} \tag{A.7a,b}$$

$$z\frac{d^2\psi}{dz^2}+(1+\nu)\frac{d\psi}{dz}-k^2\psi=0,\quad \psi=z^{-\nu/2}\left\{C_1I_\nu\left(2k\sqrt{z}\right)+C_2K_\nu\left(2k\sqrt{z}\right)\right\} \tag{A.8a,b}$$

Note that equation (A.6a) is related to the governing equation of the motion of non-uniform bars with a polynomial variation in area.

Consider a combination of equations (A.7a) and (A.8a) such as

$$\left[z\frac{d^2}{dz^2}+(1+\nu)\frac{d}{dz}+k^2\right]\left[z\frac{d^2}{dz^2}+(1+\nu)\frac{d}{dz}-k^2\right]\psi=0 \tag{A.9}$$

When it is expanded, a differential equation of 4th order is obtained as

$$z^2\frac{d^4\psi}{dz^4}+2(2+\nu)z\frac{d^3\psi}{dz^3}+(1+\nu)(2+\nu)\frac{d^2\psi}{dz^2}-k^4\psi=0 \qquad \text{(A.10)}$$

Note that this equation is related to the governing equation of the motion of non-uniform beams with a polynomial variation in area and the second moment of area. The general solution to equation (A.10) is given by

$$\psi=z^{-\nu/2}\left[C_1H_\nu^{(1)}\left(2k\sqrt{z}\right)+C_2H_\nu^{(2)}\left(2k\sqrt{z}\right)+C_3I_\nu\left(2k\sqrt{z}\right)+C_4K_\nu\left(2k\sqrt{z}\right)\right] \qquad \text{(A.11)}$$

A.3 Recurrence relations

The Bessel function of the first kind, $J_\nu(z)$, satisfies

$$\frac{\mathrm{d}}{\mathrm{d}z}\left[z^\nu J_\nu(z)\right]=z^\nu J_{\nu-1}(z),\quad \frac{\mathrm{d}}{\mathrm{d}z}\left[z^{-\nu}J_\nu(z)\right]=-z^{-\nu}J_{\nu+1}(z) \qquad \text{(A.12a,b)}$$

Expanding the derivatives appearing in equation (A.12) gives

$$zJ_\nu'(z)+\nu J_\nu(z)=zJ_{\nu-1}(z),\quad zJ_\nu'(z)-\nu J_\nu(z)=-zJ_{\nu+1}(z) \qquad \text{(A.13a,b)}$$

where $(\,)'$ denotes the derivative over z. Alternatively, subtracting (A.13b) from (A.13a) or adding them gives

$$J_{\nu+1}(z)=\frac{2\nu}{z}J_\nu(z)-J_{\nu-1}(z),\quad J_\nu'(z)=\frac{1}{2}\left\{J_{\nu-1}(z)-J_{\nu+1}(z)\right\} \qquad \text{(A.14a,b)}$$

Equations (A.12) to (A.14) are called the recurrence relations of Bessel functions and also hold for the functions $Y_\nu(z)$, $H_\nu^{(1)}(z)$ and $H_\nu^{(2)}(z)$.

Similarly, the recurrence formulas of the modified Bessel functions are summarized as

$$\frac{d}{dz}\left[z^\nu I_\nu(z)\right]=z^\nu I_{\nu-1}(z),\quad \frac{d}{dz}\left[z^{-\nu}I_\nu(z)\right]=z^{-\nu}I_{\nu+1}(z) \qquad \text{(A.15a,b)}$$

$$zI_\nu'(z)+\nu I_\nu(z)=zI_{\nu-1}(z),\quad zI_\nu'(z)-\nu I_\nu(z)=zI_{\nu+1}(z) \qquad \text{(A.16a,b)}$$

$$I_{\nu+1}(z)=-\frac{2\nu}{z}I_{\nu}(z)+I_{\nu-1}(z),\qquad I'_{\nu}(z)=\frac{1}{2}\{I_{\nu-1}(z)+I_{\nu+1}(z)\} \tag{A.17a,b}$$

$$\frac{d}{dz}\left[z^{\nu}K_{\nu}(z)\right]=-z^{\nu}K_{\nu-1}(z),\qquad \frac{d}{dz}\left[z^{-\nu}K_{\nu}(z)\right]=-z^{-\nu}K_{\nu+1}(z) \tag{A.18a,b}$$

$$zK'_{\nu}(z)+\nu K_{\nu}(z)=-zK_{\nu-1}(z),\qquad zK'_{\nu}(z)-\nu K_{\nu}(z)=-zK_{\nu+1}(z) \tag{A.19a,b}$$

$$K_{\nu+1}(z)=\frac{2\nu}{z}K_{\nu}(z)+K_{\nu-1}(z),\qquad K'_{\nu}(z)=-\frac{1}{2}\{K_{\nu-1}(z)+K_{\nu+1}(z)\} \tag{A.20a,b}$$

A.4 Bessel functions of half-integral order

Bessel function of half-integral order $(2n+1)/2$, where n is an integer, can be expressed in closed form in terms of elementary functions. Several of them are

$$H^{(1)}_{1/2}(z)=-\mathrm{i}\sqrt{\frac{2}{\pi z}}e^{\mathrm{i}z}=-\mathrm{i}H^{(1)}_{-1/2}(z) \tag{A.21a,b}$$

$$H^{(1)}_{3/2}(z)=-\sqrt{\frac{2}{\pi z}}\left(1+\frac{\mathrm{i}}{z}\right)e^{\mathrm{i}z} \tag{A.22}$$

$$H^{(2)}_{1/2}(z)=\mathrm{i}\sqrt{\frac{2}{\pi z}}e^{-\mathrm{i}z}=\mathrm{i}H^{(2)}_{-1/2}(z) \tag{A.23a,b}$$

$$H^{(2)}_{3/2}(z)=-\sqrt{\frac{2}{\pi z}}\left(1-\frac{\mathrm{i}}{z}\right)e^{-\mathrm{i}z} \tag{A.24}$$

$$I_{1/2}(z)=\sqrt{\frac{2}{\pi z}}\sinh z,\qquad I_{-1/2}(z)=\sqrt{\frac{2}{\pi z}}\cosh z \tag{A.25a,b}$$

$$I_{3/2}(z)=\sqrt{\frac{2}{\pi z}}\left(\cosh z-\frac{1}{z}\sinh z\right) \tag{A.26}$$

$$K_{1/2}(z)=\sqrt{\frac{\pi}{2z}}e^{-z}=K_{-1/2}(z) \tag{A.27a,b}$$

$$K_{3/2}(z)=\sqrt{\frac{\pi}{2z}}\left(1+\frac{1}{z}\right)e^{-z} \tag{A.28}$$

A.5 Limiting behaviour

When $|z|>>1$ and z is real, the Bessel functions asymptote to

$$H_\nu^{(1)}(z)\approx\sqrt{\frac{2}{\pi z}}e^{\mathrm{i}\left(z-\frac{1}{4}\pi-\frac{1}{2}\nu\pi\right)},\qquad H_\nu^{(2)}(z)\approx\sqrt{\frac{2}{\pi z}}e^{-\mathrm{i}\left(z-\frac{1}{4}\pi-\frac{1}{2}\nu\pi\right)} \tag{A.29a,b}$$

$$I_\nu(z)\approx\frac{e^z}{\sqrt{2\pi z}},\qquad K_\nu(z)\approx\sqrt{\frac{\pi}{2z}}e^{-z} \tag{A.30a,b}$$

Thus it follows that

$$\frac{H_{\nu+1}^{(1)}(z)}{H_\nu^{(1)}(z)}\approx-\mathrm{i},\quad \frac{H_{\nu+1}^{(2)}(z)}{H_\nu^{(2)}(z)}\approx\mathrm{i},\quad \frac{H_{\nu+2}^{(1)}(z)}{H_\nu^{(1)}(z)}\approx-1,\quad \frac{H_{\nu+2}^{(2)}(z)}{H_\nu^{(2)}(z)}\approx-1 \tag{A.31a,b,c,d}$$

$$\frac{I_{\nu+1}(z)}{I_\nu(z)}\approx\frac{I_{\nu+2}(z)}{I_\nu(z)}\approx\frac{K_{\nu+1}(z)}{K_\nu(z)}\approx\frac{K_{\nu+2}(z)}{K_\nu(z)}\approx1 \tag{A.32a,b,c,d}$$

Now consider the case when $|z|<<1$. When $\nu=0$, the Bessel functions tend to

$$H_0^{(2)}(z)\approx-H_0^{(1)}(z)\approx-\mathrm{i}\frac{2}{\pi}\{\ln(z)+\gamma-\ln(2)\} \tag{A.33a,b}$$

$$I_0(z)\approx1,\qquad K_0(z)\approx-\ln(z) \tag{A.34a,b}$$

where $\gamma\approx0.577216$ is Euler's constant. When the real value of ν is positive, they are

$$H_\nu^{(2)}(z)\approx-H_\nu^{(1)}(z)\approx\mathrm{i}\frac{\Gamma(\nu)}{\pi}\left(\frac{2}{z}\right)^\nu \tag{A.35a,b}$$

$$I_\nu(z)\approx\frac{1}{\Gamma(\nu+1)}\left(\frac{z}{2}\right)^\nu,\qquad K_\nu(z)\approx\frac{\Gamma(\nu)}{2}\left(\frac{2}{z}\right)^\nu \tag{A.36a,b}$$

where $\Gamma(\nu)$ is the gamma function.